UNIVERSITY OF LONDON THESIS

Degree PhD Year 2007 Name of Author KONSTANTINOS LYKOSTRATIS

University College London

PhD Thesis

MATHEMATICAL MODELLING OF SHEAR STRESS SIGNALLING IN ENDOTHELIAL CELLS

London – April 2007

Konstantinos Lykostratis

ProQuest LLC
789 East Eisenhower Parkway
P.O. Box 1346
Ann Arbor, MI 48106-1346

ABSTRACT

In recent years it has become clear that cell signalling pathways are not simple linear chains of events as was once thought but frequently diverge, converge and employ positive and negative feedback. As a result signals show a complex pattern of spatial and temporal activity that is difficult to explain despite a wealth of experimental data. Systems Biology attempts to predict and understand the behaviour of complex systems by integrating information from diverse sources and principles drawn from a large number of different scientific disciplines.

The signalling pathways regulating endothelial responses to shear stress have been extensively studied, since perturbed fluid flow contributes significantly to the development of heart disease. Shear stress activates many signals in endothelial cells, from ion influxes to protein phosphorylation and gene expression, and induces changes in endothelial morphology. Here a modelling and Systems Biology approach was taken to investigate and understand better the endothelial signal transduction networks that convert fluid flow stimulation into biochemical signals. A static signal transduction network was built from integrin cell surface receptors to activation of the tyrosine kinases focal adhesion kinase (FAK) and Src. Parameters for each reaction in this network were collected from the literature or, when necessary, estimated.

To model how fluid flow initiates signalling in this network, the shear stress-induced calcium influx and the viscoelastic response of transmembrane receptors such as integrins to mechanical force were examined by means of mathematical modelling, using ordinary differential equations. These effects were used as primary activators of the shear stress response in endothelial cells, allowing quantitative analysis of the intracellular signal transduction flow which propagates from integrin to paxillin, FAK and Src activation. The magnitude and dependencies of each influence were examined individually and in conjunction with each other. The model was used to investigate the role and dynamic regulation of previously unstudied molecules in the network and the simulated results were compared against experimental data in order to validate hypotheses and increase our understanding of the molecular processes underlying the shear stress response.

LIST OF FIGURES

LIST OF TABLES

ABBREVIATIONS

Ab	antibody
AFCS	Alliance for Cell Signalling
AFM	atomic force microscope
BAECs	Bovine aortic endothelial cells
BIND	Biomolecular Interaction Database
BHK	baby Hamster kidney
CCE	capacitative Ca^{2+} entry
CHO	Chinese Hamster ovary
CICR	Ca^{2+} -induced Ca^{2+} release
CMC	Cell Migration consortium
Csk	c-Src terminal kinase
DAG	diacylglycerol
DIP	database of Interacting Proteins
DNA	deoxyribonucleic acid
ECs	endothelial cells
E.Coli	*Escherichia Coli*
ECM	extracellular matrix
EDTA	ethylenediaminetetraacetic acid
EGFR	epidermal growth factor receptor
ER	endoplasmic reticulum
ERK	extracellular signal-regulated protein kinase
FAK	focal adhesion kinase
FAT	focal adhesion targeting
DOQCS	Database of Quantitative Cellular Signalling
GAP	GTPase activating protein
GDI	guanine nucleotide dissociation inhibitor
GDP	guanosine bisphosphate
GEF	guanine nucleotide exchange factor
GHK	Goldman-Hodgkin-Katz

GPCRs	G-protein coupled receptors
GRAF	GTPase activating protein for Rho associated with FAK
Grb2	growth factor receptor binding protein 2
GTP	guanosine trisphosphate
HUVECs	Human umbilical vein endothelial cells
HPRD	Human Protein Reference Database
Ig	immunoglobulin
ILK	Integrin linked kinase
IP_3	inositol (1,4,5) trisphosphate
KEGG	Kyoto Encyclopedia of Genes and Genomes
LIM	Lin-11, Isl-1 and Mec-3 genes
LMW-PTP	Low molecular weight protein tyrosine phosphatase
MAPK	mitogen activated protein kinase
NMR	nuclear magnetic resonance
NF-kB	nuclear factor kappa beta
NO	nitric oxide
ODEs	ordinary differential equations
PAR	proteolytically activated receptor
PCA	principal component analysis
PECAM-1	platelet/endothelial adhesion molecule
PIP2	Phosphatidylinositol bisphosphate
PIPKIγ661	phosphatidyl-inositol-4-phosphate 5-kinase isoform 1γ661
PI3K	phosphoinositide 3-kinase
PKC	protein kinase C
PLC	phospholipace C
PLS	partial least squares
PTB	phosphotyrosines binding
PtdIns(4,5)P_2	phosphatidylinositol 4,5-bisphosphate
PTK	Protein tyrosine kinase
PTP	protein tyrosine phosphatase
pSTIING	Protein, Signalling, Transcriptional Interactions & Inflammation Networks Gateway

RNA	ribonucleic acid
RNAi	RNA interference
RPTPα	Receptor protein tyrosine phosphatase alpha
RTKs	receptor tyrosine kinases
SH2	Src homology 2
SH3	Src homology 3
SOS	Son Of Sevenless
VEGFR	vascular endothelial growth factor receptor

ACKNOWLEDGEMENTS

The words contained within these pages represent four years of my life filled with constant reading, simulation, and lot of head scratching – four years made possible by a great many people.

First and foremost, I would like to thank my PhD supervisors, Dr Anne J Ridley and Marketa Zvelebil who have provided invaluable assistance and support throughout the years of my PhD, with irreplaceable suggestions and remarkable proof-reading skills and whose breadth of scientific knowledge, continuous enthusiasm and passion for biological innovation have been a constant inspiration.

Hamid Bolouri and his group in the Institute for Systems Biology in Seattle, US for a crash course in mathematical modelling. I must also thank them for looking after me and making bearable fourteen-hour days spent in front of the computer screen. I am grateful to Daehee Hwang for his tutorship in chemical engineering and Matlab applications and for helping me with maths when my equations became a bit longer than I could handle.

Mike Waterfield, Buzz Baum, David Sims, Maria Christodoulou and the members if the bioinformatics groups were of great assistance in discussing biology and approaches of investigation.

Finally, I would like to express my gratitude to my family and friends, who kept me going when things got tough, whose faith in me has always been unflinching, and to whom I owe everything. And to a couple special friends, who kept me sane during my endless hours of reading publications and coding equations in Matlab.

This work was funded by the Ludwig Institute for Cancer Research and an internal graduate fellowship (Bogue) generously provided by University College London.

Kostas Lykostratis
April 2007

1 CHAPTER 1 – INTRODUCTION

1.1 Modelling In Biology

What of information without knowledge?
What of knowledge without wisdom?

1.1.1 Information, many variables.

"The most advanced tools for computer process description seem to be also the best tools for the description of biomolecular systems."
Ehud Shapiro 2001

Technological advancements in molecular biology in the last 20 years (e.g. DNA arrays, DNA sequencing, mass spectrometry, nanotechnology) have led to thousands of papers being published in biological journals and millions of experiments being carried out every day. Today there are many repositories and databases trying to store all this "information", which consist of partially processed numbers and/or raw data. This data explosion has made it difficult for analysis to take place quickly and efficiently. Without understanding of this information all this only is an encyclopaedia written in a foreign language. All this information expansion leads to an ever-increasing awareness of the complexity of living systems which by no means makes our comprehension of biological responses and systems any easier. Our understanding of signalling pathways is being refined every day. New molecules and interactions are being discovered so quickly that, genetic and protein networks have increased in size to the point that they cannot be distinguished in 2D space anymore. Diagrams that attempt to illustrate the interplay between metabolic and protein pathways frequently resemble a hybrid of an enormous spider web with a complicated underground railway map. Each new piece of information reveals a new "black" box, a new problem. Signalling pathways are tortuous, frequently converging and diverging, making it very difficult to study their operation in isolation. Computers are now extremely important tools in the arsenal of biologists. They are now being used as an integral part of the discovery pipeline, rather than just an elaborate calculator.

1.1.2 Knowledge – putting pieces of the puzzle together

"Although the road ahead is long and winding, it leads to a future where biology and medicine are transformed into precision engineering."
(Kitano, 2002)

The highly successful approach of molecular biology for the past 20-30 years has been, in most cases, to investigate individual genes or proteins one at a time. This is essentially a reductionist approach. Whether the experiments involve use of PCR (polymerase chain reaction), immunoprecipitation, western blots, DNA sequencing, DNA arrays or proteomics, the aim is always the same; to isolate specific molecular components by taking the system apart in order to generate as much information as possible that can be used to identify and describe the structure and function of individual molecules. This approach has been ideal for understanding the properties of such molecular structures and has led to the rise of bioengineering and biotechnology that allow sophisticated manipulation of proteins and genes for better clinical applications and healthcare. Nevertheless, one of the main objectives of biology which has been to understand the way cells communicate with each other and how they determine shape, size, cell division, nutrient intake, cell motility and a variety of other phenomena, still remains unconquered. The reduction-based efforts of biology research in the past two decades led to the realisation that it is extremely difficult to understand the mechanism of function of biological systems and how they are regulated by internal or external influences by analysis of isolated biological components alone. In contrast to the situation when investigating life sciences 50 years ago, and now in the 21st century more than ever, the scientific community is no longer constrained by a lack of information in most fields of biological research. Recent efforts have been promoting information integrative-based research initiatives towards the understanding of large biological systems (Figure 1.01).

These efforts have been supported by a paradigm shift in biological research, known as Systems Biology. Systems Biology complements and strengthens molecular biology by investigating the behaviour and relationships of all elements in a particular biological system while it is functioning. It employs a holistic approach of attacking biological questions, where isolated studies are replaced with combinations of experimental

measurements, sophisticated data analysis and modelling (Figure 1.02). Systematic experiments take place by manipulating the biology of cells in various ways (additions of drugs, gene knockouts, nutrient conditions, etc) and subsequently measuring the effect of each manipulation by a variety of technologies (Figure 1.02).

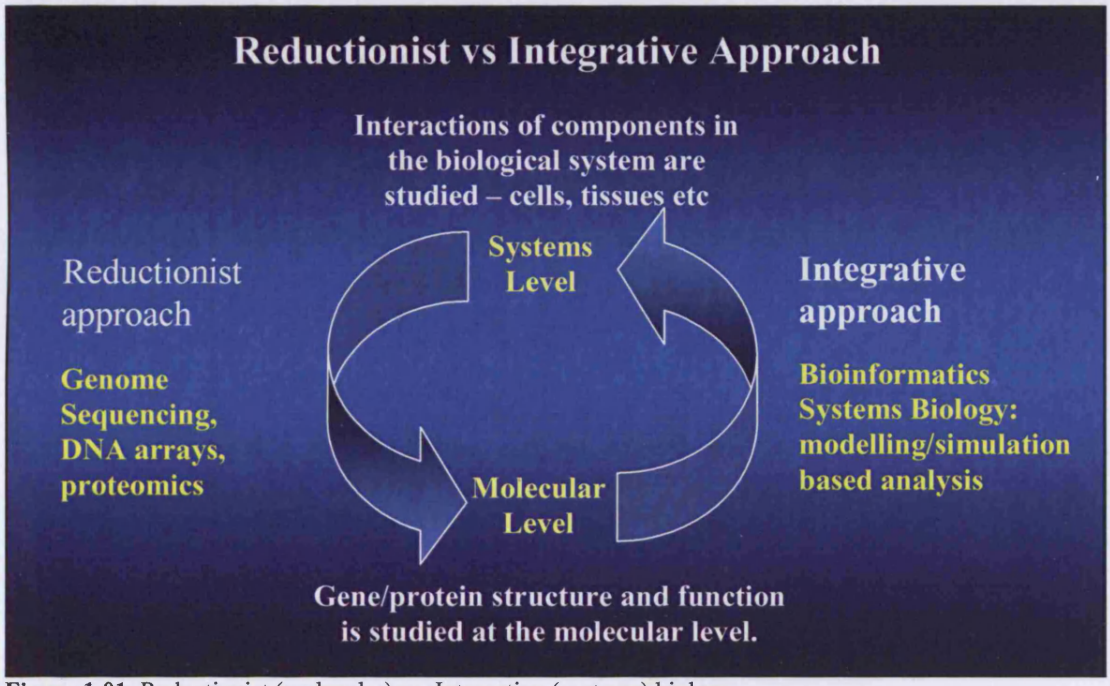

Figure 1.01. Reductionist (molecular) vs. Integrative (systems) biology.

The data generated from the experiments are then analysed/mined to extract useful information that can be used to aid our understanding of biological processes. This analysis frequently employs computational methods and tools which generally aid in the manipulation of the data and are indispensable in cases of high-throughput experimentation. The real primacy of this paradigm of research however, is revealed in the novel utility of well defined numerical models (discussed in section 1.2) along with experimental data. One of the reasons of the importance of modelling which is frequently missed, is that models, formal or numerical, are highly efficient and effective mechanisms to store and propagate knowledge. This knowledge is integrated, processed information specifically selected to describe the regulation, function and emergent properties of a particular biological system.

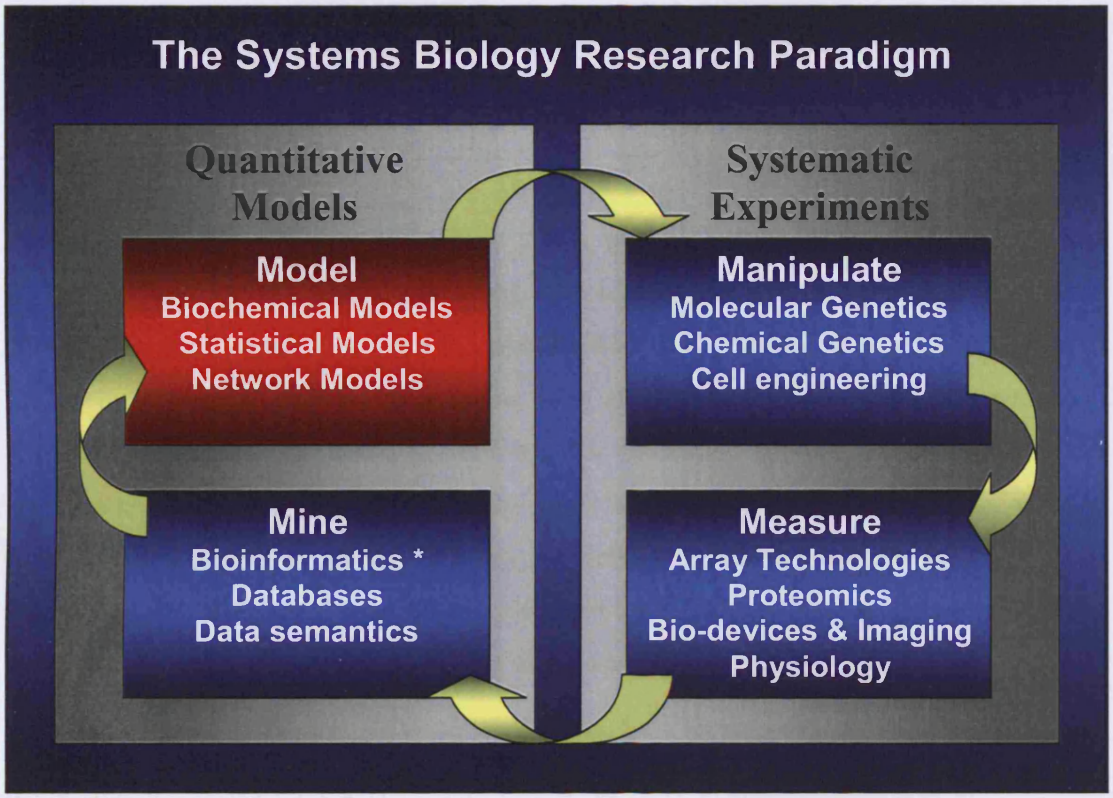

Figure 1.02 An operational definition of the systems biology research paradigm, linking experimental biology to quantitative modelling (Ideker et al., 2006). Quantitative and/or multi-variable systematic experimentation is coupled with computation that elucidates hypotheses (mining) and facilitates predictions (modelling). Information stored in databases and literature.

As a practice Systems Biology can be envisaged as combination of two aims:

- First to acquire sufficient understanding of biological processes and systems. This is achieved by integrating all knowledge and data produced by molecular biology and other disciplines in order to examine and understand the properties of the cell and its function at the system level; focusing on the responses, the measure of robustness and the overall total control.
- Second, to use this understanding in order to generate sufficient predictive power and capacity for rational manipulation of biological systems. This achieved by continuously attempting to predict the quantitative behaviour of an in vivo biological process under realistic perturbation, where the quantitative treatment derives its power from explicit inclusion of the process components, their interactions and realistic values for their concentrations, locations and local states.

1.1.3 The requirement for modelling

"Physical reality is constituted by particles of matter in motion"
Sir Isaac Newton

The general systems theory in biology is not new. It was developed by Ludwig von Bertalanffy more than 60 years ago along with his concept of live organisms as physical systems and their complexity (von Bertalanffy, 1969). His fundamental studies have been followed by several attempts to examine cells at a systems level. The advancement of computers in the last 30 years allowed computer simulation applications to take place for systems research in biology as for many other areas of research as well (e.g. weather prediction programs). In modern biology, modelling excitable cells and systems took a giant leap forward when Alan Hodgkin and Andrew Huxley published their equations for the squid giant axon, an achievement for which they received the Nobel Prize for Physiology or Medicine in 1963.

Modelling can be seen as an iterative process of interaction between mathematics and experimentation, involving successive approximations towards predictive capability. Mathematical models consist of a series of equations describing the relationship between the properties of the system, often with respect to time. Sometimes these equations are tractable to mathematical analysis providing a complete understanding of the model. If all or a large amount of the properties of the model match the experimental results, we have gained knowledge of the system. The more reactions that are added to the system modelled, however, the more that system becomes intractable to mathematical analysis. Such limitations however can be bypassed by implementing the mathematical model on computer and by means of numerical calculations determine its behaviour.
Computer simulation refers to a translation of the model into a computer program which can perform numerical analysis if the model consists of differential equations, or even use a stochastic algorithm to calculate a probabilistic model. Even though the terms 'simulation' and 'modelling' are often used interchangeably they hold distinctive meanings. Simulation makes no explicit reference to experimental data, whereas modelling links each experimental measurement to some function of the state variables of the model and then assesses the model's ability to reproduce these measurements.

Simulation therefore is only a part of the modelling process which permits us to know with precision what the model predicts. Simulation algorithms can be applied to nearly every model, irrespective of its size and complexity. This makes the computer simulation a very powerful and flexible tool in understanding physical reality. It is important however to take care in constructing the model and using an appropriate algorithm.

Besides their ability to handle detailed and extensive models of biological systems, computer simulation allows:

- **Validation of hypotheses** – one of the first things we all realize is that out of every experimental paper, at least one hypothesis is born. If a suitable model, containing the idea to be tested, is simulated, and the results of the simulation match that of the biological systems, the hypothesis can be accepted as a feasible explanation for the observed behaviour.
- **Direction of research efforts** – simulation of alternative models can highlight key areas of a system, providing an experimental strategy, and suggesting specific experiments that could be performed to select between competing theories.
- **Flexibility of inputs and environment** – models can be tested with any combination of intrinsic and extrinsic factors, such as genotype background, physical parameters and kinetic data.
- **Elimination of random errors** – with any experimental measurement there is an associated error, which often approaches the magnitude of the measurement itself. As there is no "measurement", as such, in a simulation, these errors are avoided.
- **Study of slow or fast changes** – many operations within biological systems take place on time-scales that cannot be measured practically, from the brief existence of a reaction intermediate to evolutionary steps taken over millions of years. Computer simulations can run at a faster or slower rate as required.
- **Expensive, difficult or impossible experiments** – financial or physical constraints very often limit experimental study. Simulation rarely suffers from the same limitations, allowing, for instance, the measurement of intermediates in a biological pathway or testing the global effects of changes of an ecosystem even when no assays exist. Moreover, all but the most powerful of computers are inexpensive compared to the likes of modern laboratory equipment and reagents.

For all the above reasons simulation is becoming increasingly one of the core tools in biological research. Fifteen years ago, only a handful of systems had been simulated: population dynamics in ecosystems, simple models of cell signalling pathways and motions of reacting molecules (Goldbeter et al., 1990; Rand and Wilson, 1991). Within the last decade however, dynamic models have been created (or at least attempted) for almost the complete spectrum of biological systems (Figure 1.03), including models on intramolecular forces and molecular dynamics (Vinter and Gardner, 1994), models on cellular signalling pathways (Bhalla and Iyengar, 1999; Goldbeter et al., 1990; Kholodenko et al., 1999; Schoeberl et al., 2002), models on metabolic pathways and gene expression (Arkin et al., 1998; Sauro, 1993) and the evolution of Man (Gibson, 1989).

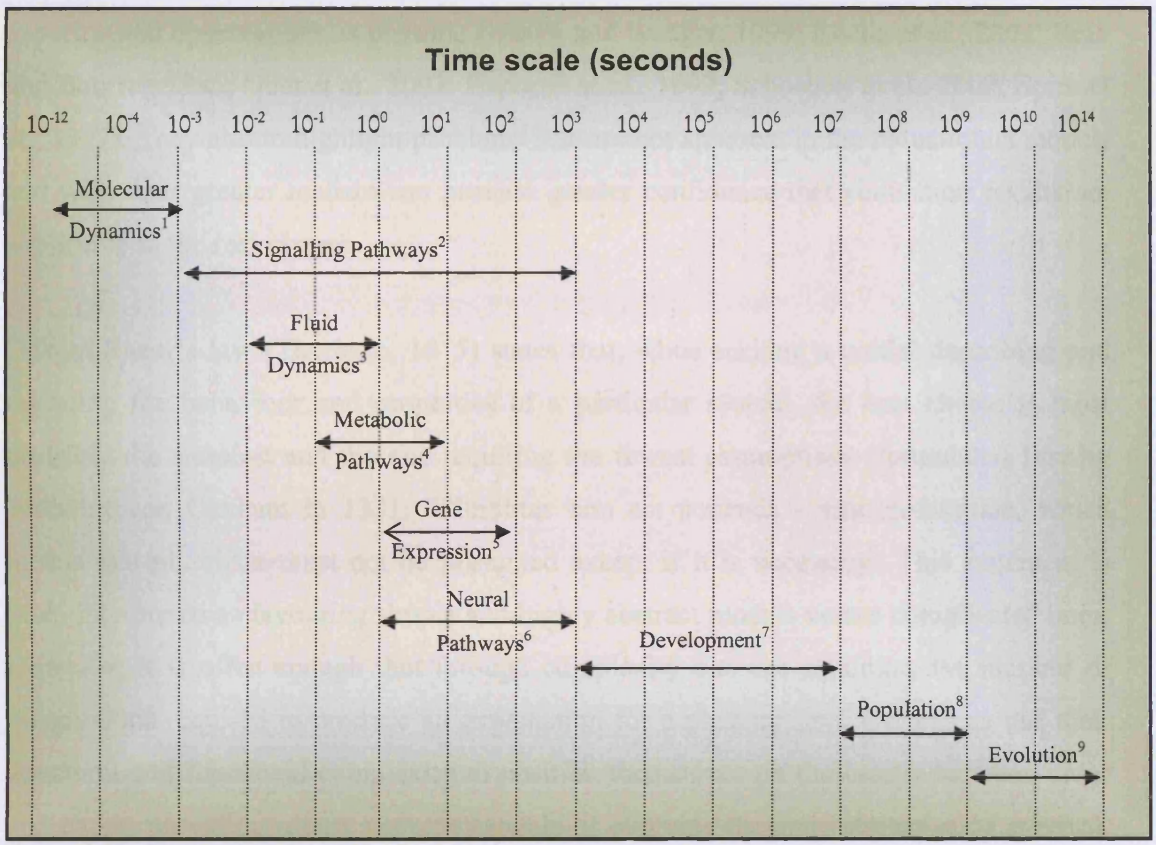

Figure 1.03. Time scales of modelled biological systems.
[1] Rational drug design (Vinter and Gardner, 1994), [2] Ca^{2+} oscillations (Dupont and Goldbeter, 1992; Goldbeter et al., 1990), EGFR signalling (Kholodenko et al., 1999; Schoeberl et al., 2002), MAPK cascade signalling (Bhalla and Iyengar, 1999), [3] Medium flow (Wiesner et al., 1997), [4] Metabolic control analysis (Sauro, 1993), [5] Phage lambda (Arkin et al., 1998), [6] Cardiac electrical activity (Cannell, 1997), [7] Cell culture growth (Kohn, 1998), [8] Epidemics (Rand and Wilson, 1991), [9] Evolution (Gibson, 1989).

1.1.4 Evolution of modelling in molecular biology and complexity expansion

Up to a decade ago, and before the exponential rise of computer processing power, the majority of models were derived from a simplification of the real system; either due to lack of knowledge of the system's true complexity (lack of information) or because the focus was on the investigation of fundamental mechanisms, in a way that might permit straightforward analytical methods. Such models generally were not aiming to incorporate the complete system, explain all experimental observations or simulate pathways in a physically realistic manner (Tang and Othmer, 1994; Valkema and Van Haastert, 1994). Recently, with the explosive generation of data describing mechanistic details of biological systems has there been a gradual shift towards information-integrated models. These encompass a greater part of the biological system and attempt to reproduce as many experimental observations as possible (Bhalla and Iyengar, 1999; Bhalla et al., 2002; Bray and Bourret, 1995; Guet et al., 2002; Hartwell et al., 1999; Schoeberl et al., 2002; Spiro et al., 1997). They aim to highlight problems that are not apparent in the reductionist models and with their greater realism can provide greater confidence that simulation results are applicable to the real system.

Ockam Razor's law (Thorburn, 1915) states that, when seeking a model describing and revealing the behaviour and properties of a particular system, the best choice is most probably the simplest and the one requiring the fewest assumptions (formulated first by Wilhelm von Ockham in 1321: "Pluralitas non est ponenda - sine necessitate, which means that pluralism must not be presumed except if it is necessary). This statement is often interpreted as favouring simple and highly abstract models versus complicated ones. However, it is often enough that through complexity one can minimise the number of assumptions required to produce an explanation for a phenomenon. Organisms use their structural and functional complexity to position themselves on the border between order and chaos, providing robust systems capable of evolving dynamic strategies of survival. Generally, highly dynamic complex systems and especially in biology manifest emergent properties such as oscillatory behaviour and regulatory feed-forward and feedback loops. It is for this reason that complexity should be preserved in the model if possible (i.e. sufficient computational power for simulation) so it also preserves any emergent properties of the system that will otherwise be missed.

1.1.5 Biochemical systems and pathways

"Though signalling pathways are often drawn as simple linear chains of events, they are rarely that simple. Frequently there is feedback, cross-talk between pathways and enough branching to make one want to change to a less complicated field of biology. In order to fully understand these pathways, we need a convenient and powerful model to complement the experimental research. Though there have been relatively few attempts to model signalling pathways using computers, it seems likely that this will very soon become a major area of study."

J Michael Bishop, Novel Laureate (Weintraub et al, 1995).

A biochemical pathway can simply be defined as a series of chemical reactions leading from one compound to another, these usually being proteins. Protein molecules are long folded-up strings of amino acids with precisely determined, but often mechanically flexible, three- dimensional shapes. If two proteins have surface regions that are complementary (both in shape and in charge), they may stick to each other, forming a protein complex where a multitude of small atomic forces creates a strong bond between individual proteins. They can similarly stick highly selectively to other substances. During a complexation event, a protein may be bent or opened, thereby revealing new interaction surfaces. Through complexation many proteins act as enzymes: they bring together compounds, including other proteins, and greatly facilitate chemical reactions between them without being themselves affected. Proteins may also chemically modify each other by means of phosphorylation, acetylation or methylation by attaching phosphate, acetyl or methyl groups respectively at specific sites. Each such site acts as a Boolean switch (either true-occupied or false-unoccupied): over a dozen of them can be present on a single protein and can influence the functionality of each protein. For example, each phosphorylation may reveal new interaction surfaces, and each surface interaction may expose new phosphorylation sites. The balance between phosphorylation and dephosphorylation of target proteins frequently determines whether cellular responses are transient or sustained.

For easier examination of cellular processes, biochemical pathways can be divided (although they are linked in reality) into metabolic pathways, which contain proteins responsible for material processing (flux) and energy transduction (de Atauri et al., 2005),

gene regulatory networks that includes various transcription factors involved in the control of cellular states and programs (Bolouri and Davidson, 2002; Davidson et al., 2002; Longabaugh et al., 2005), and signal transduction pathways that include information (signal) transmission and processing (Schoeberl et al., 2002). Signal transduction pathways sense changes in the environment, convert these into signals within the cell and ultimately stimulate a response. Overall, the operation machinery of these pathways constitutes the control system that ensures proper function of the cell in the context of the environment (Bray, 1998). All such biological pathways and systems can be described by a measure of robustness, which is a distinct feature of complexity in biology.

1.1.6 Biochemical systems and optimal robustness

Robustness is a term used to describe systems that maintain their state and functions against external and internal perturbations and is an essential feature of biological systems even if the use of this term is not frequently used (Morohashi et al., 2002). Robust systems are both insensitive to alteration of internal parameters and able to adapt to changes in their environment. Optimally robust systems are those that achieve a useful balance between robustness to frequent variations and the concomitant sensitivity to some rare events. Much investigation into robustness in biology has been done on bacterial chemotaxis as a model. Based on their work on bacterial chemotaxis, Carlson and Doyle have proposed that robustness to common variations is achieved in a system at the cost of system complexity; the more the complexity of a system the higher the robustness (Carlson and Doyle, 2000). Robust behaviour has been reported for a variety of biochemical networks (Alon et al., 1999; Yi et al., 2000) and robustness is now widely accepted in metabolism (Fell, 1997), the cell cycle (Borisuk and Tyson, 1998), apoptosis (Dartnell et al., 2005) and inter-cellular signalling (Freeman, 2000). Similarly to engineering systems, properties of biological system robustness and stability are achieved by feedback, redundancy, modularity and structural stability:

Feedback: There are various control schemes found in biological systems. The best example comes from those that take the form of feed-forward and feedback control loops. Both these loops consist of predefined sets of reaction sequences that are triggered by

certain stimuli with the difference that the feed-forward is a one-direction open-loop control while the feedback is a closed-loop that detects the difference between desired output and actual output and compensates for such difference by modulating the input. Whether such modulation is actually enhancing or down-regulating the input signal defined whether the feedback loop is called positive or negative. For good examples of robustness of biological signalling feedback loops see Bhalla and Iyengar (2002) and Alon et al (1999).

Redundancy: Redundancy comes to life by mechanisms whereby multiple components with equivalent functions are introduced and when signal transduction mechanisms have complementary functionality under different conditions. Both can act as backup mechanisms in order to maintain a particular function when damage is induced. A typical example of this comes from the appearance of duplicated genes and genes with similar functions or different pathways that lead in the activation of the same transcription factor (Gu et al., 2003).

Modularity: Network subdivisions are protected by modularity preventing damage from one such module spreading limitlessly to other parts of the network leading eventually to cell functional breakdown. , and also improves ease of evolutionary upgrading of some of the components. Furthermore modules can complement functionality when parts in other modules are failing. Modularity can easily be seen at compartmentalised but interacting signalling pathways (Bruggeman and Kholodenko, 2002).

Structural Stability: Some gene regulatory circuits are built to be stable for a broad range of parameter variations and genetic polymorphisms. Such circuits often incorporate multiple attractors, each of which corresponds to functional state of the circuit; thus its functions are maintained against change in parameters and genetic polymorphisms. Such intrinsic mechanisms are built to promote stability.

Understanding the mechanism behind robustness is particularly important because it provides in-depth understanding on how the system maintains its functional properties against various disturbances. Specifically, we should be able to understand how organisms respond to (1) changes in environment (deprived nutrition level, chemical attractant, exposure to various chemical agents that bind to receptors, temperature) and (2) internal failures (DNA damage, genetic malfunctions in metabolic pathways). Obviously, it is

critically important to understand the intrinsic functions of the system, if we are eventually to find cures for diseases.

Moreover, understanding robustness is necessary since it is not always an advantage as for instance in cancer therapy (Kitano, 2003). Cancer cells are extremely robust for their own growth and survival against various perturbations. They continue to proliferate, driven by the cell cycle, eliminating communication with their external environment, thus becoming insensitive against external perturbations. Generally, investigation into properties of robustness becomes very important for complex cellular phenomena like for example cell morphology changes (organisation of cytoskeleton regulated by physical force and molecular signalling pathways) and cell migration. Understanding the function of such mechanisms requires the consideration and integration of as many as possible mechanisms of adaptation, cellular function and robustness (Kitano, 2004; Stelling et al., 2004).

1.2 Modelling approaches and types of models.

1.2.1 Model detail according to objective of research

In the process of building a model, if the objective is to mimic the behaviour of the system, then maximum detail is needed. Large mathematical systems that build simulations in time and space provide the best if not the only accurate way to reach such an objective (Noble, 2004). If the objective is to only identify general conceptual principles or laws for behaviour of the system, then only minimal detail is needed (or desired). A simple mathematical metaphor can describe such system and succeed in identifying general principles for behaviour of a system (Scholey et al., 2003). Such models are not constrained by need of large sets of detailed data and can benefit from simplification (Figure 1.04). Nevertheless, careful design is still required since a hugely simplified system could suffer from loss in accuracy and predictive power. Finally, if the objective is to develop sufficient understanding to rationally influence the system behaviour, only the crucial detail is needed, neither minimal nor maximal. The key is to decide what to include and what not. Most models used in engineering applications are based on such objective.

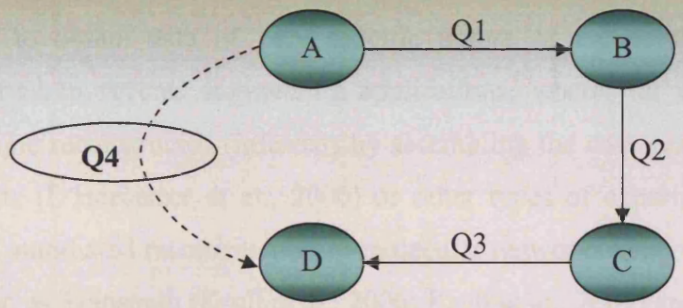

Figure 1.04. Model simplification. A case where equations Q1 to Q3 represent the unidirectional activation reactions of molecules A to D. Assume that each equation contains two parameters X(i) where i=1-6 and $0<X(i)<\infty$. We can create a system of equations to describe the behaviour of the system and activation cascade, as for example: [B]=Q1(X1,X2;[A]), [C]=Q2(X3,X4;[B]), [D]= Q3(X5,X6;[C]).
However we could potentially simplify the system by creating a new equation Q4 where D is function of [A] and two new parameters Z1 and Z6 that produce an equal regulated activation of D in the system of investigation as: [D]=Q4(Z1,Z2;[A]). Such simplification can reduce the complexity of the system by sacrificing information, accuracy and predictive power. Very rarely will a pathway A→ D equal A→ B→ C→ D with any random perturbation of the parameter values. However, simplification can be useful when focus is given only on certain behavioural questions.

1.2.2 Modelling approach based on hypothesis and data perspective

The bottom-up approach is 'data driven' and 'hypothesis neutral'.

The bottom-up approach aims to construct regulatory networks based on the compilation of independent experimental data for the identification of a fully comprehensive set of components and the behaviour arising from such compilation. Biochemical models for example can be built by combining detailed kinetic information about each reaction and they grow by expanding coverage i.e. adding reactions (Figure 1.05).

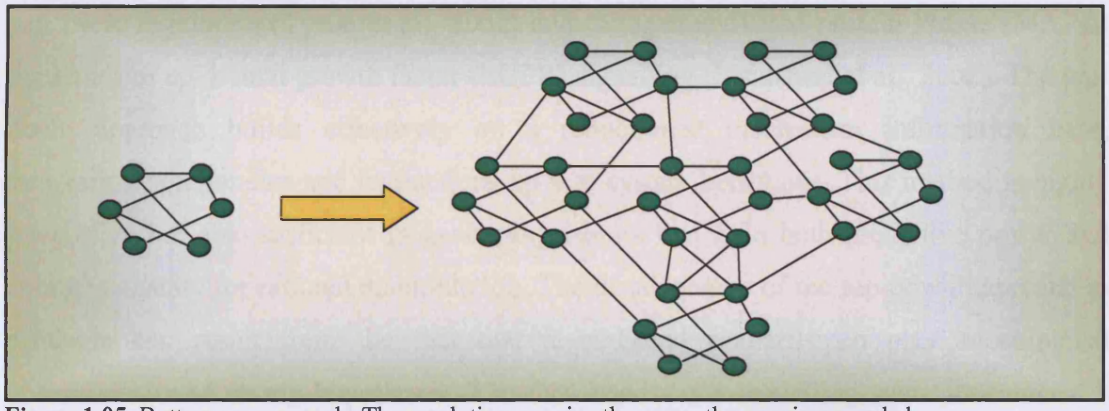

Figure 1.05. Bottom-up approach: The resolution remains the same, the map is expanded.

The bottom-up approach is based mostly on literature searches and some specific experiments to obtain data of very specific nature of the network of interest. It is frequently used in reverse engineering applications, where, for example, a molecular network can be reconstructed (inferred) by assembling the data generated by DNA array measurements (D'Haeseleer et al., 2000) or other types of experiments. Databases that specialise in automated reconstruction of molecular networks using various types of large datasets, such as Transpath (Krull et al., 2006; Krull et al., 2003) and pSTIING (Ng et al., 2006) also present a good example of bottom-up reverse engineering applications. The bottom-up approach is integrative but lacks in generating results of sufficient predictive power. Its biggest drawback is that hypotheses and the objectives of investigation frequently do not exist until after the model (i.e. molecular network) has been constructed. It is clear that the most useful devices are not constructed in the best way by combining related components to see what actions might result. For example, computer software; it

would be not be very effective to put pieces of related software code together and see what functions the program can perform.

The top-down approach is 'behaviour driven' and 'hypothesis central'.

The top-down approach aims to start from observed phenomena to determine the components and interactions required to generate observations. The top-down approach is frequently preferred in construction of biochemical models. Biochemical models can start with unbiased phenomenological information and grow by increasing detail, uncovering hidden variables (Figure 1.06). Well known top-down biochemical models are those of cell cycle regulation (Tyson et al., 2002) and mitogen activated protein kinase (MAPK) dynamics of epidermal growth factor (EGFR) signalling (Schoeberl et al., 2002). The top-down approach builds effectively on a reductionist mechanism information base, integrating components and interactions up into system behaviour. This method is highly integrative but also sufficient in generating results that hold both predictive power and enough capacity for rational manipulation. The disadvantage of the top-down approach in principle can result from the fact that it is based primarily on phenomenological observations and strong hypotheses. The data needed for modelling such phenomena is often not available and an attempt to create comprehensive models might result in masses of required complexity making the examination of a system difficult and impractical.

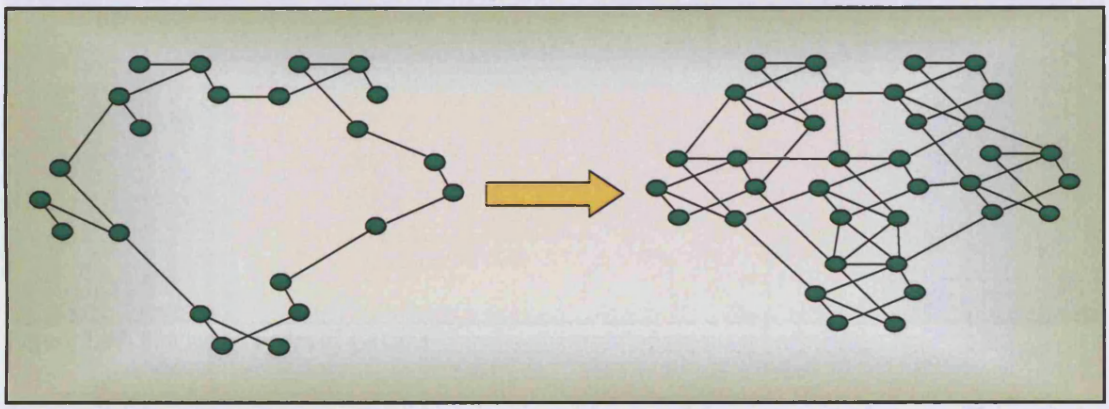

Figure 1.06. Top-down approach: The initial modes and the size of the map remain the same. The resolution of the map is increased.

The middle-out approach is 'behaviour driven', 'hypothesis central' and 'data driven'.

The middle-out approach is also integrative and can be seen as a combination of both bottom-up and top-down approaches (Noble 2005, Novartis_Foundation, 2001). This combination makes it a more flexible method of investigation in principle and usually presets cells as the fundamental operational unit in biological systems (Noble, 2006). Cell biology is modelled in terms of molecular interactions while tissue/organ physiology in terms of cellular mechanisms and their products (e.g. metabolites). The data are collected from both molecular experiments (mechanistic modelling) and system-level observations (phenomenological modelling). A biochemical model can start at any level where data is available provided that is supported by a strong hypothesis and expand both in resolution and coverage (Figure 1.07).

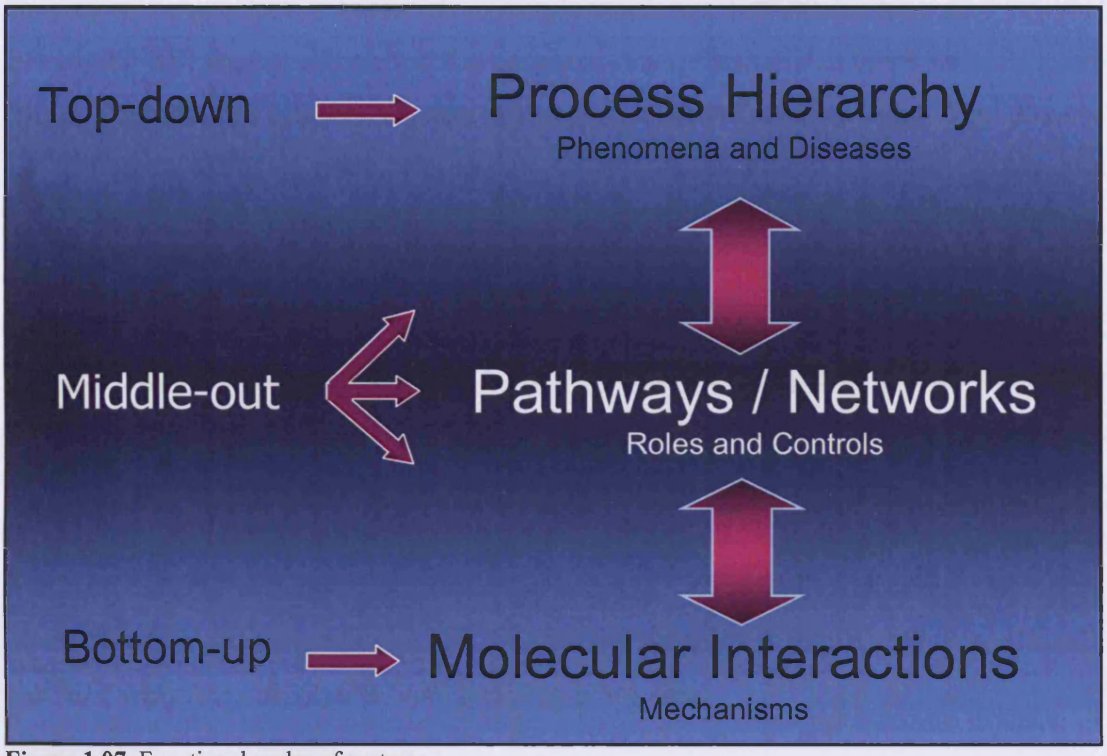

Figure 1.07. Functional scales of systems

With the currently available biological data and techniques of experimental investigation, the middle out approach method is thought to be the most efficient for generating understanding, predictive power and capacity for rational manipulation. A well known example of middle out model approach is the work on the virtual heart project (Noble,

2002; Noble, 2004). This particular project was developed over the past 40 years (Noble, 1960), was expanded in both directions and now models physiological properties of the heart as an organ down to the molecular reactions taking place in its cell. For a review on middle-out and bottom-up approaches see Noble 2004).

1.2.3 Discrimination of models by type of information focus

Descriptive models:

Descriptive models only aim to obtain a brief description of the system, and do not have mechanistic data in detail. These are easier to produce compared to mechanistic ones because they do not require much detailed data in hand and can be less time consuming. For example neural networks, which in simple words are machine learning mathematical techniques that employ algorithms that generate output results from given input data, are frequently used for analysis of data and construction of networks and can produce descriptive models (Hawkins and Boden, 2006). Another way to conceptualise and qualitatively model a system is to use Workflow/Petri net approaches (Hardy and Robillard, 2004; Peleg et al., 2002). The workflow models represent nesting and ordering of processes, the components that participate in the processes and the roles they play. Petri Nets are networks where tokens (i.e. molecules) located in places initiate transitions according to given conditions that result in the generation of new tokens in the output places (Nagasaki et al., 2004). Petri Nets can be used for comparison of data from various sources and allow for verification of formal properties of systems and qualitative simulation (for a review see Hardy and Robillard, 2004). Such approaches are mostly useful for interpolative prediction, and less for extrapolative prediction. They are usually preferred when the quantitative biological data is missing.

Mechanistic models:

If all physico-chemical (molecular, cellular) interactions in time and space are desired, then the model is bound to be mechanistic. Mechanistic models require high detail and their formulation is more difficult due to restrictions from lack of available data. An example of a mechanistic model is the model of the virtual heart (Noble, 2002; Noble,

2004) and the model describing cell cycle as core function regulated by molecular signalling by Tyson et al (2002). Mechanistic models can be created by either top-down, bottom-up of middle-out approaches. Biochemical kinetic models of intracellular signalling are usually created mechanistically in attempt to convey accurate (i.e. realistic) representations and calculate the dynamics of the examined system. For a good review on mechanistic models see (Kholodenko, 2006).

1.2.4 Discrimination of models by type of simulation.

Continuous models:

These are models incorporating any fraction of time, space and/or any other dynamic model parameters. In a continuous state-space, the time-course of a reaction will be a continuous line in a two-dimensional space. This most commonly includes algebraic equations describing general signal transfer and ordinary differential equations (ODEs) based models (e.g. kinetics, steady-state and temporal effects). Examples are the computational models created to analyze the dynamics of the epidermal growth factor receptor signalling pathway (Kholodenko, 2006; Kholodenko et al., 1999; Schoeberl et al., 2002; Shvartsman et al., 2002) or the dynamically regulated stem cell proliferation and self-renewal (Loeffler et al., 1984).

Discrete models:

Discrete models include dynamic values such as time and/or space which occur only in intervals, each model containing a finite number of these values. In a discrete state-space, each variable can take only integer values, so the time-course will be a series of collinear points. Examples include Petri nets as described above and Boolean circuit models (Huang, 1999; Kauffman et al., 2003), governed by activation/deactivation, phosphorylation/ dephosphorylation and on/off states, circuit design and overall regulation of signal flux (Huang, 1999; Somogyi and Sniegoski, 1996). In Boolean approaches the network is represented as a graph of nodes, with directed edges between nodes and a function for each node (Ideker et al., 2000a; Ideker et al., 2000b; Shmulevich et al., 2002a;

Shmulevich et al., 2002b). Application of boolean networks is common way for producing models of genetic regulatory systems (Davidson et al., 2002).

Stochastic models:

Stochastic simulation of biochemical systems is a common technique, typically based on the physically well-characterized Gillespie algorithm (Gillespie, 1977), which originally was devised for reaction-oriented descriptions. Stochastic models include random events which result in different produced outputs from the same original input. These are frequently called "noise effects". In a stochastic model, the state of the system is represented by a set of values with a certain probability distribution, such that the evolution over time is dependent on a series of probabilistic events. Stochastic simulation is particularly effective for systems with a relatively low number of interactions of any given kind, as is frequently the case in cellular-scale systems. It frequently reveals behaviour that is difficult to anticipate, and that may not even correspond to continuous deterministic approximations (McAdams and Arkin, 1999; Szallasi, 1999). One of the well known stochastic models produced is the one investigating bacterial chemotaxis coming from the work of Morton-Firth and Bray (Morton-Firth and Bray, 1998). In their model they apply a unique variant of Gillespie algorithm in order to compute the probabilities of molecular collisions based on individual thermodynamic properties of each molecule (Morton-Firth and Bray, 1998). Similarly, in signalling pathways, stochastic events can be investigated in theory by providing a computation of the probability of molecular interactions from the individual free energy considerations.

Deterministic models:

All models that do not consider stochastic events but assume that every molecule has constantly equal access to any other molecule are deterministic. The state of the system at any moment in time completely specifies the system for all times, which simply means that the rates of molecular reactions are governed by fixed rate laws with constant parameter values through-out the duration of the simulation. It is important however to be aware of the limitations of deterministic models. When the number of molecules involved in a biological process is relatively small, the effects of stochasticity and random collisions could be decisive. The combination of deterministic processes with stochastic

events (such as those controlled by differential thermodynamic properties of proteins) can produce a model accounting for a more complete and realistic description of a biological system's behaviour and would naturally be expected to yield greater predictive power. Nonetheless, this is often impractical since stochastic modelling requires intensive computation. When it is already known or strongly indicated that the stochastic effects in a certain cellular process have minimal contribution to the overall regulation of its dynamics with proportionally non-significant fluctuations, these are often excluded.

Statistical models:

These are models that examine the distributional properties of the data and classify components into separate collections according to their patterns of behaviour. The methods applied in statistical models vary from t-tests, clustering, principal component analysis (PCA) and partial least squares analysis (PLS) which are commonly applied in analysis and classification of DNA array data to sophisticated techniques such as probabilistic Bayesian networks for elucidation of molecular networks based on multi-parameter data (Hwang and Zhang, 2005; Sachs et al., 2005). Bayesian networks combine directed acyclic graphs with a conditional distribution for each random variable (Friedman et al., 2000; Pe'er et al., 2001). They follow *Baye's* rule describing the probability of an event (i.e. interaction) occurring (likelihood) given that another specific event has been preceded. Detailed description of the mathematical formalism for Bayesian networks (as also for Boolean networks, Petri nets, etc) is beyond the scope of this document. For a comprehensive literature review on various modelling and simulation approaches see (de Jong, 2002) and (Neves and Iyengar, 2002).

Temporal models:

These are the models that depend on the computational integration of time as a differential parameter. Temporal models are not concerned with spatial effects and exclude integration of space or any other differential parameters. Most available signalling pathway models in the literature are temporal models.

Spatial models:

Spatial models depend on computational integration of space as a differential parameter in addition to time. Processes such as molecular diffusion and protein translocation are extremely significant since they affect spatial protein concentration gradients that result in different reaction rate dynamics. Moreover one needs to also account for events and phenomena that are also sensitive to external stimuli (such as electrical and mechanical properties of molecules and cell components e.g. molecular or membrane deformation – molecular mechanics). These can also be included in the collection of spatial models; especially if calculation of such phenomena requires use finite difference of finite element methods (Mackerle, 2005). Spatial models are frequently used in fluid mechanics research.

1.2.5 Discrimination of models according to physical scale

Often it is crucial to select an appropriate physical scale for the model where important events are not ignored and at the same time the model is not overly complex. This is based on the belief that individual events occurring at the microscopic scale will not impact on the behaviour of the macroscopic system.

Macroscopic models:

Macroscopic models are concerned with global changes in the system of chemical reactions which is assumed to be of infinite size and homogeneous, so spatial effects are not considered. The majority of deterministic models of biochemical reactions are macroscopic.

Mesoscopic models:

Mesoscopic models are those that lie between macroscopic and microscopic models. The individual nature of the molecule is represented, making the models discrete, but spatial and intramolecular effects are largely ignored, although not always (Reguera et al., 2005). The reaction kinetics may be deterministic or stochastic.

Microscopic models:

Microscopic models contain physical descriptions of force and movement at the intramolecular and intermolecular scale. Due to the complexity of such models, only a very small number of particles can be represented. Three-dimensional molecular models of proteins are typical examples of microscopic models.

1.2.6 Model construction is governed by availability of data

Models can be described as topological, stoichiometric or kinetic based on the available data in hand that can be used to build them.

Topologicals models are created by data that only provide data regarding connectivity. These are the most frequent and usually the first to build before proceeding to a more detailed model. Graph theory is usually the key player in designing these models as their quality is assessed based on the quality and connectivity of the graphs. Topological network models can either be characterised as exponential or scale-free (Figure 1.08). Exponential networks have all their substrates more or less equally connected, each one involved in a certain amount of reactions (Figure 1.08). Therefore the addition of a new substrate results in an exponential increment in the total number of reactions. Scale-free networks have most of their substrates involved in very few reactions and few substrates involved in a large number of reactions. Therefore an addition of a new substrate might results on only a single new reaction.

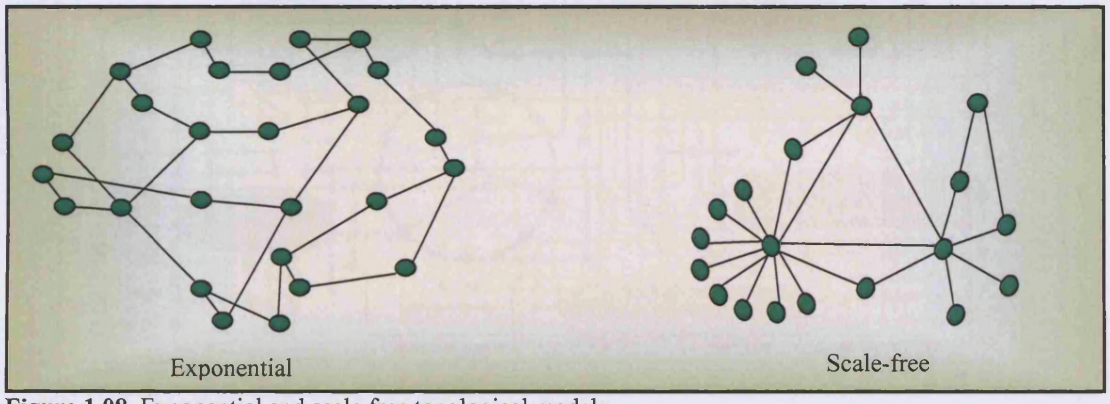

Figure 1.08. Exponential and scale free topological models.

Practically, whether the topological model is exponential or scale free depends exclusively on the interaction data available used to create the models. This data however, often reveals unique properties of certain networks that are structured specifically either for purposes of fast signal transition or as back-up/fail-safe networks that add to overall robustness. Databases that use interaction data in order to automatically generate topology based interaction networks use graph theory. A good example of a topological model is the one shown in Figure 1.09 created by Jeong et al (Jeong et al., 2000).

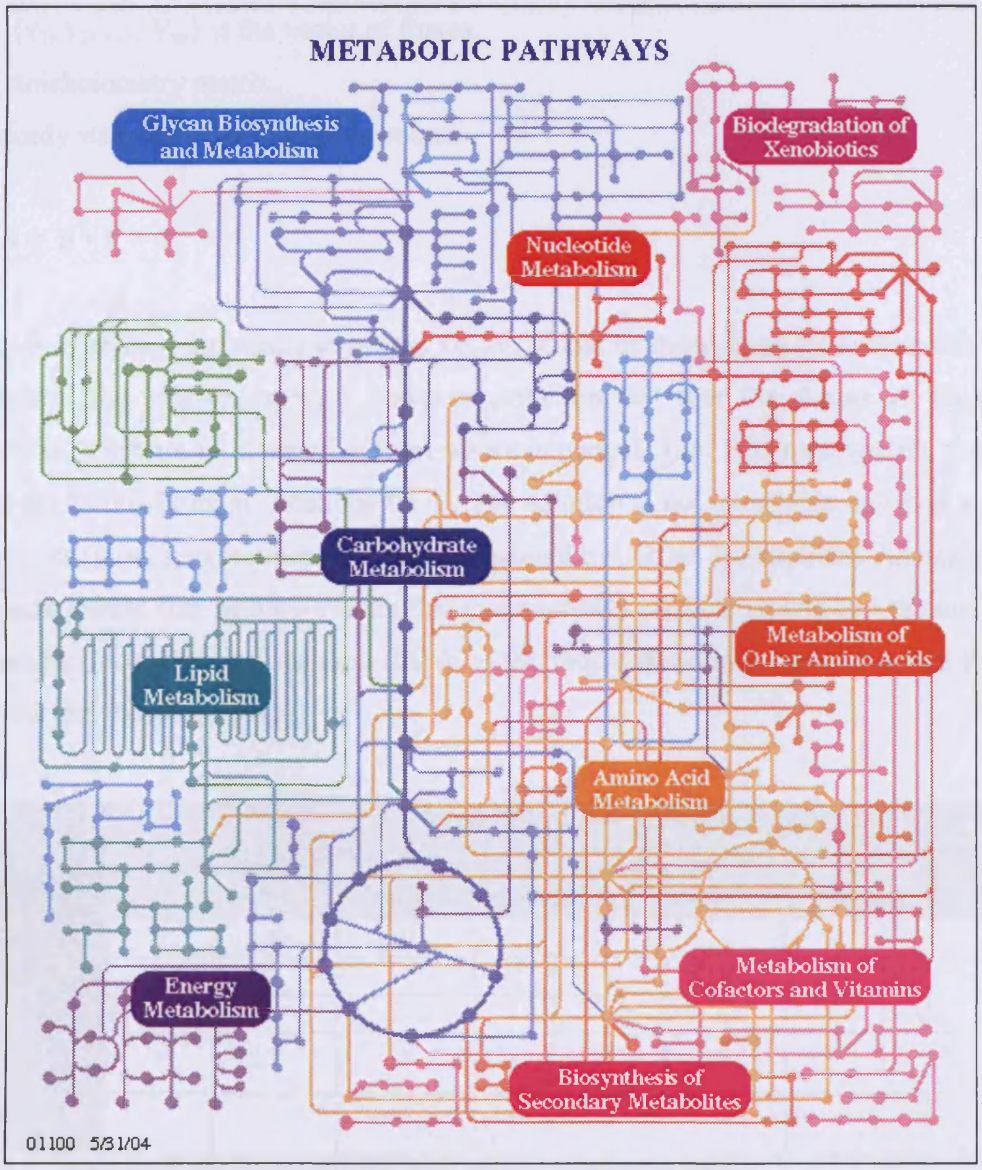

Figure 1.09. Metabolic networks (Jeong et al., 2000).

If more details regarding the reactions are known such as the stoichiometric properties then these can be used to write rate laws, and a stoichiometric model can be build. When the stoichiometry of the reaction network is known, a mass balance for the components can be written in the form:

$dX/dt = S \bullet V$, where:

$X = \{x_1, x_2, \ldots. X_n,\}$ is the vector of components,

$V = \{v_1, v_2, \ldots. V_n,\}$ is the vector of fluxes,

S = stoichoiometry matrix.

At steady state the mass balance becomes

$dX/dt = S \bullet V = 0.$

Since S is known, the steady state flux vector, v, can be determined by solving this linear equation. The problem appears however from the fact that for almost all biological networks, there are more reaction rates than components (i.e., S is rectangular), therefore there are infinitely many solutions for V. The solution is not intractable however and can be solved by using experimental data accompanied by certain assumptions. An example of a stoichiometric flux balance system that quantitatively predicts growth and the metabolic by-product excretion in wild type E.Coli is the model developed by Varma and Palsson (Varma and Palsson, 1994).

Level of output and input detail	Modelling Techniques								
	Kinetic (ODEs)	Stoichoio metric	Molecular Mechanics	Petri Nets	Boolean Nets	Bayesian Nets	Neural Nets	PCA PLS	PDEs
Mechanisms	√	√	√		-	-	-	-	√
Influences	-	-	-	√	√	√	√	-	-
Relationships	-	-	-	-	-	√	√	√	
High detail (specified)	√	√	√	-	-	-	-	-	√
Lower detail (abstracted)	-	-	-	√	√	√	√	√	-

Table 1.1. Input detail and generated output from various modelling techniques.

Finally if explicit values are known for the reaction laws of the interactions then a dynamic kinetic model can be formulated (Ozbudak et al., 2004). These models will be discussed in greater detail in later chapters. Table 1.1 shows the level of input detail required for each modelling application and the nature of biological output generated.

1.2.7 Applying modularity in modelling signalling pathways

Much debate in modelling signalling pathways is generated around application of modularity for both the construction and the examination of molecular systems. As described in section 1.1.6, molecular networks need to be highly complex (robustness achieved at cost of complexity) and employ surrounding control loops to ensure the tight and robust regulation of even simple operations (e.g. glucose metabolism in E.coli) (Edwards and Palsson, 2000).. The implication is that these networks and pathways may be modelled in terms of such operation modules, where dynamic properties of the module models are governed by parameters that depend on the physico-chemical properties of regulatory molecular interactions (Bruggeman and Kholodenko, 2002; Bruggeman et al., 2002). Generally, there are no defined laws as to how a network can be divided into regulatory modules and how many components a module should embrace. Such decisions are often intuitive and are subject to the depth of understanding of the network. Empirically however, there some direction that can aid in the definition of modules when the system under investigation is large. For example, a module can be defined as:

a) An independent part of a model involving both feed forward and feedback loops, as for example the MAPK pathway (Wolkenhauer et al., 2005).
b) A model part that can be examined in isolation with a certain input and output, when its intermediated components do not influence and are not influenced by other modules. Although this is thought to be the case in the cell, in terms of modelling it is always an assumption, since we do not possess all knowledge regarding cellular signalling to date in order to confidently argue that intermediated components of a given pathway do not interact with any other components of intracellular signalling.
c) A network pathway that is redundant in function with another. This is also possible in the cell (especially in signalling pathways leading to activation of transcription

factors) and is believed to be a cellular mechanism that provides robustness to external or internal variations and signal knockouts, however it is not a interesting area of research in biology (i.e. focus is given on identifying novel components or novel functions and not components of redundant function) and not much knowledge is available to allow for modules to be constructed based on their redundancy.

d) A distinct pathway that needs to be separated as a module due to its size and biological importance as for example the nuclear factor kappa beta (NF-kB) pathway (Hoffmann et al., 2002).

In principle, even if the system examined is very small, it can still be modelled in a modular way. Each pair of molecules could be modelled as a separate module provided such decision agrees with the cases above. However, in practise this is often unnecessary since the dynamics of very small systems can be observed, analysed and understood easily. Modules are defined as independent building blocks of a network when systems are extremely large and cannot be sufficiently modelled on the individual function of certain molecules. Thus, modular design arises as a need for functional value/use hierarchy and is achieved as described above.

1.2.8 Modelling molecular pathways

There has been much interest in the literature regarding the methodology (Figure 1.10) for either qualitative and/or quantitative hypothesis testing in biological pathways using models. It is well accepted that the choice of the pathway and system to be examined is possibly the most important part of the process. If the functionalities of and components of the pathway are well known, the process might yield interesting results, however availability of knowledge and data are frequently the limiting factors in creating a comprehensive model. A model should not be expected to be perfectly accurate. A model aims to complement experimental research with certain investigative facilities that can be obtained through simulation allowing questions to be addressed such as:

- Which are the components that impair the system's functionality when missing?
- What are the gaps in the current knowledge of a biological pathway?

- Does the model identify any novel molecular interactions?
- Which molecules control and balance the system most and which pathway modules are more robust or sensitive to changes?
- Could the system be influenced by addition of chemical compounds and what are the side effects?

Answering these questions will aid in the identification of targets and the design of better drugs for treating human diseases.

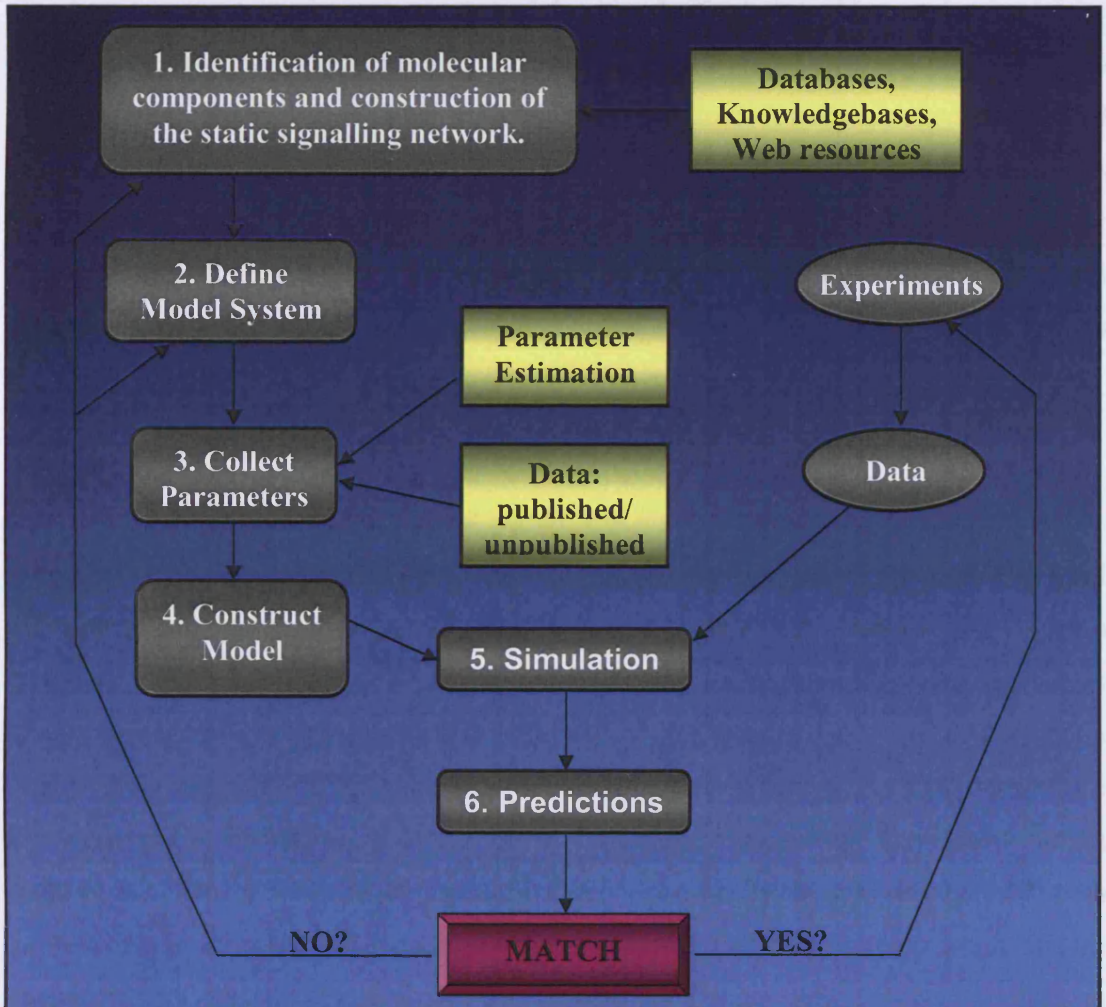

Figure 1.10. Network reconstruction and mathematical modelling. The numbers indicate the order of steps carried out. The process is completed through a series of successive steps. Steps 1 and 2 Parameter estimation takes place using data fitting analysis software employing well known algorithms (e.g. least squares fitting). Note that the data used to construct the network and match the predictions of the model must be different. Very often, the model can not possibly match experimental data at initial stages therefore both biological knowledge and an element of intuition are proved to be necessary in the model building and refining process.

1.3 The Shear Stress Response in Endothelial Cells

The environment of a cell may impinge on it in many ways. Different kinds of molecules, such as mitogens, growth factors and cytokines may bind to transmembrane receptors initiating signalling cascades or even the cell surface may be stretched or sheared. Frequently certain cells respond to such extracellular stimuli with significant changes in their shape and morphology. Endothelial cells (ECs) are known to have such responses. They can be stimulated by various molecules of the extracellular matrix (ECM) but are also very sensitive to shear stress caused by blood circulation. The mechanism(s) by which shear stress is converted from a mechanical stimulus to a biochemical response has not been fully understood yet. However their sensitivity to both molecular and mechanical influences allows them to uphold many important physiological functions, such as maintaining anticoagulant properties, controlling lumen diameter and regulating vascular permeability. Pathologically, they are involved in acute inflammation, wound healing and cardiovascular disorders such as the development of atherosclerosis (Davies, 1995; Davies et al., 1995).

1.3.1 Properties of blood fluid, blood vessels and shear stress

Blood is the cell-containing fluid that circulates through the body carrying vital components and oxygen to tissues and organs and carrying waste matter away. Its main components include red cells, platelets, white cells and plasma. Its fluid properties, such as density (measure of mass per unit of volume) and viscosity (measure of the resistance of a fluid to deformation under shear stress), play a major role in developing shear stresses on the endothelium. Blood is a non-Newtonian fluid which means that its viscosity is not constant but changes with the applied shear force. Specifically, its viscosity depends both on the volume of packed red blood cells in the specimen (what is clinically known as the hematocrit) and the rate of shear. This property makes blood a very complex and difficult fluid to study in fluid mechanics (the discipline that studies fluids, liquids and gasses). Such studies however have allowed researchers to investigate the relationship of the anatomical structure and the dynamic forces in the blood (Kamm, 2002). For basic fluid mechanics models blood is treated as a homogeneous Newtonian fluid in order to avoid

complexity and is given a constant viscosity 0.04 Poise (1 Poise = 0.1 Pa s = 0.1 N-s/m^2) and kinematic viscosity (ratio of viscosity to density) of 4 mm^2/sec (Ku, 1997).

Blood vessels have a simple layered architecture with cylindrical symmetry (Figure 1.11). Arteries and veins are composed of three major tissue layers (Figure 1.12), the tunica intima (or tunica interna), the tunica media and the tunica adventitia (or tunica externa). The tunica intima is the innermost layer of arteries and veins. In arteries this layer consists of a monolayer of endothelial cells adhered to a self-assembled extracellular matrix, and an internal elastic lamina that separates the intima from the central layer. Veins do not contain the internal elastic lamina that is found in arteries however. The tunica media is the middle layer of the walls of arteries and veins and is composed of elastic smooth muscle cells, elastic lamina, elastic fibrils, and bundles of collagen fibres. The tunica adventitia is the strong outer covering and is composed of elastic and collagen fibres covered or intermingled with fibroblasts, smooth muscle cells, and nutrient vessels and nerves.

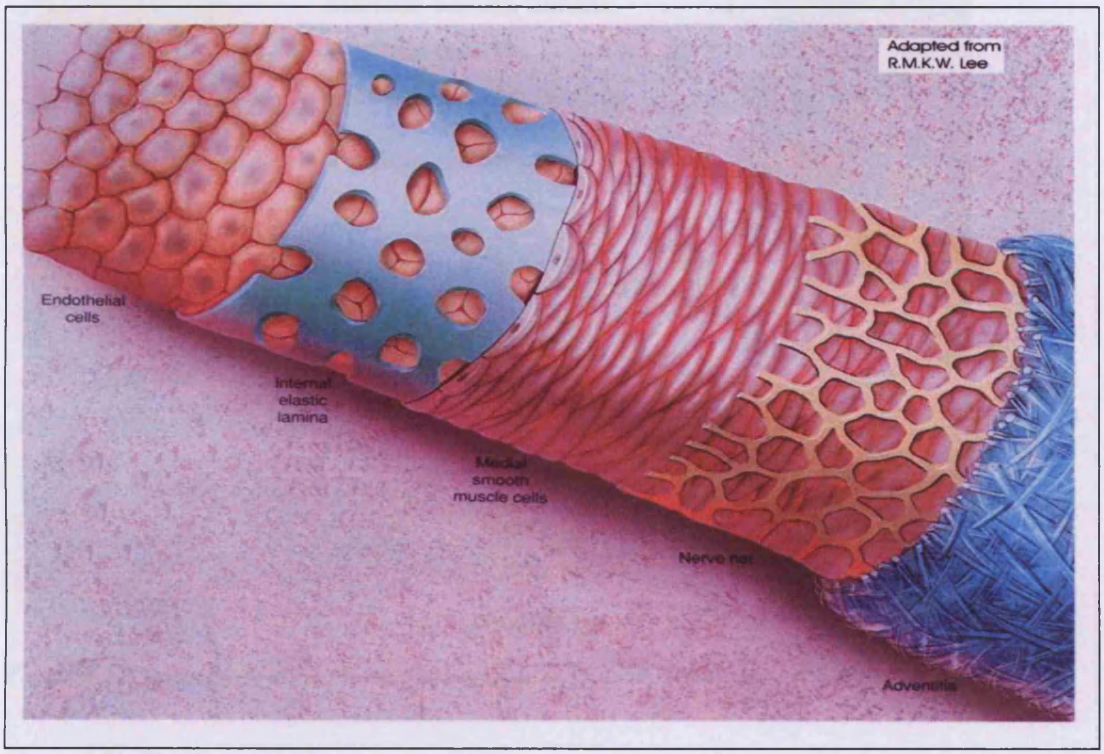

Figure 1.11. Blood vessel architecture (Lee, 1989).

Arteries have generally thicker walls compared to veins and carry the blood away from the heart (Figure 1.12). They get smaller as they progress further away from the heart until the become arterioles which are smaller in diameter and closer to the target organs. The arterioles in turn, branch into even smaller vessels called capillaries (Figure 1.12). Capillaries do not contain smooth muscle cells and so cannot selectively constrict or dilate like arteries or veins. Veins on the other hand have thinner walls and carry the blood to the heart. Some veins have one way flap valves (venous valves) that prevent the backflow of blood caused by the force of gravity. These valves are needed as the venous blood pressure is considerably lower than the arterial blood pressure. Veins run between skeletal muscle fibres and as the fibres contract (skeletal muscle action), blood is forced through the venous valves (Figure 1.12).

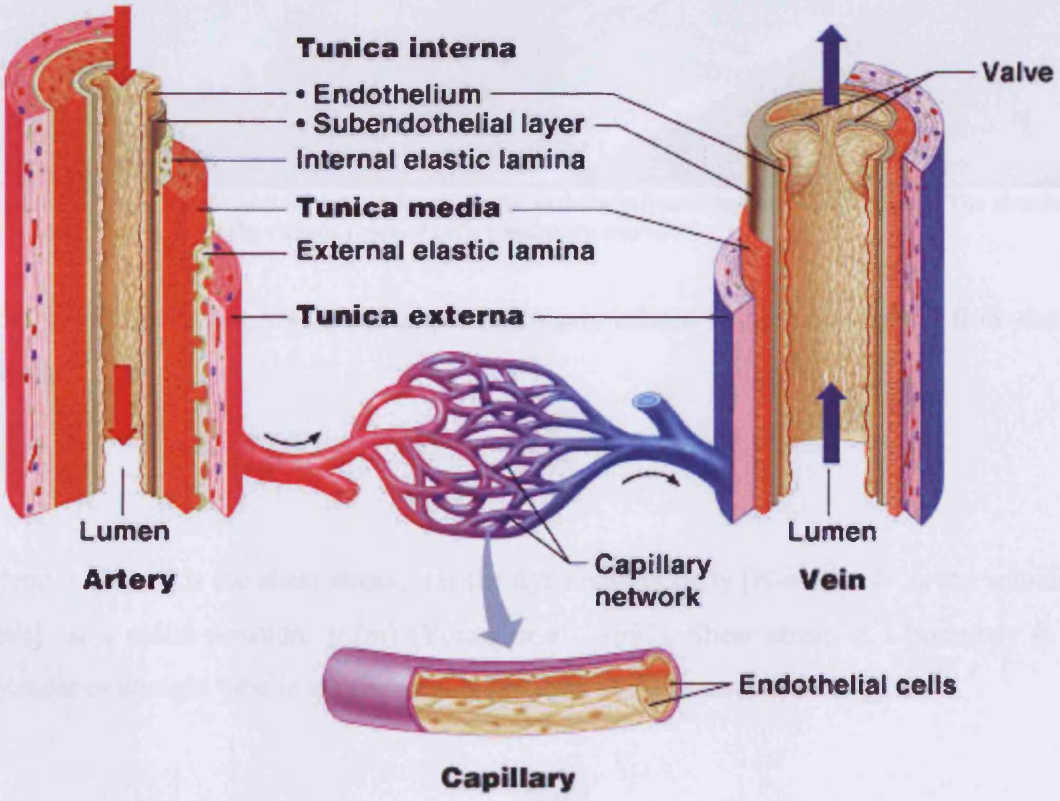

Figure 1.12. Diversity of arteries, veins and capillaries (Marieb, 2004).

The forces created in the blood vessels due to the bulk flow of blood are called haemodynamic and can be resolved into two principal forces: pressure and shear stress (Figure 1.13) Pressure acts perpendicular to the vessels and imposes circumferential

deformation on blood vessels. Shear stress is the frictional force acting at the interface between the circulating blood and the endothelium of the vessel wall and regulates cellular function via mechanical activation of signal transduction pathways.

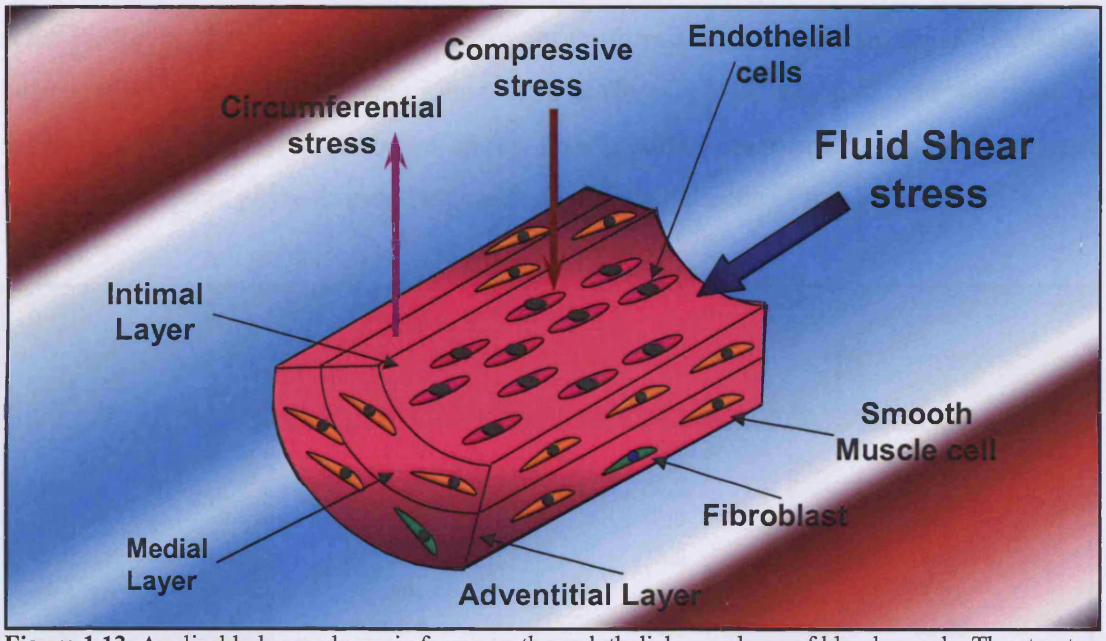

Figure 1.13. Applicable haemodynamic forces on the endothelial monolayer of blood vessels. The structure of the blood vessels and the various types of cells present are shown.

For Newtonian fluids, wall shear stress is linearly related to the rate of fluid flow shear (dU/dy),

$$\tau = \mu \frac{dU}{dy}$$

where τ [N/m^2] is the shear stress, μ is the dynamic viscosity [N-s/m^2], U is the velocity [m/s] at a radial position y [m] (Young et al., 1997). Shear stress at a boundary in a cylinder or straight tube is expressed as a function of the measured flow Q,

$$\tau_{\text{wall}} = \frac{32\mu Q}{\pi D^2}$$

where μ is the fluid viscosity and D the diameter of the cylinder. This expression is a reasonable estimate of the mean wall shear stress in arteries although it becomes less accurate for pipes/cylinders of very small diameter (Ku, 1997).

Wall shear stress has considerable clinical relevance because it provides information about both the magnitude of the force that the blood exerts on the vessel wall as well as the force exerted by one fluid layer on another. In healthy blood vessels the shear stress is generally low (~5-20 dynes/cm^2, where 1 dyne/cm$_2$ = 0.1 N/m^2) and it is not harmful to endothelial cells. However, the shear stress levels are not uniform between different types of vessels. Differences in vessel diameter, along with differences in structure and function of different types of vessels as shown above, greatly affect the average wall shear stresses and the subsequent physiological responses of endothelial cells (Table 1.2).

Blood vessel geometry and shear stress			
Vessel Type	**Average Diameter (cm)**	**Average Velocity (cm/s)**	**Average Wall Shear Stress (dynes/cm^2)**
Pulmonary artery	2.70	18.0	2.13
Aorta	2.50	35.0	4.48
Carotid artery	0.80	16.0	6.48
Celiac artery	0.58	12.0	6.62
Femoral artery	0.61	14.0	7.34
Small artery	0.10	10.0	32.00
Small vein	0.08	2.7	10.80
Large vein	0.55	9.0	5.24
Vena cena	3.00	28.0	3.00

Table 1.2. Relationship between blood vessel geometry and wall shear stress (Lelkes and Samet, 1999).

1.3.2 Properties of blood flow

In addition to different types of blood vessels, physiologically different types of blood flow conditions have important effects on the biology of the endothelium. Blood flow in the circulatory system is invariably unsteady and in many regions it displays a periodic behaviour and a net directional motion throughout the cycle. This type of flow is called pulsatile. If the flow has a periodic behaviour and oscillates back and forth without a net forward or reverse output then it is called oscillatory flow.

Several dimensionless quantities (pure numbers without any physical units used commonly in mathematics and physics) have been developed to relate the flow conditions in one system to those in another (e.g. fluid conditions in vascular tissue to fluid conditions in a mechanical pipe) where conditions of flow might differ. These relationships represent the degree of similitude between two systems, and allow

predictions of the velocity profiles in flow systems. The most well known dimensionless quantities are the Reynolds (Rott, 1990) and Womersley numbers that describe steady straight pipe flow, and pulsatile flow respectively (Wood, 1999).

The Reynolds number (R_e) represents the ratio of inertial forces to viscous forces and predicts the transition between steady laminar and steady turbulent flow. When viscous forces dominate (i.e. molecules remain in close proximity to their neighbours), the flow is called laminar and is characterised by a smooth motion of the fluid. Laminar flow can be thought of as if the fluid is divided into a number of layers flowing parallel to each other without any disturbances or mixing between the layers. On the other hand, when inertia forces dominate the flow is called turbulent. In turbulent flow the fluid exhibits a disturbed, random motion which is superimposed on its repeatable, main motion. In pipe flow, the Reynolds number is given by:

$$R_e = \frac{\rho UD}{\mu} = \frac{Inertial forces}{Viscous forces}$$

where ρ is the fluid's density [kg/m^3], μ is the dynamic viscosity [kg/m·s], U is the flow velocity [m/s] and D is the pipe diameter [m]. It has been determined experimentally that in a smooth-surfaced tube, flow is laminar for $R_e < 2100$ and the flow streams are smooth and straight, as the layers of liquid smoothly slide over one another (Young et al., 1997). In contrast, when $R_e > 2100$, the flow starts to become turbulent (fully developed turbulent flow is observed at $Re = 10_4$) and the motion of the liquid particles transitions from orderly to vortical and chaotic (Young et al., 1997). In the cardiovascular system, Reynolds numbers range from 10^{-2} for microcirculation up to 12,000 in the aorta. In straight veins and arteries however, it is typically well below 2000 (Lelkes and Samet, 1999).

When pressure and velocity profiles of the flow vary periodically (Period = duration of cardiac cycle [s]) with time however, therefore exhibiting the behaviour of a pulsatile flow, the Reynolds number cannot predict accurately the transition between laminar and turbulent flows. Apart from pressure distribution and the velocity profile in vessels, the

nature of the pulsatile flow also affects the point of transition from a laminar to a turbulent regime. Flow in the vessels don't become turbulent as soon or to the degree expected based on instantaneous Reynolds number values simply because there is not sufficient time provided for flow to become turbulent. For a fully developed turbulence state of flow to establish, some initial disturbance to the flow at some site must propagate throughout the entire flow field and usually the physiologic frequency of cardiac pulse does not provide the amount of time required for this to happen and the conditions of flow change constantly. This is why in healthy vessel turbulence is mostly absent and the flow exhibits vortex and "turbulent-like" behaviour at regions like bifurcations or branches. Pulsatile flow is described by the Womersley dimensionless number which both characterises the periodic nature of blood flow and provides a comparison between unsteady inertial forces and viscous forces and is given by:

$$\alpha = \frac{D}{2}\sqrt{\frac{\rho\omega}{\mu}} = \frac{Unsteady Inertial forces}{Viscous forces}$$

where ω [radians/sec] is the heart rate. In the human circulatory system α usually ranges from 10^{-3} in capillaries to 18.0 in the ascending aorta (largest artery in body) at rest. When $\alpha < 1.0$, viscous forces dominate in every region of the tube. If α starts to increase the inertial forces become more important and start to dominate, initially at the centre of the tube.

1.3.3 Atherosclerosis

Atherosclerosis comes from the Greek words *athero* (meaning gruel or paste) and *sclerosis* (hardness). It is the name of the process in which deposits of fatty substances, cholesterol, cellular waste products, calcium and other substances build up in the innermost layer (anatomy of artery shown in Figure 1.12) of blood vessels (Libby, 2003). This build-up is called atherotic plaque or atheroma. The growth of plaques results in the narrowing of the lumen, reducing the flow of blood to tissues supplied by the artery. Continuous advancement of the plaque size over time reaches a stage where the plaque becomes fragile and unstable and is very likely to rupture. Plaques that rupture cause

blood clots to form that can block blood flow or break off and migrate through the bloodstream, eventually generating an embolism at a distant site causing either a stroke or a heart attack. Atherosclerosis is one of the leading causes of mortality worldwide. Figure 1.14 illustrates the development of atherosclerosis from initial to advanced stages.

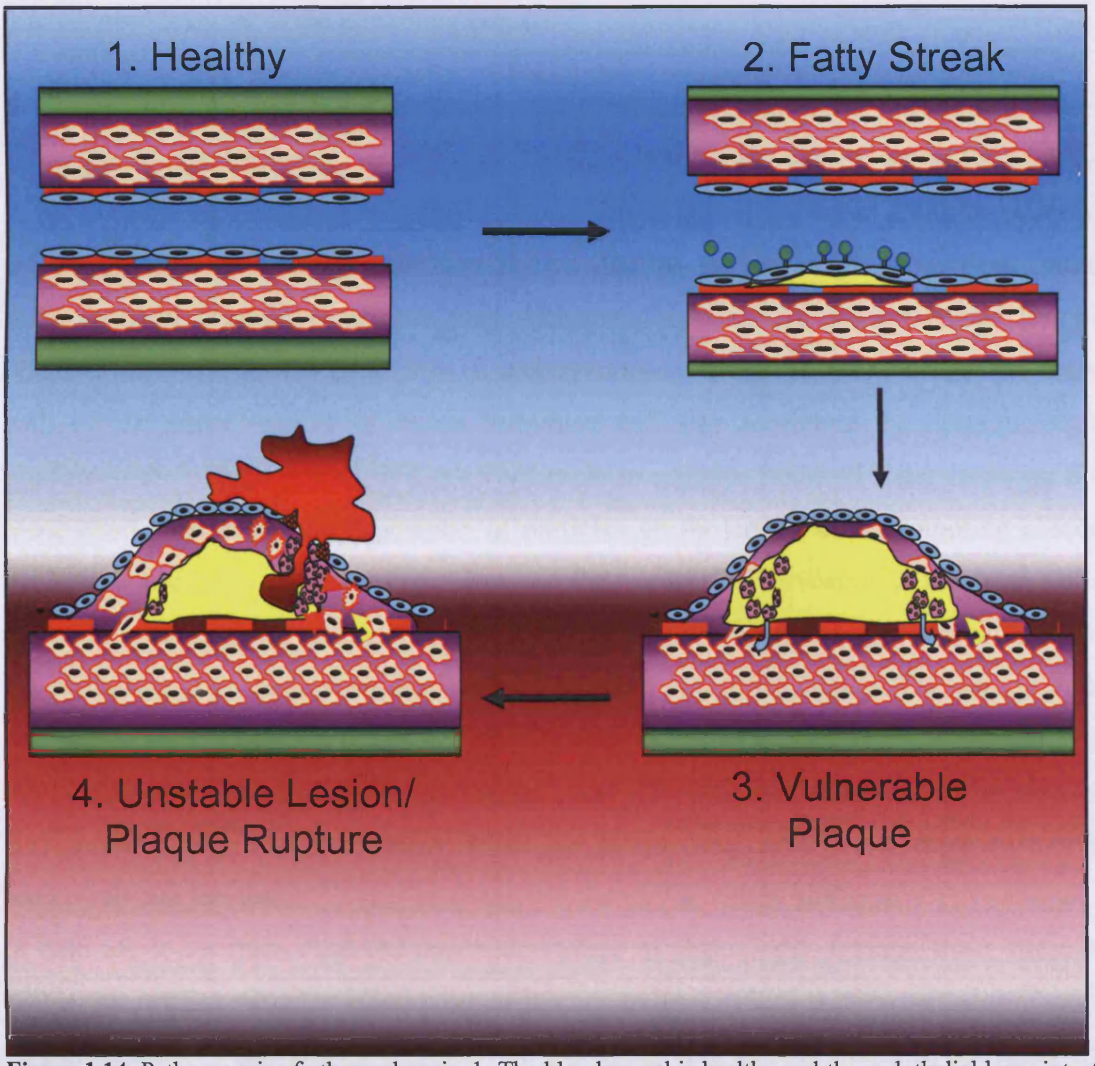

Figure 1.14. Pathogenesis of atherosclerosis. 1. The blood vessel is healthy and the endothelial layer intact. 2. Early stage of atheroma called fatty streak. Fatty streaks appear as irregular yellow discoloration near the luminal surface of the artery. 3. Further rapid growth of the atheroma that has a thin cover separating it from the bloodstream inside the arterial lumen. Tearing of the cover leads to plaque rupture. 4. Plaque rupture is depicted. Upon rupture, tissue debris spill into the blood stream resulting in severe obstruction of blood supply while that plaque becomes highly unstable and may suddenly increase in size. Blood clotting (thrombosis) on top of the site of the ruptured plaque forms and expands.

Although the pathobiology of atherosclerosis is a highly complex multifactorial process, blood flow-induced shear stress has emerged as an essential feature for atherogenesis

(development of atheroma). The fluid drag force acting on the vessel wall is mechanotransduced into a biochemical signal that results in changes in vascular behaviour. All theories on the pathogenesis of the atherotic plaques share that shear stress fluctuations play a major role as an initiating event; primarily by inducing endothelial damage, followed by a localised inflammatory response which results in the well observed microscopic features of the atherotic plaque.

Within the vascular tree, there are gradients of shear stress that typically occur near vessel bifurcations and branches, in regions of arterial narrowing and in areas of extreme curvature such as the carotid bulb (bifurcation point of the carotid artery along the sides of the neck). Clinical investigations have shown that the regions of disturbed flow (rapid shear stress fluctuations) correlate well with the distribution of atherosclerotic lesions (Caro et al., 1971; Zarins et al., 1983). Increased shear stress can both damage the inner wall of the artery leading to lesion formation and also accelerate the destabilization process of the plaque making it more vulnerable to rupture. Reduced shear stress on the other hand encourages the deposition of particles on the artery wall, promoting plaque growth. In situations of flow reversal (reverse flow occurring transiently at the outer walls of the bifurcation point of an artery due to unsteadiness/oscillations of flow), changes in the endothelium promote thrombosis (formation of a clot or thrombus). The carotid bulb provides a good example, where the medial wall experiences high shear stress and the lateral wall experiences recirculation vortexes that vary with the cardiac cycle, resulting in flow reversal and low mean shear stress: the lateral wall usually has more extensive atherosclerotic lesions.

In contrast, it has been observed that maintenance of physiologic, laminar shear stress is crucial for normal vascular functioning as it tends to have effects that are anti-thrombotic, anti-inflammatory and growth inhibitory to the underlying smooth muscles, activated via signal transduction mechanisms. Thus, shear stress is critically important in regulating both the atheroprotective, normal physiology as well the pathobiology and dysfunction of the vessel wall though complex molecular mechanisms that result in atherogenesis.

1.3.4 Experimental setup for in vitro study of shear stress

Parallel plate flow chambers (Figure 1.15) are used as models for long, straight blood vessels devoid of curves or branches. Parallel plates exhibit a one dimensional flow whose transverse velocity is uniform across the entire width of the chamber. Typically, the surface area of the plates is much greater than the distance between the plates so that they can be regarded as infinite in comparison. The parallel-plate flow chamber is used for flow stimulation of various cell types, e.g., bone cells and endothelial cells (Brown, 2000). Cells are attached to one of the internal plate surfaces. The plates are then inserted into the flow chamber and subjected to fluid flow by creating a pressure gradient across the chamber (Figure 1.15). To calculate the resulting shear stress on the cells, the mathematical model assumes a Newtonian fluid in which the shear tensor (matrix of all shear forces in all directions) is proportional to the deformation tensor (deformation of the material in all directions).

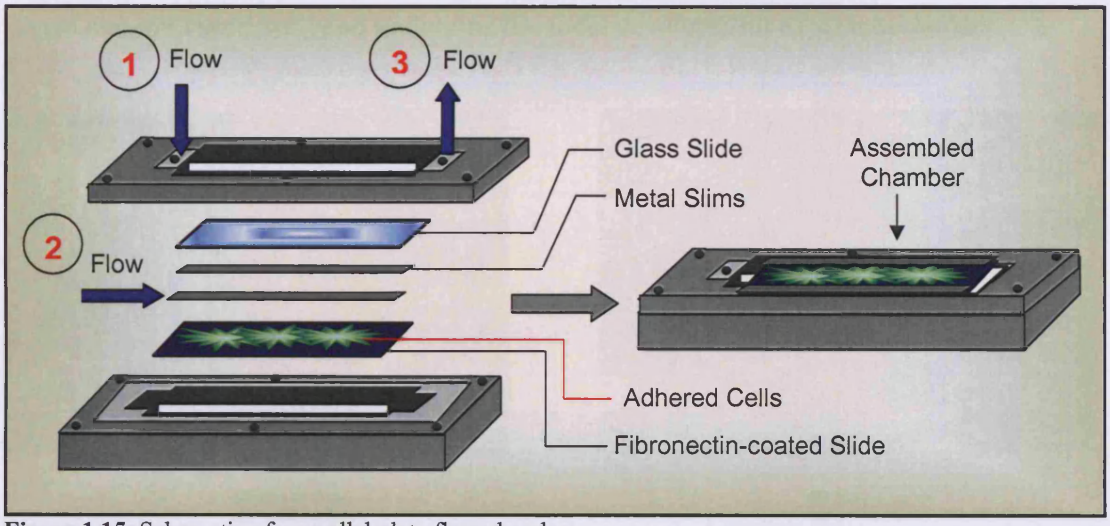

Figure 1.15: Schematic of a parallel plate flow chamber.

The flow profile in a parallel plate chamber is typically parabolic, and for steady flow between infinitely wide parallel plates, the wall shear stress is calculated as a function of the measured flow Q (perfusion rate):

$$\tau_{\text{wall}} = \frac{6Q\mu}{bh^2}$$

where μ is the fluid viscosity, b is the width of the chamber and h is the distance between plates. For finite chamber dimensions (finite b/h), the fluid velocity profile remains parabolic between the plates, but vanishes at the boundaries of the rectangular channel (Belansky and Wanser, 1993; Booij et al., 1995). The shear stress profile, calculated from the velocity gradient, has maximum magnitudes at the plate surfaces and vanishes at the corners of the channel (Schlichting, 1968).

1.3.5 Endothelial Responses to shear stress

It has been long known that blood flow is a determining factor for the axial (i.e. parallel to the direction of blood flow) organization of endothelial cell morphology that endothelial cells respond to their fluid-dynamic environment (Davies, 1995; Dewey et al., 1981; Flaherty et al., 1972; Nerem et al., 1981; Silkworth et al., 1975), indicating that these cells posses an intrinsic mechanism for sensing fluid flow (Figure 1.16). The endothelial monolayer acts as a signal transduction interface *in vivo* between forces from flowing blood and the vessel wall and underpins the focal development of atherosclerosis.

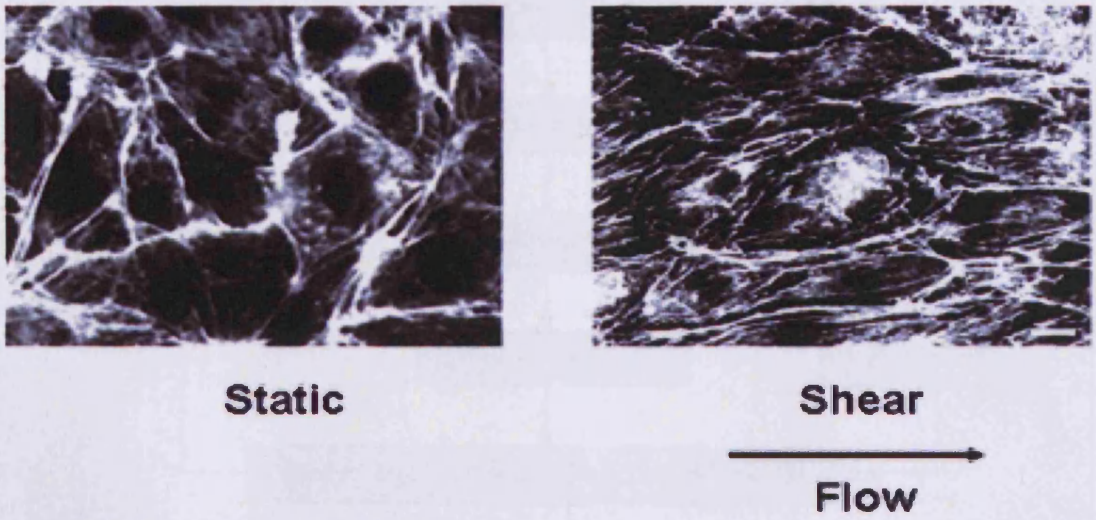

Figure 1.16. EC cells stained with rhodamine-phalloidin and observed by confocal microscopy. Left = cells in vitro under no flow conditions. Right = in vitro effects of flow, cells elongated and aligned with the direction of the flow (Tzima, 2006).

The means by which endothelial cells convert shear stress stimulation into biochemical signals have been studied intensively over the past two decades. Shear stress is exerted on the membrane of the endothelium, and is transferred from there to all structural components of the cells (Ali and Schumacker, 2002). Hypothesized mechanisms of fluid

flow-induced signal mechanosensing include: local displacement of receptors at the luminal surface (caused by asymmetries in the transbilayer pressure profile), force transduction through focal adhesion sites, force transmission through the cytoskeleton, activation of mechano-sensitive ion channels, and flow-mediated ligand delivery to receptor sites. Following the initial mechanosensing, ion influxes, downstream intracellular signalling pathways and expression of endothelial genes, all take place to modulate shear-induced biochemical function as well as shear-induced alterations in endothelial cell morphology (Figure 1.17). Integrins, G protein coupled receptors (GPCRs), receptor tyrosine kinases (RTKs) and Ca^{2+} and K^{+} ion channels are primary key players of these processes.

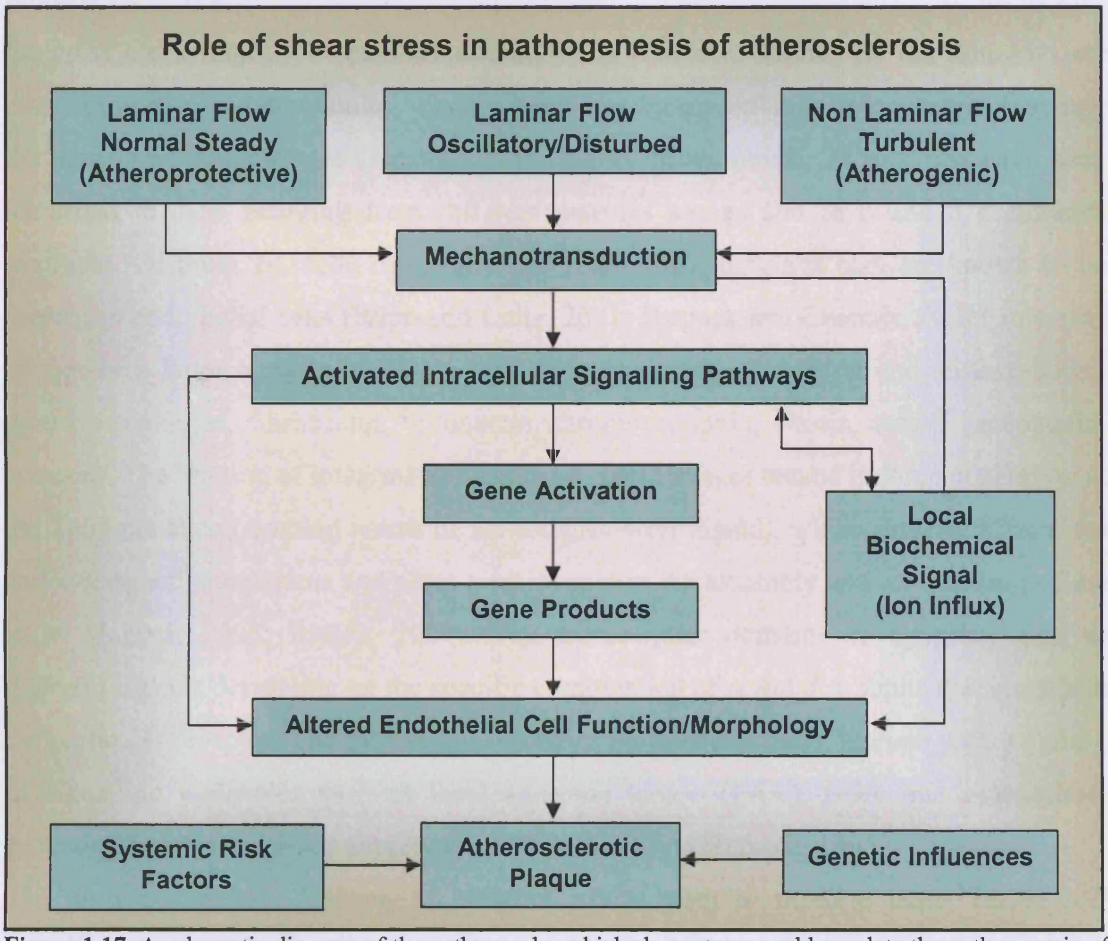

Figure 1.17. A schematic diagram of the pathways by which shear stress could regulate the pathogenesis of atherosclerosis (Cunningham and Gotlieb, 2005). The pathogenesis of the atherosclerotic plaque is modulated by shear stress regulation of atheroprotective and atherogenic influences, by systemic risk factors (diet, smoking, hypertension, etc) and by genetic influences (e.g. heritability, gene defects, Doherty et al., 2004; Scott, 2004) that affect both multiple cellular processes in the wall and the plaque as well as the response of the vessel wall to shear stress itself.

1.3.6 Molecular Mechanosensors

Fluid mechanical shear stress elicits a wide range of metabolic and structural responses in vascular endothelial cells which have been well documented (Helminger et al, 1991; Nerem et al, 1981; Davies 1995; Barakat and Davies 1998) and the nature of these responses depends on the specific form of the imposed shear stress (Helminger et al., 1991; Helminger et al., 1996). However, it is unknown how the cells are able to sense shear stress and how shear stress signalling is transmitted from the cell membrane to the cytoskeleton. Investigation of the molecular shear stress response over the years revealed selective influence of mechanical force on the activity of specific molecules.

Integrin receptors

Integrins are a family of heterodimeric adhesion receptors formed by the non-covalent association of α and β subunits. Each subunit is a transmembrane glycoprotein spanning the plasma membrane once (Arnaout et al., 2005). In mammals, 24 integrins have been identified to date, resulting from different pairings among the 18 α and 8 β subunits available. Of these 24, $\alpha_1\beta_1$, $\alpha_2\beta_1$, $\alpha_3\beta_1$, $\alpha_5\beta_1$, $\alpha_6\beta_1$, $\alpha_6\beta_4$, $\alpha_v\beta_3$ and $\alpha_v\beta_5$ are known to be present in endothelial cells (Rupp and Little, 2001; Stupack and Cheresh, 2002). Integrins recognize a large number of physiologic ligands, including soluble and surface-bound proteins (collagen, fibronectin, vitronectin, thrombospondin, elastin, tensin, osteoponin, laminin). The binding of integrins to ligands on rigid surfaces results in force generation at the focal contacts (meeting points of the integrin with ligand), which directly affects the cell's contractile apparatus and plays a major role in the assembly and remodelling of the ECM (Ingber, 2003; Ridley, 2004). The extracellular domains of integrins bind to different ligands depending on the specific combination of α and β subunits that constitute the particular receptor. The cytoplasmic domains on the other hand, interact with a variety of signalling molecules such as focal adhesion kinase (FAK), c-Src and cytoskeletal proteins like talin and a-actinin (Hynes, 1992; Sastry and Horwitz, 1993).

The unique structural features of integrins allow them to mediate both "inside-out" signalling, in which intracellular signals modulate the affinity of integrins for extracellular ligands, and "outside-in" signalling, in which ECM stimuli (e.g. ligands) induce the intracellular signalling cascade via integrin activation (Schwartz et al., 1995). Integrins are activated also by avidity modulation which is clustering of integrin receptors. Affinity

modulation involves changes in integrin heterodimer conformation that lead to increased binding to their ligands such as fibronectin or vitronectin. When the ligand binds, it induces conformational changes in integrins that lead to further association of intracellular molecules with the integrin cytoplasmic tail (Humphries et al., 2003; Liddington and Ginsberg, 2002; Shimaoka et al., 2002). Avidity modulation involves changes in lateral mobility and clustering of the integrins in order to facilitate a stronger binding to the attached surfaces.

Integrin receptors are directly activated by shear stress in endothelial cells (Wang et al 1993; Tzima et al 2001) and by mechanical stretch in fibroblasts (Katsumi et al 2005). Shear stress increases both the affinity and avidity of integrins (Chicurel et al., 1998; Davies et al., 1995; Shyy and Chien, 2002). A growing body of evidence now suggests that integrin receptors constitute one of the main mechanosensory bodies of mechanical force (Chicurel et al., 1998; Geiger et al., 2001; Katsumi et al., 2004; Munevar et al., 2004; Sheetz et al., 1998). Integrins are linked directly to the cytoskeleton and carry out some transduction via direct transmission of forces among cytoskeletal elements.

Ion Channels

An early response to shear stress is the influx of Ca^{2+} in endothelial cells (Helmlinger et al., 1996; Kanai et al., 1995; Yamamoto et al., 2000) which can in turn regulate cellular signalling and EC functions through the activation of Cl^- channels and Ca^{2+} activated K^+ channels (Nilius and Droogmans, 2001). It is the membrane potential that modulates the driving force for Ca^{2+} transmembrane fluxes since endothelial cells lack voltage-dependent Ca^{2+} channels. It has been shown that the intracellular Ca^{2+} concentration $[Ca^{2+}]$ undergoes a rapid increase within 1 minute of shear stress application (Ando et al., 1988) which is transient and subsides after 5 minutes. It has also been observed that laminar shear stress-induction of membrane-driven Ca^{2+} influx and increased Ca^{2+} -activated K^+ channel activity leads to increased synthesis of vasodilator and anti-thrombotic factors (Brakemeier et al., 2003) which might constitute an atheroprotective mechanism.

GPCRs and G-proteins

G protein activation has been shown to occur as early as 1 second after the onset of shear stress which appears to be independent of the cytoskeletal and cytosolic components

(Gudi et al., 1996). In addition, it has been shown that G proteins reconstituted in liposomes in the absence of protein receptors are capable of increasing their activity in response to shear stress (Gudi et al., 1998). It is possible that the plasma membrane itself activates G-proteins by increasing fluidity of the lipid bilayer in response to shear stress as it has also been observed (Haidekker et al., 2000).

Platelet/endothelial adhesion molecule 1 (PECAM-1)

PECAM-1 (also called CD31) is a 130-kDa glycoprotein most abundantly expressed in expressed in endothelial cells. It is also expressed by platelets, monocytes, neutrophils and leukocytes. PECAM-1 belongs to the immunoglobulin (Ig) superfamily and has 6 loops of the C2 type Ig-like domains, constituting a large extracellular portion of the molecule (Figure 1.18). It has a single transmembrane domain and a short cytoplasmic tail (Osawa et al., 1997). PECAM-1 is a cell-to-cell adhesion molecule and is located at junction sites between neighbouring endothelial cells in a confluent (cells are in contact to each other and covering about ~95% of the dish) monolayer.

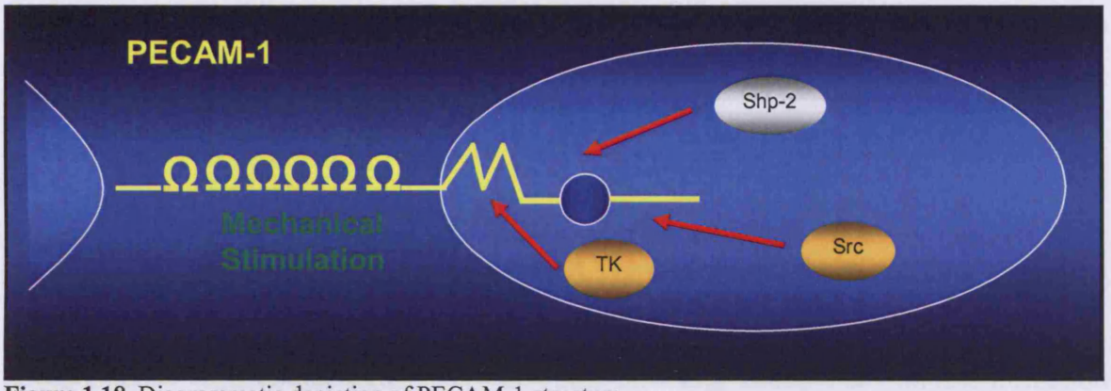

Figure 1.18. Diagrammatic depiction of PECAM-1 structure.

Studies have demonstrated a transient tyrosine phosphorylation of PECAM-1 in endothelial cells within 1 min after the application of shear stress (Harada et al., 1995; Osawa et al., 1997). Shear stress can induce the recruitment of the tyrosine phosphatases SHP-1 and SHP-2 (Freeman et al., 1992) to EC junctions within 5 min, and such translocation is dependent on PECAM-1 expression (Osawa et al., 2002). SHP-2 however binds with an affinity 5-fold higher that SHP-1 (Hua et al., 1998). It has been shown that the shear stress-induced phosphorylation of extracellular signal-regulated protein kinase

(ERK) is dependent on PECAM-1 tyrosine phosphorylation and PECAM-1 and SHP-2 activity seem to be shear stress-sensitive (Osawa et al., 2002). It was found that PECAM-1 is phosphorylated on tyrosine 686 by c-Src kinase (Lu et al., 1997), which is also stimulated by mechanical forces in endothelial cells (Traub and Berk, 1998) and binds to the phosphorylated Y686 of PECAM-1 via its SH2 domain (Masuda et al., 1997). It has also been shown that mechanically induced tyrosine phosphorylation of PECAM-1 is not downstream of Ca^{2+} influx, K^{+} channel activation and stretch-activated channel activity or protein kinase C (PKC) activation (all pathways known to be activated as fast as PECAM-1 – within the first 1 minute of shear stress stimulation) (Fujiwara et al., 2001).

Receptor tyrosine kinases (RTKs)

Shear stress also causes a transient activation of the vascular endothelial growth factor (VEGF) receptor Flk-1, an RTK on the endothelial surface (Chen et al., 1999). This is detectable within 1 min after the application of shear stress, reaches a peak in 10–15 min, and disappears by 30 (Wang et al., 2002; Chen et al., 1999). These shear-induced changes in Flk-1 are independent of its ligand VEGF (Chen et al, 1999; Jin et al, 2003). In this respect Flk-1 seems to be activated directly by mechanical forces in the same manner as PECAM-1.

1.3.7 Shear stress modulation of signalling pathways

Many cytoplasmic proteins have been reported to be implicated in shear stress signalling (Papadaki and Eskin, 1997). Integrins play a major role in the propagation of the shear stress-induced intracellular signal (Schwartz and Ginsberg, 2002). They initiate formation of protein complexes and phosphorylation of members of these complexes (Chen et al., 1999; Vuori, 1998; Zamir and Geiger, 2001). This chain of molecular interaction eventually leads to the activation of the Rho family of proteins (Rho, Rac, Cdc42) and subsequent cytoskeletal rearrangements (Tzima, 2006).

Talin-integrins

Talin is a major actin-binding protein that binds to integrins, co-localizes with activated integrins (Critchley, 2000) and plays a crucial role in integrin activation (Tadokoro et al.,

2003). Talin consists of the head domain (talin-H), which displays a significant homology to the FERM domain present in ERM proteins (ezrin, radixin and moesin) and a rod domain. It is currently thought that affinity switching of integrin receptors for their molecular targets is triggered intracellularly by the binding of the NPxY motif of the integrin β cytoplasmic tail to the PTB-like (PTB domains were initially characterised as domains that bind to phosphorylated tyrosines) F3 FERM subdomain of talin (Yan et al 2001).

Although how exactly the activation of integrins is regulated is not completely understood yet, it is possible that talin provides inside-out activation increasing the affinity of integrins for ligands which in turn as an outside-in activation step induces conformational changes that further increase integrin affinity for cytosolic proteins (Calderwood, 2004a; Calderwood, 2004b; Calderwood et al., 2002; Calderwood et al., 1999). At least two other molecules can regulate the affinity of talin for integrins. Cleavage of talin by the protease calpain separates the talin N- (head) and C- (tail) terminal domains and increases affinity of talin head for integrins (Yan et al., 2001) while binding of PtdIns(4,5)P_2 (phosphatidylinositol 4,5-bisphosphate) to talin induces a conformational change within the talin FERM domain that can enhance its association with integrin tails (β1 tails) (Martel et al., 2001).

Paxillin

Paxillin is a 557-amino acid (human), 68-KDa protein that is comprised of multiple structural domains (Figure 1.19) including 5 leucine-rich LD motifs (consensus LDXLLXXL) (Tumbarello et al., 2002) and 4 double zing finger LIM domains (Turner, 2000a). Its primary function is as a molecular adaptor or scaffold protein that provides multiple docking sites at the plasma membrane for an array of signalling and structural proteins. For example it provides a binding platform for FAK and Src which are activated as a result of integrin activation or growth factor stimulation (Figure 1.19). Phosphorylation of residues at the N-terminus of paxillin by these kinases permits the regulated recruitment of downstream effector molecules such as Crk, which (via association with p130Cas) is important for transduction of external signals into changes in cell morphology and motility. In addition, negative regulators of these pathways,

including c-Src terminal kinase (Csk, an inhibitor of Src kinase activity) and protein tyrosine phosphatase PEST (PTP-PEST, a phosphatase that dephosphorylates FAK and CAS), bind directly to paxillin, which brings them into proximity with their targets (Turner, 2000a; Turner, 2000b).

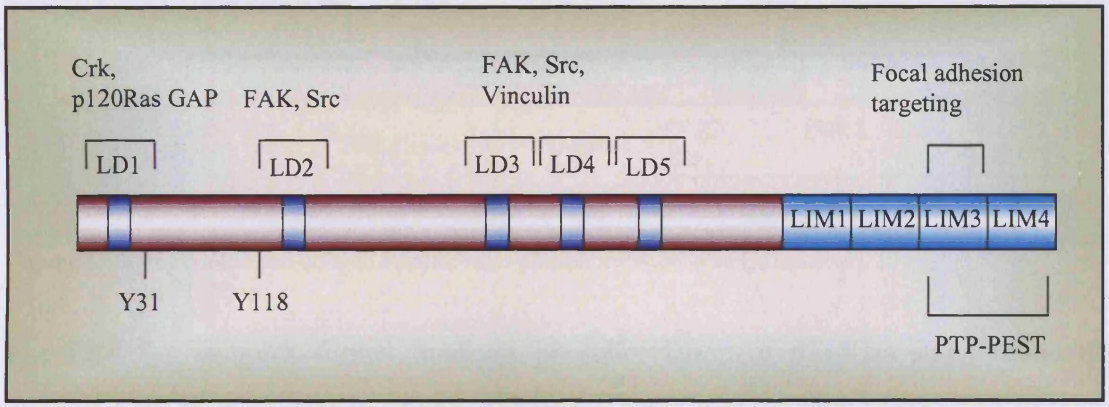

Figure 1.19. Paxillin structure and binding partners. (adapted from Brown and Turner, 2004).

FAK-Src

Integrin binding to extracellular matrix (ECM) induces a transient phosphorylation of focal adhesion kinase (FAK) in a variety of cell types (Schwartz et al., 1995). Shear stress induces tyrosine phosphorylation of FAK (Sai et al., 1999; Yano et al., 1996): kinase activity of focal adhesion kinase increases in a very rapid (after 1 minute) and transient manner (Li et al., 1997). FAK is a 125-kDa cytosplasmic tyrosine kinase that is composed of an N-terminal FERM domain, a central kinase domain, a C-terminal focal adhesion targeting domain (FAT) and three proline-rich regions which allow it to interact with multiple targets (Figure 1.20). The FAT domain associates with proteins such as talin and paxillin (Schlaepfer et al, 2004), FAK binds to the SH3 domain of the adaptor protein p130Cas (Crk-assosiated tyrosine kinase substrate p130Cas) (Harte et al., 1996) and the LD2 domain of paxillin (Calalb et al., 1995) via its proline-rich and FAT regions respectively. Upon integrin engagement, FAK localises to focal adhesions via its FAT domain (Hildebrand et al., 1993) and is activated by autophosphorylation on tyrosine 397 (Y397). When phosphorylated, Y397 becomes a binding site for Src, which phosphorylates FAK at Y576 and Y577, further stimulating kinase activity (Calalb et al., 1995), and Y861 and Y925, creating docking sites for other substrates such as the growth

factor receptor binding protein 2 (Grb2) and GTPase activating protein for Rho associated with FAK (GRAF) (Schlaepfer et al., 1994; Schlaepfer and Hunter, 1998).

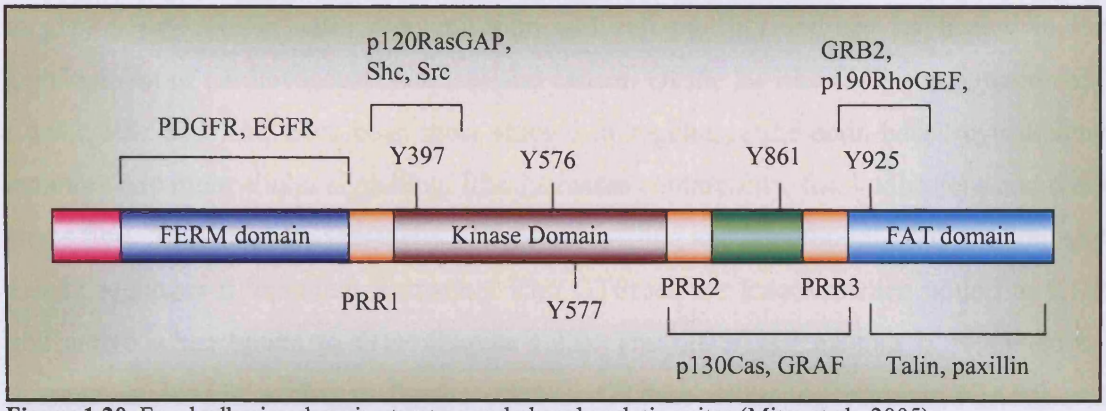

Figure 1.20. Focal adhesion domain structure and phosphorylation sites (Mitra et al., 2005).

The FAK-Src complex further mediates phosphorylation of p130Cas and paxillin on multiple sites (Turner, 2000a; Turner 2000b). SH3-mediated binding of p130Cas to FAK is linked to enhanced tyrosine phosphorylation of p130Cas at multiple sites which promotes SH2-mediated binding of the Crk adaptor protein to p130Cas. Recruitment and binding of Crk to phosphorylated p130Cas allows in turn binding of DOCK180 to the FAK-Cas-Crk complex. It has been shown that DOCK180 (also found as DOCK180-ELMO complex) is an exchange factor for the Rac GTPase (Brugnera et al., 2002; Gu et al., 2001). A schematic of the possible protein complex formation upon shear stress-induced integrin activation is shown in Figure 1.21.

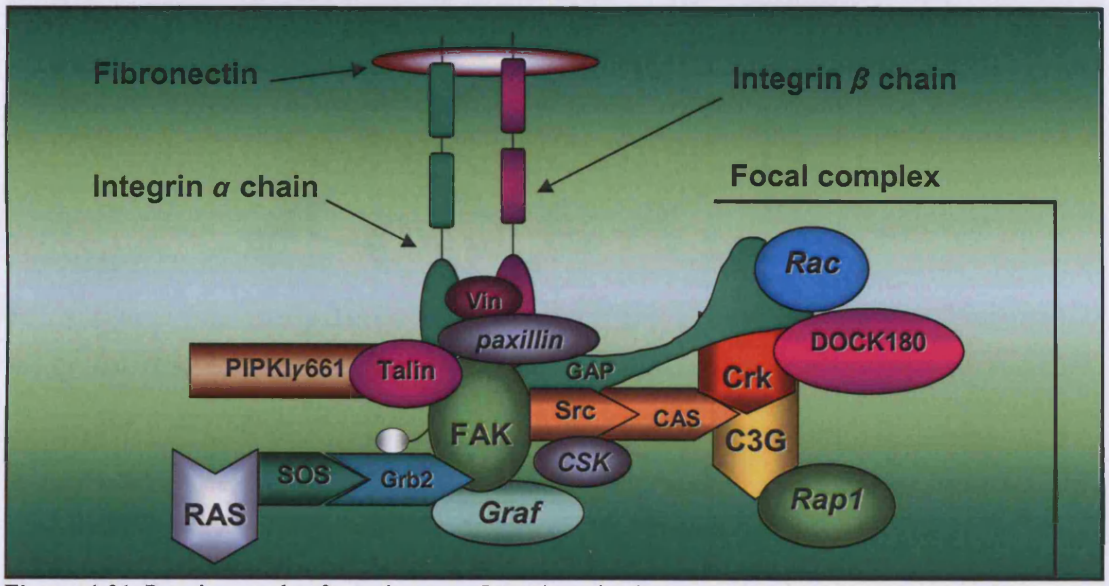

Figure 1.21. Protein complex formation upon Integrin activation.

Rho GTPases

Rho family small GTPases (Ridley, 2001) belong to the Ras superfamily. They are known to play a key role in actin reorganisation and cell motility and are implicated in the development of cardiovascular diseases and cancer. Of the 22 Rho GTPases in mammals, Cdc42, Rac and Rho have been most studied in regulating the actin-based cytoskeletal structure and intracellular signalling. Rho increases contractility, focal adhesions and actin stress fibre formation; Rac regulates membrane ruffling and lamellipodium formation; and Cdc42 regulates fillopodium formation. Rho GTPases are inactive when bound to GDP and active when bound to GTP (Figure 1.22). The GDP/GTP cycling is regulated by guanine nucleotide exchange factors (GEFs), GTPase activating proteins (GAPs) and guanine nucleotide dissociation inhibitors (Moon and Zheng, 2003; Van Aelst and D'Souza-Schorey, 1997). GEFs bind with high specificity to Rho GTPases (after GDP dissociation inhibitors (GDIs) are released) and activate them by forcing the exchange of GDP for GTP. In turn, GTP activating proteins (GAPs) deactivate the GTPases by catalyzing the hydrolysis of bound GTP to GDP returning the GTPases to their GDP-bound inactive form (where they can associate with GDIs again).

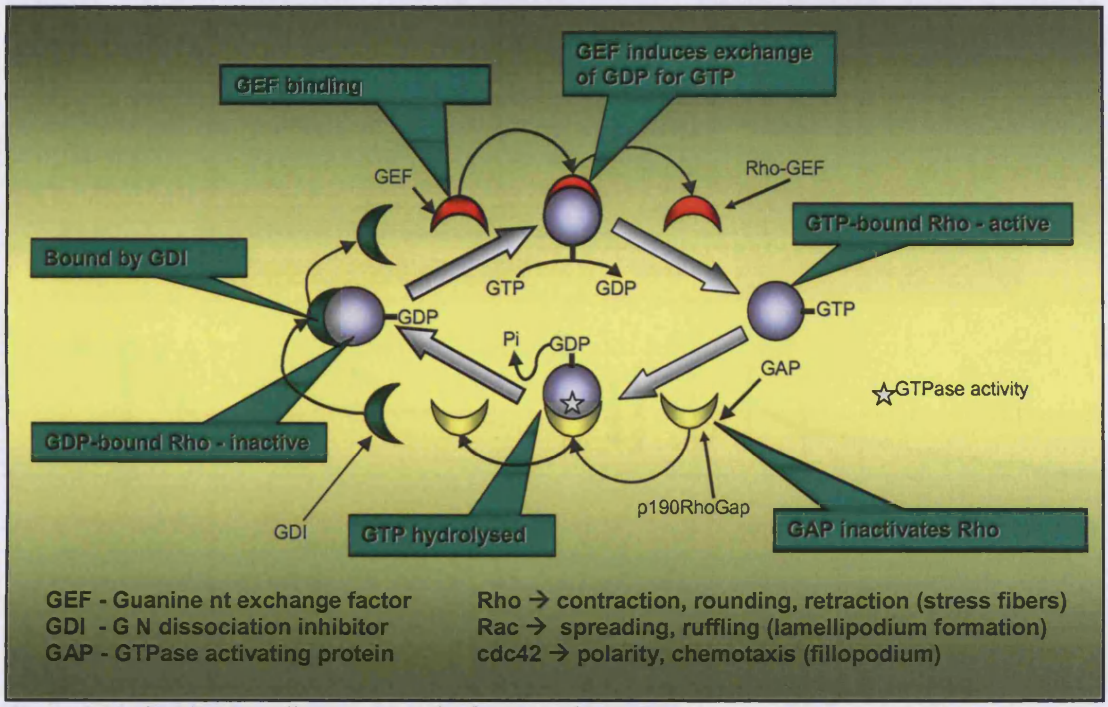

Figure 1.22. GTP/GDP cycling regulates the function of Rho GTPases.

Shear stress has been shown to cause a rapid increase of Rho activity in the range of 2.5 to 3 fold which peaks in the first five minutes (Wojciak-Stothard and Ridley, 2003; Tzima et al., 2001) and then subsides (Figure 1.23).

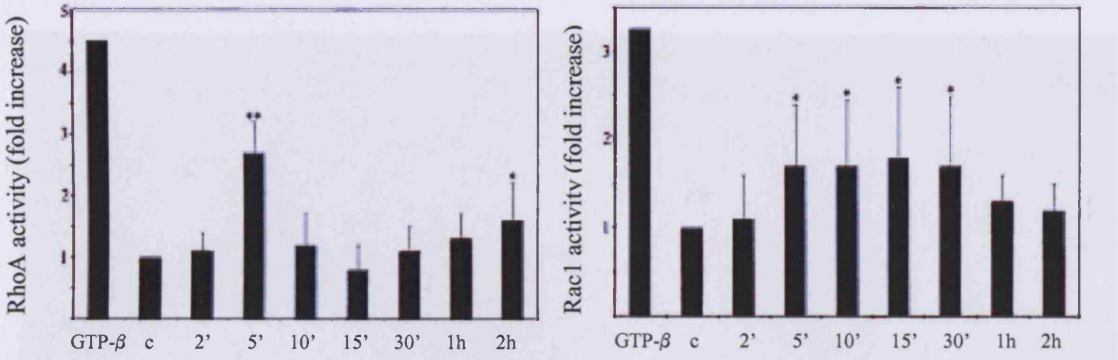

Figure 1.23. Activity observations generated by Wojciak-Stothard and Ridley, 2003. HUVECs were subjected to shear stress for the indicated times. Panels on the bottom show fold increase of RhoA and Rac activities for the indicated times respectively.

On the other hand, Rac activity (Figure 1.24) increases in the range of 2-3 fold in a slower rate (~15-30 minutes) but more sustained manner which is generally the amount of time required for the endothelial cells to morphologically adjust to shear stress (Wojciak-Stothard and Ridley, 2003; Tzima et al., 2001).

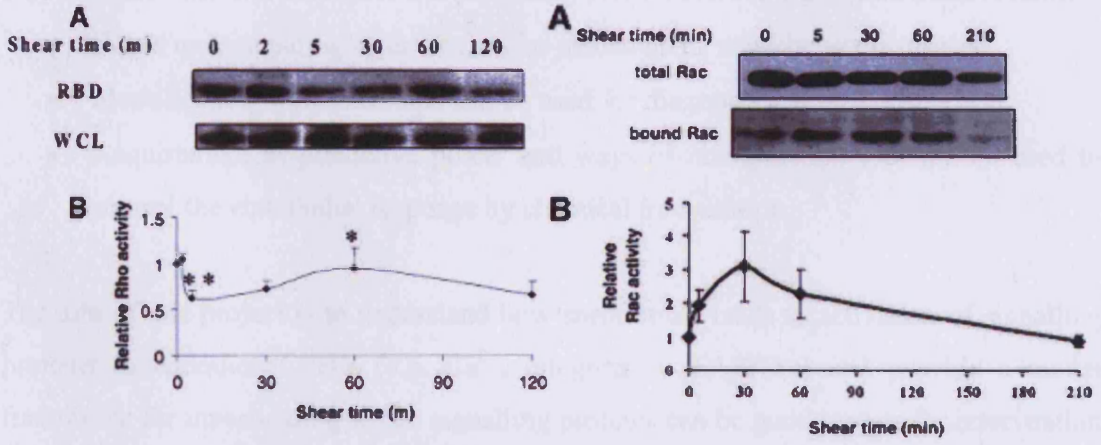

Figure 1.24. Activity profiles generated by Tzima et al. (2001). Left panel shows the fold activity of Rho under shear stress conditions subjected to BAECs for the indicated times. Right panel shows the fold activity of Rac under shear stress conditions subjected to BAECs for the indicated times (Tzima et al., 2001). For details of experimental procedure refer to the original literature.

Activation of Rho and Rac leads to cytoskeletal rearrangements such as actin polymerization, actin filament stabilization and actomyosin assembly and contraction (Figure 1.25). These together, lead to early morphological changes induced by shear stress (Tzima, 2006).

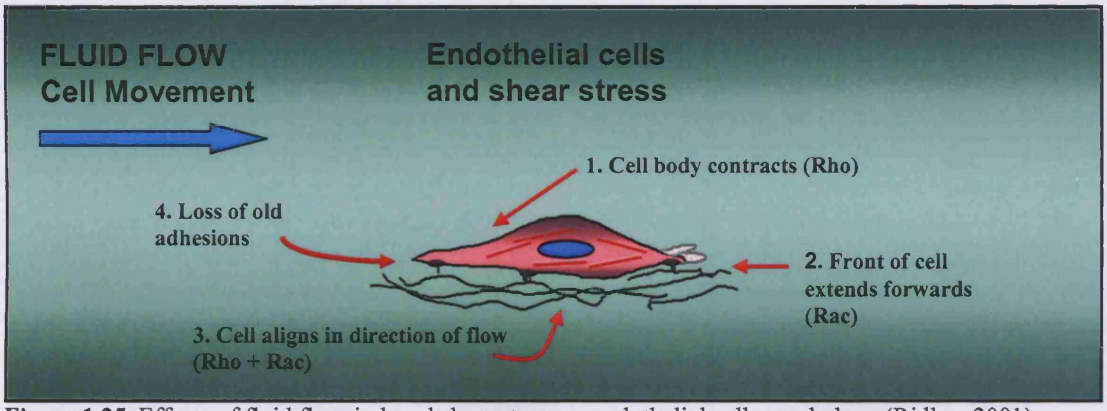

Figure 1.25. Effects of fluid flow-induced shear stress on endothelial cell morphology (Ridley, 2001).

1.3.8 Aims of the project

So far the medical community has been trying to indirectly control the fluid dynamics and shear stress fluctuations by modifying the blood pressure with hypertensive drugs. Instead it is possible that direct chemical intervention and control of the endothelial response itself may be more efficient. Solutions can potentially rise from three significant achievements:

- Better understanding of the molecular mechanisms underlying the disease,
- Identification of markers that can be used for diagnosis and prognosis,
- Acquirement of predictive power and ways of manipulation that can be used to control the endothelial response by chemical intervention.

The aim of this project is to understand how shear stress leads to activation of signalling proteins in endothelial cells (e.g. Ca^{2+}, integrins → FAK/Src) and provide a model framework for investigating which signalling proteins can be good targets for intervention (e.g. in high blood pressure). The aim involves the identification of the sequence of macroscopic and microscopic events and interactions that take place outside and within the endothelial cells under shear stress stimuli. This can be achieved by connecting the extracellular input of fluid flow and shear stress and (and how it regulates signal

transduction and propagation within the cell) to the critical interactions and molecule interrelationships of all the intracellular pathways that are known to be involved. This has formed the primary objective of this project and is represented with a workflow diagram in Figure 1.26.

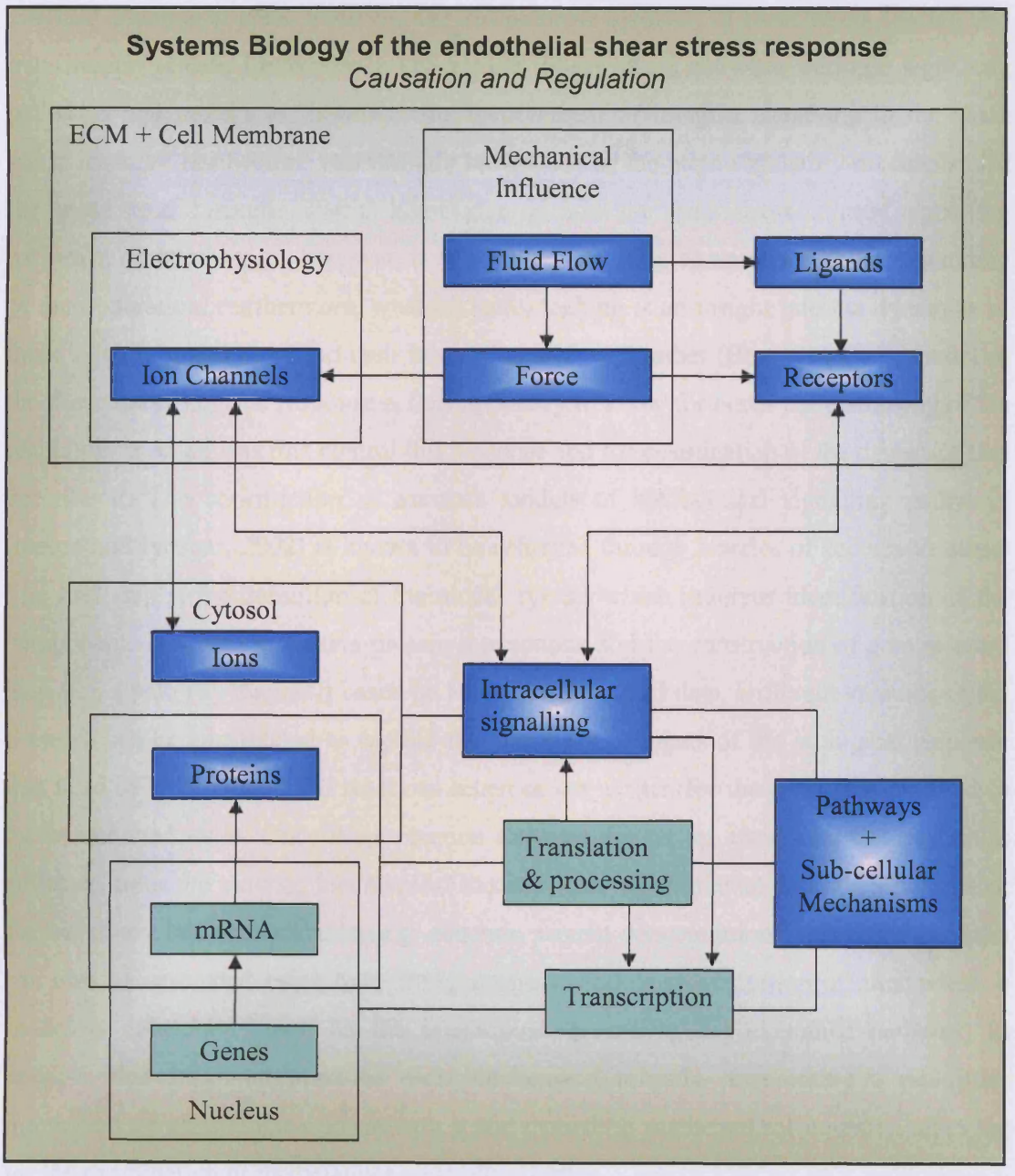

Figure 1.26. Global systems biology approach for investigating the shear stress response. Tables in blue correspond to elements which have been examined in this project. Tables in green have been left out due to time limitations.

2 THE MODEL OF THE SHEAR STRESS-INDUCED SIGNALLING

2.1 Introduction

Fluid mechanical shear stress elicits morphological, metabolic, and structural responses in vascular endothelial cells; however, the mechanisms involved in shear stress sensing and transduction remain incompletely understood. Shear stress activates multiple signalling pathways and molecules; however, the involvement of integrin signalling in the shear stress response has become increasingly recognised as the main regulatory mechanism of the shear stress response. Partial knowledge on how the shear stress-induced signalling pathways function exists, however, it is not adequate for a comprehensive understanding of their operation. Furthermore, what is clearly lacking is an insight into the dynamics of these signalling pathways and their interaction with each other (Bray, 1998). A model of the shear stress-induced response is thus necessary to allow for better understanding of the regulatory mechanisms that control this response and for examination of the dynamics that describe it. The construction of accurate models of biochemical signalling pathways (Neves and Iyengar, 2002) is known to be achieved through a series of successive steps. The first step is the definition of the model system which involves identification of the components involved in protein-protein interactions and the construction of a connection map (i.e. a pathway diagram) based on available biological data. Different versions of the network can be constructed to capture the necessary elements of the biological response that need to be modelled and reactions schemes are written for the processes captured in the constructed maps. Once these reaction schemes are set up, parameter information is collected from the existing biochemical literature and experimental data. Parameters that are necessary but not available (e.g. absolute protein concentrations and rate constants) can also be estimated using data-fitting analysis. Following collection of parameters, a model is developed based on the interactions describing the examined pathway. In practise, this is a translation of each biochemical formula representing a molecular interaction or physiological event into a corresponding mathematical equation allowing for the examination of its dynamics under shear stress.

2.2 Building a comprehensive static map for integrin signalling

2.2.1 Initial pathway information

Integrins are involved in the regulation of cell morphology, cell migration, survival and growth and can be stimulated in a variety of ways. Each stimulus (for example, adhesion to extracellular matrix proteins, mechanical force, and activation via other receptor-activated pathways) can lead to different intracellular responses causing different sets of molecules to activate (initiate signalling) and with different extent (magnitude of change in protein activities). Although integrin signalling has been researched for many years, the information regarding the molecular events involved is scattered throughout the literature and databases and no comprehensive map has been created yet as it has for the epidermal growth factor receptor signalling (Oda et al., 2005). At the beginning of the project and before any work was carried out, a first version of the pathway was available that included some of the molecules known to be involved in shear stress-induced and/or integrin signalling (Figure 2.01).

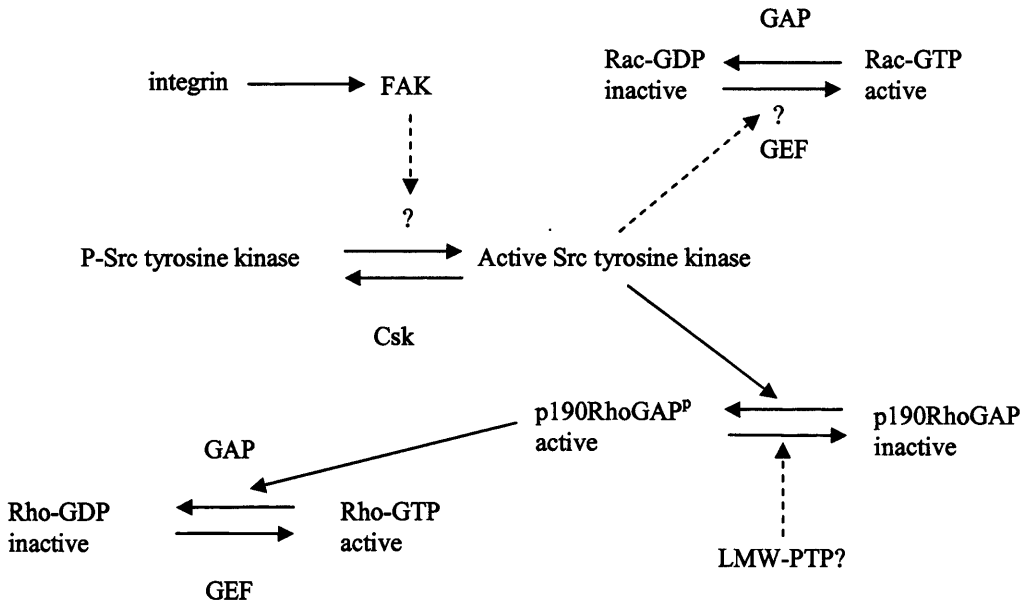

Figure 2.01. Initial shear stress response (network). Shear stress is known to activate integrins, FAK, Src, Rac and both upregulate and downregulate Rho in endothelial cells (see introduction). Regulation of Src kinase is shown to an extent. Src kinase is known to induce activation of Rac GTPase but also inactivation of Rho GTPase by first activating p190RhoGAP by phosphorylation. p190RhoGAP active in turn inactivates Rho GTPase. The interaction of Src with p190RhoGAP has been identified in endothelial cells, however it has not been investigated under conditions of shear stress.

It is clear that this pathway had to be expanded and new information added. Therefore a comprehensive static map for shear stress-induced integrin signalling was created which was necessary to a) aid in the understanding of the architectural feature of the signalling network, b) aid decisions regarding the size and the extent of the reconstruction of the mathematical (dynamic) model that was built based on this map and c) serve as a useful reference of the molecular events examined for the duration of this project. To construct a static network of molecular reactions, responses activated by integrins were identified first and subsequently filtered to create a more specific static network for the shear stress response.

2.2.2 Components and interactions of the integrin signalling pathway

The identification of components and interactions of a biochemical pathway is possibly the most critical step towards assembling a good working model. Protein-protein interactions can be identified automatically using software that collects and integrates data from various databases and subsequently generates diagrammatic layouts of protein interaction networks using graph theory. Frequently used examples of such software are Cytoscape (Shannon et al., 2003), OsPrey (Breitkreutz et al., 2003) and pSTIING (Ng et al., 2006). Generation of protein interaction maps by automated methods can be useful in identifying potential molecular interactions in a pathway and can be used for qualitative analysis to a certain extent (e.g. examination of pathway architecture, feedback loops).

However, initial attempts to obtain interaction maps from such software revealed that the automated generation of networks often incorporates many interactions that have not been sufficiently validated experimentally (e.g. many identified interactions are based only on yeast-two-hybrid experiments) and almost always suffers from many false positive interactions. This limitation made them impractical for the purpose of generating an accurate map for the integrin pathway or for quantitative analysis and modelling since their refinement and validation would take enormous amounts of time. An example of an automated protein interaction network generated by searching for integrin, FAK, Src, Rho and Rac is shown in Figure 2.02.

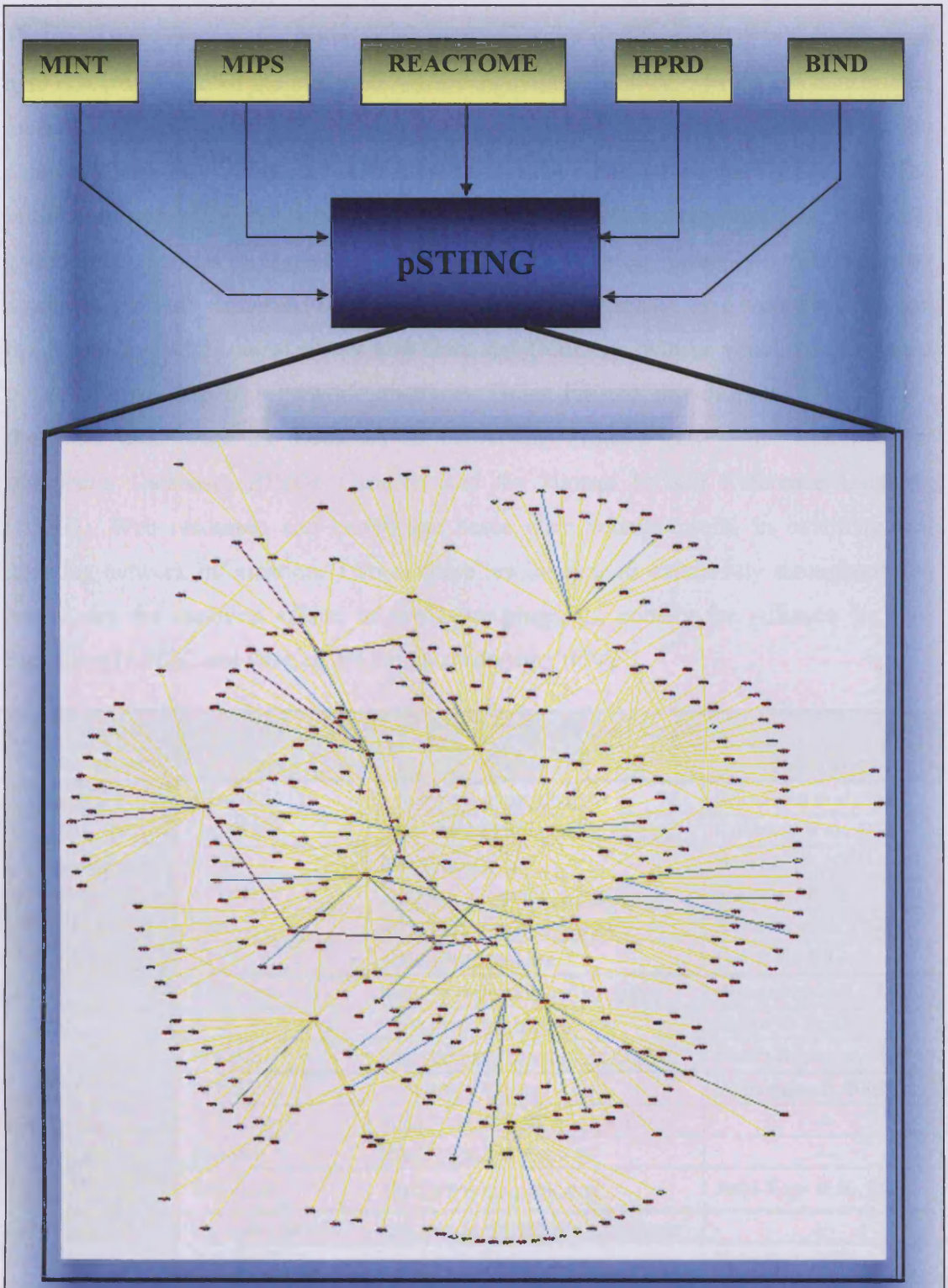

Figure 2.02. pSTIING Batch Search. 535 edges and 398 nodes shown. These represent all possible molecular interactions drawn from the data combined from a number of databases. The map was generated using the pSTIING database and searching for interactions that involved the following molecules: FAK, Paxillin, Integrins $\alpha v\beta 3$ & $\alpha 5\beta 1$, RhoA, SRC, Talin, and Rac1.

The static pathway map for the integrin signalling pathway (Figure 2.03), which will from here onwards be called the integrin/FAK/Src signalling pathway, was instead constructed manually by collecting information regarding individual components involved in the pathways and the molecular interactions and inter-relationships between them. The information regarding molecules implicated in the shear stress response (e.g. integrins) and their interactions was manually extracted from pre-existing manually-curated pathway databases and web resources (Table 2.1). The two main databases used were BioCarta and the Kyoto Encyclopedia of Genes and Genomes (KEGG), both of which contain good collections of graphical network diagrams. Other curated protein-protein interaction databases used were the Database of Interacting Proteins (DIP), the Biomolecular Interaction Database (BIND), GeneNet and the Human Protein Reference Database (HPRD). Web resources and knowledge bases were equally useful in obtaining and updating network information. Two of these resources used extensively throughout this project are the resulting efforts of two large programs, namely the Alliance for Cell Signalling (AFCS) and the Cell Migration consortium (CMC).

Data Resources used to construct the integrin/FAK/Src map			
Description	**Name**	**Web Link**	**Reference**
Qualitative descriptions of signalling interactions and networks	TRANSPATH	http://www.transpath.de/	Schacherer et al., 2001
	GeneNet	http://wwwmgs.bionet.nsc.ru/mgs/	Kolpakov et al., 1998
	BIND	http://bind.ca/	Bader et al., 2001
	KEGG	http://www.genome.jp/kegg/	Kanehisa, 2002
	DIP	http://dip.doe-mbi.ucla.edu/	Xenarios et al., 2002
	HPRD	http://www.hprd.org	Peri et al., 2004
Molecular kinetics databases	BRENDA	http://www.brenda.uni-koeln.de/	Schomburg et al., 2002
	EMP	www.empproject.com/	Selkov et al., 1996
	DOQCS	http://doqcs.ncbs.res.in/~doqcs/	Bhalla &Iyengar, 1999
Databases of signalling models	AFCS	http://www.afcs.org	Subramaniam, 2002
	CMC	http://www.cellmigration.org	---
	Biocarta	http://www.biocarta.com	---
	Reactome	http://www.reactome.org/	Joshi-Tope et al., 2005
Other web resources and databases	Signalling gateway	http://www.signalling-gateway.org/	---
	BioCyc	http://www.biocyc.org/	Karp et al., 2005
	Gene Ontology	http://www.geneontology.org/	---
	STKE	http://stke.sciencemag.org/cm/	Gough, 2002

Table 2.1. Data resources used to construct the integrin/FAK/Src map.

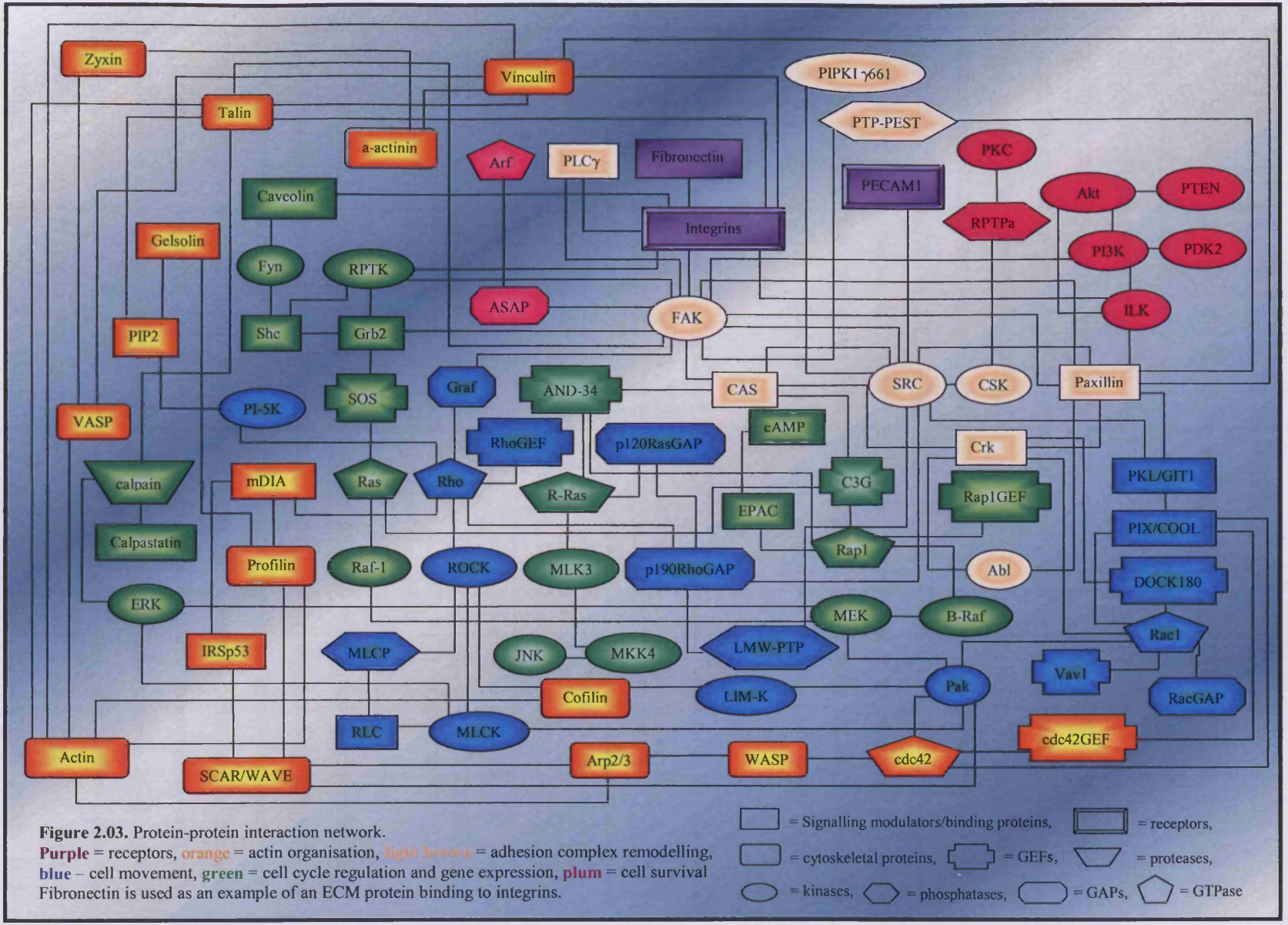

Figure 2.03. Protein-protein interaction network.
Purple = receptors, **orange** = actin organisation, **light brown** = adhesion complex remodelling, **blue** – cell movement, **green** = cell cycle regulation and gene expression, **plum** = cell survival
Fibronectin is used as an example of an ECM protein binding to integrins.

2.2.3 *Identifying the key players for the shear stress responses.*

Not all molecules from the static Integrin/FAK/Src map (Figure 2.03) have been investigated under conditions of shear stress however (a sample is given in Table 2.2, for a complete list of available protein activity profiles refer to the Excel file in the CD attached), and from protein interaction data alone, it was not obvious which molecules or interactions were important for the reported shear stress-induced phenotypic responses (Wojciak-Stothard and Ridley, 2003; Tzima et al., 2001). As mentioned before, different stimuli trigger different responses and it is possible that certain molecules that have been reported to be involved in integrin signalling under specific conditions are not involved in the shear stress response. Equally, the shear stress response involves molecular components that were not part of the static Integrin/FAK/Src map, such as intracellular calcium which was identified as an important modulator of the shear stress response (Wiesner et al., 1997).

Table 2.2: A collection sample of activity profiles

Protein activated	Cell type	LSS (d/cm2)	Detailed time points (min)	Fold activity increase/decrease (respective to time points)	REF
CAS phosphorylation	HUVEC	12	0 - 5 - 10 - 15 - 20	1 - 3.5 - 3.6 - 3.5 - 2.8	1
CAS binding to Crk	HUVEC	12	0 - 5 - 10 - 15 - 20	1 - 1.3 - 1.95 - 1.9 - 1.9	2
FAK	BAEC	12	0 - 1 - 5 - 10 - 20 - 30 -60	1 - 2.6 - 2.25 - 1.9 - 1.8 - 1.7 - 1.65	3
Src phosphorylation	BAEC	12	0 - 1 - 5 - 10 - 20	1 - 3.3 - 3.9 - 5.65 - 3.2	4
Integrins	BAEC	12	0 - 2 - 5 - 15 - 30	1 - 2 - 3 - 2 - 2	5
RAC	BAEC	12	0 - 5 - 15 - 30 - 45 - 60 - 90	1 - 2 - 2.5 - 3 - 2.7 - 2.4 - 2.2 - 2.0	6

Table 2.2. Activity profiles. 1-6 references are given here. HUVEC= Human umbilical vein endothelial cells, BAEC = Bovine aortic endothelial cells. 1 (Okuda et al., 1999), 2 (Okuda et al., 1999), 3 (Li et al., 1997), 4 (Jalali et al., 1998), 5 (Tzima et al., 2001), 6 (Tzima et al., 2002).

Furthermore, it was necessary to ensure that the information obtained from the databases and knowledgebases was correct and that all crucial information regarding the pathways was documented. This was achieved by manually curating the information present within the text of more than 300 scientific papers (reviews and research articles) accessible from PubMed and/or by extrapolating information from experimental observations and data published in research articles. Such data included temporal measurements of changes in the relative expression of activity levels of a specific molecule (which often correlated with the subsequent phenotypic changes they induce), commonly generated using western blotting techniques, immunoprecipitation experiments and biochemical assays (e.g.

western blotting-generated temporal activity profiles of integrins, FAK and Src under shear stress conditions (Table 2.2).

Using this information extracted from the literature and the static map for the Integrin/FAK/Src signalling pathway (Figure 2.03), the network map was refined and adapted to shear stress conditions (Figure 2.04) and the key components and the details of their molecular interactions relevant to the shear stress response were identified. Two fundamental processes were used to describe most of the signalling events in the shear stress pathway map:

- Transformations, which are the chemical reactions that break or make covalent bonds. These mainly included phosphorylation by kinases, dephosphorylation by phosphatases and proteolytic activities of proteases.
- Binding events, which are all intermolecular interactions and collisions such as ligand-receptor associations, allosteric regulation of enzymes and formation of multimeric protein complexes through protein-protein interactions. (e.g. SH3 domain binding to proline-rich sequences).

The refined connection map was constructed from the extracted information by linking validated functional states (various forms of the same molecules resulting from either transformations or binding events) of chemical components (section 2.3.3). This provided an initial working version of a static model for the shear stress response which starts with integrin activation and Ca^{2+} influx as initiators of the mechanical signalling and stops at the regulation of Rho and Rac GTPases. The network contains both mechanosensors (e.g. integrins, talin, PECAM-1) (see section 1.3) and molecules known to be involved in shear stress-induced signalling, such as FAK and Src. In addition, other molecules that are known to interact with the shear stress response-implicated molecules under different conditions, such as PTP-PEST, receptor protein tyrosine phosphatase alpha (RPTPα) and calpain and therefore could be involved in the shear stress response were also included, although not yet investigated experimentally. A part of the working version of the static model for the shear stress response is shown in Figure 2.05. The model was annotated to provide molecular details of each transformation or binding events. An overview of the complete shear stress response model is shown in Figure 2.06.

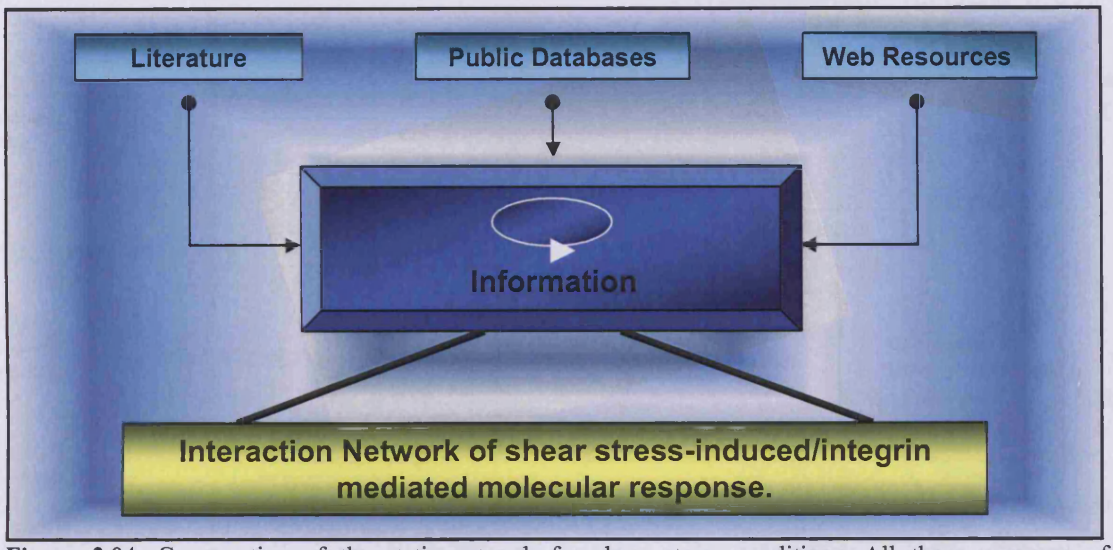

Figure 2.04. Construction of the static network for shear stress conditions. All three resources of information were used iteratively for cross correlation and elimination of false negatives.

At this stage, some of the connections in the integrin/FAK/Src pathway remained missing or uncertain due to missing or contradictory published data (e.g. phosphatase responsible for dephosphorylation of Src kinase). These were added at a later stage (Chapter 3) during construction of the dynamic model along with accompanying hypotheses supporting their role, which were tested with simulation).

In the process of identifying components and molecular interactions involved in the shear stress response the data used were not restricted to endothelial cells based on the assumption that the pathways under investigation are involved in the regulation of cell shape and morphology and are likely to be common between cell types like fibroblasts, epithelial and endothelial cells. This was necessary as the interaction information regarding pathways produced from experiments on only one cell type is incomplete and insufficient for the construction of a comprehensive network. As will be described later however (chapter 3) numerical and validation data used in the model were only taken from experiments performed on endothelial cells (Table 2.2).

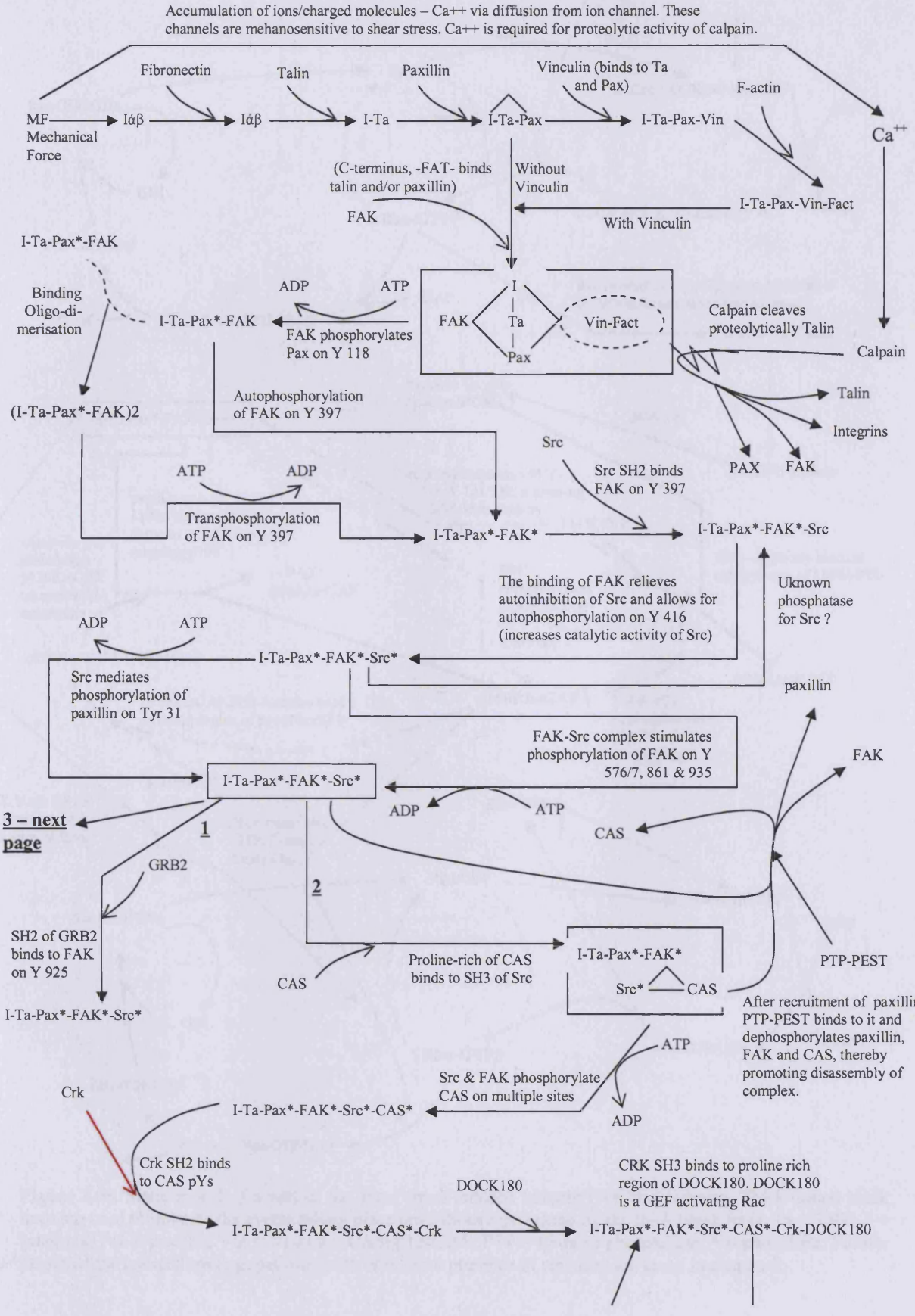
Accumulation of ions/charged molecules – Ca++ via diffusion from ion channel. These channels are mehanosensitive to shear stress. Ca++ is required for proteolytic activity of calpain.
MF Mechanical Force
Iαβ
Fibronectin
Iαβ
Talin
I-Ta
Paxillin
I-Ta-Pax
Vinculin (binds to Ta and Pax)
I-Ta-Pax-Vin
F-actin
Ca++
(C-terminus, -FAT- binds talin and/or paxillin)
FAK
Without Vinculin
With Vinculin
I-Ta-Pax-Vin-Fact
I-Ta-Pax*-FAK
Binding Oligo-di-merisation
(I-Ta-Pax*-FAK)2
I-Ta-Pax*-FAK
ADP
ATP
FAK phosphorylates Pax on Y 118
FAK
I
Ta
Pax
Vin-Fact
Calpain cleaves proteolytically Talin
Calpain
Talin
Integrins
PAX
FAK
Autophosphorylation of FAK on Y 397
ATP
ADP
Transphosphorylation of FAK on Y 397
I-Ta-Pax*-FAK*
Src
Src SH2 binds FAK on Y 397
I-Ta-Pax*-FAK*-Src
The binding of FAK relieves autoinhibition of Src and allows for autophosphorylation on Y 416 (increases catalytic activity of Src)
Uknown phosphatase for Src ?
ADP
ATP
I-Ta-Pax*-FAK*-Src*
Src mediates phosphorylation of paxillin on Tyr 31
paxillin
FAK-Src complex stimulates phosphorylation of FAK on Y 576/7, 861 & 935
FAK
I-Ta-Pax*-FAK*-Src*
ADP
ATP
CAS
3 – next page
1
GRB2
2
SH2 of GRB2 binds to FAK on Y 925
I-Ta-Pax*-FAK*-Src*
CAS
Proline-rich of CAS binds to SH3 of Src
I-Ta-Pax*-FAK*
Src*
CAS
PTP-PEST
After recruitment of paxillin, PTP-PEST binds to it and dephosphorylates paxillin, FAK and CAS, thereby promoting disassembly of complex.
ATP
ADP
Src & FAK phosphorylate CAS on multiple sites
Crk
I-Ta-Pax*-FAK*-Src*-CAS*
Crk SH2 binds to CAS pYs
DOCK180
CRK SH3 binds to proline rich region of DOCK180. DOCK180 is a GEF activating Rac
I-Ta-Pax*-FAK*-Src*-CAS*-Crk
I-Ta-Pax*-FAK*-Src*-CAS*-Crk-DOCK180

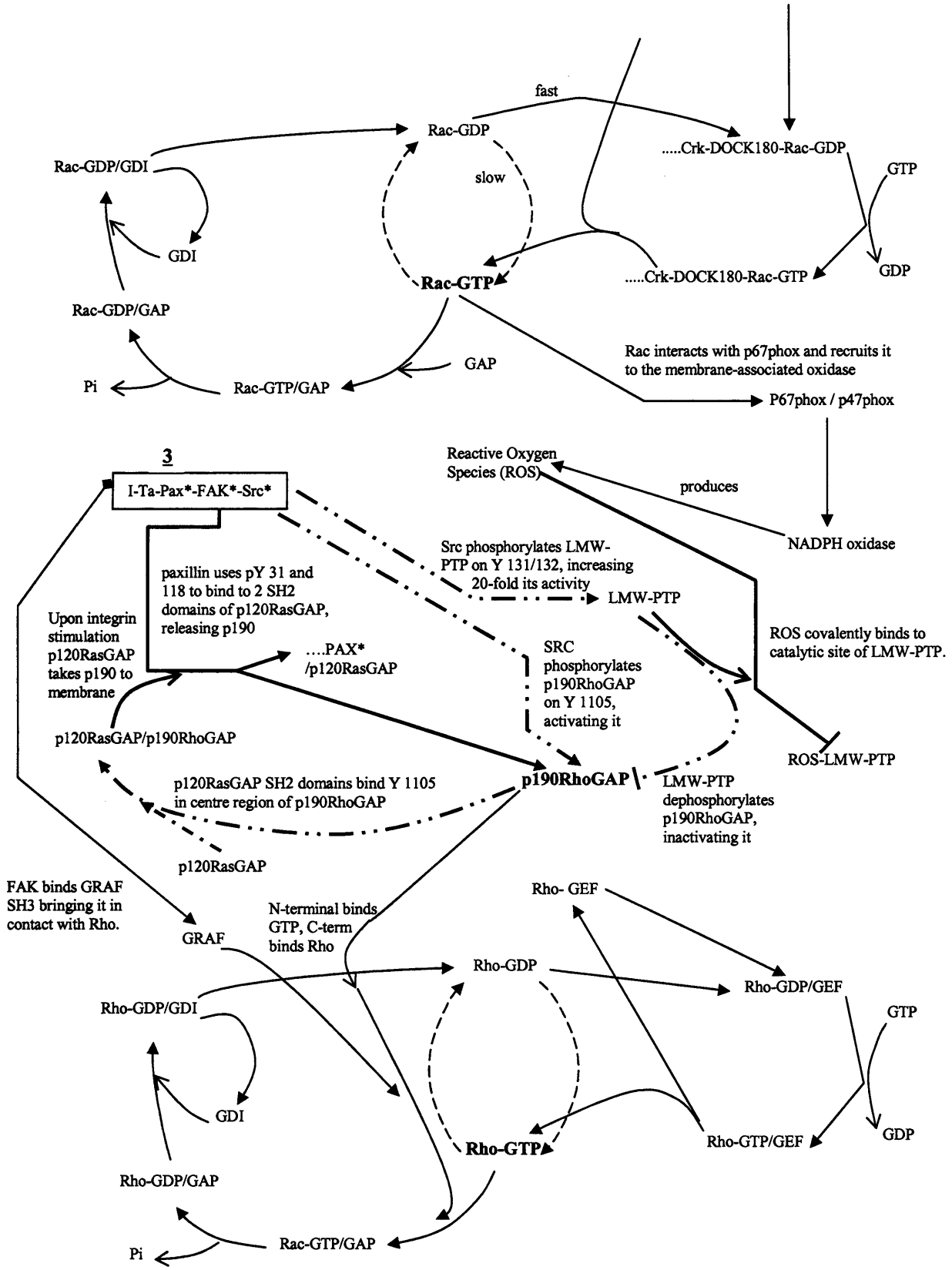

Figure 2.05. Static model of a part of the shear stress-induced Integrin/FAK/Src pathway. Thick dotted black lines are used to indicate the events taking place prior those represented by the thick black lines. Ta = Talin, I = Integrins, Pax = paxillin, Vin = Vinculin, CAS=p130CAS, PTP = tyrosine phosphatase, * = phosphate. Further details of the interactions (e.g. pathway with or without presence of vinculin) are given in chapter 3.

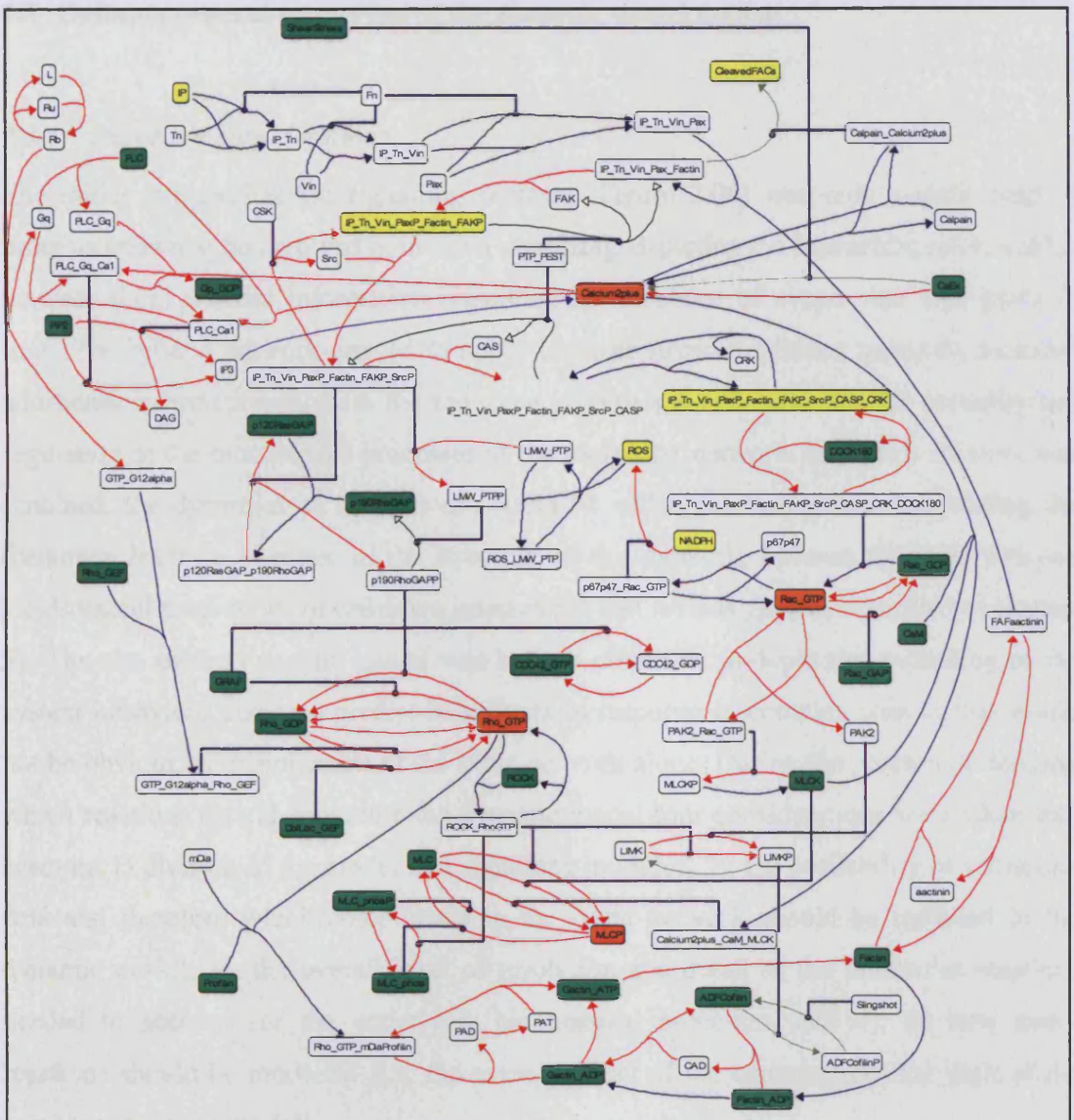

Figure 2.06. Overview of the shear stress response model.
The model includes:

- proteolytic cleavage of talin by calpain and the formation of the complex consisting of integrins, talin, FAK paxillin, Src, CAS and Crk.
- The activation of G-protein coupled receptors and downstream G-protein signalling.
- The regulation of Rac and Rho GTPases respectively and how they communicate.
- The regulation of myosin light chain and polymerisation of actin respectively. F-actin feeds back into the system by assisting focal complex formation.

2.3 Defining general properties of the dynamic model system

2.3.1 Important considerations

The initial integrin/Fak/Src signalling network (Figure 2.06) was only a static map of proteins known to be involved in integrin signalling, depicting the interaction relationships between them without information regarding the sequence of events that take place in time. The refined network created to apply to shear stress conditions however, included additional information for both the sequence of events in time and also the causality and regulation of the biochemical processes of the molecular network. Once this network was obtained, the dynamics of the network could be added (in reality however, adding the dynamics leads to changes in the structure of the network, because dynamic analysis yields useful predictions of unknown interactions and reveals gaps as described in chapter 3). The aim of the dynamic model was both to obtain an in-depth understanding of the system behaviour and also predict behaviours in response to complex stimuli that would not be obvious by examination of the static network alone. During the process of defining which reactions should constitute the dynamic model four considerations were taken into account: 1) division of the model into signalling modules, 2), the availability of validation data and therefore which components in the static network should be included in the dynamic model; 3), the overall level of resolution and detail of the molecular reactions needed to account for the underlying biochemical processes, and 4), on how many reactions should be modelled (i.e. the overall extent of the construction) for each of the components in the model.

2.3.2 Division of the model into modules

In deciding the size of the model and which parts to include, distinct signalling modules were identified. A signalling module consists of a group of molecular compounds and proteins that are spatially co-localised (not always known), function and respond together under certain conditions (Bruggeman and Kholodenko, 2002). There are no universal rules, to date, on how a module is defined and how many components should be included and thus the decisions made were subjective and based on understanding of the network (see section 1.2.7). In this model, modularity was applied at two different stages.

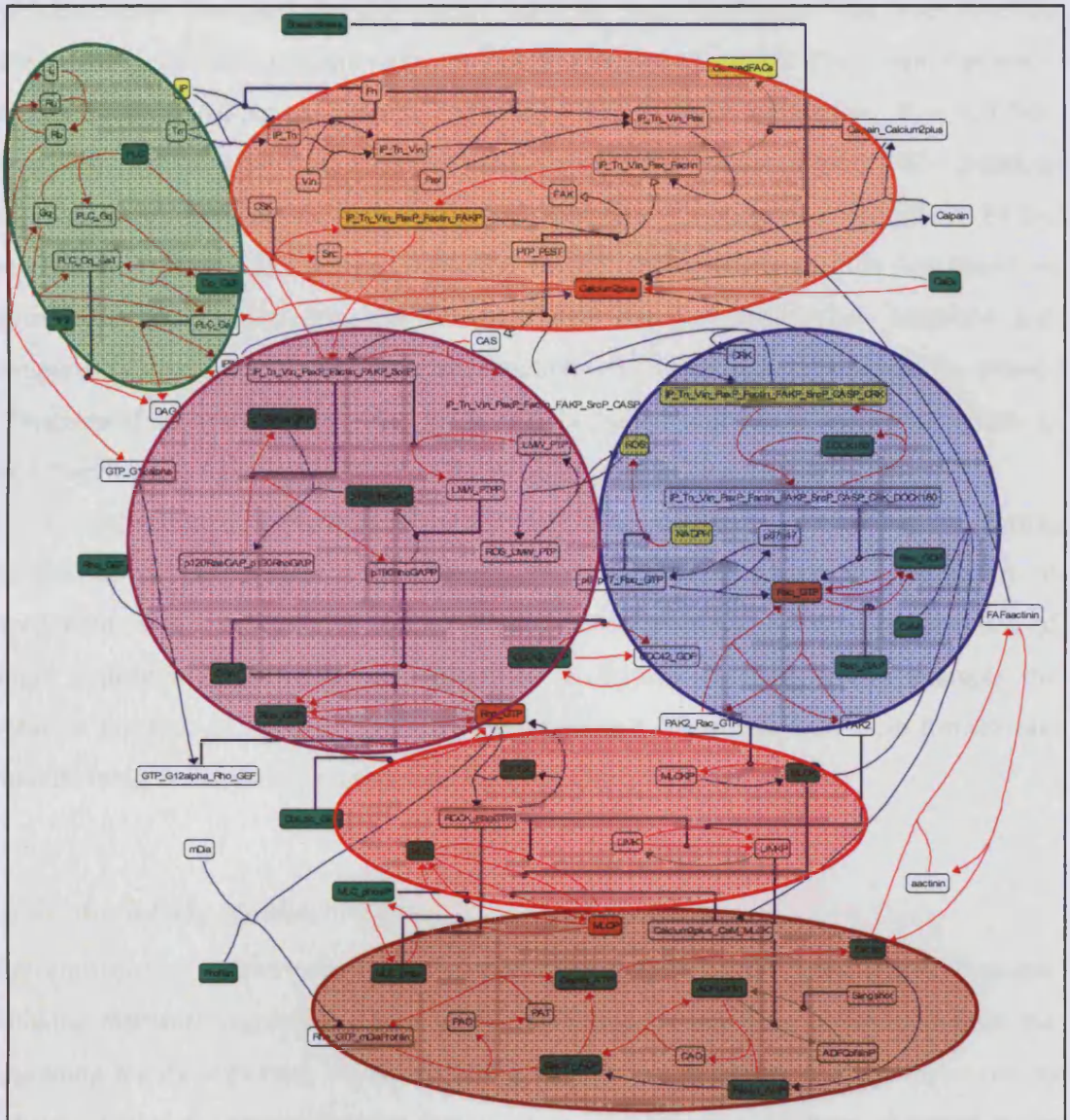

Figure 2.07. Initial modular division of the model.
The connection map was divided into 6 distinct modules. The orange module includes the proteolytic cleavage of talin by calpain and the formation of the complex consisting of integrins, talin, FAK Paxillin, Src, CAS and Crk. The green module involves the activation of G-protein coupled receptors and downstream G-protein signalling. The modules in blue and purple show the regulation of Rac and Rho GTPases respectively and how they crosstalk. The modules in red and brown include the regulation of myosin light chain and polymerisation of actin respectively. F-actin feeds back into the system by assisting focal complex formation.

The first modular division took place before testing the dynamics of the system. Six modules were identified to distinguish between large pathways that can function independently of others and can be controlled by a variety of stimuli. These modules were: integrin/FAK signalling, G-protein signalling, Rac GTPase regulation, Rho GTPase regulation, myosin light chain signalling and actin polymerisation (Figure 2.07). Building the model around these six modules helped maintain the contextual specificity of the network even though inclusion of particular components within a module was based on intuitive and subjective decisions. Module size was increased when reactions and components were added to provide more functions and responses and increase the overall robustness of the system. It was decided to restrict the dynamic modelling of the system to the integrin-FAK signalling (Figure 2.07) preceding Rac GTPase regulation.

The second modular division was considerably more detailed and was applied during simulations of the dynamics (chapter 3). In certain cases where the regulation of components was very complex and involved many interactions, the dynamic function of single molecular components were identified as distinct modules, as for example the dynamic function of FAK. In this way the interaction of calpain with talin formed one module, integrin activation another, and the FAK-Src interaction another.

2.3.3 Availability of validation data

The constructed pathway map for the molecular events of the shear stress response included elements regulating Rho and Rac GTPases, which were considered from the beginning highly important molecules in the shear stress response, as they are known to induce cytoskeletal rearrangements that mediate morphological changes observed under shear stress conditions (e.g. alignment of cells in the direction of flow). Elucidating the properties and overall control of the shear stress response requires thorough investigation of the dynamics of both Rho and Rac GTPases. During the process of creating the dynamic model, the only time-dependent experimental measurements of Rho and Rac GTPases available were from the published work of Wojciak-Stothard and Ridley (2003) and Tzima et al (Tzima et al., 2002; Tzima et al., 2001) respectively. However, the measurements of these two groups were generated by experiments performed on different cell types, confluent BAECs (Tzima et al., 2002) or sub-confluent HUVECs (Wojciak-

Stothard and Ridley, 2003) and showed different results. As data consistency and specificity was highly important to make the model applicable to a specific cellular system, more profiles (activity levels of molecules under shear stress conditions) were collected for the rest of the molecules involved in the pathways (see Table 2.2 and Excel file in CD attached) to identify whether both BAEC and HUVEC profiles were available for the processes taking place. Upon collection of additional published time-dependent measurements for other molecules it was realised that most available data had been generated from experiments using confluent BAECs. Due to this data limitation, it was decided to focus on processes that lead to activation of Rac (where BAEC profiles were available) and leave out activation of Rho which would require more HUVEC profiles for other molecules to become available to be used in conjunction with the Rho GTPase profile.

2.3.4 Resolution detail of the model

During modelling of signalling networks involving protein-protein interactions, detailed chemistry and the protein folding process are usually ignored, and each protein is treated as a collection of features (binding sites and phosphorylation sites) whose availability is affected by (de)complexation (binding to other molecules) and (de)phosphorylation interactions. A well known example of this is the model for the EGFR/Ras/ERK pathway (Schoeberl et al., 2002). In that each protein is considered as a collection of sites and switches, each of which can be, at any given time, either available or unavailable. An available switch on protein or protein complex can be turned on or off, resulting in a new state where a new collection of switches and sites is available. Proteins can join at matching sites, to form bigger and bigger complexes. Two protein complexes can combine at available sites, or one complex can split into two, resulting in a new state where a new collection of switches and sites is available. The availability of sites and switches in a complex is the state of the complex. A system is a multiset of (disjoint) complexes, each in a given state (Figure 2.08).

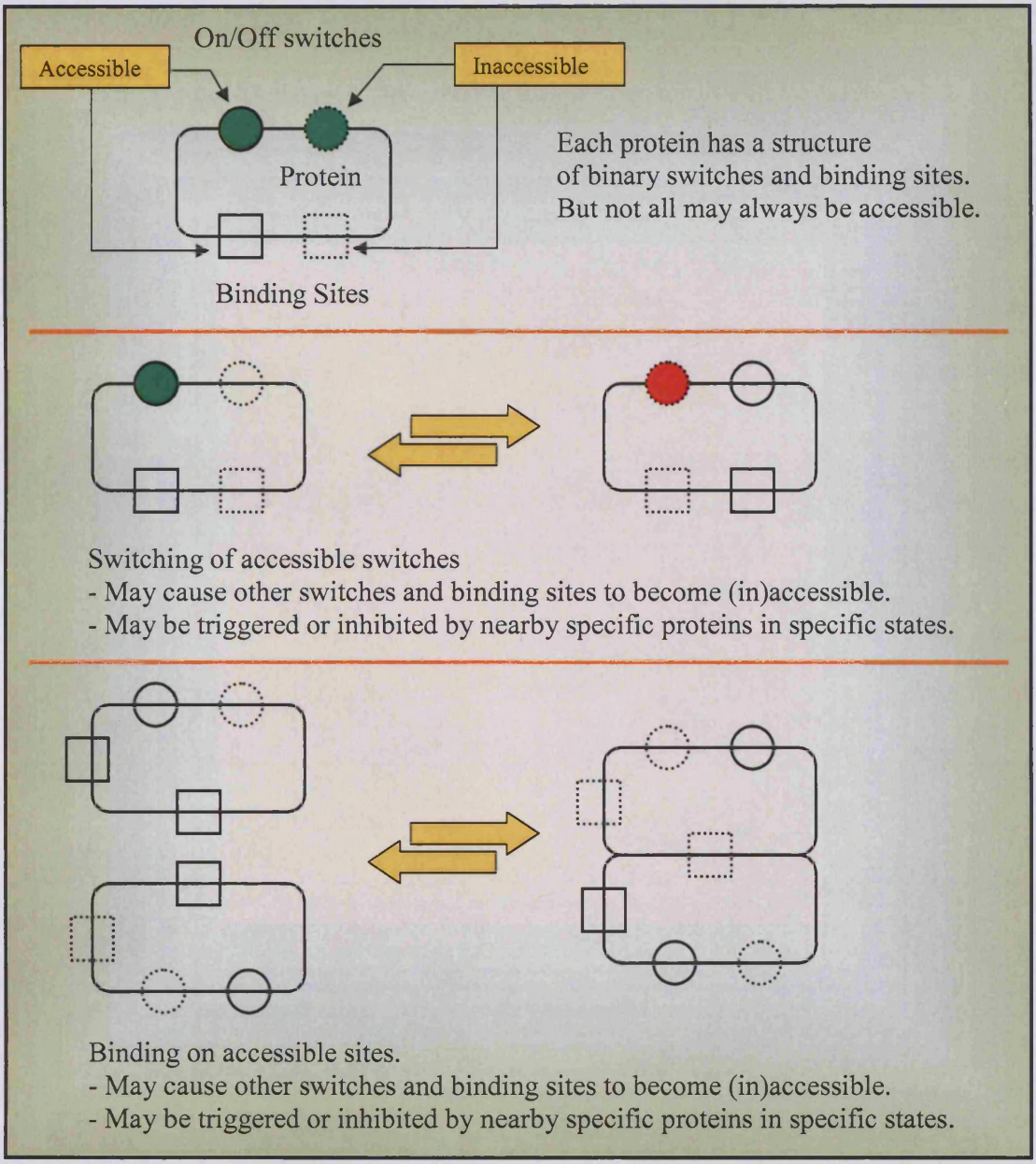

Figure 2.08. Description of protein states. Proteins are modelled as structures of binary switches and binding sites.

It was decided that it would be beyond the purpose of this work to apply the highest level of chemical resolution and detail for the biochemical processes in the integrin/FAK/Src model and thus the protein states for the model were set up as described above. For example, ATP levels and turnover were not modelled explicitly for the phosphorylation events; rather the focus was given on how many molecules of a single component were

phosphorylated and how many phosphorylation reactions affected that particular component.

2.3.5 Extent of the construction and combinatorial complexity

The third step involved defining the extent of the model: how many molecular states and reactions to include and the outer limits of the model. This is a very important process as small numbers of intracellular proteins operating in combinatorial manner can allow for a large diversity of functions in signalling networks. Specifically, the functional states of the biochemical network were much larger than the number of molecules involved simply because a single molecule can exist in more than one functional state (Figure 2.13).

Knowing the physical limits to how many reactions and states a system can contain, can be seen as additional information describing its mechanism/design and therefore aiding in higher definition of its properties. Such complexity plays a key role in the specificity and robustness of biological process. For example, molecule structures have a highly complex structure made of huge variety of amino-acid combinations. This complexity is necessary for two main reasons: to assign a unique specific function to the molecules (as the amino-acid combinations are vast) while simultaneously providing a good measure of robustness to their structure (so not every single amino acid change would easily disrupt the structure). Therefore, working towards complexity was envisaged as being an important approach to refine/increase the accuracy of the model and thus dictated the amount of molecular states and reactions that should included.

A part of the model is presented here to demonstrate how complexity affected the model in its diagrammatic representation and therefore also to its mathematical description (for more details see chapter 3). This example depicts a part of the pathway involved in the shear stress response and demonstrates how the model was expanded and improved in time by adding further molecular reactions.

Molecules

Calcium (Ca^{2+})	Calpain (protease)	Talin
Integrin receptor	ECM ligand (e.g. fibronectin)	Paxillin
FAK	PTP-PEST	Src kinase
Hypothetical Src PTP	RPTPα	Csk kinase

Molecular interactions (1,2.. indicate the number of reactions described)

Ca^{2+} binds to calpain and RPTPα and activates them. **(1,2)**

Active calpain cleaves talin into cleaved talin. **(3)**

Talin and cleaved talin bind to integrins and pre-activate them at different rates. **(4, 5)**

Fibronectin binds to integrins and fully activates them. **(6)**

Paxillin binds to functionally active integrins and FAK. **(7, 8)**

FAK phosphorylates paxillin and itself on pY1. **(9, 10)**

Src kinase binds to FAK pY1 which allows phosphorylation of Src pY2 activating it **(11)**

PTP-PEST dephosphorylates FAK and paxillin. **(12, 13)**

Phosphorylated Src on pY2 in turn phosphorylates integrins and FAK pY2. **(14, 15)**

A Src phosphatase dephosphorylates Src pY2 inactivating it **(16)**

RPTPα dephosphorylates Src pY 1 activating it. **(17)**

CSK phosphorylates Src on pY1 inactivating it. **(18)**

There are a total of 18 molecular interactions (Figure 2.09).

The diagrammatic depiction of the processes describes precisely the information given regarding the system but has neither interpolative nor extrapolative predictive power and could not successfully accommodate dynamics that would reveal regulatory responses in time that would not be "visible" by a diagram alone (i.e. emergent properties – discussed in chapters 3 and 4).

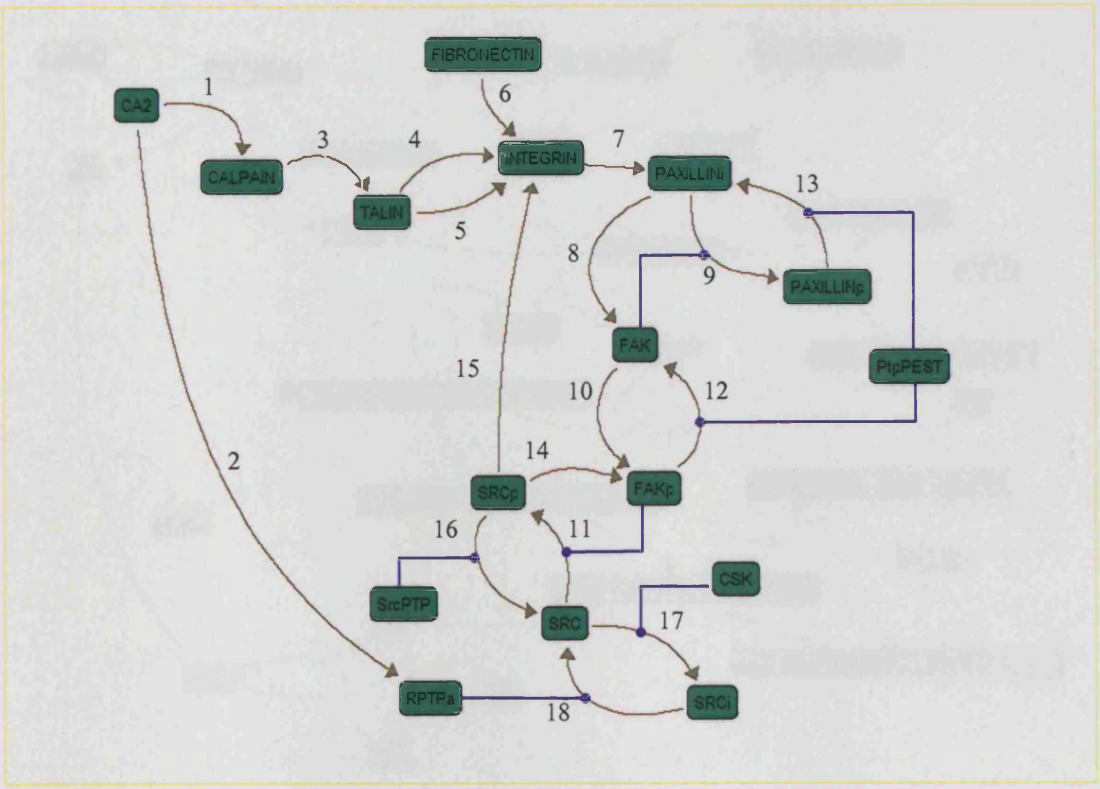

Figure 2.09. Model of 18 molecular interactions. PAXILLINi and PAXILLINp stand for the unphosphorylated and phosphorylated forms of paxillin respectively. The same notation is used for Src kinase as well (shown as SRC). FAKp is FAK phosphorylated. PtpPEST = PTP-PEST, CA2 = Ca^{2+}, RPTPa = RPTPα.

In order to allow dynamic modelling, a more complete version of the same model was built representing explicitly all the reactions that take place in the system in time. This involved the identification and representation of all intermediate products that precede the effect of molecular interactions. Specifically, if a kinase interacts with and phosphorylates a certain protein then there should be a step where the kinase and the target protein associate with each other followed by the transformation reaction itself, which involves phosphorylation (e.g. Src binding and phosphorylating FAK). The presence of the complex of the kinase with the target protein as a distinct molecular species in the model is very important as its quantity and rates of formation/disassembly affect the overall output of the interaction. By reforming the same pathway (Figure 2.09) the network this time consisted of a total of 45 molecular reactions (Figure 2.10).

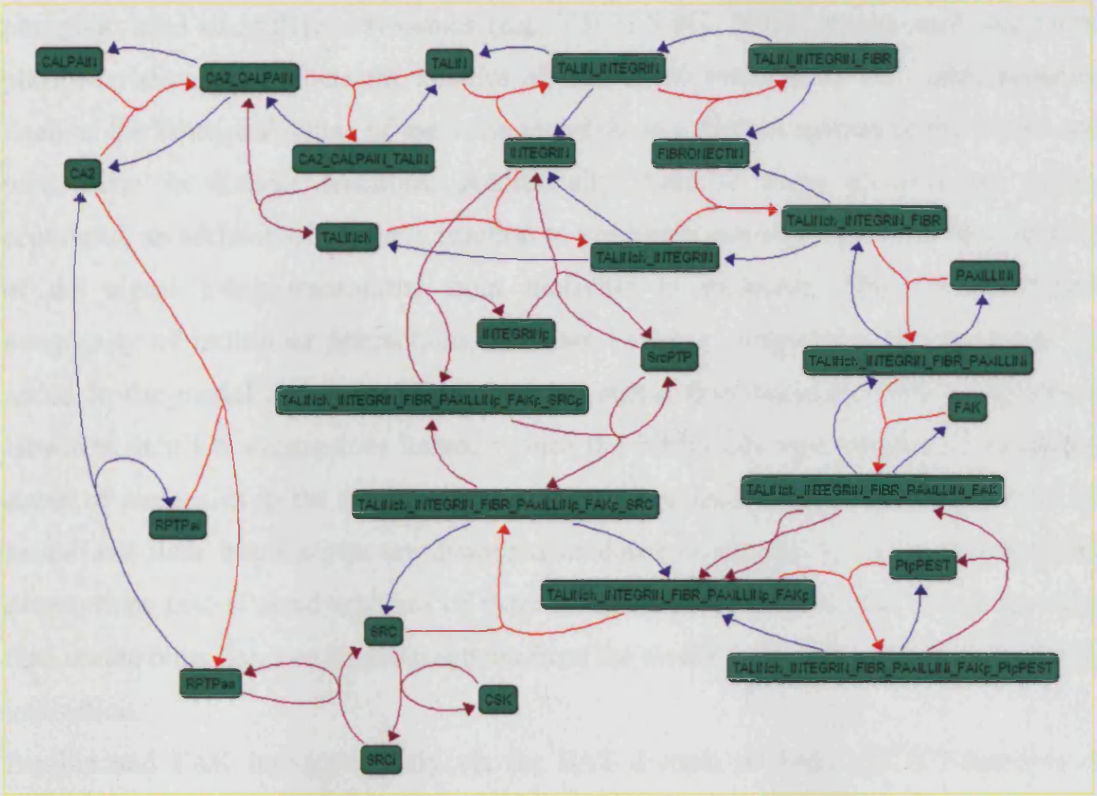

Figure 2.10. Expansion of the initial 18 reactions to 45 reactions. Notation is same as in Figures 2.08 and 2.09. Each association results in a new molecular species in the model and all reactions are represented. FIBR = fibronectin, SRCi = Src kinase inactive, RPTPaa=RPTPα active.

Even though there is a clear improvement to the model (the feedback created by interaction of Src with integrin shown in Figure 2.09 as reaction number 15, is given in the above Figure in much more detail), it still lack robustness since if one interaction is removed the system automatically collapses and its function terminated. For this reason additional detail and system complexity was added by considering multiple functional states of molecules and their interactions (through the addition of further biological information and or assumptions based on general cellular signalling principles).

2.3.6 Multiple functional states of molecules – a case example

In the model the various functional states of a molecule equal the number of different states caused by transformations and binding events (see section 3.1.3). For example FAK exists in many functional states: as a monomer, bound to one or more proteins and/or

phosphorylated on different tyrosines (e.g. Y397, Y861, Y935) where each additional phosphorylation event alters the kinetics of subsequent interactions with other proteins. Each of the functional states of the same molecule is a distinct species in the model and participates in distinct reactions. Additionally, because some proteins are highly connected, an addition of a simple reaction to a network can significantly affect the flow of the signal being transmitted from molecule to molecule. This 'combinatorial' complexity of molecular interactions increases as more components and reactions are added to the model and the regulation of the signal flow becomes more complicated. However, implicit assumptions helped reduce the potentially vast number of functional states of molecules in the model (all the assumptions made for the construction of the model and their implications are described in detail in chapter 3). An example of the assumptions that allowed addition of extra reactions to the model and the assumptions that, on the other hand, excluded reactions from the model is given here for paxillin FAK-interaction.

Paxillin and FAK interact directly via the FAT domain of FAK and LD domains of paxillin (Figures 1.19 and 1.20). However it is not clear whether these two molecules only bind to each other in cells when they are in focal complexes and via a third interface provided by integrins, or whether they can actually bind to each other outside of focal complexes. The model was therefore refined to include both conditions with the difference that when paxillin and FAK bind to each other independently of integrins, they do so at a slower rate. This assumption is derived from the fact that the interaction in the cytosol would depend on random diffusion and collision of the molecules without the help of a docking site such as a focal complex.

In either of these cases, they need to be regulated by phosphatases. This introduces certain hypotheses in the model. FAK binds to paxillin which allows for autophosphorylation of FAK on Y397 and phosphorylation of paxillin on Y118 by FAK. Although there is much debate regarding the cause of autophosphorylaton of FAK (e.g. transphosphorylation) FAK is assumed to bind to paxillin in order for Y397 phosphorylation to take place for three reasons. First, if paxillin is not required for this event its presence in the focal complex for reasons of signalling would not be required. Second, the only verified known phosphatase that interacts with FAK and paxillin is PTP-PEST which binds to paxillin (not FAK) (Shen et al., 1998) and thus without paxillin FAK dephosphorylation could not

take place. Third, if FAK is being phosphorylated by trans-phosphorylation (FAK-to-FAK), association of FAK to paxillin is required to bring multiple FAK molecules close together at focal complexes. Paxillin is not required for localisation *per se* of FAK at focal complexes but for the enhanced association of FAK with the complex (see section 3.5). The model therefore incorporates a case where phosphorylation of FAK Y397 and paxillin Y118 and dephosphorylation of FAK Y397 is dependent on association between the two molecules. The FAK-paxillin interaction however is assumed independent of phosphorylation because there is not evidence to suggest that pre-phosphorylated paxillin and FAK cannot bind to each other.

All the above lead to the following implications:

It is possible that FAK and paxillin dissociate from each upon dephosphorylation by PTP-PEST (Figure 2.11a). However it is also possible that they dissociate (at slower or faster rates) before the dephosphorylation step takes place. In that case each individual molecule may be dephosphorylated separately (Figure 2.11b) or one of the two molecules may be dephosphorylated by the phosphatase before they both bind to each other again (Figure 2.11c). This results from the fact that FAK cannot be dephosphorylated if not bound to paxillin while paxillin as a monomer could. Finally, FAK molecules could phosphorylate each other via a transphosphorylation event, dependent upon integrin clustering (Katz et al., 2002), Figure 2.11d.

It is plausible that there is a pool of each functional state for FAK and paxillin within the cell. Consideration of these events and functional states of molecules increases the number of molecular species present in the model. The addition of corresponding reactions to the mathematical model could have large effects on the overall dynamic behaviour and robustness of the system, since disruption of one event or a perturbation would not necessarily disrupt the system but could produce only a small change in the overall dynamic behaviour (see chapter 3). Since the aim of the model was both to provide insight into the shear stress response and to allow the effects of many perturbations to be predicted, it was decided to include as many functional states and reactions as feasible in the model (as demonstrated above). Molecular interactions were therefore dealt similarly for most parts of the model.

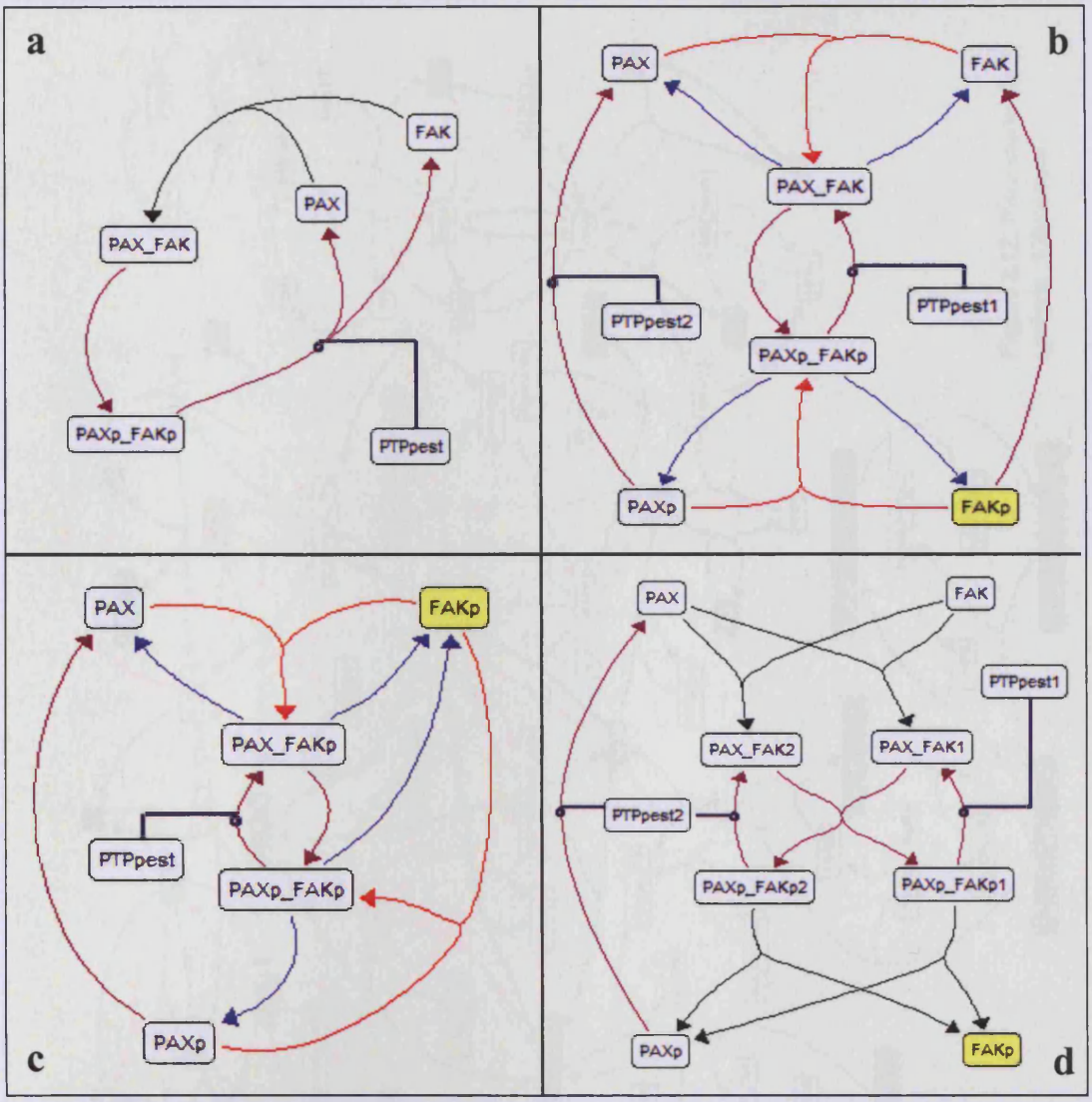

Figure 2.11. Interactions of FAK-paxillin and related molecules. PAX = paxillin. The letter (p) following the name of any species specifies they have been phosphorylated by a kinase. Associations are shown in red, dissociations in blue and transformation in brown.

This approach taken led to a considerably more complex version of the model where each molecule could exist in multiple different forms and it allowed for inclusion of molecular events that are likely to take place but frequently not considered (e.g. dissociation of talin from a protein complex that contains talin, integrins, fibronectin, paxillin, FAK and Src). The resulting model (Figure 2.12) was used to write the necessary chemical reactions describing the integrin/FAK/Src molecular pathway (see section 3.3.2 and 3.3.1).

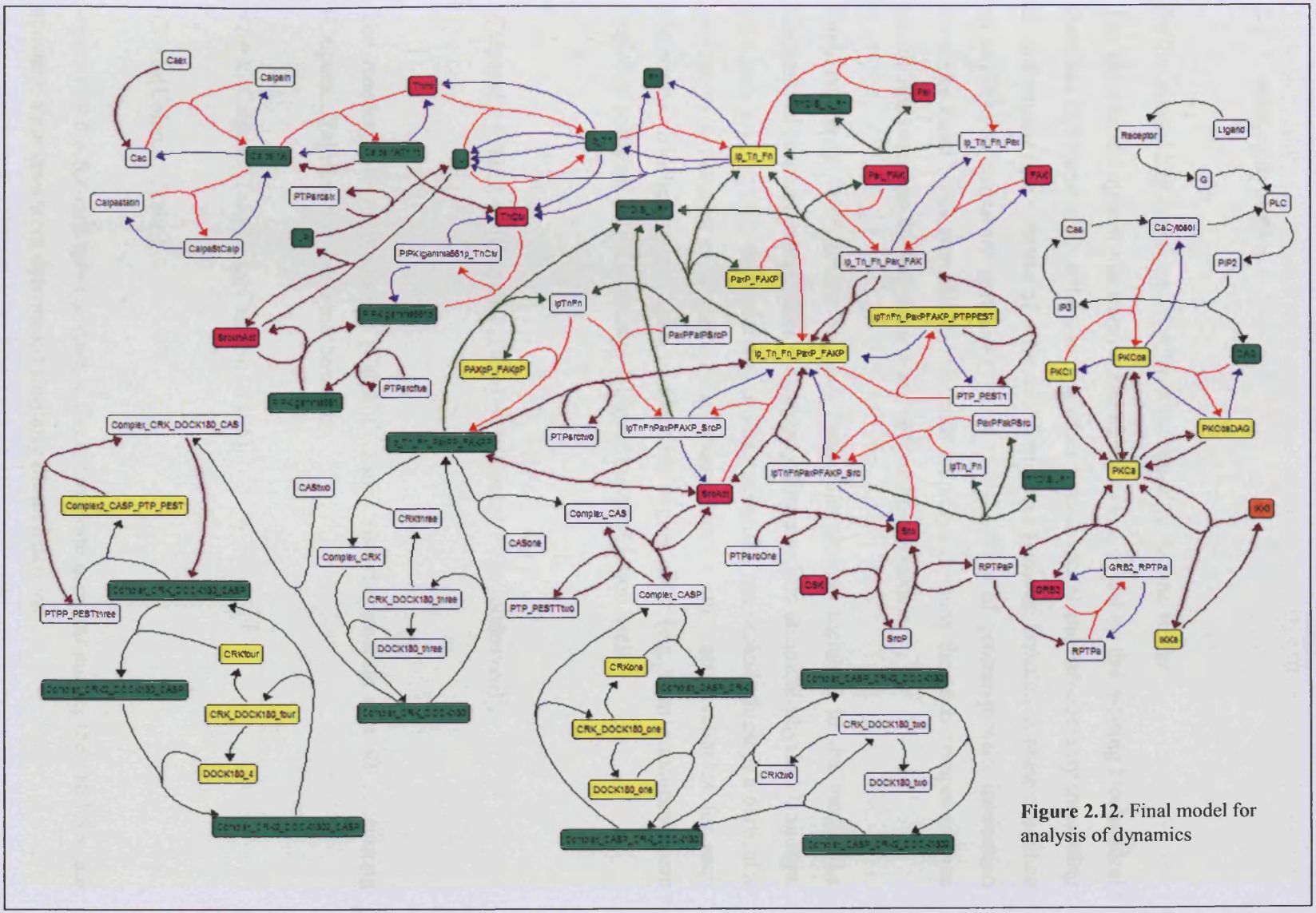

Figure 2.12. Final model for analysis of dynamics

2.4 Adding dynamics

2.4.1 Assembling the system of differential equations for the model

The static model system was transformed into a kinetic model by first writing biochemical formulae representing all molecular interactions in the model and subsequently translating these formulae into a system of ordinary differential equations. Solution of these equations required some necessary parameter values. In the case of protein-protein interaction networks these parameter values constitute the concentrations for each component and kinetic rate constants for interactions and enzymatic reactions.

First, rate laws were written for each molecular process included in the model (i.e biochemical reactions) to translate the pathway diagrams into chemical-physical language. Rate laws are algebraic expressions for a flux (molecules per second) through a particular process as a function of the molecular abundances or other state variables for each component. Biochemical reactions of second or higher order (e.g. transformations) were treated as collision of two molecules followed by the reaction itself:

$$[\text{Calpain}] + [\text{Talin}] \underset{k_2}{\overset{k_1}{\leftrightarrow}} [\text{Calpain...Talin}] \xrightarrow{k_3} [\text{Calpain}] + [\text{Talin(cleaved)}],$$

The reaction rate $v1$ producing [Calpain...Talin] and the reaction rate $v2$ consuming [Calpain...Talin] in the above reaction are:

$$v1 = k_1[\text{Calpain}][\text{Talin}] - k_2[\text{Calpain...Talin}],$$

$$v2 = k_3[\text{Calpain...Talin}],$$

where k_1 is the forward rate constant, k_2 the reverse rate constant and k_3 the catalysis rate constant. Rate laws were determined similarly for all reactions.

In order to know the number of molecules of a component that exist in any state at all times however, it is necessary to sum all inputs and outputs that lead to and from that component through a given molecular pathway at any given time. This is essentially the rate of change of concentration of each molecule in time and can be calculated with ordinary differential equations. ODEs can be generically described by the following equation:

$dx_i/dt = f_i(x_1,\ldots,x_n; p_1,\ldots,p_m)$, $i = 1,\ldots,n$

where dx_i/dt is the rate of change of concentration of the i-th component with time, f_i gives the function that describes how each of the components directly affects the rate of change of the i-th component and p_j is the value of the j-th (where j a number between 1 and m) parameter (e.g. rate constant, affinity constant). The exact forms of these functions (f) depend on the stoichiometry of the reaction network and the assumptions made about rate laws for each reaction.

The dynamic model was set up as a system of ODEs written for each molecular state by setting its rate of change to be equal to the sum of the processes or rate laws that produce this molecular species minus those processes (rate laws) that consume it, therefore representing the mass conservation for each state. This is given by the following master equation:

$$\frac{d[C_i]}{dt} = \sum v_{production} - \sum v_{consumption},$$

where C*i* represents each of the molecular species included in the model and $\sum$ represents the sum of the rate laws (**v**) that affect the concentration of that species. Accordingly, the ODE for the [Calpain...Talin] component can be written as:

$d[\text{Calpain...Talin}]/dt = v1 - v2$,

which becomes:

$$d[Calpain...Talin]/dt = k_1[Calpain][Talin] - k_2[Calpain...Talin] - k_3[Calpain...Talin].$$

2.4.2 Parameter value collection for the dynamic properties of interactions

Collection of parameter values for each of the components and their interactions is essential for the construction of a kinetic model; however their availability is also often a limiting factor (Bhalla and Iyengar, 1999). Some information regarding parameter values was obtained from public repositories such as the DOQCS (Database of Quantitative Cellular Signalling) database (Bhalla and Iyengar, 1999). In most cases however, quantitative information was manually extracted from primary research papers.

When extracting data from the literature, annotation and explicit statement of assumptions were critical factors in defining the biochemical parameters. Contextual information was found to be crucial for parameter selection and development of a realistic model; for example in cases where quantitative information was not available for a specific molecule but was available for a related molecule, this was selected instead (see sections 3.3, 3.5). In some other cases the parameter values were not measured but rather estimated in the first place and were either discarded or empirically given a lower confidence (see sections 3.3 to 3.5). This was the main reason for manually extracting biochemical parameter values and information from the literature and not automating their collection from the literature using NLP (Natural Language Processing) algorithms or other text mining protocols (Hoffmann et al., 2005) like the one used in the iHOP database (http://www.ihop-net.org/UniPub/iHOP/).

Often the parameter values needed for specific reactions were not available but could be obtained from related data using simple calculations. For example the bimolecular reaction:

$$[FAK] + [paxillin] \underset{k_r}{\overset{k_f}{\leftrightarrow}} [FAK...paxillin],$$

represents both molecular association and dissociation and can be described as:

$$d[FAK...paxillin]/dt = k_f[FAK][paxillin] - k_r[FAK...paxillin],$$

where k_f and k_r are the forward and reverse constants respectively. In many cases the values for both k_f and k_r were not available in the literature. Therefore, based on the reported K_d dissociation constants, k_f and k_r had to be calculated from:

$K_d = k_r / k_f$.

Enzymatic reactions such as phosphorylations and dephosphorylations are commonly represented by *Michaelis-Menten* reactions in which a substrate (S) binds an enzyme (E) to form an enzyme-substrate complex (ES), which undergoes a catalytic reaction, releasing the product and unaltered enzyme as:

$$E + S \underset{k_2}{\overset{k_1}{\leftrightarrow}} ES \xrightarrow{k_3} E + P, \quad \Rightarrow \quad Src + paxillin \underset{k_2}{\overset{k_1}{\leftrightarrow}} Src\text{-}paxillin \xrightarrow{k_3} Src + paxillin(Y^p).$$

where Y^p is a phosphate on a tyrosine.

The *Michaelis Menten* equations are described by two unique constants, V_{max} and K_m. V_{max} is the *maximum velocity* of an enzyme-mediated reaction and is determined by increasing the substrate [S] concentration until a constant rate of product formation is achieved. K_m is the *Michaelis* constant and represents the substrate concentration when the rate of the reaction is half of its maximum. V_{max} and K_m values are both determined by experimental observations.

For the transformations of the integrin/FAK/Rac model, the reaction rates for the first reaction, k_1 and k_2, were generally not given in the literature. However k_3, the catalysis reaction rate, can be given from the experimental K_{cat} value, by dividing the V_{max} value by the concentration of the enzyme, as:

$K_{cat} = Vmax / [E]$.

where $k_3 = K_{cat.}$

Thus, based on the K_m values and k_3 values, the *Michaelis Menten* equations were converted into association-dissociation reactions where k_1 and k_2 values were calculated from the following the equation:

$K_m = (k_2 + k_3) / k_1.$

There were no *in vivo* data available the numerical values of molecular reaction rate constants for the components of the model, therefore all parameter values were obtained from *in vitro* data. *In vitro*-generated numerical data do not necessarily apply under *in vivo* conditions but this is a limitation that cannot be avoided.

2.4.3 Optimisation (parameter estimation)

Parameter values that were necessary but not available in the literature were estimated by fitting the model to published time-dependent quantitative observations (Table 2.2). Data fitting was also used when some parameters were given but had to be calibrated to investigate certain emergent behavioural properties of the molecular network (changing the values of parameters slightly could have large influences in the dynamics). All the experimental observations used for the data fitting were the result of the measurement of differential activity of proteins upon shear stress stimulation at various time points. Since this is a model for the shear stress response any observations derived from other experimental conditions would not be relevant. Furthermore, the use of these data was restricted to those given from measurements that were performed on bovine aortic endothelial cells in order to avoid potential physiological differences. However in some cases data from experiments on human umbilical vein endothelial cells were also used due to limited availability of these profiles. From the 120 activity profiles collected (Excel file in CD attached) less than 10 were used (Table 2.2) for the integrin/FAK/Src model due to type of experiment/shear stress condition/cell type/ timescale restrictions.

The data fitting was achieved by method of optimisation. In general terms, optimization is the utilization of algorithms that search the optimal space of solutions for a specific

problem. Optimization problems are concerned with locating optima (maxima or minima) of functions. The optimization problem can be described as follows:

Given a real-valued scalar function $f(x)$ of n variables $\boldsymbol{x} = (x_1,...,x)$, find a minimum of $f(x)$ such that $g_i(x) \geq 0$ with $I = 1, ..., m$ (inequality constraints) and $h_j(x) = 0$ with $j = 1,...,m$ (equality constraints).
In general, the objective function $f(\boldsymbol{x})$ and the constraints $g_i(x)$ and $h_j(x)$ are non-linear, although frequently the only constraints are linear boundaries of the form $\alpha_i \leq x_i \leq b_i$.

The field of optimization is vast and there are many methods that can be utilised for parameter space searches in science and engineering. Optimisation has also received great attention in biological modelling (Faller et al., 2003, Kutalik et al., 2004, Swameye et al. 2003., Zak et al., 2003, Mendes and Kell, 1998, Moles et al., 2003, Rodriguez-Fernandez et al., 2005). Table 5 provides examples of various optimisation methods, however discussing the difference between all the various optimizations methods is outside the scope of this thesis. Optimisation methods are routinely used in parameter fitting problems, as a means of designing improved processes or devices, in search problems or as learning algorithms (Fletcher, 1987). In chemical kinetics, some of these methods are used in combination with simulation for parameter estimation (fitting). Linear or non-linear least squares regression is used to estimate kinetic constants from measured rates and concentrations.

Optimisation methods	
Random Search with uniform distribution	------
Steepest descent with finite differences gradient	Fletcher, 1987
Truncated Newton	Nash, 1984
Levenberg Marquardt algorithm *	Levenberg, 1944; Marquardt, 1963
Adaptive nonlinear least squares (Gauss-Newton)	Dennis et al, 1981
Hooke and Jeeves direct search	Hooke and Jeeves ,1961
Genetic algorithm based search	Michalewicz, 1994
Meta- evolutionary programming	Fogel et al, 1992
Monte Carlo simulated annealing algorithm	Corana et al, 1987

Table 2.3. Examples of optimisation methods. * The Levenberg-Marquardt algorithm was the method of choice for optimisation in the current model.

Optimisation was used in order to give certain hypotheses generated by the model the best chance to account for the available experimental data in hand. What was used as a clear measure of fit was the weighted sum of the squares of the errors between the model solution and the experimental time-dependent quantitative observations (i.e. activity profiles). Accordingly, every set of parameter values optimised corresponded to a numerical value of the weighted sum of squares. Ideally, for a perfect fit, the sum of squares would be zero; this however is not usually expected since models are not expected to be 100% accurate. The task of optimization was to determine the set of parameter values that yielded the best or most optimal fit. This was attained by allowing extension of specific parameters to defined intervals or replacement of values when more than one set of values are available for a particular molecular process. This also provided a way of assessing the validity of the extracted kinetic values, since in some cases these were also estimated (see chapter 3). Naturally, the difficulty in the exploration of the parameter space increases as the parameter space increases itself. For this reason we applied optimisation to only few parameters each time and against specified smaller signalling modules in the network rather than the whole signalling network itself.

Among the various optimisation algorithms, the Levenberg-Marquardt algorithm (Levenebrg, 1944; Marquardt, 1963) is particularly suitable in least squares problems based on sum of squares functions and was chosen as the optimization algorithm for our model. Figure 2.14 shows the specification of the generic algorithm (based on the Levenberg-Marquardt method) that was implemented to perform numerical optimization and parameter fitting. The Matlab script implementing the algorithm and used for optimisation can be found in the CD included.

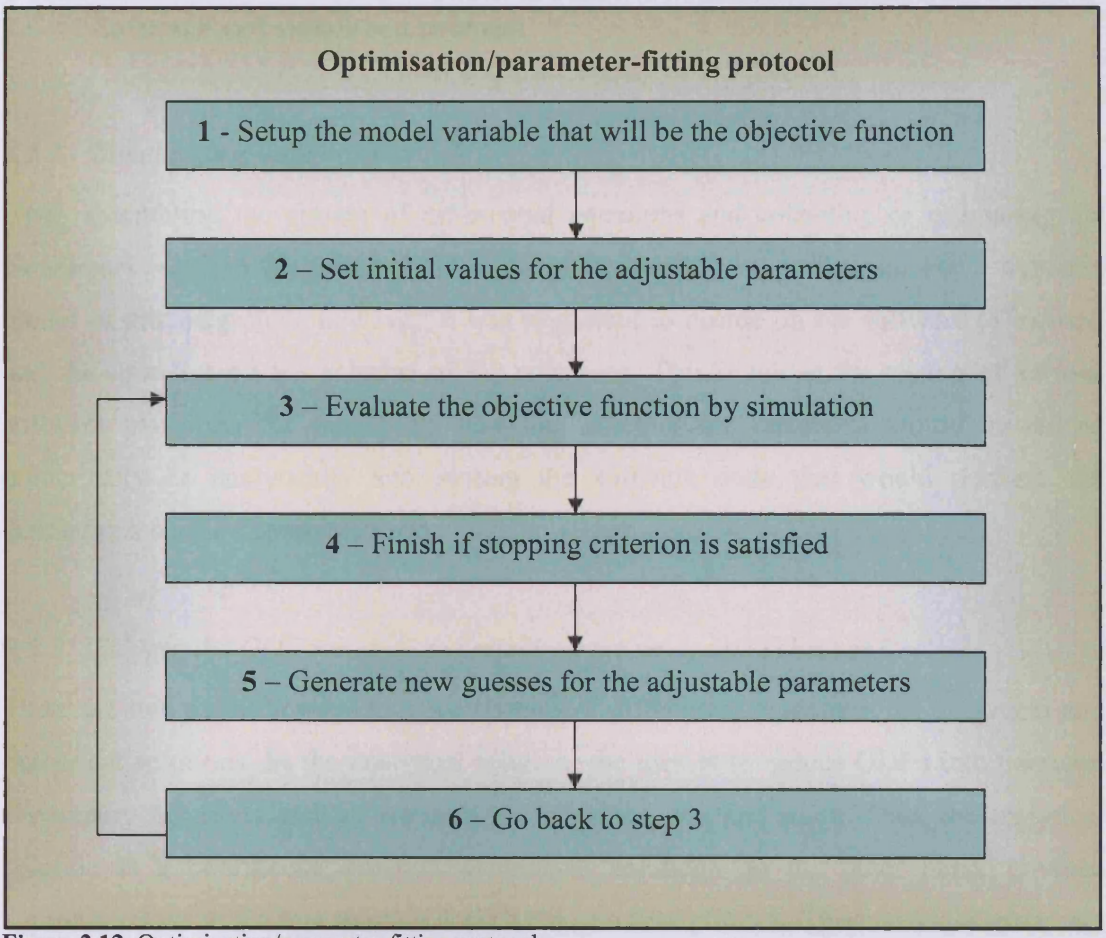

Figure 2.13. Optimization/parameter-fitting protocol.

2.5 Software and simulation protocol

2.5.1 Simulation considerations

Upon assembling the system of differential equations and collecting or estimating the parameters required for their solutions, simulations could be performed. For a dynamic model of this magnitude however, it was important to decide on the software to be used and the specifics on the solution of the equations. This involved the testing of various software platforms for modelling, choosing whether the equations would be solved numerically or analytically and writing the software code that would perform the simulations on the chosen platform.

2.5.2 Solving the ODE system – numerical versus analytical solutions

There are two possible ways to solve systems of differential equations, the analytical and numerical solutions. In the analytical solution, the idea is to reduce ODEs into common elementary functions such as exponentials (e^t), sines, cos, and so on. Thus, the analytical solution is a continuous function. Numerical solutions on the other hand, produce approximations to the true solution at each discrete time point, t_k. These become extremely useful when:

a) the system of differential equations becomes large,
b) each of the equations in the system becomes complex,
c) the equations do not have analytical solutions (e.g. for non-linear equations).

For systems containing only few chemical reactions, differential equations can be solved analytically. However, it is by far easier and more appropriate for large scale models such as the one in this study to be solved using numerical methods, such as Runge-Kutta or Euler methods (Burrage et al., 2004). The choice of method may often require the model to be modified. Euler's method for instance, is often applied to a deterministic model by calculating the changes in each chemical species in a fixed time step by assuming that the concentrations of the other species are held constant.

2.5.3 Simulation Software

Several modelling environments are now available that can be used to develop kinetic simulation of signalling pathways and networks. These programs can simulate the steady-state and kinetic behaviour of reactions. SCAMP (Jarnac) for example (Sauro, 1993) employ non-standard biochemical languages to specify a model in a series of command files. The simulator uses these to construct differential equations which it then solves using numerical integration. More recent programs like GEPASI (Mendes, 1993) allow the user to enter the stoichoiometric chemical equations using a graphical user interface; these are converted into differential equations and solved as before. Each modelling platform has particular advantages and disadvantages based on the specific purpose they were built for (some for example are designed to operate within the framework of metabolic control analysis). All of them however, at their core, use built-in mathematical solvers that integrate and solve differential equations.

Programs specialised for simulating signalling pathways like Jarnac (Sauro, 1993) and GEPASI (Mendes, 1993) were tested but they could not handle the large number of equations in the model and the 'reaction stiffness' problem that sometimes appeared. Specifically, if a system contains two chemical reactions which occur on very different time scales, the simulation algorithm must use a small time step size appropriate to simulating the faster reaction; with the result that a large number of iterations will be required to simulate the slower reaction to any appreciable degree. This is commonly called as reaction stiffness and frequently results in computers crashing while trying to perform the integrations. The mathematical suite Matlab (http://www.mathworks.com/) was chosen instead to serve as the simulation environment because it provides several powerful and flexible programming constructs able to handle large number of integration problems with algorithms able to bypass problems such as "stiff" reactions. The Matlab solvers ode45 (non-stiff problems) and ode23s (stiff problems) were engaged for the simulations (i.e. numerical solutions) of the model. For description of Matlab numerical routines and ODE solvers see
http://www.mathworks.com/access/helpdesk/help/techdoc/ref/ode23.html.

2.5.4 *Simulation protocol*

A simulation protocol is simply a timeline of predefined functions that calculate the rate of change in state variables upon specifying a set of initial (and/or boundary) conditions to be imposed on the solution of the differential equations. The standard simulation protocol followed in this project is described in Figure 2.14. The files containing the Matlab can be found in the CD attached. Programming guidelines have been followed to minimise errors, to make the source code accessible to customisation by other developers and to simplify the implementation of future modifications. The code is commented with lines describing the properties of each function.

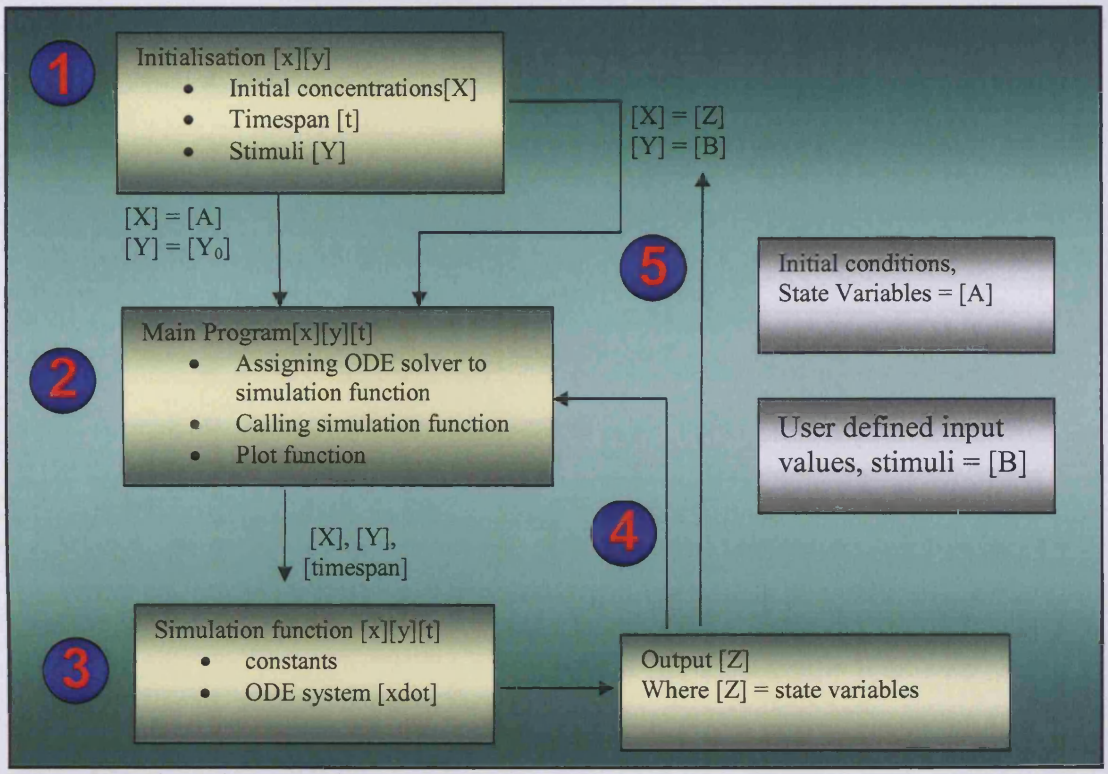

Figure 2.14. Simulation protocol.
1) User input is defined: Initial values are given to a) concentration of species (state variables), b) the stimuli that will be applied and c) the timespan (time length) and time step of simulation. The initial concentrations for the intermediate species (e.g. protein complexes) are zero in the first round to calculate the steady state of the system. **2)** The user defined input is passed to the main program: The program is responsible for a) assigning the ODE solver that will be engaged, b) calling the simulation function (that contains the ODEs) and c) for plotting the generated values (simulation results) after completion of the simulation for the given timespan. **3)** The simulation function is engaged for the length of simulation (timespan) with the predefined ODE solver and the defined user input. The simulation function contains the parameter constants and the system of ODEs (denoted as xdot). **4)** The simulation-generated values are passed back to the main program for plotting. **5)** The simulation-generated values replace the original values of state variables and steps 2 to 4 are re-iterated to calculate the concentration of species under the given stimuli (e.g. shear stress).

2.5.5 Summary

This chapter described the techniques and principles followed for building the model-system for the events describing the intracellular signal transduction which occurs in endothelial cells as a response to fluid flow. First, a comprehensive static map for integrin signalling was created for the molecular events taking place upon shear stress stimulation. A part of the static map was subsequently transformed into a dynamic model by translating the molecular reactions of interacting proteins of the model into ordinary differential equations. These equations required parameter values for their solution during simulations, which were collected (or estimated) for all the molecular reactions included in the dynamic model. The biology, details of mechanism and hypotheses regarding each molecule and their reactions in the network are discussed along with description of the dynamic model in chapter 3.

3 CHAPTER 3 - MODELLING THE SHEAR STRESS RESPONSE

3.1 Introduction

Modelling of biological systems can enable both qualitative and quantitative predictions of the system's behaviour (i.e. static model of shear stress signalling, see chapter 2). This chapter develops the mathematical description of the molecular events of the shear stress response and analyses the underlying assumptions and hypotheses that constitute the various parts of the model. Various mathematical models have been developed to describe both the different modalities by which fluid flow-induced shear stress initiates the signal that modulates the endothelial response and how this signal is propagated within the cell. Differential equations were generated as described in section 2.4.1 to express the rate of change of concentration for each molecule in the model.

3.1.1 Annotation of reactions

Part of the model is represented by state transition diagrams with various node structures (Figure 3.1). These diagrams consist of vertexes and edges and are structured in a similar way to the architecture of the process diagrams recently described (Kitano et al., 2005). There are two classes of vertices. One class of vertex (state node) represents molecules involved in the reactions, such as proteins and ions. The other class (transition node) represents modulations imposed on the reaction, such as catalysis, association and dissociation (Figure 3.01). There are also two types of edges: those from a state node to a transition node and those from a transition node to a state node. Different visual icons and arch colorations were used to distinguish between state entities transition nodes respectively.

The model was divided into modules to simplify analysis and answer questions regarding the dynamic behaviour and regulation of particular molecules. The modules were created to provoke distinct questions regarding the dynamic behaviour and regulation of particular molecules that control the overall response of the system. All equations have been numbered for easier navigation.

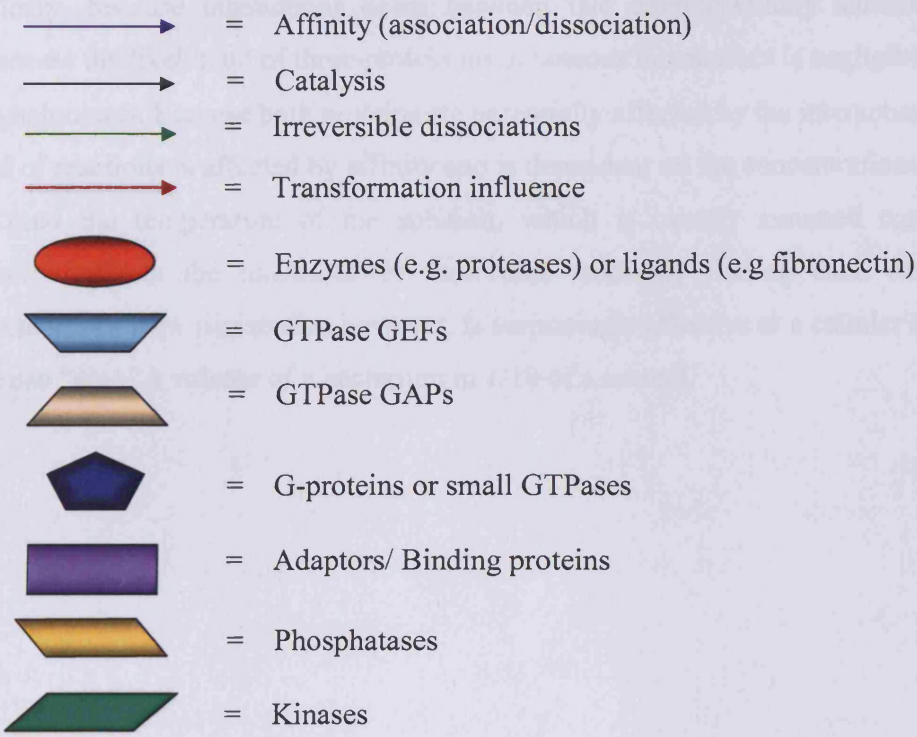

Figure 3.01. Symbols used in the model.

3.1.2 Global consideration for the entire model

The model system investigates the molecular response of endothelial cells to shear stress at relatively short periods of time (seconds to few hours). During the time period simulated by the model, additional biochemical responses will take place that cannot all be modelled in parallel in this investigation. Therefore the model is only valid under certain crucial underlying assumptions. These are:

- The cells are not regulated by external factors other than the ones considered.
- No other pathways affect any of examined molecules as a function of shear stress.
- Cells do not grow, divide, or undergo any other morphological changes over the simulation periods.

Furthermore, the model simulates the signalling operation between protein molecules as fast, synchronous, binary interactions:

- Binary, because interactions occur between two complementary surfaces and because the likelihood of three-protein instantaneous interactions is negligible.
- Synchronous, because both proteins are potentially affected by the interaction.

The speed of reactions is affected by affinity and is dependant on the concentrations of the reagents (and the temperature of the solution, which is usually assumed constant). Concentration affects the likelihood of molecules randomly finding each other by Brownian motion. Brownian motion however, is surprisingly effective at a cellular scale: a molecule can "scan" a volume of a bacterium in 1/10 of a second.

3.2 Endothelial calcium dynamics (Module 1)

3.2.1 Module description

Shear stress induces an increase in cytosolic calcium concentration [Ca^{2+}] via: 1) stretch-activated calcium channels and 2) G-protein-induced calcium release from intracellular stores. The mathematical model for calcium dynamics here is based on that of (Wiesner et al., 1996).

Calcium is a key intracellular second messenger in almost all eukaryotic cells. In endothelial cells intracellular Ca^{2+} serves as a positive or negative regulatory signal for a range of cell functions, including: secretion of vasoactive agents, such as nitric oxide (NO) and prostaglandin, adhesion molecules, growth factors and various inhibitors; cell alignment in the direction of blood flow; cell proliferation and apoptosis (Schilling and Elliott, 1992; Tran et al., 2000). Under resting conditions, the concentration of free Ca^{2+} in the cytosol is maintained at a very low level by active transport mechanisms that pump Ca^{2+} out of the cell. Ca^{2+} is also pumped into internal storage compartments, primarily the endoplasmic reticulum (ER), which contain the majority of a quiescent cell's intracellular Ca^{2+} (Alberts, 1994). Transduction of an external biochemical or mechanical signal can stimulate both a release of Ca^{2+} from internal stores and an influx of Ca^{2+} across the plasma membrane (Alberts, 1994). This can result in a single transient peak of cytosolic Ca^{2+} concentration, followed by a return towards baseline, or in sustained Ca^{2+} oscillations (Dull and Davies, 1991; Shen et al., 1992).

Ca^{2+} signalling (Figure 3.02) can be initiated by the binding of ligands to cell surface receptors, which results in activation of phospholipace C (PLC) (via activation of GPCRs and G-proteins). This leads to production of second messengers such as inositol (1,4,5) trisphosphate (IP_3). IP_3 binds to receptors on the ER membrane, opening Ca^{2+} channels and thus allowing stored Ca^{2+} to be released into the cytosol (Tran et al., 2000). Depletion of the internal stores appears to stimulate influx of Ca^{2+} into the cell via plasma membrane ion channels (a process known as capacitative Ca^{2+} entry or CCE) (Putney et al., 2001), and can also accelerate the rate of release of Ca^{2+} from the ER into the cytosol (a phenomenon termed Ca^{2+} -induced Ca^{2+} release or CICR) (Berridge, 1990; Berridge,

1997). The mechanical force acting on the EC surface due to fluid shear stress appears to contribute to Ca^{2+} signalling by activating plasma membrane stretch-activated Ca^{2+} channels, thus allowing further influx (Kwan et al., 2003). Shear stress may also activate other receptors (e.g. VEGFR) linked to the IP_3 signalling pathway (Resnick et al., 2003), thus increasing the rate of internal Ca^{2+} release (Tseng et al., 1995).

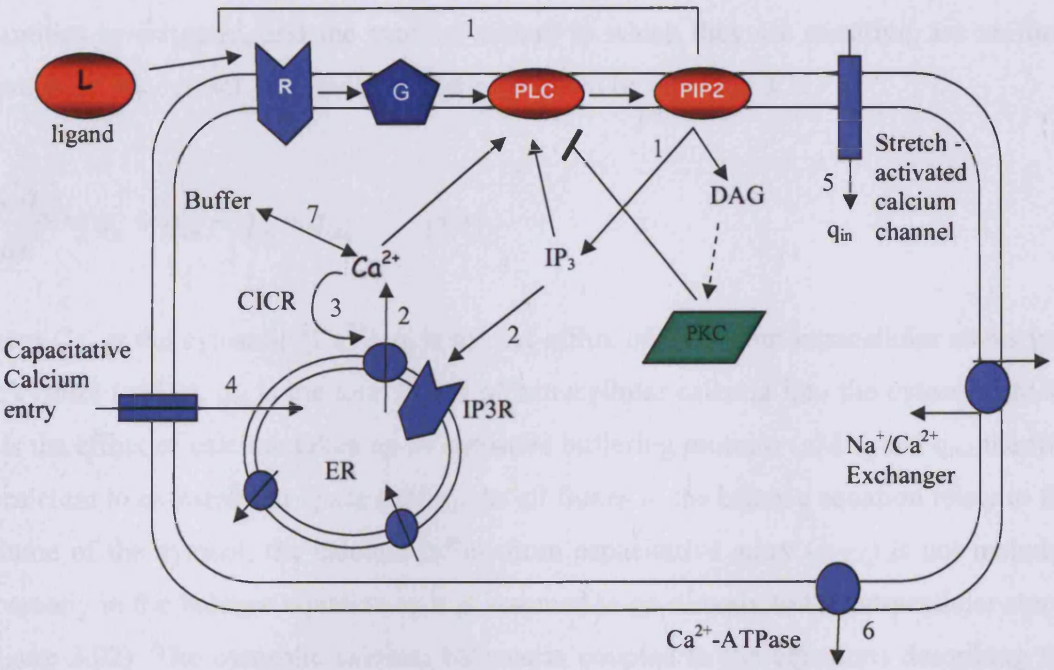

Figure 3.02. Major mechanisms that regulate calcium levels in ECs.
1. Binding of ligand to surface receptors reversibly forms a receptor–ligand complex which involves the activation of heterotrimeric G-proteins and phospholipace C and the cleavage of phosphatidylinositol bisphosphate (PIP_2) which results in internal production of IP_3.
2. IP_3 opens Ca^{2+} channels in the ER, so the rate of internal Ca^{2+} release is dependent on IP_3 concentration.
3. Both the rate of IP_3 production and the rate of internal Ca^{2+} release can be enhanced by cytosolic free Ca^{2+}. This is a part of the CICR mechanism (see text).
4. The rate of Ca^{2+} influx due to CCE is an increasing function of the degree of depletion of ER Ca^{2+} below resting levels, as well as the Ca^{2+} concentration difference across the plasma membrane (i.e. the difference between the external and cytosolic concentrations).
5. The rate of Ca^{2+} influx through shear-gated (i.e. stretch activated) channels is an increasing function of the mechanical shear stress to which the EC is exposed.
6. Cytosolic Ca^{2+} is re-sequestered back into the ER by a Ca^{2+} -ATPase and is pumped out of the cell by plasma membrane Ca^{2+} - ATPases and Ca^{2+} (cytosolic) - Na^+ exchangers.
7. Cytosolic Ca^{2+} is reversibly buffered to proteins such as calmodulin and calpain.

3.2.2 Describing the species balance for calcium

The model of calcium dynamics derived by Wiesner et al (1996) is described by a species balance of four quantities: the calcium efflux levels from intracellular stores, influx of extracellular calcium from mechanically-activated calcium channels, extrusion (and exchange) of cytosolic calcium to the extracellular space and buffering of cytosolic calcium by cytoplasmic proteins. The model assumes that the concentrations of the four quantities investigated, and the external stimuli to which they are sensitive, are uniform throughout the cytosol. The species balance is given by equation 3.1:

$$\frac{dCa_c}{dt} = q_s + q_{in} - q_b - q_{out} \quad (3.1)$$

where Ca_c is the cytosolic $[Ca^{2+}]$, q_s is the net efflux of Ca^{2+} from intracellular stores into the cytosol (μM/s), q_{in} is the total influx of extracellular calcium into the cytosol (μM/s), q_b is the efflux of calcium taken up by cytosolic buffering proteins (μM/s) and q_{out} the flux of calcium to extracellular space (μM/s). As all fluxes in the balance equation relate to the volume of the cytosol, the calcium influx from capacitative entry (q_{CCE}) is not included separately in the balance equation as it is assumed to go directly to the intracellular stores (Figure 3.02). The cytosolic calcium balance is coupled to the equations describing the calcium concentration in intracellular stores and to the calcium complexed to buffering proteins. The Ca^{2+} in the stores is given by:

$$\frac{dCa_s}{dt} = \frac{V_c}{V_s}(q_{CCE} - q_s) \quad (3.2)$$

where Ca_s is the concentration of $[Ca^{2+}]$ in the ER, V_c is the volume of cytosol (litres) and V_s the volume of intracellular stores (litres).

The rate of change of buffered calcium (Ca_b) is given by:

$$\frac{dCa_b}{dt} = q_b \quad (3.3)$$

Under condition of calcium homeostasis (i.e. steady state) all rates of change are zero. Thus the steady state for equations 3.1-3.3 is:

$$q_{in}(Ca_c, Ca_{ex}) + q_{CCE}(Ca_{ex}, Ca_s) = q_{out}(Ca_c)$$

$$q_s = q_{CCE}$$
$$q_b = 0 \qquad (3.4)$$

Under steady state the net exchange of calcium among intracellular compartments is zero and the influx of exogenous calcium is balanced by efflux of calcium. The intracellular calcium levels depend solely on the extracellular calcium levels.

3.2.3 Release of calcium from intracellular stores

The rate of release of calcium from intracellular stores depends on the stores concentration, the cytosolic concentration and the cytosolic level of IP_3. The rate of generation of IP_3 depends on the number of membrane receptors activated, either by ligands or by force-induced molecular deformation (described in section 3.6) in the absence of receptor bodies. Wiesner et al (1996) considered the case of the thrombin protease that stimulates the proteolytically activated receptors PAR1 and PAR2 (although activation of VEGFR and other GPCRs can equally stimulate PLC (G-proteins). Thrombin binds reversibly to the receptors and undergoes an irreversible cleavage producing a proteolytic fragment and the activated receptor (R^*). The activated receptor then triggers the IP_3 pathway of $[Ca^{2+}]$ release. The above processes are given by the following equations:

$$\frac{dR_u}{dt} = -k_{on}R_uC_s + k_{off}R_b \qquad (3.5)$$

$$\frac{dR_b}{dt} = k_{on}R_uC_s - k_{off}R_b - k_dR_b \qquad (3.6)$$

$$\frac{dR^*}{dt} = k_d R_b \qquad (3.7)$$

where R_u is the concentration of the unbound receptors, R_b is the concentration of bound receptors, k_{on} is the association rate of thrombin for its receptor, k_{off} is the dissociation rate of thrombin, R^* is the concentration of cleaved active receptors, k_d is the rate of receptor proteolysis and C_s is the concentration of ligand at the cell surface. Considering that initially all receptors are unoccupied, the initial conditions for equations 3.5-3.7 at t = 0 are:

$$\begin{aligned} R_u(0) &= R_T \\ R_b(0) &= R^*(0) = 0 \end{aligned} \qquad (3.8)$$

where R_T is the total concentration of receptors. The bound receptors activate PLC via G proteins which in turn catalyses the hydrolysis of PtdIns(4,5)P_2 (PIP_2) to IP_3 and diacylglycerol (DAG). Wiesner et al give the rate of change of [IP_3] generation as:

$$\frac{dI}{dt} = k_1 R^* - k_2 I \qquad (3.9)$$

where I is the cytosolic concentration of IP_3 and k_1 and k_2 the rate constants for IP_3 generation and degradation respectively.

IP_3 binds to and opens a Ca^{2+} channel receptor (Figure 3.02) on the ER thereby releasing Ca^{2+}. The binding stoichoiometry indicates that at least 3 molecules of IP_3 are required to open the channel. The rate of IP3-mediated calcium release (q_{rel}) is proportional to the fraction of channels open and the concentration of calcium in the ER and is given by (Meyer and Stryer, 1988) as:

$$q_{rel} = k_3'(Ca_c)\left(\frac{I}{K_2 + I}\right)^3 Ca_s \qquad (3.10)$$

where K_2 is IP_3 concentration at which half of the IP_3 receptors are occupied (assuming an equilibrium between IP_3 and its receptor in the ER) and $k_3'(Ca_c)$ the rate of cytosolic calcium released from intracellular stores (calcium-induced-calcium-release; CICR) which is given by Wiesner et al (1996) by Michaelis-Menten kinetics as:

$$k_3'(Ca_c) = k_3\left(\frac{k_{CICR}Ca_c}{K_{CICR} + Ca_c}\right) \quad (3.11)$$

where k_{CICR} is an amplification factor of CICR and K_{CICR} the cytosolic $[Ca^{2+}]$ at which CICR is half-maximal. The ER also contains a Ca^{2+}-ATPase that transports $[Ca^{2+}]$ back into the organelle. As the $[Ca^{2+}]$ in the stores (Ca_s) increases, the rate of transport drops. The net rate of transport is given by Meyer and Stryer (1998) as:

$$q_{res} = k_4\left(\frac{Ca_c}{K_3 + Ca_c}\right)^2 - k_5 Ca_s^2 \quad (3.12)$$

where k_4 is rate for transport of Ca_c, K_3 is the dissociation constant between Ca^{2+} and ER Ca^{2+}-ATPase and k_5 the rate for reverse transport of ER Ca^{2+}-ATPase.

The rate of calcium efflux from the stores can now be given by subtracting equation 3.12 from equation 3.10:

$$q_s(i, Ca_c, Ca_s) = k_3\left[\left(\frac{k_{CICR}Ca_c}{K_{CICR} + Ca_c}\right)\left(\frac{I}{K_2 + I}\right)\right]^3 Ca_s - k_4\left(\frac{Ca_c}{K_3 + Ca_c}\right)^2 + k_5 Ca_s^2 \quad (3.13)$$

The flux of calcium into the stores from capacitative calcium entry (Figure 3.02) occurs in response to depletion of calcium in the intracellular stores and is given by an equation that predicts a flux proportional to the extent of depletion of the store and the concentration difference between the ECM and the store:

$$q_{CCE} = k_{CCE}(Ca_{s,0} - Ca_s)(Ca_{ex} - Ca_s) \qquad (3.14)$$

where k_{CCE} is the rate constant for CCE (Table 3.01).

3.2.4 Calcium buffered to proteins

The rate of buffering is considered by Wiesner et al (1996) for the protein calmodulin which has four calcium binding sites. The rate of calcium-calmodulin reversible complexation is proportional to the free calcium concentration and the concentration of free binding sites. Therefore the rate of calcium buffering by proteins is given by:

$$q_b = k_6 Ca_c(BT - Ca_b) - k_7 Ca_b \qquad (3.15)$$

where k_6 and k_7 are the forward and reverse rate constants for buffering respectively (Table 3.01) and BT the total concentration of calcium binding sites. Following Wiesner et al (1996), the buffering of Ca^{2+} in the ER is not explicitly included in the model, since the rate of buffering in the ER is very fast and thus contributes only a scale factor to the equations (Sneyd et al., 1995).

3.2.5 Flux of calcium to extracellular space

Calcium efflux (q_{out}) is mediated by plasma membrane Ca^{2+}-ATPases and Na^+/Ca^{2+} exchangers. The rate of ATPases is given by (Valant et al., 1992) as a sum of two Hill functions:

$$q_{ATPase} = \frac{V_p Ca_c^{1.7}}{K_4^{1.7} + Ca_c^{1.7}} + \frac{V_{hi} Ca_c^{4.4}}{K_{hi}^{4.4} + Ca_c^{4.4}} \qquad (3.16)$$

where the first term represents the capacity of the ATPase in the basal state and the second term represents the activated high capacity mode of the ATPase which forms upon exposure to elevated levels of cytosolic calcium. V_p is the maximal rate of pumping of

calcium in the basal state, K_4 is the calcium concentration at which the extrusion is half-maximal in the basal state and V_{hi} and K_{hi} are analogous quantities for the high capacity term.

Similarly, the rate of the Na^+/Ca^{2+} exchanger is given by Valant et al., 1992 as:

$$q_{ex} = \frac{V_{ex} Ca_c}{K_5 + Ca_c} \qquad (3.17)$$

where K_5 is the calcium concentration at which the rate of exchange is half-maximal. The total rate of calcium efflux to the extracellular space is the sum of q_{ATPase} and q_{ex}:

$$q_{out} = \frac{V_p Ca_c^{1.7}}{K_4^{1.7} + Ca_c^{1.7}} + \frac{V_{hi} Ca_c^{4.4}}{K_{hi}^{4.4} + Ca_c^{4.4}} + \frac{V_{ex} Ca_c}{K_5 + Ca_c} \qquad (3.18).$$

By substituting the above equations for the various fluxes into equations 3.1-3.3 along with the equation of IP_3 generation a system of four coupled non-linear ODEs is generated:

$$\frac{di}{dt} = k_1 R^* \left(\frac{Ca_c}{K_1 + Ca_c} \right) - k_2 I$$

$$\begin{aligned} \frac{dCa_c}{dt} &= k_3 \left[\left(\frac{k_{CICR} Ca_c}{K_{CICR} + Ca_c} \right) \left(\frac{I}{K_2 + I} \right) \right]^3 Ca_s - k_4 \left(\frac{Ca_c}{K_3 + Ca_c} \right)^2 \\ &+ k_5 Ca_s^2 - k_6 Ca_c (BT - Ca_b) + k_7 Ca_b \\ &- \frac{V_p Ca_c^{1.7}}{K_4^{1.7} + Ca_c^{1.7}} - \frac{V_{hi} Ca_c^{4.4}}{K_{hi}^{4.4} + Ca_c^{4.4}} - \frac{V_{ex} Ca_c}{K_5 + Ca_c} + q_{in} \end{aligned} \qquad (3.19)$$

$$\frac{dCa_s}{dt} = \frac{V_c}{V_s}\left\{\begin{array}{l} K_{CCE}(Ca_{s,0} - Ca_s)(Ca_{ex} - Ca_s) \\ -\left\{\begin{array}{l} k_3\left[\left(\frac{k_{CICR}Ca_c}{K_{CICR}+Ca_c}\right)\left(\frac{I}{K_2+I}\right)\right]^3 Ca_s \\ +k_4\left(\frac{Ca_c}{K_3+Ca_c}\right)^2 + k_5 Ca_s^2 \end{array}\right. \end{array}\right\} \quad (3.20)$$

$$\frac{dCa_b}{dt} = k_6 Ca_c(BT - Ca_b) - k_7 Ca_b \quad (3.21)$$

where the concentration of active receptors (R^*) is obtained either by solving equations 3.5-3.7 if ligand is present or by a model of molecular deformation (section 3.6). In the above system of equations, the only value that remains to be defined dynamically is the influx of extracellular calcium (q_{in}) into the cytosol.

3.2.6 Influx of extracellular calcium

The influx of extracellular calcium takes place via shear stress-activated calcium channels which have been identified in endothelial cells (Hoyer et al., 1994; Popp et al., 1992). Ions migrate through the ion channels in the membrane of a cell (Figure 3.03). Normally, the cell maintains an electric potential difference across the membrane, denoted by $\Delta\varphi$. As indicated in Figure 3.03 the interior of the cell is negative relative to the exterior (Alberts, 1994). Under physiological conditions, the concentration of extracellular calcium (Ca_{ex}) is four orders of magnitude larger than the concentration of intracellular calcium (Ca_c) (Alberts, 1994). Thus, extracellular calcium ions are subjected to two inward driving forces, a concentration gradient and an electric potential gradient.

The steady-state flux of an ion across the membrane (Figure 3.03) is described by the Goldman-Hodgkin-Katz equation (GHK) also known as the constant field equation (Patuzzi, 1998) given by 3.22:

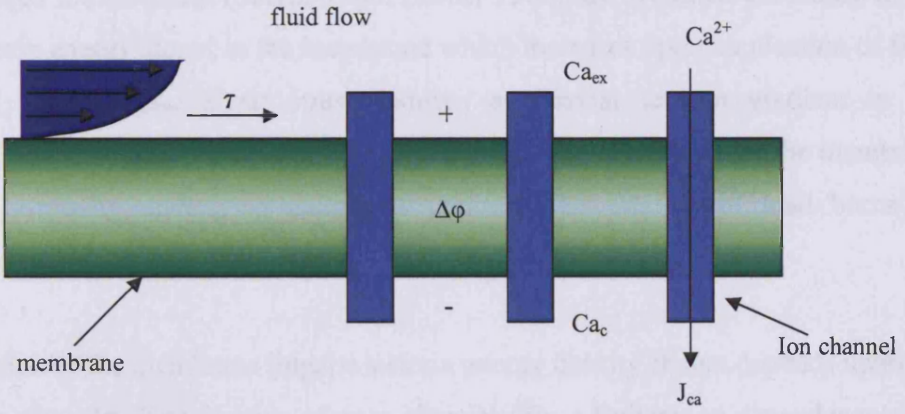

Figure 3.03. Ion flux through the ion channels of a membrane.

$$q_{in} = -\frac{PzF\Delta\varphi}{RT}\left(\frac{Ca_{ex} - Ca_c \exp\left[\frac{zF\Delta\varphi}{RT}\right]}{1 - \exp\left[\frac{zF\Delta\varphi}{RT}\right]}\right) \qquad (3.22)$$

where z is the charge on the ion (+2 in the case of calcium), F is the Faraday number (96.500 coulombs/equivalent), R is the universal gas constant and T is the absolute temperature. Δφ denotes the membrane electric potential and P is the permeability coefficient and is equal to D/h where D is the effective diffusion coefficient of the ion in the membrane and h is the membrane thickness.

The GHK equation depends in part upon the membrane permeability coefficient *P*. Wiesner et al (1997) reflected the value of this permeability coefficient in their model by the fraction of open ion channels that are in the open state. Based on Kirchoff's law for parallel conductors and the relationship between the membrane permeability and membrane conductance, the permeability is linearly related to the open channel fraction f_0 and the permeability of the membrane when all channels are open is P_{max}, i.e:

$$P = f_0 P_{max.} \quad (3.23)$$

Stretch-activated ion channels (Sachs, 1986; Sachs, 1988) are activated according to the amount of strain energy stored in the membrane which increases upon application of fluid flow-induced shear stress. Shear stress induces a uniaxial tension gradient in the membrane which inevitably deforms it. Part of the applied load is borne by the membrane and part is borne by underlying cellular structures. The fraction of load borne by submembranous structures is denoted as ϵ.

The deformation of the membrane imparts a strain energy density W that depends upon the applied shear stress (τ). The fraction of open channels has a Boltzmann dependence upon the level of gating energy in the membrane. The gating energy in turn can be related to the strain energy density. A fraction of the strain energy is considered to gate the shear stress-activated channels. This fraction is designated as *fe*. Thus, the fraction of channels in the open state, $f_o(\tau)$ depends upon the strain energy density (Wiesner et al 1997):

$$f_o(\tau) = \frac{1}{1 + \alpha * \exp\frac{-f_e W(\tau)}{kTN}} \qquad (3.24)$$

where N is the number of channels (no./unit area), k is the Boltzmann constant, T is the absolute temperature, and α (dimensionless) is a measure of the probability that a channel is in the open state in the no-load case (no shear stress).

The relationship of the strain energy density to the applied shear stress $W(\tau)$ also need to be developed to allow for calculation of $f_o(\tau)$. Employing a simplifying analysis, (Fung and Liu, 1993) demonstrated that the equations of mechanical equilibrium for the endothelial cell membrane can be reduced to:

$$dT_z/dz + (1 - \epsilon)\tau = 0, \qquad (3.25)$$

and $T_x = 0$. (3.26)

where T_z and T_x are the tensions in the directions of flow and orthogonal to flow in the plane of the membrane respectively. The quantity of ϵ is the fraction of the stress absorbed by the interior of the cell and the complex net of actin filaments preserving solidly the shape of the cell. The tension gradient in the direction of flow is related to the fraction of load borne by the membrane $(1 - \epsilon)\tau$.

Fung and Liu (1993) assumed the tension in the direction perpendicular to the flow T_x to be very small based on the tension field hypothesis (which states that the membrane cannot support compressive stresses in its own plane because its thickness is small compared with its length and width) and for the sake of simplification was taken as zero making the stress in the cell membrane a uniaxial tension field in the direction of flow. Evans and Skalak (Evans and Skalak, 1979a; Evans and Skalak, 1979b) give a constitutive relationship for cell membranes in pure shear deformation under uniaxial tension:

$$T_z = \mu (\lambda_z^2 - \lambda_z^{-2}), \qquad (3.27)$$

where the quantity λ_z is the stretch ratio in the direction of flow. The elastic constant μ is the membrane shear modulus (elasticity constant for deformation of membranes). (Skalak et al., 1973) give a strain energy density function, W, for a two dimensional membrane. Integration of that expression and equation 3.25 yields the relationship between strain energy density and the applied shear stress as given by Wiesner et al (1997):

$$W(\tau) = \frac{\left[(1-\varepsilon)\tau L + \sqrt{16\mu^2 + \tau^2 L^2(\varepsilon^2 - 2\varepsilon + 1)} - 4\mu\right]^2}{8\left[(1-\varepsilon)\tau L + \sqrt{16\mu^2 + \tau^2 L^2(\varepsilon^2 - 2\varepsilon + 1)}\right]} \qquad (3.28)$$

where L is the length of the cell in the flow direction.

The dynamics of extracellular calcium influx as described so far require knowledge of membrane electric potential, kinetics of ion channel activation and viscoelasticity of the membrane. The membrane hyperpolarizes, i.e. becomes more negative in response to shear stress (Nakache and Gaub, 1988). Membrane electric potential depends upon currents of potassium, sodium and chloride ions and it has been reported that shear-stress

activated potassium channels exist in endothelial cells (Olesen et al., 1988). However little is known about sodium channels and sodium and potassium exchangers in endothelial cells (for review see (Nilius and Droogmans, 2001). For the sake of simplicity Wiesner et al (1997) have used an empirical relationship between shear stress and membrane electric potential $\Delta\phi(t, t)$, given as:

$$\Delta\phi(t,\tau) = -E_r - \Delta E_m(\tau)\left(1 - e^{\frac{-t}{t_\phi}}\right) \qquad (3.29)$$

where E_r is the resting membrane potential, $\Delta E_m(\tau)$ is the hyperpolarisation of the membrane potential due to shear stress and t_ϕ is the time constant of hyperpolarisation.

The calcium influx is not established immediately but over a period of ~70 seconds upon application of shear stress. This could be due to the viscoelastic nature of the cell membrane where a delay in membrane deformation would result in a delay in the accumulation of strain energy within the membrane. Consequently there would be a delay in the approach of the permeability coefficient to its steady state value. Supporting the idea that the membrane viscoelasticity contributes to the dynamics of membrane permeability, Wiesner et al (1997) produced a relationship (3.29) between shear stress and the temporal aspect of membrane permeability (equation 3.23) as:

$$P(t,\tau) = \left\{ f_o(0) + \tanh\left[\frac{\pi t}{t_f}\right]\left[f_o(\tau) - f_o(0)\right]\right\} P_{max} \qquad (3.30)$$

where f_0 is the fraction of open ion channels at a given time (equation 3.23), t_f is the constant for channel opening time (by relaxation of membrane deformation) and tanh is the hyperbolic tangent (tanh(0)=0, tanh(∞)=1) which gives a basal value of $f_o = f_o(0)$ at time t = 0 and equal to $f_o(\tau)$ at time t = ∞

With the dynamics of membrane potential and membrane permeability the transduction of a shear stress signal via Ca^{2+} influx were simulated. This was achieved by first calculating

the strain energy density (W) for the applied shear stress, the product of which was used to calculate the fraction of channels (f_o) in the open state as a function of membrane strain energy density. This fraction (f_o) was then given in equation 3.30 to calculate the permeability (P) coefficient of the ion channels. The relationship between shear stress and membrane potential ($\Delta\varphi$) was solved to get the rate of change for membrane electric potential as a function of time and membrane hyperpolarisation.

The derived values were then put in the GHK equation (3.22) to calculate the steady-state flux of calcium (q_{in}) across the endothelial cell membrane. Solution of the above set of equations then provided the Ca^{2+} influx as a function of fluid flow-induced shear stress. q_{in} was then added to the balance equation (3.1) for cytosolic Ca^{2+} (Ca_c) to calculate the complete calcium dynamics under shear stress stimulation (including ligand/G-protein).

3.2.7 Parameter values

The total intracellular calcium (Ca_T) is not constrained to be a constant but it given as a sum of species that exist in the cell as:

$$Ca_T = Ca_c + Ca_b - \frac{V_s}{V_c} Ca_s \qquad (3.30)$$

The quantities of C_s, Ca_{ex} are concentrations present in the medium (Table 3.02). The initial condition for the model is taken to be the steady state for an unstimulated cell, where the surface concentration of ligand is taken to be zero, there are no receptors activated and the calcium influx (q_{in}) is zero. From this it follows that the concentration of IP_3 is also zero. By substituting these values to equation 3.20, the initial concentration of Ca^{2+} in intracellular stores is as:

$$Ca_{s,0} = \sqrt{\frac{k_4}{k_5}} \left(\frac{Ca_{c,0}}{K_3 + Ca_{c,0}} \right) \text{(3.31)},$$

where $Ca_{c,0}$ the initial level of cytosolic free calcium.

Similarly, the initial condition of buffered calcium can be obtained by setting equation 3.21 to zero as:

$$Ca_{b,0} = \frac{k_6 Ca_{c,0}}{k_6 Ca_{c,0} + k_7} B_T \quad (3.32),$$

As few data are available on the positive feedback mechanisms of CICR and Ca^{2+}-sensitive IP_3 production, the values for K_{CICR} and K_1 were taken as $K_{CICR} = K_1 = 0$ following Wiesner et al (1996), which means that there is no positive feedback on Ca^{2+} release from stores.

Table 3.01 Parameter values for calcium module

Constant	Description	Value	Units	Source
k_1	IP_3 generation	1.24×10^{-6}	$\mu M/s$	Wiesner et al., 1996
k_2	IP_3 degradation	2	s^{-1}	Meyer & Stryer 1988
k_3	Basal rate for IP_3 release from internal stores	6.64	s^{-1}	Meyer & Stryer 1988
k_4	rate for re-sequestration of Ca	5	$\mu M/s$	Meyer & Stryer 1988
k_5	rate for reversal of ER Ca^{2+}-ATPase	10^{-7}	$\mu M^{-1}s^{-1}$	Wiesner et al., 1996
k_6	forward rate for calcium buffering	100	$\mu M^{-1}s^{-1}$	Bayley et al., 1984
k_7	reverse rate for calcium buffering	300	s^{-1}	Bayley et al., 1984
K_1	dissociation between calcium and PLC	0	μM	Wiesner et al 1996
K_2	binding of IP3 to ER IP3 receptor channels	0.2	μM	Wiesner et al 1996
K_3	dissociation between Ca^{2+} and ER Ca^{2+}-ATPase	0.15	μM	Meyer & Stryer 1988
K_4	Hill's const. where membrane Ca^{2+}pumping is ½ max	0.08	μM	Valant et al., 1992
K_5	Michaelis-Menten const. for Na/Ca exchanger	0.321	μM	Wiesner et al., 1996
K_{hi}	analogous to K4 for high-capacity term	0.38	μM	Valant et al., 1992
k_{CCE}	rate constant for CCE	0	$\mu M^{-1}s^{-1}$	Wiesner et al., 1996
k_{CICR}	amplification factor of CICR	1	-	Wiesner et al., 1996
K_{CICR}	cytosolic Ca conc. at which CICR is ½ max	0	μM	Wiesner et al., 1996
V_p	max rate of pumping by Ca^{2+}-ATPase	1.63	$\mu M/s$	Valant et al., 1992
V_{hi}	analogous to V_p for high-capacity term	4.76	$\mu M/s$	Wiesner et al., 1996
V_{ex}	maximal rate of exchange by Na^{2+}/Ca^{2+} exchanger	18.33	$\mu M/s$	Valant et al., 1992
V_c/V_s	volume cytosol/volume of intracellular stores	3.5	-	Voet and Voet 1990
B_T	total concentration of buffering proteins	120	μM	Jafri et al., 1992

Table 3.01. Parameter values for calcium dynamics module. The original references for the values given by Wiesner et al (1996, 1997) can be found in the respective articles.

Table 3.02 Parameter values for calcium module – cont.				
RT	total number receptors	$4.4x10^4$	No./cell	Lollar et al., 1980
k_d	Catalysis rate for receptor-ligand	0.12	s^{-1}	Wiesner et al., 1996
k_{off}	Reverse rate constant for ligand binding	142.8	s^{-1}	Wiesner et al., 1996
k_{on}	Forward rate constant for ligand binding	5316.7	$\mu M^{-1}s^{-1}$	Wiesner et al., 1996
$q_{in,pass}$	Passive ECM influx of Ca^{2+} into cytosol	5.33	$\mu M/s$	Johns et al 1987
ϵ	load fraction borne by cytoplasm	0.90	-	Wiesner et al 1996
Ca_{ex}	extracellular calcium concentration	1500	μM	Alberts, 1994
μ	membrane shear modulus	0.01	dynes/cm	Sato et al., 1987
D	diffusivity	$8.76x10^{-7}$	cm^2/sec	Sober 1970
L	length of an endothelial cell	$35x10^{-4}$	cm	Levesque & Nerem, 1985
P_{max}	maximum permeability coefficient	$6.87x10^{-8}$	cm/sec	Wiesner et al 1997
S	en face are of cell	$611x10^{-8}$	$cm^2/cell$	Levesque & Nerem, 1985
f_e	gating fraction	0.044	-	Wiesner et al 1996
c_s	Concentration of ligand in the media	1U/ml = 9	nM	Wiesner et al., 1997
N	Ion channel density	$1.38x10^{-16}$	$channel/cm^2$	Wiesner et al., 1997
α	Factor for f_o at zero shear	36.4	-	Wiesner et al., 1997
t_r	time constant for relaxation of deformation	60	secs	Wiesner et al., 1997
$\Delta E_m(\tau)$	Hyperpolarisation potential	$0.235\tau^{0.876}$	Volt	Wiesner et al., 1997
$t\phi$	time constant for hyperpolarisation	100	secs	Nakache & Gaub 1988
ER	membrane resting potential	$-27x10^{-3}$	Volt	Adams et al., 1989
VC	volume of cytosol	$3x10^{-12}$	litres	Voet and Voet 1990
RG	gas constant,	1.987	cal/mol/Kelvin	Wiesner et al., 1997
Z	charge on calcium	2	-	Wiesner et al., 1997
FA	Faraday number	$2.3x10^4$	cal/volt/equivalent	Wiesner et al., 1997
KB	Boltzmann constant	$1.38x10^{-16}$	ergs/Klevin/channel	Wiesner et al., 1997
T	absolute temperature	310	Kelvin	Wiesner et al., 1997

Table 3.02. Parameter values for calcium dynamics module. The original references for the values given by Wiesner et al (1996, 1997) can be found in the respective articles.

3.2.8 Shear stress-induced calcium dynamics, results and discussion

After constructing the model and coding the respective equations in Matlab (CD included) the dynamics of intracellular calcium was investigated upon application of shear stress equal to τ = 12 dynes/cm^2. Parametric studies (i.e. evaluation and optimisation of parameter values) were not performed here as these have been described and discussed in detail by Wiesner et al (1996, 1997). Calculation of the dynamics of [Ca^{2+}] however was necessary for a complete examination of the molecular shear stress response as calcium regulates the function of molecules (see chapter 2) such as calpain by direct interaction

(section 3.3) and Src kinase via the PKC pathway (section 3.8). Accurate calculation of $[Ca^{2+}]_c$ upon application of shear stress will therefore allow for the determination of the influence calcium has on downstream pathways and for a more accurate determination of the dynamics of downstream molecules.

According to the model of calcium dynamics constructed here after Wiesner et al (1996, 1997), while ligand binding and IP_3 production contributes to the initial rise in $[Ca^{2+}]_c$ (peak), the overall $[Ca^{2+}]$ increase (plateau) is mostly influenced from the stretch-activated calcium channels (Wiesner et al 1997). This increase reaches a plateau as the membrane pumps/exchangers balance the calcium concentration difference.

Calcium dynamics in the model is highly dependent on the fraction of the shear stress-produced load that is borne by submembranous structures denoted by ϵ, the value of which has not been experimentally determined to date. As discussed by Wiesner et al, altering the value of ϵ alters the threshold value of shear stress and the shear dependent range to which q_{in} responds. As more stress is absorbed by the membrane (i.e. increasing the value of ϵ), the threshold level of the q_{in} decreases (less strain energy is available to gate the mechanosensitive ion channels) and the shear-sensitive range narrows (Wiesner et al 1997).

Wiesner et al gave an initial value estimate of $\epsilon = 0.90$, based upon the micropipette experiments of Sato et al (1987) in which the main load-bearing component of the cell was found to be the cytoskeleton. They assumed ϵ to be constant and non-changing in time. This leads to an elevation of calcium influx q_{in} which reaches a plateau level (sustained influx) upon application of shear stress but never returns to basal level (Figure 3.04) (Wiesner et al 1997). As a result, the model by Wiesner et al (1997) for the synergistic effect of sustained shear stress-induced calcium influx and agonist stimulation when compared with the experimental observations (Helmlinger et al., 1996; Helmlinger et al., 1991) under similar conditions, predicted the $[Ca^{2+}]_c$ accurately for most of the time course (particularly in the peak region) but not for the recovery phase. The experimental data showed that $[Ca^{2+}]_c$ returns to the initial baseline within 5 minutes when stimulated with both ligand (i.e. thrombin) and shear stress (Helmlinger et al., 1996).

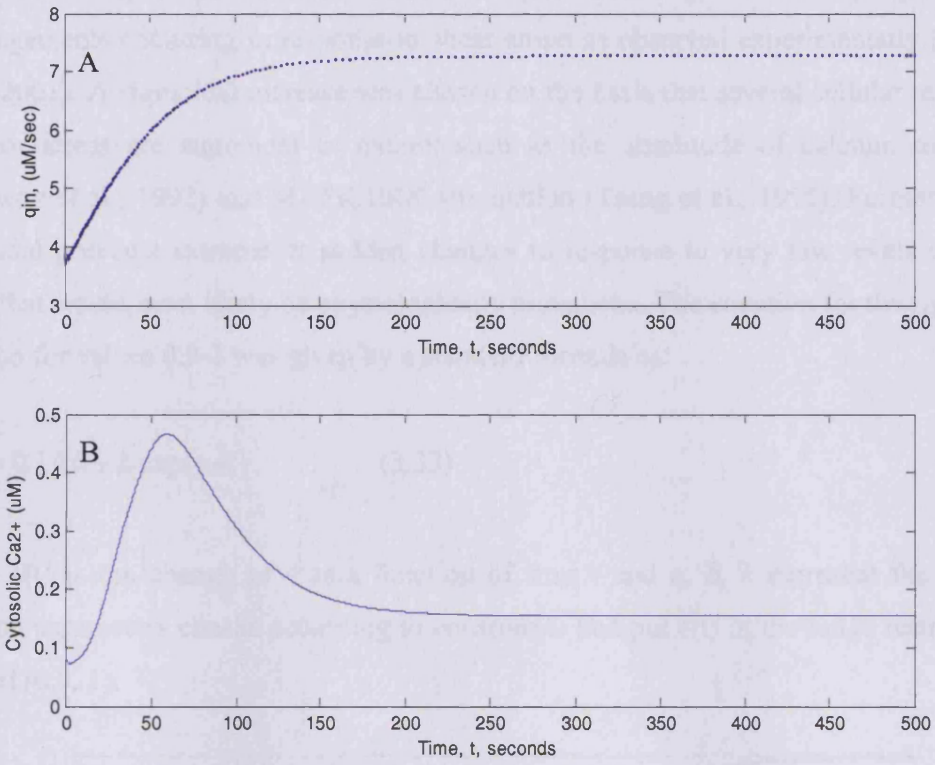

Figure 3.04. Original calcium dynamics. A; calcium influx q_{in} reaches a sustained plateau when ϵ is fixed *a priori* at 0.90. B) calcium dynamics in time similarly to the predictions resulted from the simulation of Wiesner et al (1997). After recovery Ca_c reaches a plateau of ~0.2μM and never returns to the original basal levels (0.1 μM).

It is well known that shear stress (e.g. 12 dynes/cm^2) induces changes to the shape of endothelial cells and cytoskeletal rearrangements that influence the cell's morphology under conditions of fluid flow and shear stress (Davies, 1995; Dewey et al., 1981; Nerem et al., 1981). As the deformation of the membrane depends upon its load-bearing capacity relative to submembranous structures, the changes on the cytoskeleton could account for the difference between the calcium dynamics observed experimentally (return of calcium to basal levels) (Helmlinger et al., 1995) and the ones predicted by the model of Wiesner et al (1997).

When searching for a mechanism to explain the return of calcium level to the initial baseline it was realised that inclusion of cytoskeletal changes embodied in the factor ϵ would account for the experimentally observed calcium dynamics. A sigmoid increase of 10% was added to the initial value of ϵ that peaked within 500 seconds at ϵ = ~1 (Figure

3.05), indicating an increase in stiffness of the membrane caused by cytoskeletal rearrangements occurring in response to shear stress as observed experimentally (Bausch et al., 2001). A sigmoidal increase was chosen on the basis that several cellular responses to shear stress are sigmoidal in nature, such as the amplitude of calcium transients (Schwartz et al., 1992) and MAPK/ERK stimulation (Tseng et al., 1995). Furthermore, a sigmoidal prevents extreme or sudden changes in response to very low levels of shear stress that would most likely be physiologically unrealistic. The equation for the sigmoidal function for values 0.9-1 was given by a standard formula as:

$$\varepsilon(t) = 0.1/(b + k\exp(-at), \qquad (3.33)$$

where ϵ(t) is the change of ϵ as a function of time t and a, b, k represent the logistic function parameters chosen according to constraints that put ϵ(t) in the range restricted to interval (0.9, 1).

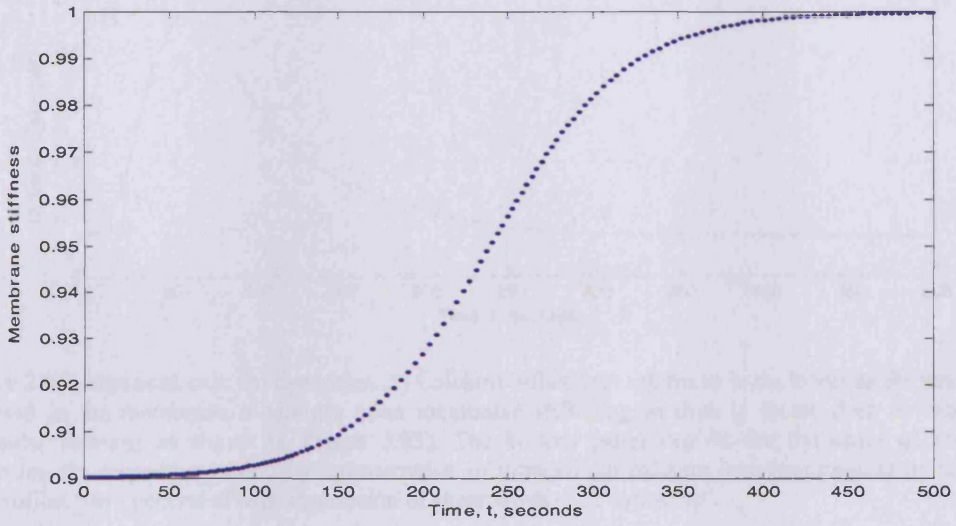

Figure 3.05 Adaptive sigmoidal increase of membrane stiffness (equation x.32) in response to shear stress. The values for b, k and α were chosen as 1, 400 and 0.025 respectively to produce the curve in this plot which when incorporated in the model of calcium dynamics best reproduces the response curves of intracellular $[Ca^{2+}]_c$ as observed experimentally (Helmlinger et al., 1995).

An increase of the value of ϵ in time suggests that after certain time the cytoskeletal rearrangements that take place within the cell act as an adaptation mechanism to external forces allowing the submembranous structures to be able to bear more force load. This hypothesis also agrees with the observation of cell shape changes and subsequent

movements shortly after fluid flow is applied. Applying this increase of ϵ in the model resulted in calcium dynamics of a biphasic character (Figure 3.06), matching the calcium peak in response to 12 dyne/cm^2 shear stress but also allowing [Ca^{2+}] to slowly decay to its initial basal level (within ~4 minutes) consistent with the experimental observations on BAECs and HUVECs (Chen et al., 1992); Helmlinger et al 1995; Nilius and Droogmans, 2001).

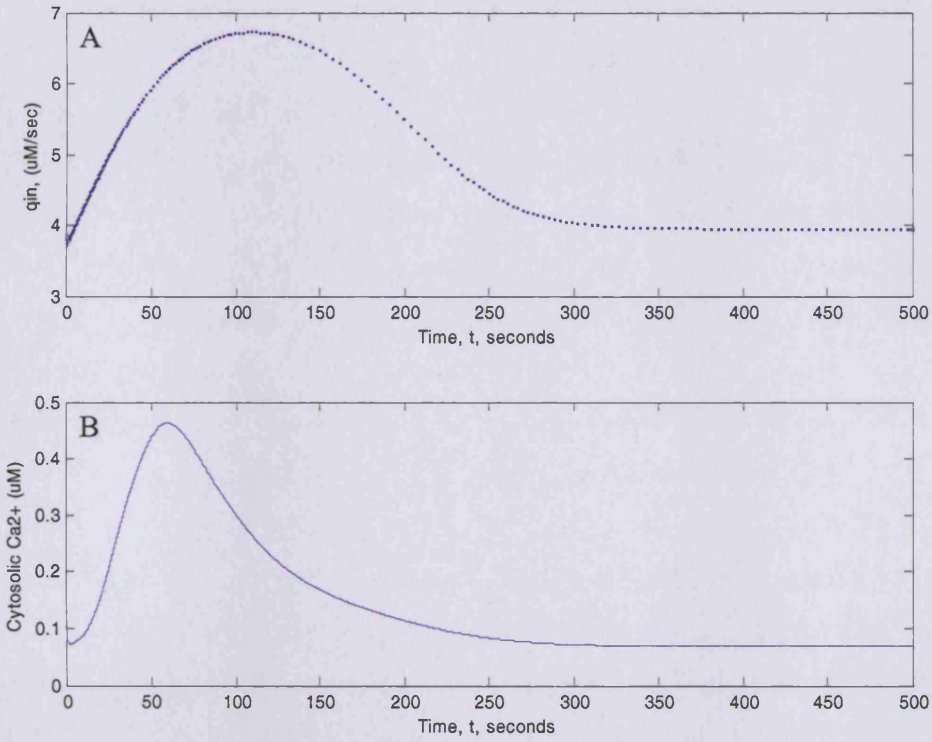

Figure 3.06. Improved calcium dynamics. A) Calcium influx (q_{in}) returns to basal levels as the strain energy imparted in the membrane minimizes upon membrane stiffening in time (ϵ factor rises to value 1 in a simgoidal fashion) as shown in Figure 3.05). The bottom panel depicts the dynamics of calcium by presenting the respective molecular concentration of intracellular calcium ions (micromolar units) in time. The profiles were generated with application of shear stress = 12 dynes/cm^2.

3.2.9 Summary and conclusions

This section described the dynamics of $[Ca^{2+}]_c$ focusing on shear stress-induced calcium influx and how shear stress affects membrane activated-calcium ion channels (membrane permeability changes by membrane deformation). A previously published mathematical model of calcium dynamics model was used as a base in order to account for the contribution of calcium to the overall shear stress response.

It was necessary to apply certain changes to the original model regarding the effects of shear stress on the membrane's permeability to extracellular calcium to allow calcium to return to basal levels after application of shear stress. In the original model the membrane did not adapt to the force applied, while the modified model included gradual stiffening of the membrane resulting in membrane electric potential recovering, channels closing and calcium dynamics decaying to initial baseline.

3.3 Calpain proteolytic activity and cleavage of talin (Module 2)

3.3.1 Module description

Calpain cleaves a number of proteins such as integrins, FAK, Src, talin, PTP1B and ERK (Franco and Huttenlocher, 2005). While it is not clear to date what the molecular consequence is of cleaving most of these proteins, it has been reported that cleavage of talin by calpain results in conformational changes promoting its binding to integrin β-tails (Yan et al., 2001), which is known to be crucial for inside-out activation of integrins. Cleavage of talin by calpain separates the talin N- and C- terminal domains, releasing the auto-inhibitory structural loop of talin and making the structural 'head' of talin more accessible to binding partners. Both intact talin and cleaved talin can bind to integrins with the difference that the cleaved form has a higher affinity for integrins; both 20-fold and 16-fold higher K_a for the cleaved talin have been reported in different cases (Calderwood et al., 2002; Yan et al., 2001).

Calpains recognize bonds between domains rather than specific amino acid residues, therefore hydrolysing substrate proteins in a very limited manner (Suzuki et al., 2004). The two calpains differ in calcium sensitivity in vitro. μ-calpain requires 3-50 μM of cytosolic Ca^{2+} ($[Ca^{2+}]_c$) for half maximal activity while m-calpain requires 400-800 μM (Cong et al., 1989; Goll et al., 2003; Saido et al., 1994a; Saido et al., 1994b; Suzuki, 1991). Both μ- and m-calpains are heterodimers containing an identical 30-kDa regulatory subunit (Figure 3.07) and different 80-kDa catalytic subunits (Figure 3.07) which share 55–65% sequence homology between the two proteases (Suzuki et al., 1990). The 30K subunit is not essential for protease activity but plays a role as a chaperone and is essential for the 80K subunit to have the correct conformation (Pal et al., 2001; Yoshizawa et al., 1995). Calpain exists in the cytosol as an inactive enzyme and translocates to the membrane in response to increases in $[Ca^{2+}]_c$ levels. Both μ- and m-calpains dissociate into their subunits (autolysis) in the presence of Ca^{2+} and phospholipids (Tompa et al., 2001) and the dissociated 80K subunit functions as the active protease for substrates (Moldoveanu et al., 2002; Tompa et al., 2001) after release from the membrane (Yoshizawa et al., 1995). Although not uncommon for proteases, the autolysis of calpains presents them with some unique features: brief autolysis in vitro in the presence of 1 mM or greater $[Ca^{2+}]_c$ reduces the $[Ca^{2+}]_c$ concentration required for half-maximal proteolytic

activity of μ-calpain from 3–50 to 0.5–2.0 μM and that of m-calpain from 400–800 to 50–150 μM (Goll et al., 2003) without affecting the specific activity of either enzyme (Edmunds et al., 1991). Whether intact calpain is capable of enzymatic activity is unknown however autocatalytic hydrolysis seems to occur consistently under conditions where the calpains are proteolytically active (Goll et al., 1992).

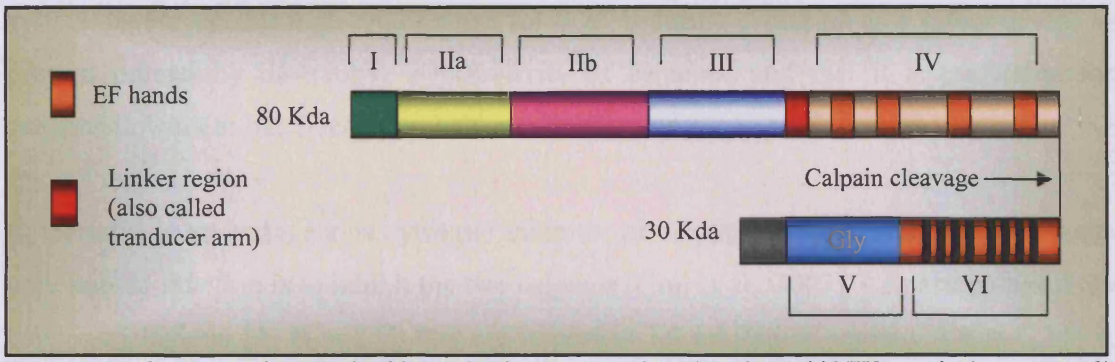

Figure 3.07. Structure of μ-calpain. 80 K subunit structure: 1) a 19-amino acid NH2-terminal sequence; 2) and 3) two domains that constitute the active site, IIa and IIb; 4) domain III; 5) an 18-amino acid extended sequence linking domain III to domain IV; and 6) domain IV, which resembles the penta EF-hand family of polypeptides similar to those found in calmodulin. 30 K subunit structure: 1) a NH_2-terminal domain V which is hydrophobic and believed to bind phospholipids in the plasma membrane (Imajoh et al., 1986) and 2) a COOH-terminal domain VI structurally similar to domain IV (Blanchard et al., 1997). Domains IV and VI interact together to form the heterodimer comprising of the 30 K and 80 K subunits.

As revealed by X-ray crystallography, the mechanism of activation of calpain requires 4 Ca^{2+} ions and comprises two stages (Moldoveanu et al., 2002). The first stage is the binding of Ca^{2+} to domains VI and III domains (Figure 3.07) which results in the release of the constraints imposed by I-VI and II-III domain interactions, thus allowing for autolysis and dissociation of the calpain subunits. These Ca^{2+}-induced structural changes are necessary for activation to form a functional catalytic site (Moldoveanu et al., 2002; Reverter et al., 2001a; Reverter et al., 2001b). The second stage is the rearrangement of the active site cleft caused by binding of two Ca^{2+} ions to the protease domain. Activation by the second stage occurs only after release of the constraints freed by the first stage (Moldoveanu et al., 2002). The requirement of 4 Ca^{2+} ions for proteolytic activation by conformational change allows for sufficient activation of calpain only in the presence of large amounts of intracellular calcium. It should be noted however that in the case of m-calpain, these Ca^{2+} binding events must occur at physiological $[Ca^{2+}]_c$ concentrations, which are in the range of 50–300 nM and much lower than the reported requirements for half-maximal m-calpain activity in vitro. It has also been reported however that the

binding of phospholipids to calpains significantly decreases the $[Ca^{2+}]_c$ requirements in vitro (Arthur and Crawford, 1996; Melloni et al., 1996; Suzuki et al., 1992; Tompa et al., 2001). Similarly, regulation of calpain by protein-protein interactions also changes the requirements of calpain for $[Ca^{2+}]_c$ (Melloni et al., 1998; Michetti et al., 1991). Whether this is also the case in vivo conditions is unknown. Friedrich has recently provided an explanation for this apparent paradox (Friedrich, 2004) where he proposes that the calpain system developed this high requirement for $[Ca^{2+}]_c$ during evolution as a safety device to prevent potentially destructive hyperactivity of calpains, and that it is preferable for calpains to work at much less than half-maximal activity.

Calpastatin is an endogenous cytosolic inhibitor of calpains (Wendt et al., 2004) whose only known function is to inhibit the two calpains (Goll et al., 2003). Calpastatin has three conserved regions (A, B and C) that are important for inhibition: regions A and C block binding of calpain to the membrane while region B reduces the rate of autocatalytic hydrolysis by binding at or near the active site (Tompa et al., 2002). It has been reported that Ca^{2+} is required in vitro for calpastatin binding and inhibition of calpains (Barnoy et al., 1999; Tullio et al., 1999). However, there is no evidence that calpastatin binds Ca^{2+} so the Ca^{2+} requirement for the calpastatin/calpain interaction must originate from the calpain molecule (Kapprell and Goll, 1989; Otsuka and Goll, 1987). The $[Ca^{2+}]_c$ required for calpains to bind to calpastatin is significantly lower than that required to initiate their proteolytic activity (Kapprell and Goll, 1989). It has also been recognized that calpastatin can only inhibit dimeric calpain (both IV and VI domains are required) and dissociated 80K subunits escape from the regulatory actions of calpastatin (Suzuki et al., 2004).

3.3.2 Considerations for mathematical description

The model for calpain regulation (Figure 3.08) was formulated based on the following data: a) calpastatin binds to and inhibits only dimeric calpain, b) Ca^{2+} is required for calpain to bind to calpastatin, c) dissociation of the calpain subunits and activation of the catalytic site of the calpain requires binding of 4 Ca^{2+} in total, two Ca^{2+} ions introducing conformational changes and two Ca^{2+} ions activating the catalytic site of calpain and d)

the region B of calpastatin masks the catalytic site of calpain (where the third and fourth Ca^{2+} ions bind to activate calpain).

Based on data b) and d), calpastatin is assumed to be able to bind to calpain only after the first stage of calpain activation which involves binding of two Ca^{2+} ions. The binding of calpastatin to calpain however is reversible which means that there is some unsequestered calpain that is complexed with Ca^{2+}. Binding of calpain to two more Ca^{2+} ions (to a total of four) results in its autolysis and full activation. Based on data a) and c) and taken that chelation of Ca^{2+} releases calpain from calpastatin in intact form (Kapprell and Goll, 1989; Otsuka and Goll, 1987), the model assumes that calpastatin cannot bind to calpain after its full activation by binding of four Ca^{2+} atoms. This formulation agrees with the observations that the requirement of $[Ca^{2+}]_c$ for calpastatin binding to calpain is lower (close to half) compared with the $[Ca^{2+}]_c$ required to activation of proteolytic activity of calpains (Kapprell and Goll, 1989). As a result, calpastatin inhibits calpain activation during small transient increases of $[Ca^{2+}]_c$, allowing calpain to play an active role only when calcium rises to high or more sustained levels. The exact mechanism of calpastatin regulation is not known and thus it is assumed that calpastatin is constitutively active (not regulated by other factors) and functions as an attenuation rather than preventive mechanism by sequestering a percentage of the active form of calpain. To avoid depletion of intact calpain and accumulation of dissociated 80K subunit occurring by irreversible autolysis (change in mass by removal of 18 and 26 amino acids from the 80K subunit during autolysis), slow degradation rates for 80K and constitutive production of intact calpain were introduced. Upon degradation of calpain 80K, the Ca^{2+} ions are released into the cytosol. The role of the calpain 30K subunit following dissociation is not known and the dynamics of the 30K subunit are therefore not examined. The effect of interaction between phospholipids and calpain on the proteolytic activity of calpain remains controversial and has not been included.

Although not proven yet, the interaction of calpain with talin is expected to influence the speed of inside-out activation of integrins. It is reasonable to assume that at all times intact talin is available and some percentage of it is cleaved depending on the concentration of the dissociated and proteolytically active calpain 80 K. The binding of calpain 80K to talin

is assumed to be reversible if the proteolysis does not occur (Figure 3.08). Similarly to calpain, to avoid depletion of the full length (intact) talin due to irreversible cleavage by calpain, slow rates of degradation for cleaved talin and constitutive production of new talin were introduced. These rates were adjusted to keep the total levels of talin constant in the cytosol.

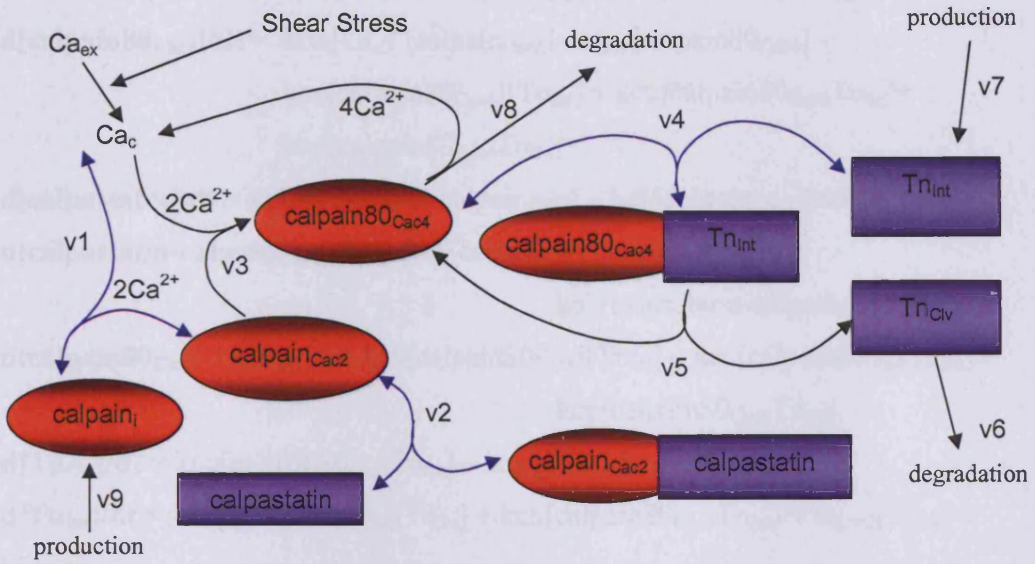

Figure 3.08. Regulation of calpain and cleavage of talin. $calpain_i$ = inactive form of calpain, $calpain_{Cac2}$ = calpain bound to 2 Ca^{2+} ions, $calpain_{80Cac4}$ = calpain subunit 80K bound to 4 Ca^{2+} ions . Tn_{Int} = full length talin, Tn_{Clv} = cleaved talin. The reversible binding reactions are shown with bidirectional blue arrows. The catalytic reactions are given by unidirectional black arrows. Numbers v1-v9 represent all reactions included in the module.

Calpain activation and cleavage of talin are given by the following reactions:

v1, $[calpain_i] + 2[Ca^{2+}] \leftrightarrow [calpain_{Cac2}]$,

v2, $[calpain_{Cac2}] + [calpastatin] \leftrightarrow [calpastatin\text{-}calpain_{Cac2}]$,

v3, $[calpain_{Cac2}] + 2[Ca^{++}] \rightarrow [calpain80_{Cac4}]$

v4, $[calpain80_{Cac4}] + [Tn_{Int}] \leftrightarrow [calpain80_{Cac4}\text{–}Tn_{Int}]$,

v5, $[calpain80_{Cac4}\text{–}Tn_{Int}] \rightarrow [calpain80_{Cac4}] + [Tn_{Clv}]$,

v6, $[Tn_{Clv}] \rightarrow$ degraded,

v7, production $\rightarrow [Tn_{Int}]$,

v8, $[calpain80_{Cac4}] \rightarrow$ degraded + $4[Ca^{2+}]$,

v9, production $\rightarrow [calpain_i]$,

The ODEs calculating the rate of change of the concentration of each molecular species in this module are given below. The ODEs for subsequent modules were constructed in the same manner and are given in the Matlab code (Appendix X).

$$\mathbf{d[calpain_i]/dt} = kcc_r[calpain_{Cac2}] - kcc_f[Ca_c]^2[calpain] + kc_{prod}[calpain_i]$$

$$\mathbf{d[calpain_{Cac2}]/dt} = kcc_f[Ca_c]^2[calpain] - kcc_r[calpain_{Cac2}] - kcl_f[calpain_{Cac2}][calpastatin] + kcl_r[calpastatin\text{-}calpain_{Cac2}] - kcc_f[Ca_c]^2[calpain_{Cac2}]$$

$$\mathbf{d[calpain80_{Cac4}]/dt} = kcc_f[Ca_c]^2[calpain_{Cac2}] - kc_{deg}[calpain80_{Cac4}] - kct_f[calpain80_{Cac4}][Tn_{Int}] + kct_r[calpain80_{Cac4}Tn_{Int}] + kcp[calpain80_{Cac4}Tn_{Int}]$$

$$\mathbf{d[calpastatin]/dt} = kcl_r[calpastatin\ calpain_{Cac2}] - kcl_f[calpain_{Cac2}][calpastatin]$$

$$\mathbf{d[calpastatin\text{-}calpain_{Cac2}]/dt} = kcl_f[calpain_{Cac2}][calpastatin] - kcl_r[calpastatin\text{-}calpain_{Cac2}]$$

$$\mathbf{d[calpain80_{Cac4}\text{-}TnInt]/dt} = kct_f[calpain80_{Cac4}][Tn_{Int}] - kct_r[calpain80_{Cac4}Tn_{Int}] - kcp[calpain80_{Cac4}Tn_{Int}]$$

$$\mathbf{d[Tn_{Clv}]/dt} = kcp[calpain80_{Cac4}Tn_{Int}] - ktt_{deg}[Tn_{Clv}]$$

$$\mathbf{d[Tn_{Int}]/dt} = - kcp[calpain80_{Cac4}Tn_{Int}] + kct_r[calpain80_{Cac4}Tn_{Int}] + kt_{prod}[Tn_{Int}]$$

3.3.3 Parameter values

Parameter values used in the calpain-calpastatin-talin module				
Constant	Description	Value	Units	Source
kcc_f	Association of calpain and Ca^{2+}	0.01	$\mu M^{-1}s^{-1}$	After Goll et al., 2003
kcc_r	Dissociation of calpain and Ca^{2+}	0.25	s^{-1}	After Goll et al., 2003
kcl_f	Association of calpain and calpastatin	3	$\mu M^{-1}s^{-1}$	Takano et al., 1995; Yang et al., 1994
kcl_r	Dissociation of calpain and calpastatin	0.009	s^{-1}	Takano et al., 1995; Yang et al., 1994
kct_f	Association of calpain and talin	0.1	$\mu M^{-1}s^{-1}$	After Goll et al., 2003
kct_r	Dissociation of calpain and talin	0.3	s^{-1}	After Bhalla and Iyengar, 1999
kcp	Rate of talin cleavage by calpain 80K	1.2	s^{-1}	Palecek et al., 1999
kt_{deg}	Degradation rate of cleaved talin	0.006	s^{-1}	After Bhalla and Iyengar, 1999
kc_{deg}	Degradation rate of calpain 80K	0.006	s^{-1}	After Bhalla and Iyengar, 1999
$calpain_t$	Total calpain concentration	0.1	μM	Lane et al., 1992
$calpastatin_t$	Total calpastatin concentration	0.1	μM	Lane et al., 1992
$talin_t$	Total talin = total integrins	0.17	μM	Faull et al., 1993; Palecek et al., 1999

Table 3.03. Parameter values used in the calpain-calpastatin-talin module.

The parameter values for the rates of association and dissociation of calpain and Ca^{2+} and for calpain and calpastatin could not be found in the literature. Dissociation constants (K_d) for these processes however have been reported (Goll et al., 2003). The parameter values needed for most of the reactions in this module were extrapolated from and evaluated based on various sources of experimental data.

Studies on calpain reported that μ-calpain binds ~5–8 Ca^{2+}/molecule with a K_d of ~21–61 μM, whereas m-calpain binds ~11–20 Ca^{2+}/molecule with a much higher K_d of ~ 322–1,300 μM (Goll et al., 2003). These K_d values for the two calpains reflect their respective Ca^{2+} requirements for proteolytic activity. However as the $[Ca^{2+}]_c$ produced by the calcium dynamics module is within the range required for activation of μ-calpain but not high enough for m-calpain (see Figure 3.06), only the K_d reported for μ-calpain was considered for this module. Since only 4 Ca^{2+} are required to activate calpain in the module, a low K_d value (K_d =25 μM) within the range reported was chosen for simulations. Having the K_d value and knowing that $[Ca^{2+}]_c$ levels between 3-50 μM is required for half-maximal activity of calpain (Goll et al., 2003), the model was run for high shear stress conditions (>18 dynes/cm^2) that increased the $[Ca^{2+}]_c$ levels to ~3.5 μM (Figure 3.14). For these shear stress conditions a large number of different sets of forward and reverse rate values were tested with K_d =25 μM in order to identify which rates allowed calpain to reach its half-maximal activity (i.e. 0.5 μM calpain80K_{Cac4} activated). Only one set of values (i.e. kcc_f = 0.01 M^{-1} s^{-1}, kcc_r = 0.25 s^{-1}) best satisfied these conditions (Figure 3.14) and was chosen for the simulations.

Calpastatin is a very tightly binding inhibitor of calpain with a dissociation constant K_d = ~3 nM (Crawford et al., 1990). Studies using subdomains of the calpastatin molecule showed that a 14-amino acid subdomain that was conserved among the four domains of calpastatin (Goll et al 2003) bound specifically to calpain (Takano et al., 1995; Yang et al., 1994) in a Ca^{2+}- dependent manner with K_d = 3.1 nM (= 0.03 μM). Based on this K_d, the values for the forward and reverse rates for calpastatin-calpain interaction were initially estimated as kcl_f = 3 $\mu M^{-1}s^{-1}$ and kcl_r = 0.009 s^{-1} (i.e. Kd = kcl_r/kcl_f, see section 2.4.2). To examine whether these estimates affected the dynamics of downstream molecules, the values were varied over two orders of magnitude in either direction (see section 2.4.3) while keeping the K_d constant. This resulted in very little change in the simulation

dynamics of cleaved talin (Figure 3.09). This is because the calpastatin-calpain interaction is mostly governed by the K_d value and concentration of [calpain-$2Ca^{2+}$] .

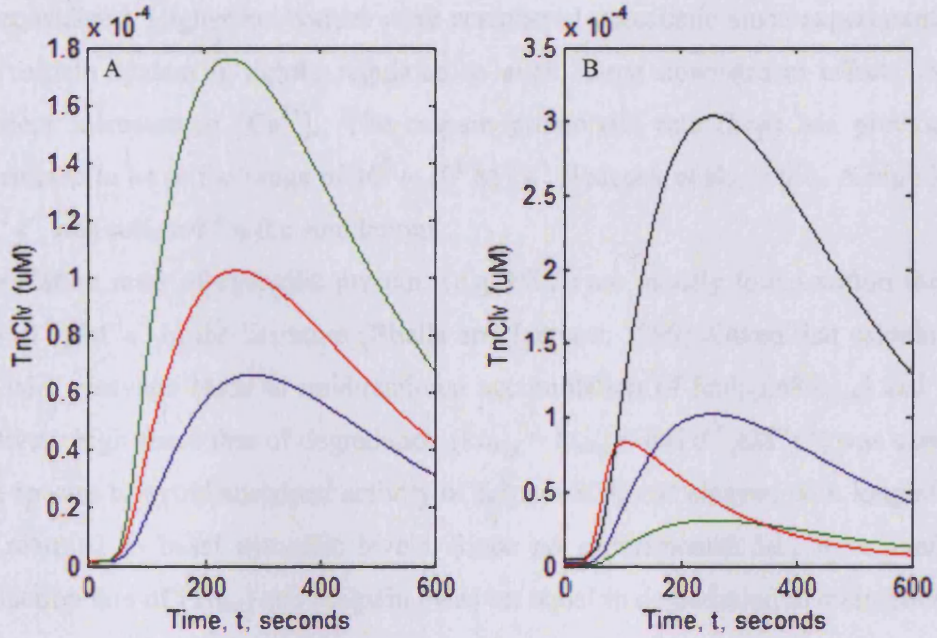

Figure 3.09. Evaluation of parameter values for talin cleavage.
A: Green plot: kclf = 300, kclr = 0.9; Red plot: **kclf = 3, kclr = 0.009**; Blue plot: kclf = 0.03, kclr = 0.00009. The values of kclf and kclr between green and blue plots differ by a magnitude of 10^4 but only result in ~2-fold difference in maximal [Tn_{Clv}]. Thus the sensitivity of downstream dynamics on the values of these parameters was not very significant. The values of kclf = 3, kclr = 0.009 were chosen for simulations.
B: Red plot: [$calpain80_{Cac4}$] dynamics; Black, blue and green plots show the [Tn_{Clv}] dynamics for kctf = 0,3 (black), 0.1 (blue) or 0.01 (green) respectively. Kctf = 0.1 leads to a total [Tn_{Clv}] production approximately proportional to [$calpain80_{Cac4}$]. Higher values (e.g. black plot) result in disproportionally larger amounts of cleaved talin from lower [$calpain80_{Cac4}$].

The forward and reverse rates for the interaction of calpain and talin were also not available in the literature. kct_r was calculated from the ratio kcp/kct_r. Following Bhalla and Iyengar (1999), the ratio $kcp/kct_r = 4$ was applied because it results in a low percentage of an enzyme sequestered in a complex with a substrate over most of the physiological range of enzyme and substrate concentrations. By setting this ratio equal to 4 (Bhalla and Iyengar, 1999), a value of $k_r = 0.3\ s^{-1}$ was obtained (table 3.03). Additional data however to estimate the ratio kcp/kct_r would be very useful in constraining the model. Studies with artificial polypeptides have shown that calpain binds to most substrates with a K_d between 0.1 and 10 μM (Goll et al., 2003). Although these values might deviate from conditions in vivo, $K_d = 3\ \mu M$ was chosen for simulations giving $kct_f = 0.1\ \mu M^{-1}s^{-1}$ ($k_f = k_r/K_d$, see section 2.4.2). Simulations showed that this value for kct_f resulted in [Tn_{Clv}] being

approximately proportional to the [calpain80$_{Cac4}$] (Figures 3.09, 3.11B, 3.11D). Higher values for kct$_f$ resulted in disproportionally large amounts of [Tn$_{Clv}$] from small amounts of [calpain80$_{Cac4}$] (Figure 3.09) (which can result from low amounts of [Ca^{2+}]$_c$) and were not considered. Higher kct$_f$ values were considered unrealistic since experiments indicate that calpain system is tightly regulated to avoid large downstream effects from small transient increases in [Ca^{2+}]$_c$. The calpain proteolytic rate (kcp) has previously been determined to be in the range of $10^2 - 10^6$ M^{-1} s^{-1} (Palecek et al., 1999). A high kcp of 1.2 μM^{-1} s^{-1} was selected for the simulations.

Degradation rates of cytosolic proteins (e.g. PKC) are usually found within the range of 10^{-3}-10^{-6} $\mu M^{-1}s^{-1}$ in the literature (Bhalla and Iyengar, 1999). Given that calpain autolysis and talin cleavage leads to unidirectional accumulation of [calpain80$_{Cac4}$] and [Tn$_{Clv}$], a relatively high fixed rate of degradation (kc$_{deg}$ = kt$_{deg}$ = $6x10^{-3}$ $\mu M^{-1}s^{-1}$) was used here for both species to avoid sustained activity of calpain 80K and cleaved talin long after [Ca^{2+}] has returned to basal cytosolic levels. Since no experimental data were available, the production rate of [Tn$_{int}$] and [calpain$_i$] was set equal to degradation to maintain a constant concentration of each species.

The calpain concentration in the cytosol has been reported to be between $10^{-9} - 10^{-6}$ M (Lane et al., 1992). A value within this range was chosen (0.1 μM). It was assumed that there are approximately equal numbers of calpain and calpastatin molecules in the cell, allowing calpastatin to sequester calpain freely when [Ca^{2+}]$_c$ levels are low. [Ca^{2+}]$_c$ is provided by the calcium dynamics module (section 3.2). The cytosolic concentration of talin is not known and was considered to be equal to the amount of integrins (i.e. there should be one talin molecule available per integrin in a cell). There are approximately 10^5 integrin molecules per endothelial cell (Faull et al., 1993; Garcia et al., 1998; Palecek et al., 1999). As diffusion and spatial events are not considered *per se* for the signalling pathways in this model the volume of the membrane was not considered separately when calculating the concentration of integrins. Considering integrins as molecules existing within the same cell volume their concentration was determined by:

$\eta = n/N$,

where η = number of moles, n = number of molecules and N = 6.023×10^{23} molecules/mole (Avogadro's number), and C = η/V, where C = moles/litre and V (volume) of the cell = 10^{-12} litres (Wiesner et al., 1996; Wiesner et al 1997), it was deduced that 1 μM = 1e-18 moles/cell = 6.023×10^5 molecules/cell. Thus, 10^5 integrins per cell ~= 0.17 μM. Similar conversions were performed for all parts of the model when needed.

Given that there is always $[Ca^{2+}]_c$ available, it is not assumed that at time t = 0 no calpain is bound to Ca^{2+} nor that all talin is intact. The initial conditions for the interacting species of the module were obtained under conditions of steady state in the absence of shear stress or receptor-induced Ca^{2+} influx.

3.3.4 Steady state analysis of species concentrations

Simulations were first run to obtain the concentrations of species at steady state in the absence of shear stress stimulation but in the presence of the inhibitor (calpastatin) (Figure 3.10 A-D). Steady state conditions were attained almost immediately for calpain complexed to two calcium atoms (Figure 3.10A). Calpastatin induced a small attenuation of calcium-induced calpain activation by inhibiting certain amount of calpain (Figure 3.10C) but more significantly a delay in complexation of calcium to the last two calcium atoms that fully activate [calpain80Cac4] as can be seen from (Figure 3.10A) and (Figure 3.10B). Following delayed activation of calpain, the cleavage of talin was also delayed compared to [calpain80Cac4] and the levels of talin cleavage at physiological levels of intracellular calcium (0.1 μM) were found to minimal ~= 0.001 % percentage of total talin (Figure 3.10D).

The simulations were also run in the absence of calpastatin (Figure 3.10 E-H). For basal $[Ca^{2+}]_c$ the absence of inhibitors does not change the amount of concentration of species generated significantly, although this generation occurs much faster due to the elimination of the delay occurring from calpastatin inhibition. Calpastatin reduces significantly the generation of active calpain and cleavage of talin only following increases in $[Ca^{2+}]_c$ as will be demonstrated later.

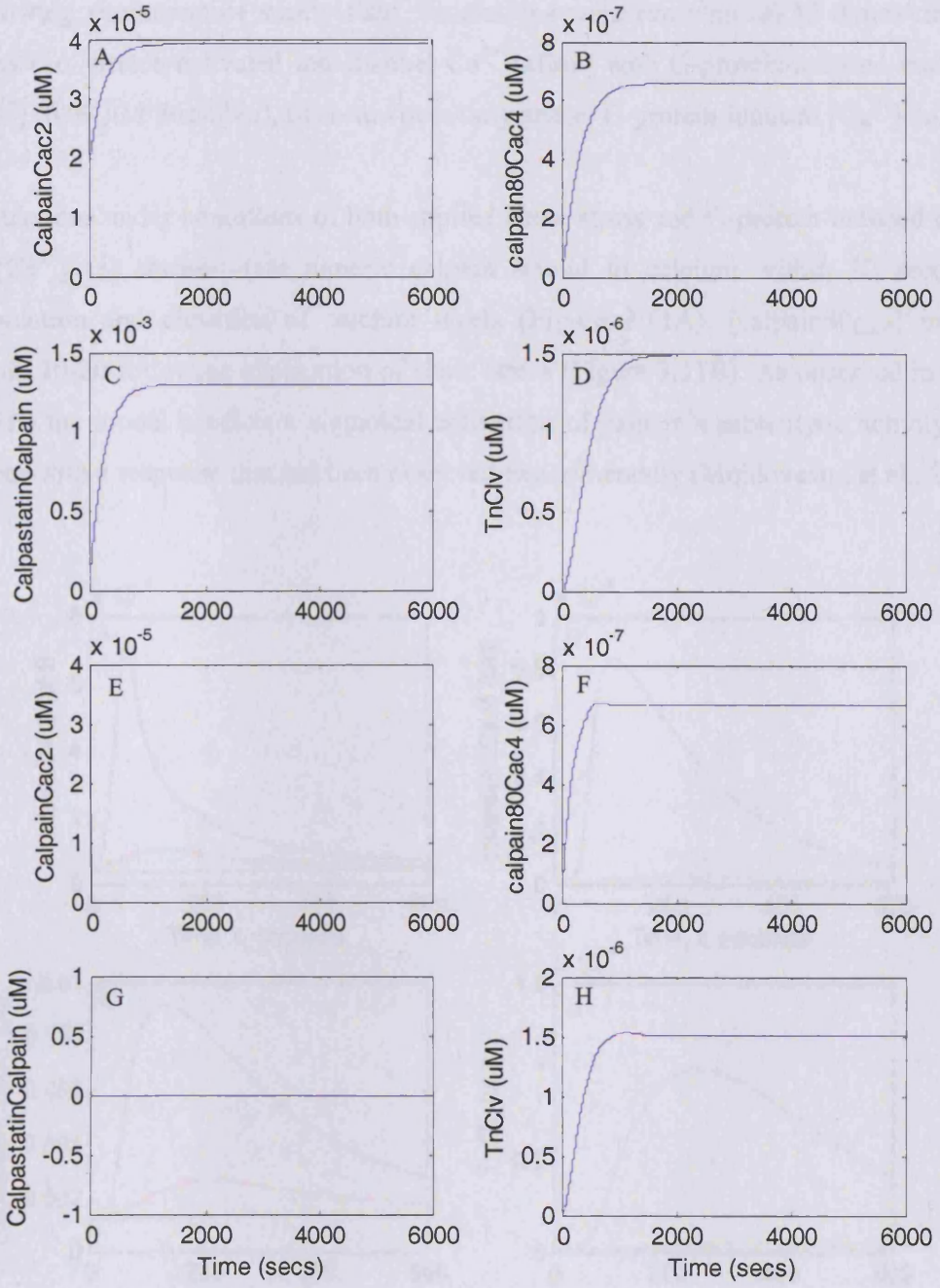

Figure 3.10 Dynamics of species concentrations at steady state (calpain module). A to D examine the dynamics of species in the presence of calpastatin. E to H show the dynamics of species in the absence of calpastatin. For nomenclature of species names see Figure 3.08. uM = μM.

3.3.5 *Analysis of simulation results under shear stress conditions*

Following attainment of steady state, simulations were run with :a) 12 dynes/cm^2 shear stress (i.e. stretch-activated ion channel Ca^{2+} influx) with G-protein-induced increase in [Ca^{2+}] (0.09 μM thrombin), b) shear stress only and c) G-protein-induced [Ca^{2+}] only.

Simulations under conditions of both applied shear stress and G-protein-induced increase of [Ca^{2+}] (a) showed that dimeric calpain bound to calcium within 10 seconds of stimulation and elevation of calcium levels (Figure 3.11A). [calpain80$_{Cac4}$] increased within 10-20 following application of shear stress (Figure 3.11B). As observed in (Figure 3.11B) the model predicts a sigmoidal activation of calpain's proteolytic activity which agrees with a response that has been observed experimentally (Moldoveanu et al., 2002).

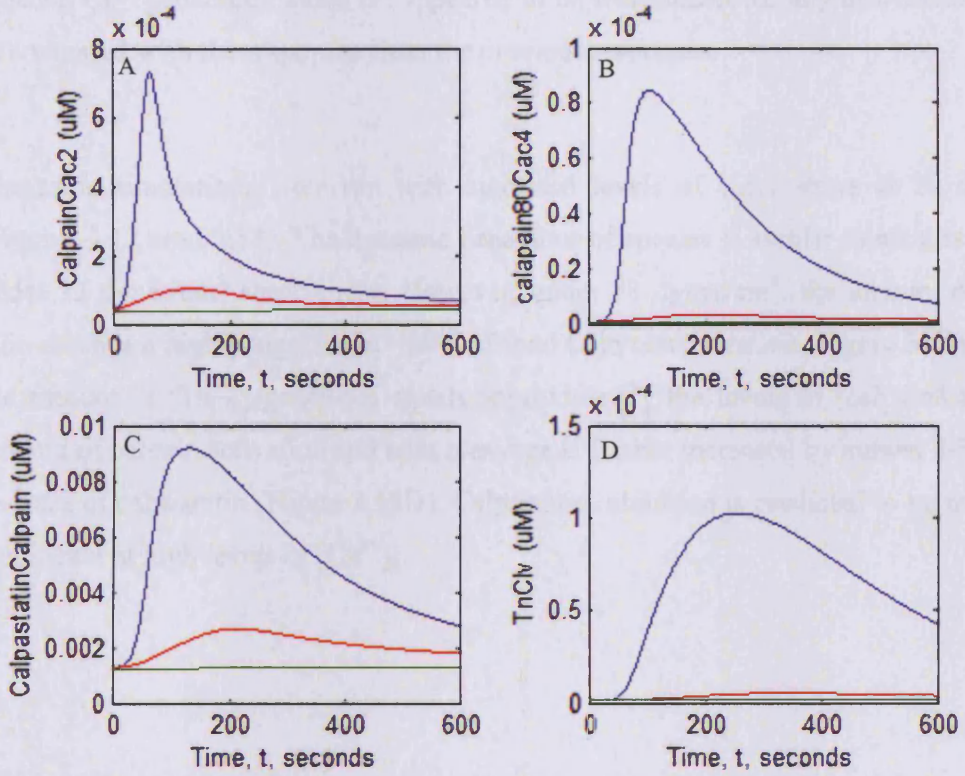

Figure 3.11. Effect of applied stimuli on species concentration dynamics (calpain module). Combination of both shear stress (12 dynes/cm^2) and G-protein-induced Ca^{2+} generation is shown in blue, shear stress 12 dynes/cm^2 alone is shown in red, G-protein-induced Ca^{2+} generation alone is shown in green.

Calpastatin attenuates calpain activation by sequestration of a proportionally large amount of calpain when calcium levels increase (Figure 3.11 B and C). Generation of [Tn_{Clv}] was slightly delayed compared to the generation of [$calpain80_{Cac4}$] and observed after 45-55 seconds of stimulation (Figure 3.11 D). The amount of talin cleavage increased somewhat proportionally with the levels of [$calpain80_{Cac4}$] (Figure 3.11 B and D). At time t = 0 (absence of stimulation) and basal levels of calcium, there was some free calpain complexed to calcium (Figure 3.11 A) and also sequestered by calpastatin (Figure 3.11 B), but a 100-fold less amount of [$calpain80_{Cac4}$]. The model showed that [$calpain80_{Cac4}$] was being activated significantly only after elevation of intracellular calcium levels. Conditions of shear stress of 12 dynes/cm^2 alone (b) showed observable but much lower influence on dynamics of species compared with those that result from synergistic stimulation of shear stress and G-protein-induced [Ca^{2+}] generation. Finally, G-protein-induced Ca^{2+} generation alone (c) appeared to be insufficient for any downstream effects as compared with the responses from the previous responses.

The same simulations were run with increased levels of shear stress at 18 dynes/cm^2 (Figures 3.12 amd 3.13). The dynamic behaviour of species is similar to what is observed under 12 dynes/cm^2 shear stress. However, under 18 dynes/cm^2, the amount of cleaved talin reaches a highly significant ~15% of total talin concentration (Figure 3.12G). Again the amount of [Tn_{Cln}] generated equals approximately the levels of [$calpain80_{Cac4}$]. The amount of calpain activation and talin cleavage is further increased by almost 2-fold in the absence of calpastatin (Figure 3.13D). Calpastatin inhibition is predicted to be much more significant at high levels of $[Ca^{2+}]_c$.

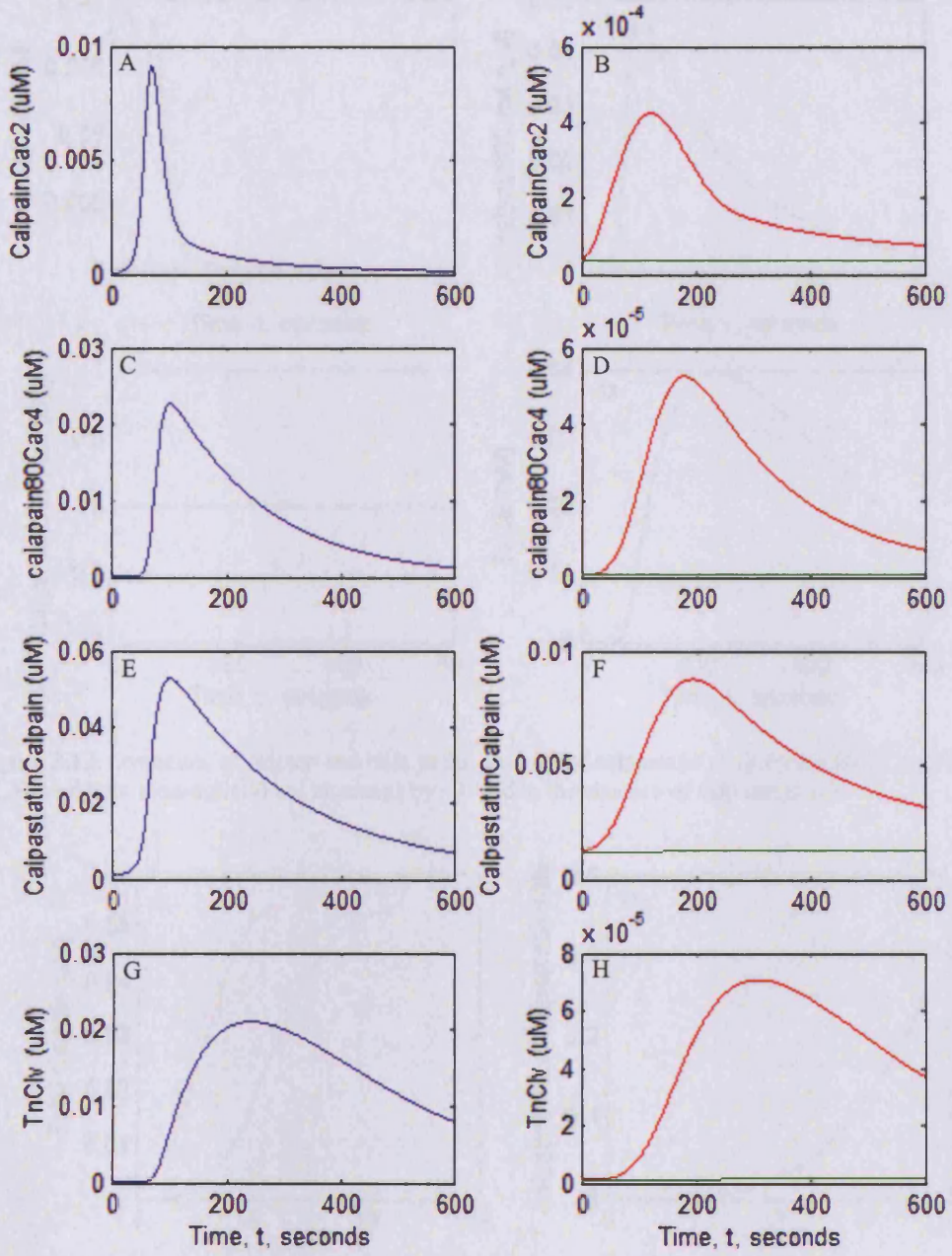

Figure 3.12 Effect of enhanced stimuli on species concentration dynamics. Combination of both shear stress of 18 dynes/cm^2 and G-protein-induced Ca^{2+} generation is shown in blue, shear stress 18 dynes/cm^2 alone is shown in red, G-protein-induced Ca^{2+} generation alone is shown in green.

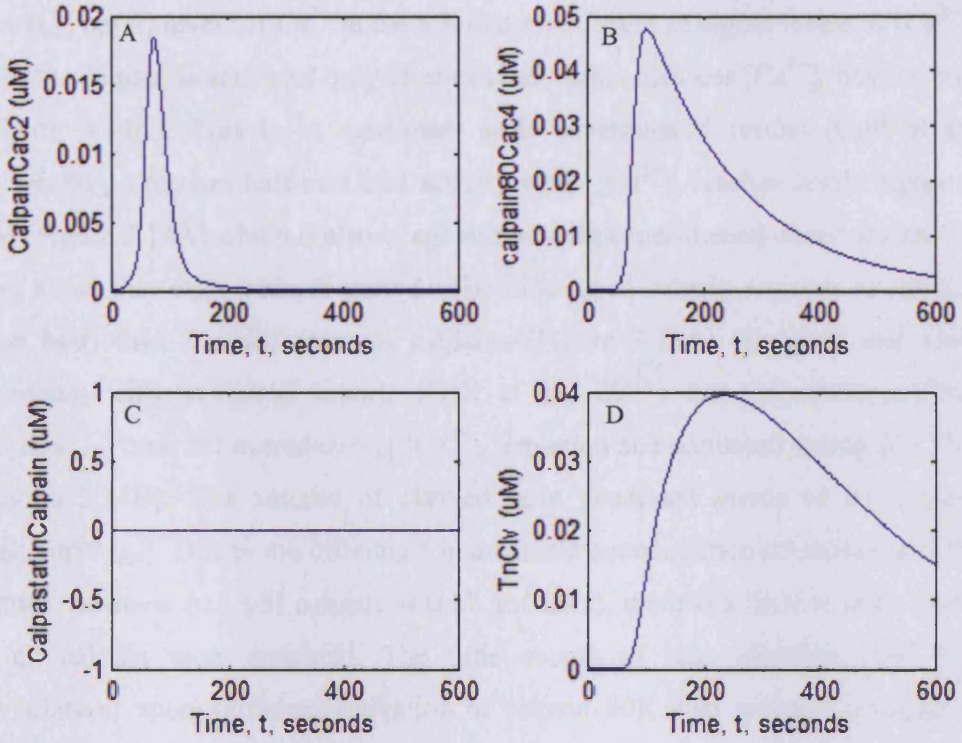

Figure 3.13. Dynamics of calpain and talin in the absence of calpastatin at 18 dynes/cm^2. Calpain activation (A, B) and talin cleavage (D) are increased by ~2-fold in the absence of calpastatin (C).

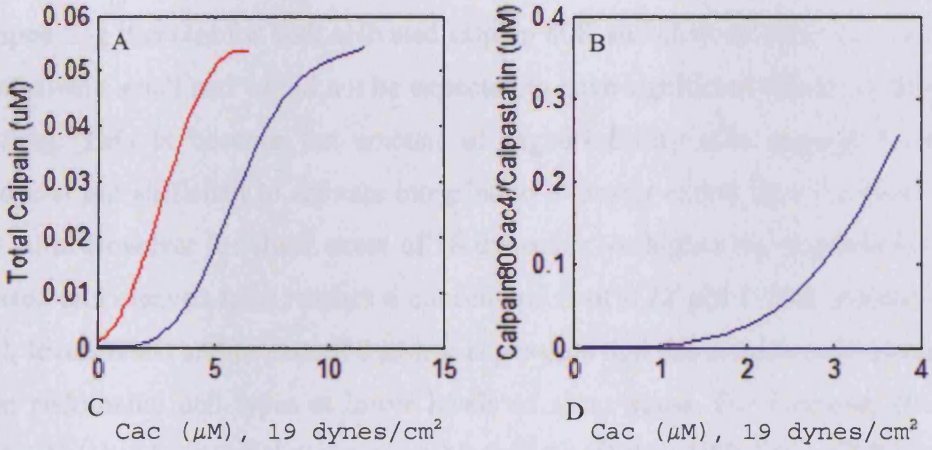

Figure 3.14. Analysis of species dynamics at shear stress equal or greater than 18 dynes/cm^2 (19 dynes/cm^2). Plots demonstrate requirement of $[Ca^{2+}]_c$ for activation of calpain and calpastatin. A: Red plot shows the relationship between $[Ca^{2+}]_c$ levels and produced $[calpain_{Cac2}]$ that can complex with calpastatin. Blue plot shows the relationship between $[Ca^{2+}]_c$ levels and $[calpain80_{Cac4}]$. As observed, the requirement of calcium [] levels for $[calpain80_{Cac4}]$ reaching its half maximal activity (>0.05μM) is 3 μM and above which is in agreement with experimental reports (Goll et al., 2003).B: Plot shows the ratio of total active calpain to complexed calpastatin-calpain $[calpain80_{Cac4}]/[calpastatin\text{-}calpain_{Cac2}]$. This ratio increases at higher levels of cytosolic calcium.

Overall the model predicts that calpastatin inhibits calpain activation to a certain extent at low (i.e. basal) levels of Ca^{2+} in the cell and much more at higher levels of $[Ca^{2+}]_c$ (Figure 3.14A). Calpain is activated only after calcium influx elevates $[Ca^{2+}]_c$ beyond basal levels (Figure 3.14A). This is in agreement with experimental results (Goll et al., 2003). $calpain80_{Cac4}$ reaches half-maximal activity when $[Ca^{2+}]_c$ reaches levels higher than of 3 μM (Figure 3.14A) which is also in agreement with experimental observations. The results also show that calpastatin (Figure 3.14B) binding to calpain requires lower $[Ca^{2+}]$ (less than half) than the activation of calpains (Figure 3.14A) (Kapprell and Goll, 1989). Agreeing with published reports (Goll et al., 2003) the $[calpain80_{Cac4}]$/$[calpastatin\text{-}calpain_{Cac2}]$ ratio is lowered during $[Ca^{2+}]_c$ depletion and increased during $[Ca^{2+}]_c$ repletion (Figure 3.14B). The amount of cleaved talin generated seems to be proportional to $[calpain80_{Cac4}]$. Due to the difference in available concentration of calpain and talin in the cytosol however (0.1 μM calpain vs 0.17 μM talin), there is a limit to talin cleavage even if all calpain were activated. The time course of talin cleavage (>45 seconds of stimulation) upon sufficient activation of calpain 80K also matches accurately recently produced experimental observations (unpublished, courtesy of Christodolou M).

For the increase in $[Ca^{2+}]_c$ at applied shear stress of 12 dynes/cm^2 however, the corresponding increase for both activated calpain 80K and cleaved talin (e.g. ~$1x10^{-4}$ μM) was relatively small and would not be expected to have significant effects on downstream signalling. This is because the amount of higher-affinity talin generated by calpain cleavage is not sufficient to activate integrins to a greater extent than the basal levels of intact talin. However for shear stress of 18 dynes/cm^2 or higher the response is markedly increased and cleaved talin reaches a concentration of 0.22 μM (~13K molecules) when $[Ca^{2+}]_c$ levels reach and/or exceed 3 μM. It is possible that this result would be obtained in certain endothelial cell types at lower levels of shear stress. For example, BAECs can withstand higher levels of shear stress (>16 dynes/cm^2) than HUVECs which may be due to differences in membrane stiffness between these cell types resulting from different cytoskeletal organization, different lipid or ion channel composition and integrin-substrate adhesion. As membrane deformality and stiffness governs the levels of calcium influx, it is possible that the significant differences modeled here in BAECs at shear stress of >=18 dynes/cm^2 to be equivalent with a similar response in HUVECs at lower shear stress levels

(e.g. different Ca^{2+} influx). The difference between HUVECs and BAECs clearly needs further investigation and would lead to a better understanding of the observations recorded with different cell lines and experimental conditions.

3.3.6 Conclusions and discussion

It is not yet understood why calpain cleaves talin thereby inducing activation of integrins while at the same time cleaving integrins, FAK and paxillin (Carragher et al., 1999; Cooray et al., 1996) which would reduce the assembly of focal adhesions. Three possible mechanisms are presented here to explain this: First, that cleaved talin prevents calpain from interacting with the focal complexes containing cleaved talin but not intact talin. This would be valid if calpain binds only to talin but is able to cleave other proteins nearby. As the amount of cleaved talin is much lower than that of intact talin, stimulation by calcium and increased active calpain would result in an overall decrease of the amount of focal adhesions observed macroscopically but also in bigger and stronger focal adhesions free of proteolysis from calpain (fewer but bigger focal complexes and adhesions). Second, that talin competes with calpain access to molecules such as integrins, FAK and paxillin (assuming that calpain can bind directly to these molecules) and resulted cleavage possibly by requiring the same binding surface/access for function. As cleaved talin has an apparent K_a 16-fold higher (resulting from a 100-fold increase in association rate of cleaved talin to integrins, Yan et al 2001) that the K_a of intact talin for binding to integrins, this would mean that calpain binds and cleaves 16 intact talin containing-focal complexes and only 1 cleaved talin-containing focal complexes in the same amount of time. Thus, although the total turn-over of focal complexes would be increased due to calpain activation, the ratio of large-strengthened focal complexes/normal focal complexes would also be increased which would likely result in macroscopic observations similar to the first mechanism. Inhibition of calpain on the other hand, would result in a decreased focal complex turnover, which is in agreement with the phenotype of slow focal adhesion turn-over in cells expressing calpain-resistant talin (Franco et al., 2004), but the focal complexes and adhesions formed would not be as strong and potentially large compared to those containing cleaved talin from calpain. Investigation of the influences of calpain activation on the morphology adaptation of the endothelial cells would shed light in this

question. The third mechanism can be derived upon structural and experimental data on certain molecules. Intact talin has it head domain masked by the rod domain. Calpain cleavage however removes the rod inhibition from the talin head and results in generation of rod and head fragments. It is also known however that the rod domain of talin contains several binding sites for the actin-binding adaptor protein vinculin and a major F-actin binding site (Critchley, 2004). Therefore it is possible that calpain-mediated cleavage of talin could disrupt/inhibit the interaction of integrins with the actin-linking proteins and actin cytoskeleton therefore decreasing formation of focal adhesions (Giannone et al., 2004) while simultaneously promoting integrin activation by increased binding of talin to integrins. This mechanism would be in agreement with experimentally observed morphological changes that have shown that subconfluent endothelial cells contract and retract in response to application of fluid flow-induced shear stress which likely occurs as a result of Rho activation (Wojciak-Stothard and Ridley, 2002; Wojciak-Stothard and Ridley, 2003) and dissociation of integrin-fibronectin bonds. Furthermore, it would be in agreement with observations showing that activated talin-bound β_3 integrins can cluster without being associated with actin filaments and that truncated talin (i.e. calpain-cleaved) enhances clustering (Cluzel et al., 2005). Clustering occurs because talin has two head domains positioned at both ends (Isenberg and Goldmann, 1998) that can cross link integrin receptors. It is possible that the third mechanism takes place in conjunction with one of the first two mechanisms to regulate both intracellular signalling and morphological adaptation of endothelial cells to shear stress. Nevertheless, because cleavage of talin is not sufficient to affect the activation of integrins significantly as it will be shown in the next section, it may be that its primary purpose is to induce integrin clustering while influencing signalling dynamics significantly only at high levels of applied shear stress. No evidence supporting this exists however and further research is required for better understanding of the significance of the cellular roles of these molecules.

Overall, the model predicts quantitatively and matches the dynamic behaviour of observed molecular responses, gives insight on the timing of each molecular response and shows clearly the effects of activation and inhibition and the dependence of the magnitude of responses on the cytosolic calcium levels. Careful construction of this module and

predictions of satisfactory accuracy make it easily fit for integration with further upstream and downstream modules of molecular dynamics.

3.4 Activation of integrins by talin cleavage (Module 3)

3.4.1 Module description

Talin is an elongated (approx. 60 nm) 260 kDa flexible molecule (Winkler et al., 1997) consisting of a N-terminal approximately 50 kDa globular head and a 220 kDa c-terminal rod (Critchley, 2000; Critchley, 2005). It is known to bind to β1A, β1D, β2, β3 and β5 integrin tails (Calderwood et al., 1999; Critchley, 2000). The major integrin-binding site lies within the talin head (Calderwood et al., 1999; Yan et al., 2001) although the rod also contains a lower-affinity integrin-binding site (Calderwood et al., 1999; Yan et al., 2001). Talin binds to integrins via a FERM domain located in the talin head (Calderwood et al., 2002; Calderwood et al., 1999). The FERM domain consists of F1, F2 and F3 subdomains out of which the F3 subdomain which resembles a PTB domain is primarily responsible for binding to integrins (Calderwood et al., 2002; Calderwood et al., 1999). RNAi knockdown of talin expression has revealed that talin is essential for β1 and β3 integrin activation in a variety of cells (Tadokoro et al., 2003) and that requirement for talin cannot be bypassed by physiological agonists or by expression of other putative integrin-activating proteins (Tadokoro et al., 2003). Prior to talin binding, the membrane proximal regions of integrin α and β subunit cytoplasmic tails are held together by a disulfide bridge between R^{995} and D^{723} that keep integrins in inactive state (Hughes et al., 1996). Talin binding disrupts this salt bridge thereby inducing cytoplasmic tail separation that results in integrin activation (Kim et al., 2003; Luo et al., 2004; Vinogradova et al., 2002).

Although the mechanism and regulation of integrin activation is still under investigation, considerable evidence now supports that integrin activation (transition from low- to high-affinity state for targets) requires talin binding to the β tail (Calderwood et al., 1999; Carman and Springer, 2003; Kim et al., 2003). It is believed that talin binding to integrin β cytoplasmic domains initiates integrin activation by inducing conformational changes to integrins resulting in the unfolding of the extracellular domain of integrins which opens up permitting for binding of the ligand and full activation of integrin receptors (Calderwood, 2004a; Calderwood, 2004b; Campbell and Ginsberg, 2004; Cram and Schwarzbauer, 2004; Ratnikov et al., 2005; Xiong et al., 2003). Cleavage of talin by calpain regulates its interaction with integrins as cleavage of intact talin releases the head domain and results in a 16-fold increase in apparent association constant (Yan et al., 2001).

At molecular level, talin contains several binding sites for F-actin, vinculin and integrins (Critchley, 2000; Xing et al., 2001). However, as vinculin and F-actin are structural elements that promote linkage of integrins to cytoskeleton (Critchley, 2000) and are not known to influence downstream signalling dynamics, they are not considered here. Cell attachment to ECM is primarily mediated by integrin binding to ligands such as fibronectin, vitronectin, laminin or collagen (see 1.3.6). Different ligands bind to different integrins of endothelial cells, for example collagen binds mainly to $\alpha_2\beta_1$ and $\alpha_1\beta_1$ (Davis et al., 2000; Senger et al., 1997), laminin preferentially binds to $\alpha_6\beta_1$ (Wixler et al., 1999), vitronectin binds to $\alpha_v\beta_3$ and fibronectin mainly binds to $\alpha_v\beta_3$ and $\alpha_5\beta_1$.

3.4.2 Considerations for mathematical description

Because the β_1- and β_3-containing integrins are predominant in BAECs (Dejana, 1993; Dejana et al., 1993) and the available time-dependent observations of integrin activity originate from experiments performed on $\alpha_v\beta_3$ and $\alpha_5\beta_1$ integrins (Goldmann, 2000; Li et al., 2005a; Li et al., 2005b; Li et al., 1997; Tzima et al., 2001), these were considered for the model. Fibronectin was chosen as the ligand molecule of preference in the model because it binds mainly $\alpha_v\beta_3$ and $\alpha_5\beta_1$ (Li et al., 2005) and most of the evidence around integrin-ligand binding originates from experiments using fibronectin (Garcia and Boettiger, 1999; Garcia et al., 1999). Because experimental observations for activation dynamics of integrins in shear stress conditions were available for $\alpha_v\beta_3$ (Tzima et al., 2001), $\alpha_v\beta_3$ was chosen as the integrin receptor in the model.

The model presents the case where one talin molecule (either in full-length or cleaved form) and one fibronectin molecule bind to one integrin receptor with a stoichoiometry 1:1:1. Binding of talin and fibronectin to integrins as a two-step mechanism result in their activation and allows them to further interact with downstream targets at basal affinity rates. Although it is possible that fibronectin binds to integrins at lower affinities prior to their activation by talin this is not included in the model as it is currently believed that activation of integrins must initiate from inside-out. In the model fibronectin can only bind and activate integrins only after association of integrins with talin.

Both binding of talin and fibronectin to integrins are standard affinity reactions and considered to be reversible in the model (Figure 3.15). However the model includes the

possibility of dissociation of talin from the complex when both talin and fibronectin are bound to integrin receptors (Figure 3.15). This was included because talin binds intracellularly while fibronectin extracellularly (not physically attached to each other) and there has not been any experimental indication that binding of fibronectin prevents the dissociation of talin from integrin. Therefore talin could still dissociate at physiological rates after fibronectin has bound to integrins. On the basis of activation of integrins (fibronectin binding requires conformational changes of integrins resulting from talin binding) it is assumed that dissociation of talin from the complex will also result in spontaneous dissociation of fibronectin (integrins return to initial conformation). The same logic has been applied in subsequent reactions in the model. While it is possible that the bigger the focal protein complex becomes it is biochemically less likely for such abstract dissociation to occur, this was not considered due to lack of related data regarding such events. It is also possible that different integrins have different association/dissociation rates, however only $\alpha_v\beta_3$ (and $\alpha_5\beta_1$) integrins are considered in the model.

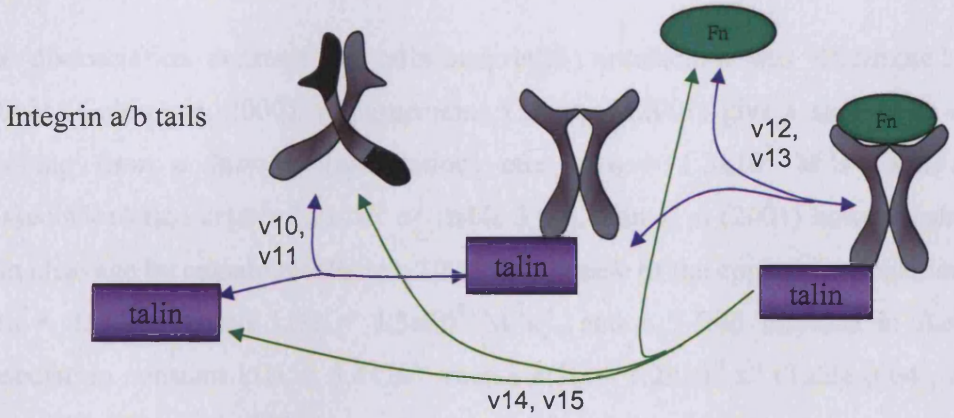

Figure 3.15. Binding of talin and fibronectin to integrin. Reactions rates v10-v15 depict the binding and unbinding events for both intact talin and cleaved talin respectively. Fn stands for fibronectin (which has an oval-like structure as shown in the Figure). Reactions v14 and v15 depict the unbinding of talin (intact talin and cleaved talin respectively) from integrins resulting in complete dissociation of the protein complex.

The activation of integrin receptors is given by the following equations:

v10, $[Tn_{Int}] + [\alpha_v\beta_3] \leftrightarrow [Tn_{Int}\text{-}\alpha_v\beta_3]$,

v11, $[Tn_{Clv}] + [\alpha_v\beta_3] \leftrightarrow [Tn_{Clv}\text{-}\alpha_v\beta_3]$,

v12, $[Tn_{Int}\text{-}\alpha_v\beta_3] + [Fn] \leftrightarrow [Tn_{Int}\text{-}\alpha_v\beta_3\text{-}Fn]$,

v13, $[talin_{Clv}\text{-}\alpha_v\beta_3] + [Fn] \leftrightarrow [Tn_{Clv}\text{-}\alpha_v\beta_3\text{-}Fn]$,

v14, $[Tn_{Int}\text{-}\alpha_v\beta_3\text{-}Fn] \rightarrow [Tn_{Int}] + [\alpha_v\beta_3] + [Fn]$

v15, $[Tn_{Clv}\text{-}\alpha_v\beta_3\text{-}Fn] \rightarrow [Tn_{Clv}] + [\alpha_v\beta_3] + [Fn]$

3.4.3 Parameter values

Parameter values used in the talin-integrin-fibronectin module				
Constant	Description	Value	Units	Source
$kt1i_f$	Binding of intact talin with integrins	0.0013	$\mu M^{-1}s^{-1}$	Yan et al., 2001
$kt1i_r$	Unbinding of intact talin with integrins	0.00072	s^{-1}	Yan et al., 2001
$kt2i_f$	Binding of cleaved talin with integrins	0.14	$\mu M^{-1}s^{-1}$	Yan et al., 2001
$kt2i_r$	Unbinding of cleaved talin-integrins	0.0054	s^{-1}	Yan et al., 2001
kfi_f	Binding of fibronectin to integrins	0.0117	$\mu M^{-1}s^{-1}$	Akiyama and Yamada, 1985
kfi_r	Unbinding of fibronectin to integrins	0.01	s^{-1}	Akiyama and Yamada, 1985
[Talin]	Total talin = total integrins	0.17	μM	Faul et al., 1993; Garcia et al., 1998
[Fn]	Total fibronectin	$5x10^5$	molecules	After Bhalla & Iyengar, 1999
$[\alpha_v\beta_3]$	Total integrins	0.17	μM	Palecek et al., 1999; Faul et al., 1993; Garcia et al., 1998

Table 3.04. Parameter values used in the talin-integrin-fibronectin module

The disscociation constant for talin-integrin(β_3) interaction was determined as K_d = 400nM (Goldmann, 2000). In agreement, Yan et al (2001) give a similar K_d of 550nM resulting from a forward (association) rate $kt1i_f = 1.3x10^3\ M^{-1}s^{-1}$ and a reverse (dissociation) rate $kt1r_r = 7.2x10^{-4}\ s^{-1}$ (table 3.04). Yan et al (2001) however showed that talin cleavage by calpain results in a 100-fold increase of the apparent association constant $kt2i_f = 1.4x10^5$ versus $kt1i_f = 1.3x10^3\ M^{-1}s^{-1}$, and a 7-fold increase in the apparent dissociation constant $kt1i_r = 5.4x10^{-3}$ versus $kt1i_r = 7.2x10^{-4}\ s^{-1}$ (Table 3.04), relative to intact talin (Yan et al., 2001).

Some affinity constants for integrin-fibronectin binding were found in the literature. (Akiyama and Yamada, 1985) evaluated the association rate at $kfi_f = 7x10^5\ M^{-1}\ min^{-1}$ (= 0.0117 $\mu M^{-1}\ s^{-1}$) and the dissociation rate at kfi_r = 0.6 min^{-1} (= 0.01 s^{-1}) giving a dissociation constant K_d =0.8547 μM (Lauffenburger and Linderman, 1993). The dissociation constant however has been shown to vary from $4x10^{-8}$ (McKeown-Longo and Mosher, 1985) to >1 μM (Wu, 1997), depending on cell type. Goldmann (2000) reported a dissociation constant of binding of fibronectin to integrins at K_d = 0.4 μM (Goldmann, 2000) at a molar ratio 1:1. Garcia et al (1998) and Faul et al (1993) have reported also a

K_d = 0.1-1 μM. Because the only values for reverse and forward rates originate from the work of Akiyama and Yamada and also because the dissociation constant derived by their experiments is also in very close proximity with the one given by Goldmann (2000) and within the Kd range reported by Garcia et al (1998) and Faul et al (1993) these values were used in the model.

Similarly to calpain activation, by expecting that there is always a basal amount of cleaved talin present in the cytosol, and that integrins form bonds with the fibronectin coated surface before application of shear stress, the initial conditions for the intermediate produced interacting species of the module are obtained upon conditions of steady state in absence of shear stress force stimuli and receptor-induced calcium generation.

The total concentrations of talin and integrin have been given in section 3.3.3. Fibronectin was given at $5x10^5$ molecules available per endothelial cell (10μg/ml).

3.4.4 Steady state analysis of species concentrations

Steady state runs were first generated from the model to obtain the initial concentrations of talin-integrin and talin-integrin-fibronectin complexes for both intact and cleaved talin. The talin consumption (Figure 3.16 A) is equal to consumption of integrins (Figure 3.16 C) and fibronectin (Figure 3.16 D) and the resulted formation of talin-integrin complexes. Some amount of talin exists in cleaved form and unbound (Figure 3.16 B) at steady state as given by module 2, although at low basal levels. The amount of integrin-fibronectin bonds formed at steady state is linearly proportional to the amount of talin-integrin bonds (Figure 3.16 E and C). Furthermore, the concentration of cleaved talin bound to integrins is 3-fold higher than the concentration of free cleaved talin in the cell (Figure 3.16 B, F and H). This results from the high affinity rate of cleaved talin. Interestingly however, the concentration of complexes with fully activated integrins by cleaved talin and fibronectin (Figure 3.16 H) equal the concentration of free cleaved talin (Figure 3.16 B).

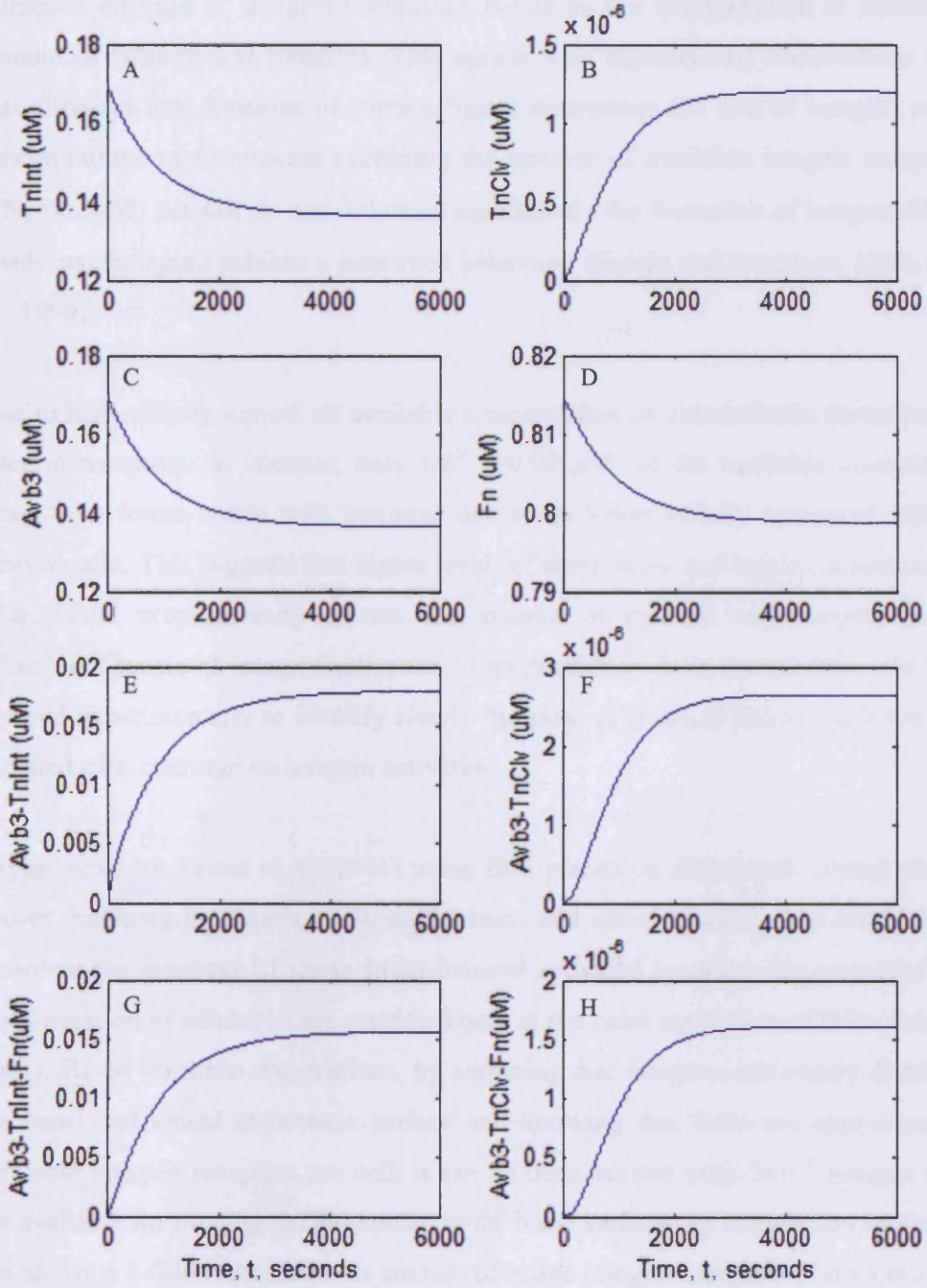

Figure 3.16. Initial concentrations and consumption of reactants after 6000 secs of incubation. The dynamics of steady state (equilibrium) concentrations attained for free species ($\alpha v\beta 3$, fibronectin, talin) and the four complexes forming at the membrane (intermediate species) resulting from binding of intact/talin and fibronectin to integrins are shown.

The model predicts that the available concentration of fibronectin molecules does not influence the rate of integrin-fibronectin bonds as the complexation is limited by the amount of talin-primed integrins. This agrees with experimental observations reporting that although low densities of surface ligand determines the rate of integrin activation, concentrations of fibronectin exceeding the number of available integrin receptors (e.g. [FN]> 0.3μM) per cell do not influence significantly the formation of integrin-fibronectin bonds, as the ligand exhibits a saturation behaviour (Garcia and Boettiger, 1999; Garcia et al., 1999).

Due to high affinity almost all available concentration of cleaved talin forms bonds with integrin receptors. In contrast, only $1/8^{th}$ (~0.02 μM) of the available concentration of intact talin forms bonds with integrins due to its lower affinity compared with that of cleaved talin. This suggests that higher levels of shear stress and larger amounts of cleaved talin would proportionally elevate the amount of cleaved talin-integrin bonds and subsequent levels of integrin activation. This prediction from the model could be easily verified experimentally to identify clearly the ratio of $[talin_{int}]/[talin_{clv}]$ and the effect of elevated talin cleavage on integrin activation.

Experiments by Tzima et al (2001) using ECs placed on fibronectin coated plates have shown that integrins localize both on the basal and apical membrane of endothelial cells. However the presence of shear stress-induced activated integrins (by increased affinity) and formation of adhesions are restricted only at the basal membrane of ECs (Tzima et al., 2001). Based on these observations, by assuming that integrins are evenly distributed on the basal and apical membrane surface and knowing that there are approximately 10^5 available integrin receptors per cell, it can be deduced that only $5x10^4$ integrin receptors are available for binding to fibronectin on the basal surface. As stimulation by shear stress has shown a 3-fold increase in the amount of active integrin receptors (Tzima et al., 2001), the amount of basal integrin-fibronectin bonds (i.e. active integrins) prior to shear stress stimuli can be empirically evaluated in the order 10^3 activated integrins (approximately 0.017 μM in concentration units). The simulation results based on the kinetic values used, predict an equilibrium basal concentration of active integrins (prior to shear stress) of approximately 0.16 μM which is in good agreement with the expected value.

3.4.5 *Analysis of simulation results under shear stress conditions*

Following identification of the basal levels of active integrins at steady state, simulations at applied shear stress 12 dynes/cm^2 were applied for ~30 minutes of real time (2000 secs). Upon shear stress initiation and calcium influx, calpain activation (taken from module 2) elevates the amount of cleaved talin in the cell in a transient manner. As the concentration of cleaved talin increases it results also in increased bonds with integrin receptors and their final activation by fibronectin (Figure 3.17 B and D). The amount of intact talin-integrin bonds does not increase/decrease to noticeable levels upon application of shear stress (Figure 3.17 A and C). This is because the amount of reduction in available intact talin concentration due to talin cleavage is very low and thus does not affect the affinity for integrins.

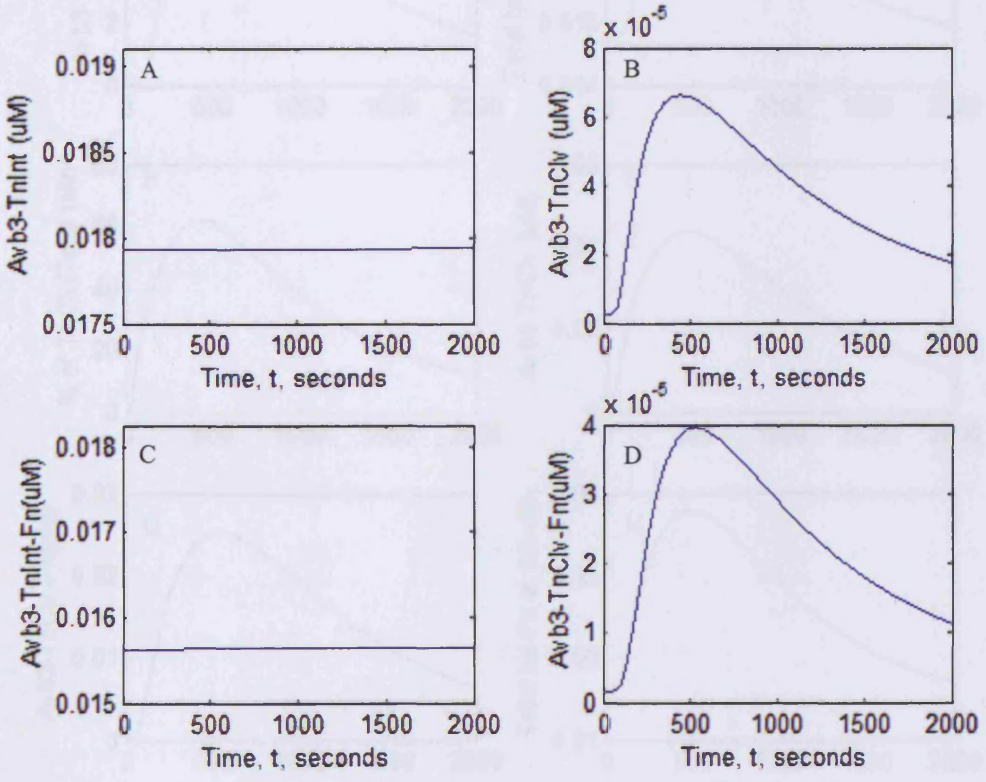

Figure 3.17. Fibronectin-integrin binding at shear stress 12 dynes/cm^2.

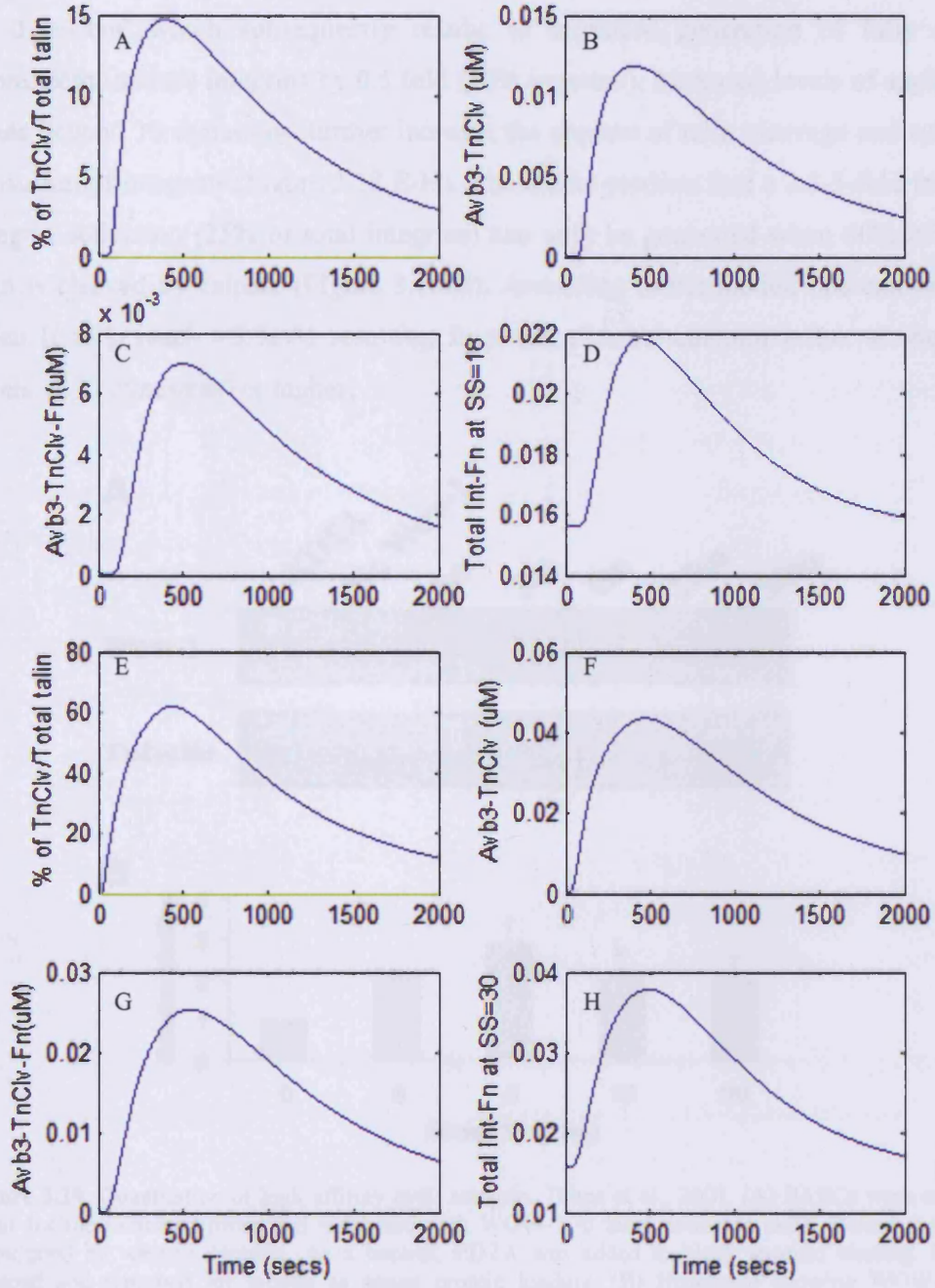

Figure 3.18. Fibronectin-integrin binding at shear stress of 18 (A-D) and 30 dynes/cm^2 (E-H).

Simulations were also run for shear stress of 18 dynes/cm^2 (Figure 3.18 A,-D) and beyond 18 dynes/cm^2. The model predicts an elevation of [Tn_{Clv}] to a total of 15% of total talin at 18 dynes/cm^2 which subsequently results in increased generation of fully activated (fibronectin-bound) integrins by 0.5 fold (50% increase). Increased levels of applied shear stress beyond 18 dynes/cm^2 further increase the amount of talin cleavage and subsequent activation of integrins (Figure 3.18 E-H). The model predicts that a 2.5-3-fold increase in integrin activation (25% of total integrins) can only be generated when 60% of the total talin is cleaved by calpain (Figure 3.18 E). According to the model, this can only occur when $[Ca^{2+}]_c$ reach >3.5mM resulting from ion channel calcium influx at shear stress levels of 30 dynes/cm^2 or higher.

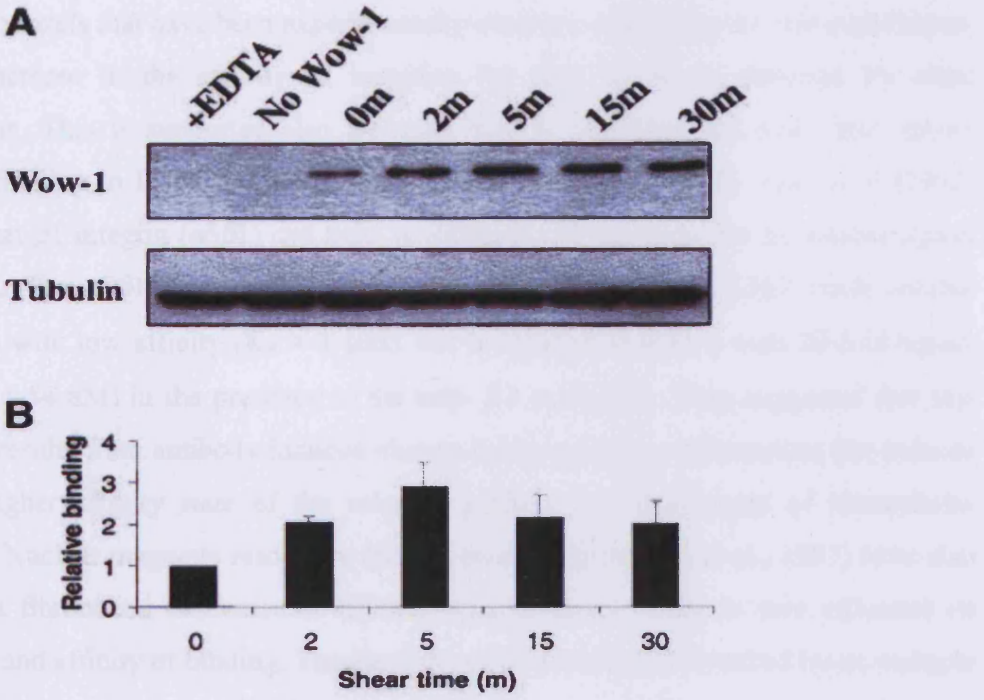

Figure 3.19. Quantitation of high affinity $\alpha v\beta 3$ integrin. Tzima et al., 2001. (**A**) BAECs were subjected to shear for the indicated times and incubated with WOW-1 to label activated $\alpha v\beta 3$. Bound antibody was quantitated by western blotting. As a control, EDTA was added to block specific binding. Blots were stripped and reprobed for tubulin to assess protein loading. (**B**) Histogram showing WOW-1 binding normalized to tubulin. Values are means ± SEM (n = 4 independent experiments) relative to cells at time 0, values are statistically significant as defined by a student's t-test (P <0.01).

Whether talin cleavage by calpain is sufficient to activate integrins, is a question that has received much attention (Calderwood, 2004a; Calderwood, 2004b) but has not yet been answered. At this stage of the model, simulations incorporating shear stress stimuli show

an overall increase in integrin activation only by elevation of intracellular calcium levels and increased amounts of cleaved talin-integrin-fibronectin complexes. This increase in activated integrins (at shear stress of 12 dynes/cm^2) however is very low approximately reaching at its peak a value of ~$4x10^{-5}$ μM. In contrast with these results however, Tzima et al (2001) have shown that shear stress of 12 dynes/cm^2 on BAECs stimulated a 2.5-3-fold increase in activation of integrins ($\alpha_v\beta_3$ bound to ligand) which resulted not from an increase in surface expression of the receptors but from a specific increase in the affinity of integrins receptors for its ligand (Figure 3.19). As the simulations have showed, the experimentally observed increase in integrin activation could only result from shear stress levels of 30 dynes/cm^2. The model thus shows that 12 dynes/cm^2 shear stress induced calcium influx and cleavage of talin is not sufficient to increase the activation of integrin receptors to levels that have been experimentally observed suggesting that the shear stress-induced increase in the affinity of integrins for their ligand is mediated by other mechanisms. This is supported also by other studies reporting that $\alpha5\beta1$ also shows increased binding to ECM following shear stress (Jalali et al., 2001). Faul et al (1993) reported that $\beta1$ integrin ($\alpha5\beta1$) can exist in different affinity states for its soluble ligand fibronectin. The $\alpha5\beta1$ expressed by the erythroleukemic cell line K562 binds soluble fibronectin with low affinity (Ka > 1 μM), but is induced to bind it with 20-fold higher affinity (Kd-54 nM) in the presence of the anti- β 1 mAb 8A2. They suggested that this activation results from antibody-induced change in the receptor conformation that induces a much higher affinity state of the receptor without the requirement of intracellular signalling. Nuclear magnetic resonance (NMR) studies (Spitzfaden et al., 1997) have also shown that fibronectin can exist in different rigidity states which in turn influence its specificity and affinity of binding. The elasticity of fibronectin is controlled by its multiple fibronectin type III repeats (Garcia et al., 1999; Krammer et al., 1999; Ugarova et al., 1995a; Ugarova et al., 1995b) which act as molecular springs that may reversibly expose important cell-binding and/or multimerisation domains much like a mechanical switch (Hocking et al., 1996; Ingham et al., 1997; Morla et al., 1994; Zhong et al., 1998). All these together provide strong evidence that stretching-induced conformational changes can alter the binding characteristics of the molecule and that shear stress-induced activation of integrin receptors may results from conformational changes of molecular structures.

3.4.5 Conclusions

The model has shown that shear stress results in activation of calpain which subsequently cleaves talin, however such mechanism is not sufficient for significant activation of integrin receptors as observed experimentally. Before attempting to investigate the reason of deviation of the simulation results with the experimental observations at this stage, it was decided to first also investigate the dynamics of FAK activation to aid our understanding of the integrin-induced signalling mechanisms.

3.5 Paxillin and FAK activation, membrane and cytosolic events (Module 4)

3.5.1 Module description

Activation of integrins by binding of talin and fibronectin allows their association with downstream signalling molecules such as paxillin and FAK.

FAK is a cytoplasmic protein tyrosine kinase (PTK) that localizes to focal contacts and adhesions as the name implies. Despite early studies supporting the idea of direct binding of β-integrins to the FAK N-terminal FERM domain (Parsons, 2003; Schaller, 2001), accumulated evidence now supports an indirect association of FAK with integrins through binding of the C-terminal focal adhesion targeting FAT domain of FAK to integrin-associated proteins (Schlaepfer and Mitra, 2004; Schlaepfer et al., 2004). This FAK FAT region contains binding sites for integrin-associated proteins such as paxillin and talin (Schaller, 2001; Turner, 2000a; Turner, 2000b).

Paxillin (chapter 1.3.7) serves as a docking protein to recruit both specific cytoskeletal linker proteins (e.g. vinculin, actopaxin) and signalling molecules (e.g. ILK, FAK) into a complex to mediate downstream signalling (Schaller, 2001). Paxillin is known to bind to the FAT region of FAK (chapter 1.3.7) via its LD2 and LD4 sequences (Brown et al., 1996; Turner and Miller, 1994).

It has been shown that paxillin-null fibroblasts exhibit reduced fibronectin (FN)-stimulated FAK phosphorylation (Hagel et al., 2002) and mutations of FAK within the FAT domain that disrupt paxillin binding exhibit reduced integrin-stimulated phosphorylation in cells (Zhao et al., 1998). Paxillin null embryonic stem cells are also impaired in tyrosine phosphorylation of FAK (Wade et al., 2002). Mutation studies revealed that every mutant of FAK that fails to target focal adhesions is also defective for paxillin binding (Cooley et al., 2000; Hildebrand et al., 1995; Tachibana et al., 1995). Paxillin can bind directly with β1 and β3 chains of integrins (Cheng et al., 2002; Schaller et al., 1995; Schaller and Parsons, 1995; Tanaka et al., 1996) and it has been suggested that paxillin acts as a dual catalyst by forming the scaffold for signal transduction (thereby serving as the docking partner of FAK at focal sites) and by aiding reorganisation of the actin cytoskeleton and cell migration (Parsons, 2003; Parsons et al., 2000; Yano et al., 2004).

FAK activity correlates with its tyrosine phosphorylation which is stimulated upon integrin activation (Burridge et al., 1992; Guan and Shalloway, 1992; Schwartz et al., 1995). The mechanism of FAK activation likely involves its autophosphorylation of Y397 that takes place upon intramolecular release of conformation restraints of the FERM domain induced by binding of FAK FAT domain to proteins in focal adhesions (Schlaepfer and Mitra, 2004; Schlaepfer et al., 2004). Phosphorylation of FAK Y397 in response to integrin engagement correlates with increased catalytic activity of FAK (Calalb et al., 1995; Lipfert et al., 1992) and appears to be important for tyrosine phosphorylation of proteins located at adhesions/complexes (Cobb et al., 1994; Schaller et al., 1999) as well as phosphorylation at Y576 and Y577, two highly conserved residues positioned within the catalytic loop of the FAK kinase domain (Owen et al., 1999).

Paxillin is phosphorylated by FAK on Y118 (Cooley et al., 2000) and is dephosphorylated by PTP-PEST, a 125-kDa tyrosine phosphatase with an N-terminal catalytic domain and a long C-terminal domain containing proline-rich sequences and PEST sequences (Charest et al., 1995; Yang et al., 1993). Paxillin binding to one of the proline-rich regions of PTP-PEST (Cote et al., 1999; Shen et al., 2000; Shen et al., 1998) is necessary for dephosphorylation of paxillin (Cote et al., 1999; Shen et al., 2000).

Although FAK itself does not bind directly to PTP-PEST, the recruitment of PTP-PEST by paxillin mediates the inactivation of FAK by dephosphorylation (Cote et al., 1999; Shen et al., 1998). However, PTP-PEST binds to the region of paxillin that functions in focal adhesion targeting (FAT domain). PTP-PEST is a cytoplasmic phosphatase that does not localise to focal adhesions (Charest et al., 1995) and associates with paxillin not in focal adhesions. It is believed that PTP-PEST ensures dephosphorylation of paxillin as it exits from focal adhesions in order to maintain the cytoplasmic pool of paxillin in an unphosphorylated form (Schaller, 2001). FAK is also reported to be negatively regulated by other phosphatases such as SH2-containing tyrosine phosphatase 2 (SHP2) (von Wichert et al., 2003a; Yu et al., 1998), low molecular weight tyrosine phosphatase (LMW-PTP) (Chiarugi, 2003), PTP1B (Liang et al., 2005) and RPTPα (Zeng et al., 2003).

3.5.2 Considerations for mathematical description

On the basis of experimental observations reporting that recruitment of paxillin to sites of force application requires the presence of talin (Giannone et al., 2003), in the model paxillin is allowed to bind to integrins only after they bind talin and fibronectin (Figure 3.21). In turn the binding of FAK FAT domain to paxillin induces a conformational change in FAK that facilitates FAK tyrosine autophosphorylation on Y397 resulting in its activation and phosphorylation of paxillin on tyrosine Y118 (Cooley et al., 2000). Phosphorylation of Y118 on paxillin is not considered as a separate reaction in the model but as a two-step mechanism: first FAK binds to paxillin reversibly and then spontaneously phosphorylates both Y397 on itself and Y118 on paxillin. FAK is also activated by transphosphorylation resulting from integrin clustering (Katz et al., 2002). This was not considered explicitly here and is assumed to be part of one phosphorylation event upon binding of FAK to paxillin.

The phosphatase PTP-PEST binds to paxillin (not FAK) and dephosphorylates both FAK and paxillin (Figure 3.20) in the cytosol but cannot bind to paxillin when associated with integrins. This dual transformation is considered as a one-step reaction in the model. PTP-PEST is also able to bind and dephosphorylate paxillin when not bound to FAK but cannot bind and dephosphorylate FAK when not bound to paxillin. PTP-PEST is not regulated by other molecules in the model (due to lack of relevant data) thus the mechanism of dephosphorylation acts as a filtering mechanism in this case. Because FAK cannot be dephosphorylated by PTP-PEST when not complexed with paxillin and considering that FAK can be dephosphorylated by other PTPs (e.g. LMW-PTP, SHP2, PTP1B, RPTPα), a tyrosine phosphatase (possibly PTP1B) (Liang et al., 2005) was added to the module to dephosphorylate and prevent limitless accumulation of phosphorylated unbound FAK.

Because FAK is recruited to integrin complexes upon stimulation but is not solely localized at these sites, it is assumed that FAK is evenly distributed throughout the cytosol and thus a percentage of the available FAK is located near the membrane and the talin:integrin:fibronectin complexes. The model presumes that FAK can associate with paxillin in the cytosol (see section 2.3.6) without the need for paxillin to be pre-bound to

integrins (Figure 3.20). This is considered to be dependent on diffusion and collision limitations and takes places at a significantly slower rate than the membrane events. This was included on the basis that integrin:paxillin complexes act as molecular docking site where proteins bind at faster rates (high concentration of available docking surfaces allows for more frequent molecular collisions). This assumption supports/predicts: a) that focal complexes influence/enhance the localization and binding of FAK and paxillin to integrins rather than paxillin solely influencing the localization of FAK near the membrane and b) that there is some basal activity of FAK at all times even when integrins have not been engaged by ligands (i.e. FAK^P in suspension cells) and signalling is never depleted to zero. The slower binding events taking place in the cytosol were produced by introducing an extra 'delay coefficient' that decreases the association rates for the FAK:paxillin interaction when occurring in the cytosol.

As a result of these cytosolic events there are some pre-bound paxillin:FAK complexes (Figure 3.20) which can associate as one molecular unit with the talin:integrin:fibronectin complex (Figure 3.21). Furthermore, their interaction in the cytosol allows for dephosphorylation by PTP-PEST (and PTPB1) which cannot occur at integrin complexes. Similarly to section 3.4 and in support of fluorescence imaging experiments showing that focal complexes and adhesions are highly dynamic (Webb et al., 2004) this module was also designed to accommodate the dynamic turnover of integrin complexes. Talin can dissociate from the receptors inactivating integrins as before and paxillin dissociation following binding of FAK results in release of active receptors and paxillin:FAK complexes. This dissociation can occur before or after phosphorylation by FAK. Proteolysis of FAK and paxillin by calpain is not investigated in the model (due to time limitations).

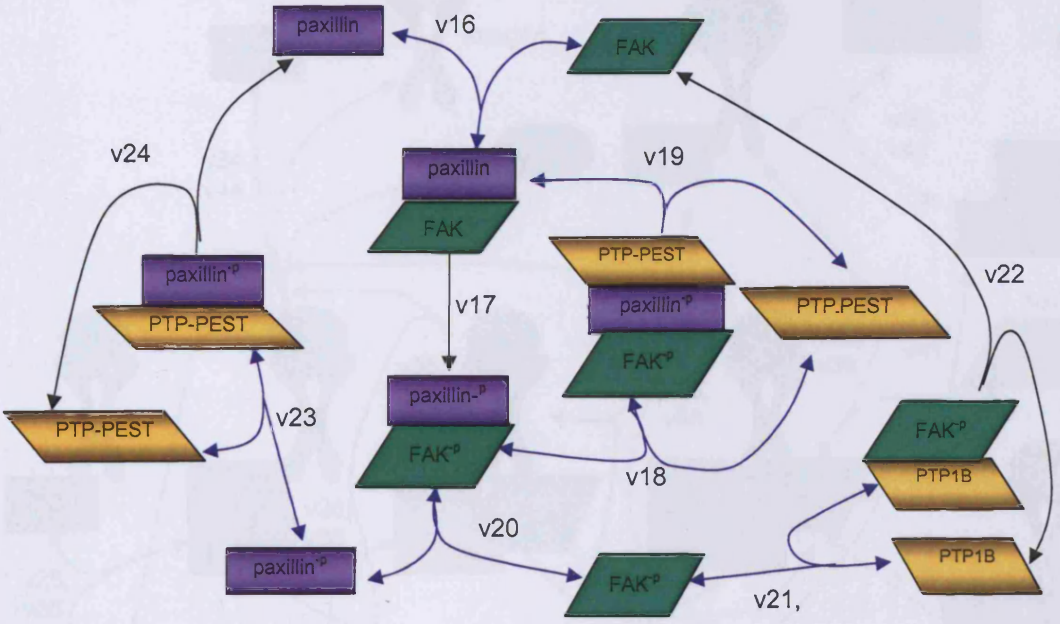

Figure 3.20. Association of paxillin and FAK in the cytosol and subsequent catalytic events. Dissociation of the complex can take place at any time.

The interaction events of paxillin, FAK and tyrosine phosphatase catalytic activities in the cytosol are given by the following equations:

v16, [paxillin] + [FAK] ↔ [paxillin-FAK]

v17, [paxillin-FAK] → [paxillin^{P}-FAK^{P}]

v18, [paxillin^{P}-FAK^{P}] + [PTP_PEST] ↔ [paxillin^{P}-FAK^{P}-PTP_PEST]

v19, [paxillin^{P}-FAK^{P}-PTP_PEST] → [paxillin-FAK] + [PTP_PEST]

v20, [paxillin^{P}-FAK^{P}] ↔ [paxillin^{P}] + [FAK^{P}]

v21, [FAK^{P}] + [PTP1B] ↔ [FAK^{P}-PTP1B]

v22, [FAK^{P}-PTP1B] → [FAK] + [PTP1B]

v23, [paxillin^{P}] + [PTP_PEST] ↔ [paxillin^{P}-PTP_PEST]

v24, [paxillin^{P}-PTP_PEST] → [paxillin] + [PTP_PEST]

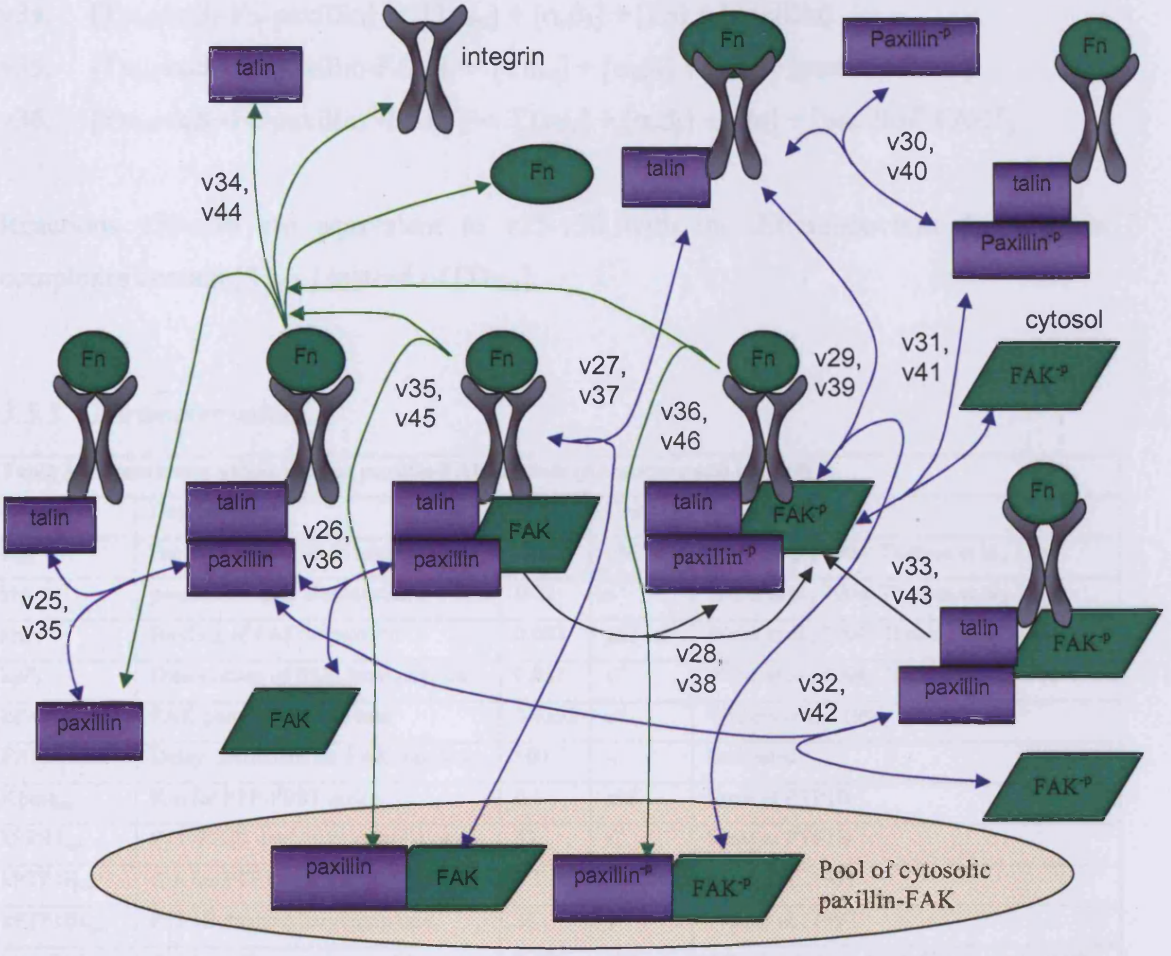

Figure 3.21. Interaction of FAK and paxillin with integrin complexes at the membrane. Preformed paxillin:FAK complexes from cytosolic events are also included.

The interaction events of paxillin and FAK and catalytic activities with integrin ($\alpha_v\beta_3$) complexes are given by the following equations:

v25, $[Tn_{Int}\text{-}\alpha_v\beta_3\text{-Fn}] + [\text{paxillin}] \leftrightarrow [Tn_{Int}\text{-}\alpha_v\beta_3\text{-Fn-paxillin}]$

v26, $[Tn_{Int}\text{-}\alpha_v\beta_3\text{-Fn-paxillin}] + [\text{FAK}] \leftrightarrow [Tn_{Int}\text{-}\alpha_v\beta_3\text{-Fn-paxillin-FAK}]$

v27, $[Tn_{Int}\text{-}\alpha_v\beta_3\text{-Fn}] + [\text{paxillin-FAK}] \leftrightarrow [Tn_{Int}\text{-}\alpha_v\beta_3\text{-Fn-paxillin-FAK}]$

v28, $[Tn_{Int}\text{-}\alpha_v\beta_3\text{-Fn-paxillin-FAK}] \rightarrow [Tn_{Int}\text{-}\alpha_v\beta_3\text{-Fn-paxillin}^P\text{-FAK}^P]$

v29, $[Tn_{Int}\text{-}\alpha_v\beta_3\text{-Fn}] + [\text{paxillin}^P\text{-FAK}^P] \leftrightarrow [Tn_{Int}\text{-}\alpha_v\beta_3\text{-Fn-paxillin}^P\text{-FAK}^P]$

v30, $[Tn_{Int}\text{-}\alpha_v\beta_3\text{-Fn}] + [\text{paxillin}^P] \leftrightarrow [Tn_{Int}\text{-}\alpha_v\beta_3\text{-Fn-paxillin}^P]$

v31, $[Tn_{Int}\text{-}\alpha_v\beta_3\text{-Fn-paxillin}^P] + [\text{FAK}^P] \leftrightarrow [Tn_{Int}\text{-}\alpha_v\beta_3\text{-Fn-paxillin}^P\text{-FAK}^P]$

v32, $[Tn_{Int}\text{-}\alpha_v\beta_3\text{-Fn-paxillin}] + [\text{FAK}^P] \leftrightarrow [Tn_{Int}\text{-}\alpha_v\beta_3\text{-Fn-paxillin-FAK}^P]$

v33, $[Tn_{Int}\text{-}\alpha_v\beta_3\text{-Fn-paxillin-FAK}^P] \rightarrow [Tn_{Int}\text{-}\alpha_v\beta_3\text{-Fn-paxillin}^P\text{-FAK}^P]$

v34, $[Tn_{Int}\text{-}\alpha_v\beta_3\text{-Fn-paxillin}] \rightarrow [Tn_{Int}] + [\alpha_v\beta_3] + [Fn] + [paxillin]$

v35, $[Tn_{Int}\text{-}\alpha_v\beta_3\text{-Fn-paxillin-FAK}] \rightarrow [Tn_{Int}] + [\alpha_v\beta_3] + [Fn] + [paxillin\text{-}FAK]$

v36, $[Tn_{Int}\text{-}\alpha_v\beta_3\text{-Fn-paxillin}^P\text{-}FAK^P] \rightarrow [Tn_{Int}] + [\alpha_v\beta_3] + [Fn] + [paxillin^P\text{-}FAK^P]$

Reactions v35-v46 are equivalent to v25-v36 with the difference that the integrin complexes contain $[Tn_{Clv}]$ instead of $[Tn_{Int}]$.

3.5.3 Parameter values

Table 3.05 Parameter values used in paxillin-FAK module (membrane and cytosol)

Constant	Description	Value	Units	Source
kip_f	Binding of paxillin to integrin	0.06	$\mu M^{-1} s^{-1}$	Webb et al., 2004; Thomas et al., 1999
kip_r	paxillin:integrin dissociation	0.02	s^{-1}	Webb et al., 2004; Thomas et al., 1999
kpF_f	Binding of FAK to paxillin	0.083	$\mu M^{-1} s^{-1}$	Webb et al., 2004; Thomas et al., 1999
kpF_r	Dissociation of FAK from paxillin	0.033	s^{-1}	Webb et al., 2004; Thomas et al., 1999
$kFAK_{cat}$	FAK phosphorylation rate	0.0292	s^{-1}	Withers et al., 1996
FAKdelCof	Delay coefficient for FAK:paxillin	100	-	Estimated
$Kpest_{km}$	Km for PTP-PEST action	0.1	μM^{-1}	Same at PTP1B
$kPEST_{cat}$	PTP-PEST dephosphorylation rate	37	s^{-1}	Same at PTP1B
$kPTP1B_{km}$	Km for PTP1B action	0.1	μM^{-1}	Flint et al., 1997
$kPTP1Bk_{cat}$	PTP1B dephosphorylation rate	37	s^{-1}	Flint et al., 1997
[paxillin]	Total paxillin = total integrins	0.17	μM	After Faul et al., 1993; Garcia et al., 1998
[FAK]	Total FAK = total integrins	0.17	μM	After Faul et al., 1993; Garcia et al., 1998
[PTP-PEST]	Total PTP-PEST = total paxillin	0.1	μM	Estimated
[PTP1B]	Total PTP1B = total FAK	0.1	μM	Estimated

Table 3.05. Parameter values for the paxillin:FAK module.

The affinity of interaction between FAK and the paxillin LD2 motif and LD4 motif has been estimated by surface plasma resonance (Thomas et al., 1999). The dissociation constant (Kd) for the interaction of the C-terminal domain of FAK with the paxillin LD2 and LD4 motifs separately is 4 μM for each. The dissociation constant (Kd) for the interaction of the C-terminal domain of FAK with paxillin containing both LD2 and LD4 together is 0.25-0.6 μM (Thomas et al., 1999). Fluorescence studies of Webb et al (2004) reported the rates of loss/dissociation of paxillin and FAK from focal sites at $k_{r,\ paxillin}$ (kip_r) = 0.02 s^{-1} (taken as the dissociation rate of paxillin from integrins) and $k_{r,\ FAK}$ (kpF_r) = 0.033 s^{-1} (taken as the dissociation rate of FAK from paxillin) respectively. Based on the

above Kd values reported for FAK:paxillin interaction by Thomas et al (1999) and the dissociation rates by Webb et al (2004), the calculated forward rate of FAK:paxillin binding is $kpF_f = 0.083\ \mu M^{-1}s^{-1}$ for a mid range Kd = 0.4 μM. Because Webb et al (2004) reported that the rates of incorporation of FAK and paxillin at focal sites (apparent association rates) where comparable to each other, an association rate of equal order was given for the binding of paxillin to integrins at $kip_f = 0.06\ \mu M^{-1}s^{-1}$. The kinetic studies of Withers et al (1996) reported the phosphorylation rate of FAK at k_{cat} = ~14nmol/min/mg (autophosphorylation of FAK). The kcat was converted to s^{-1} units based on $1g = 1mole/Mw$ and the Mw of FAK (~125K) which gives the FAK catalytic rate $kFAK_{cat} = 0.0292\ s^{-1}$. For the formation of paxillin:FAK complex in the cytosol a delay was given to the association rate that decreased the affinity of FAK for paxillin by 100-fold (Kd = 40 μM).

The affinity and catalytic rate values for the phosphatases of the module were not available in the literature. Some rates have been reported for PTPB1 (Flint et al., 1997) but these were determined with artificial peptide substrates and could deviate significantly from rates with protein substrates. The rate of dephosphorylation for PTP1B was taken from the kinetic studies of Flint et al (1997) as kcat = 37 s^{-1}. For Km, a value similar to the Km of RPTPα (Lim et al., 1997) was given as Km = 33μM. PTP-PEST was presumed to exhibit similar behaviour and the same reaction rates were given.

The total concentration of Paxillin and FAK was estimated as equal to the total concentration of integrins on the basis that there should be at least one molecule available of paxillin and FAK in the cytosol per integrin receptor. For the phosphatases in the model slightly lower concentrations were estimated at 0.1 μM considering they are highly catalytic.

3.5.4 Analysis of species dynamics in the absence of ligand

Simulations were first run in the absence of shear stress and also absence of fibronectin (i.e. no adhesions present similarly to cells in suspension) to observe the basal levels of FAK Y397 and paxillin Y118 phosphorylation in the cytosol (Figure 3.22). The model predicts 0.1% of total FAK is phosphorylated on Y397 which is in agreement with the

observations of Hotchin et al (1999) (0.1 to 1 % [FAK^p] of total FAK) of FAK phosphorylation in cells in suspension. The same predictions were also observed for paxillin phosphorylation.

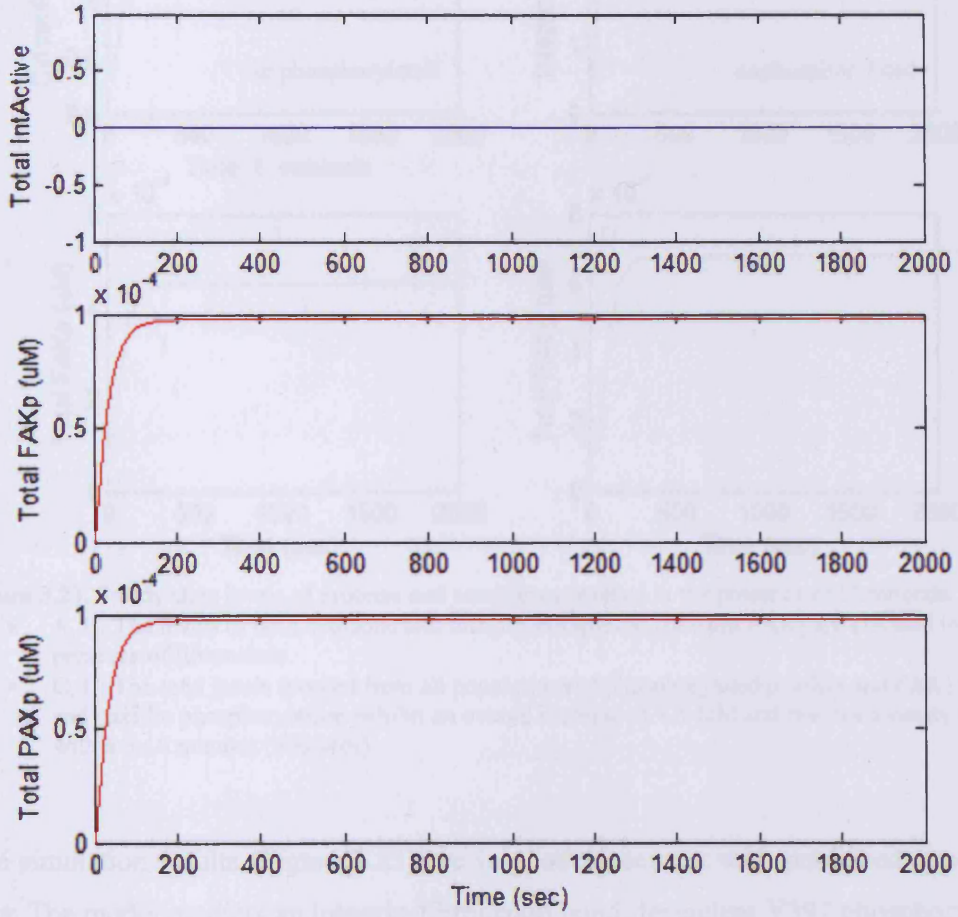

Figure 3.22. Steady state levels of phosphorylated FAK and paxillin in the absence of shear stress stimulation and fibronectin. Low levels of FAK and paxillin phosphorylation are observed. As there is no fibronectin present, there are no activated integrins and thus no FAK and paxillin bound to integrins.

3.5.5 Analysis of species dynamics in the presence of adhesions

Simulations were subsequently run in the presence of fibronectin and in the absence of shear stress (Figure 3.23).

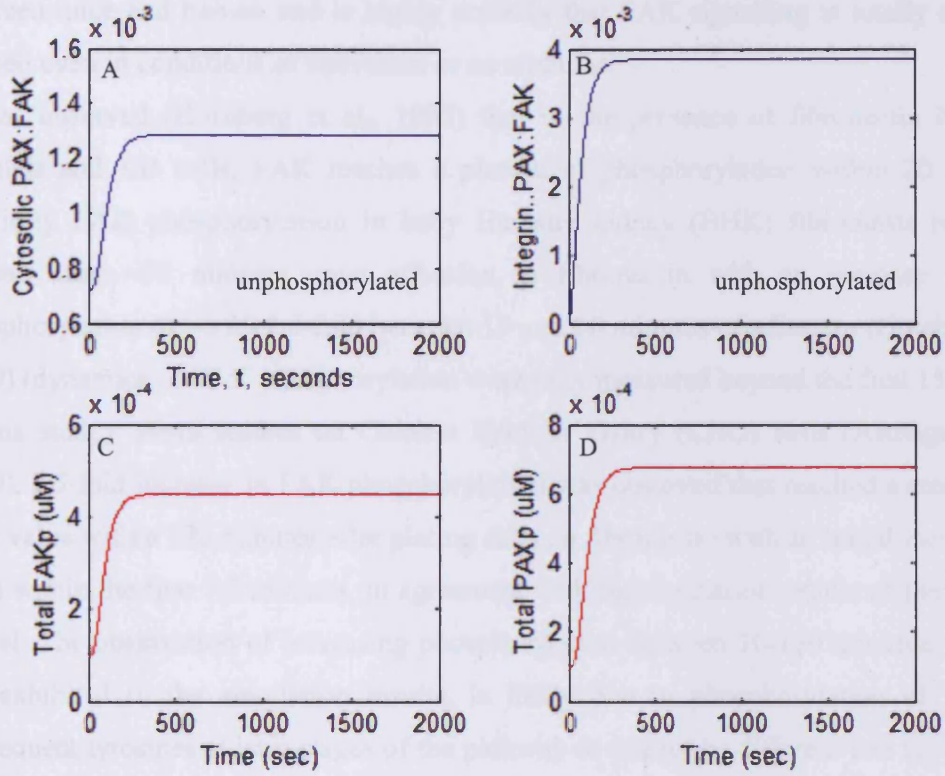

Figure 3.23. Steady state levels of proteins and complexes reached in the presence of fibronectin.

- A, B: The levels of both cytosolic and integrin-complexed [paxillin:FAK] are elevated in the presence of fibronectin.
- C, D: The total levels (pooled from all populations of phosphorylated paxillin and FAK) of FAK and paxillin phosphorylation exhibit an overall increase of 4.5-fold and reaches a steady maximal within 8-10 minutes (500 secs).

The simulation results (Figure 3.23) are in good agreement with published experimental data. The model predicts an integrin-fibronectin bond-dependent Y397 phosphorylation of FAK upon fibronectin stimulation that exhibits a total of 4.2-fold increase reaching a plateau level of phosphorylated FAK approximately equal to 0.5% of total FAK within 600 seconds. Most of the increase of phosphorylation (~4 fold) takes place within 300 seconds and exhibits an approximately 0.2 fold increase between 5-10 minutes as it reaches the plateau maximal activity. The model here predicts a low basal phosphorylation of FAK even in the absence of ligand. Considering that deletion of the genes encoding FAK or fibronectin in mice leads to remarkably similar devastating phenotypes such as defective assembly of a patent circulatory system and absence of a beating heart (Furuta et al., 1995; George et al., 1997) and that it is also known that FAK is very highly conserved

between mice and human and is highly unlikely that FAK signalling is totally absent in the cell even in conditions of starvation or no stimulus.

It was observed (Kornberg et al., 1992) that in the presence of fibronectin ligand in platelets and KB cells, FAK reaches a plateau of phosphorylation within 20 minutes. Similarly FAK phosphorylation in baby Hamster kidney (BHK) fibroblasts reaches a plateau after ~30 minutes upon adhesion to fibronectin with an increase of FAK phosphorylation of ~0.25-0.4 fold between 15 and 30 minutes of adhesion (Hotchin et al., 1999) (dynamics of FAK phosphorylation were only measured beyond the first 15 minutes in this study). From studies on Chinese Hamster Ovary (CHO) cells (Asthagiri et al., 1999), a 5-fold increase in FAK phosphorylation was observed that reached a steady-state state value within 120 minutes after plating cells on fibronectin with an initial increase (~3 fold) within the first 7.5 minutes, in agreement with the simulation results of the working model. The observation of increasing phosphorylation between 10-120 minutes, which is not exhibited in the simulation results, is likely due to phosphorylation of FAK on subsequent tyrosines at later stages of the pathway or due to the different cell type used in the experiments.

The model also predicts that the increase of FAK phosphorylation is coincident coincident and roughly proportional to the integrin-fibronectin bonds (similar dynamic behaviour as shown by slope of increase, not equal concentration levels). In agreement with this, it was reported that the adhesion strength of the cells and the phosphorylation of FAK increases almost linearly with the amount of integrin-fibronectin bonds formed in the absence of applied force (Garcia and Boettiger, 1999) suggesting that FAK phosphorylation is directly proportional to the number of receptor-ligand complexes under conditions of steady state.

A sudden peak of FAK phosphorylation at approximately 120 (Hotchin et al., 1999) and 60 minutes (Asthagiri et al., 1999) of stimulation respectively, which is not observed in the model. This is likely due to other downstream effects taking place such as positive feedback or subsequent phosphorylation of FAK after Src activation or co-operation in integrins with other receptors. It has been reported that although the paxillin binding site extensively overlaps with the FAT sequence, binding to paxillin is unlikely to be the only way to target FAK to integrin complexes because there is a single mutation of FAK that

fails to bind paxillin but is still able to localize to sites of focal complexes and adhesions (Schwartz et al., 1995). Talin also binds to FAK, however talin has been separated from focal adhesion targeting because a mutant of FAK that fails to target focal adhesions still binds talin (Schwartz et al., 1995). Because stimulation of integrins and a host of soluble agonists that act through G proteins and PTK-dependent receptors also to induce phosphorylation of FAK on tyrosine and its enzymatic activation, it is apparent that multiple distinct signalling pathways converge on a single PTK, presumably to elicit a common response (Schwartz et al., 1995). It would therefore be very interesting to include additional receptor-initiated signalling pathways to identify both the magnitude of influence of each receptor (including other integrins) and their synergistic effect on FAK phosphorylation dynamics.

As shown in the simulation results (Figure 3.23), the phosphorylation time course of paxillin on Y118 is similar to Y397 FAK. This is in good agreement with recent observations from experiments on identical conditions (unpublished, courtesy of Christodolou M).

The model predicts that almost half of FAK^P and $paxillin^P$ is in the cytosol (Figure 3.24). This is in good agreement with the observations of Webb et al (2004) which, based on kinetic analysis of disassembly of these molecules (from quantitative fluorescence studies) reported FAK and paxillin depart from focal adhesions at the same time. The model however shows that the phosphorylation levels are only elevated in presence of fibronectin (exhibiting an increase proportional to integrin-fibronectin bonds). Thus integrin stimulation functions as an activator of FAK without limiting presence of FAK to integrin complexes. These results are in agreement with the observations of Giannone et al (2004) indicating that there is a rapid exchange of FAK between cytosolic and membrane compartments. This also supports the hypothesis that an activated FAK signalling complex can dissociate from focal contacts to allow downstream cytosolic interactions (Schlaepfer, 2004). Such mechanism would be further supported when considering cleavage of integrin complexes by calpain and release of proteins into the cytosol.

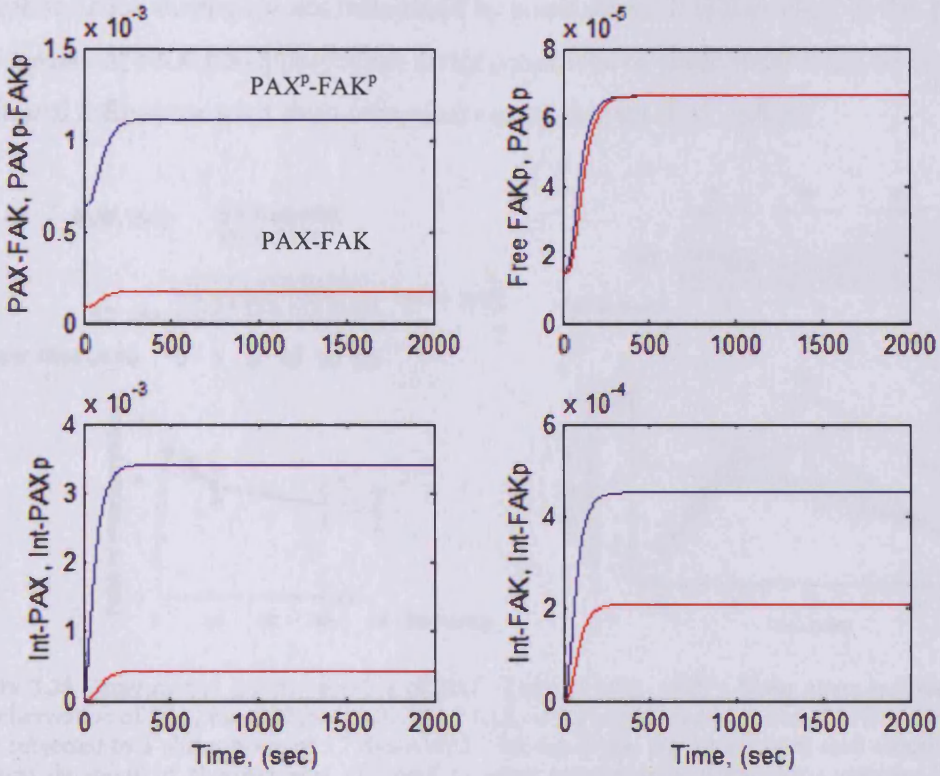

Figure 3.24. Steady state of FAK, paxillin and integrin complexes reached in the presence of fibronectin. Comparison between levels of phosphorylation for bound and free species. Red lines show phosphorylation of species. Blue lines show unphosphorylated species. Int-PAX = integrin complex containing paxillin (but not FAK). Int-FAK= integrin complexes containing both paxillin and FAK.

3.5.6 Analysis of species dynamics under shear stress

Following development of steady state levels in the absence of shear stress, simulations were run for shear stress 12 dynes/cm^2 using the concentrations obtained from steady state (Figures 3.5.2 and 3.5.3) as a starting point. Shear stress is known to activate FAK and downstream signalling (Ishida et al., 1996) Li et al., 1997; (Lehoux et al., 2005). Both Li et al (1997) and Lehoux et al (2005) observed under shear stress and pressure conditions respectively a very rapid increase of FAK phosphorylation levels that reached a peak of 2-fold within 1-10 minutes (Figure 3.25). The model however did not match this response under the same conditions of shear stress (Figure 3.26). Although an increase in FAK phosphorylation (Figure 3.26) is observed due to increased talin cleavage and integrin activation this is very small compared with experimental observations and not sufficient to change the overall levels of FAK-induced signalling. Similar behaviour was observed for paxillin phosphorylation under shear stress (not shown) while the cytosolic

phosphorylation events are not influenced by shear stress. It is thus clear at this point, that the increase of FAK phosphorylation under conditions of shear stress must be the result of additional influences apart from talin cleavage by calpain (Ca^{2+} influx).

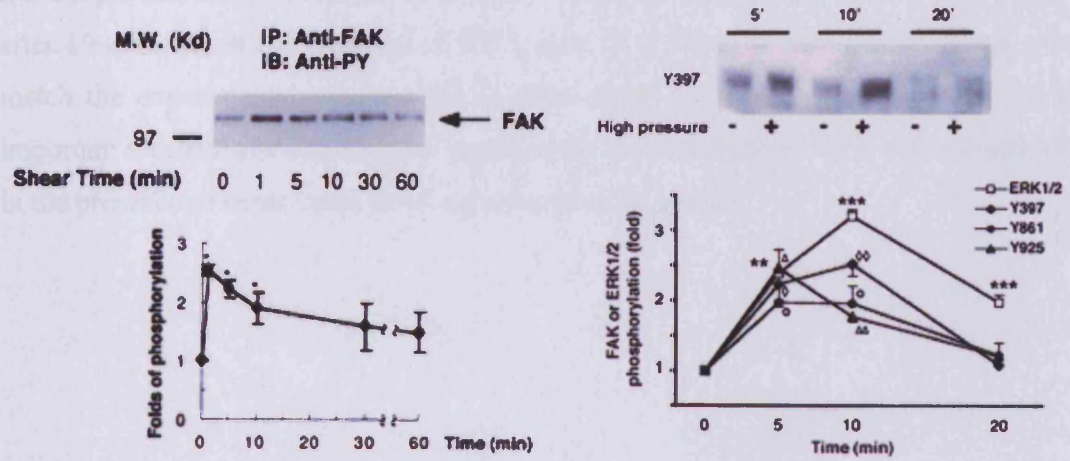

Figure 3.25 Experimental activity profiles of FAK. Left (Li et al., 2001). Shear stress increases tyrosine phosphorylation of FAK and the kinase activity of FAK. After serum-starvation for 15 h, BAEC monolayers were subjected to a shear stress of 12 dynes/cm2. 500 mg of the cell lysate from each sample following different durations of shearing was subjected to immunoprecipitation (*IP*) with a polyclonal anti-FAK antibody and immunoblotting (*IB*) with PY20 anti-phosphotyrosine mAb. Right (Lehoux et al., 2005). Kinetics of FAK and ERK1/2 phosphorylation induced by pressure. Aortic segments were cannulated and maintained at 80 mm Hg for 90 minutes, and then intraluminal pressure was readjusted to 150 mm Hg in some segments for indicated times. Pressure-induced phosphorylation of Tyr-397, Tyr-861, and Tyr- 925 was maximal by 5 minutes and remained high at 10 minutes, returning to baseline thereafter.

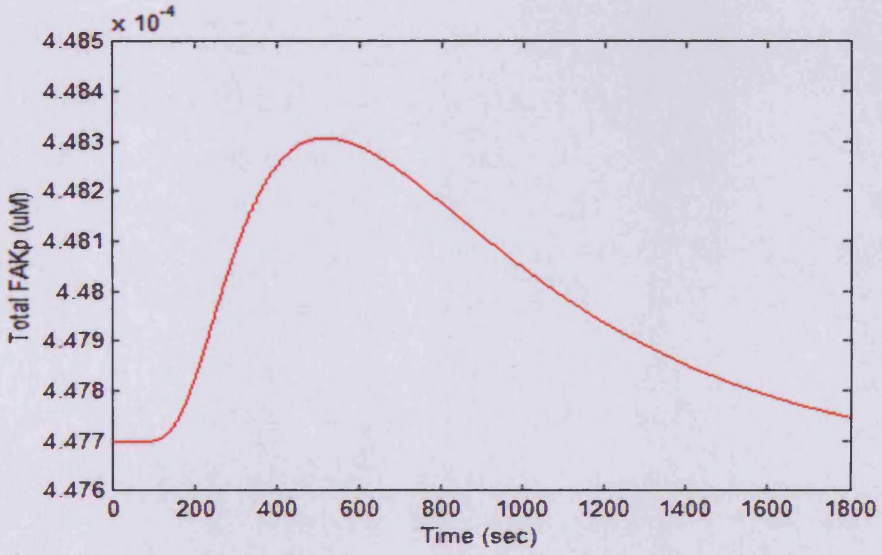

Figure 3.26. Model simulation of total FAK phosphorylation under 12 dynes/cm^2 shear stress conditions. A very low non-significant increase is observed resulting from an elevation of activated integrins (due to calcium-induced talin cleavage).

3.5.7 Summary and conclusions

The dynamics of FAK phosphorylation have been examined in this section. The model predicts a non-basal level of FAK phosphorylation in unstimulated cells or in suspension and a rapid increase of FAK phosphorylation levels (in the first 5 minutes reaching plateau after 19 minutes) in the presence of fibronectin. However the model at this stage cannot match the experimental observations in shear stress condition and it was realized that important mechanisms that increase significantly the activation of FAK above basal levels in the presence of shear stress were not present in the model.

3.6 Molecular Deformation of receptors (Module 5)

3.6.1 Introduction – additional evidence

After including in the model all the known interactions of integrin signalling which still failed to match the experimentally observed activation of FAK, it was realised that certain mechanisms of FAK activation (present physiologically) were absent in the model. A potential mechanism for the observed responses was identified after accumulation of further information:

- Experiments by magnetic bead microrheometer, optical tweezers and atomic force microscope (AFM) (Figure 3.27) have demonstrated that certain membrane molecular structures are characterised by changes in their molecular structure and their activity in response to mechanical force or stretching (Bao and Suresh, 2003; Matthews et al., 2004; Osawa et al., 2002; Wang et al., 1993).
- There is evidence that the extracellular mechanical force can be sensed by either cytoskeleton-linked receptors or the cytoskeleton structure itself. Application of force on integrin adhesion receptors increases the stiffness of the cytoskeleton while force applied on non-adhesion receptors does not (Matthews et al., 2004).
- It has been shown that stresses applied to focal adhesions lead to enhanced localization of FAK and one of its binding partners, paxillin (Sawada and Sheetz, 2002). This could occur, for example, subsequently to a conformational change in the integrin receptor itself or in talin, if such a change were to increase the binding affinity of either to FAK. Paxillin localization could then occur either as a direct result of FAK localization, or might possibly be augmented by a force-induced conformational change in FAK since once bound to the focal adhesion, it too becomes part of the force transmission pathway.
- Cells grown on flexible substrates show enhanced rates of cell migration compared with rigid substrates (Pelham and Wang, 1997). Interestingly, FAK phosphorylation on Y397 has been shown to be sensitive to the tethering of integrins to a rigid substratum (Shi and Boettiger, 2003); When binding of proteins from cell lysates to isolated detergent-insoluble cytoskeletons was assayed, stretching of the cytoskeleton increased binding of both FAK and paxillin (Sawada

and Sheetz, 2002). Thus, FAK appears to be a key component of the mechanotransduction apparatus and both FAK and its interacting proteins are candidate transducers. It has been proposed that tension alters the conformation of certain force-sensitive components of focal complexes to induce new binding interactions or direct modulation of enzymatic activity (Katsumi et al., 2004).

- Kaam and Kaazempur-Mofrad used steered molecular dynamics techniques and observed that changes in the molecular conformation of FAK FAT, induced by direct application of force, would significantly increase its binding affinity to paxillin (Kaazempur Mofrad et al., 2005; Kamm and Kaazempur-Mofrad, 2004).
- It is likely that tension alters the conformation of certain-force-sensitive components of the FA to induce new binding interactions or direct modulation of enzymatic activity. Such an effect has been shown for fibronectin, providing one mechanism for force-dependent matrix assembly (Zhong et al., 1998).
- The details of the mechanosensory processes occurring at the membrane are still elusive. It is generally accepted however that the response of cells to mechanical stimulation is determined by both extrinsic (e.g. cell size and surface) and intrinsic (i.e. material properties) properties. Just as springs and ratchets can store and release energy and rectify motion in physical systems, their analogues can perform similar functions in biological systems (Mahadevan and Matsudaira, 2000).

Based on this information a new consideration was raised regarding mechanisms of shear stress-induced applied force that could directly activate membrane receptors. Three possible mechanisms of force-induced activation were identified: 1) altered conformation of receptors due to membrane deformation which could potentially affect signalling rates. 2) force-induced deformation of the extracellular part of receptors with potential effects on ligand/receptor interactions and 3) deformation of receptors with subsequent conformational changes in their intracellular tail that affect affinity and signalling rates.

3.6.2 Membrane deformation

The membrane bilayer of the cell is known to be deformable upon application of external force and is believed to have potential deformation influences proteins spanning the bilayer (Hamill and Martinac, 2001). The deformation-sensitive membrane parameters

that may likely influence membrane protein conformational changes include membrane dilation (i.e. increased area occupied by lipid molecules), the accompanying membrane thinning (i.e. assuming membrane incompressibility) and local changes in membrane curvature or bending (Hammill and Martinac, 2001). When a membrane protein is inserted in the membrane bilayer (vesicle transport) it produces a mechanical deformation that depends on the coupling between hydrophobic regions of the protein and the membrane bilayer (Figure 3.28).

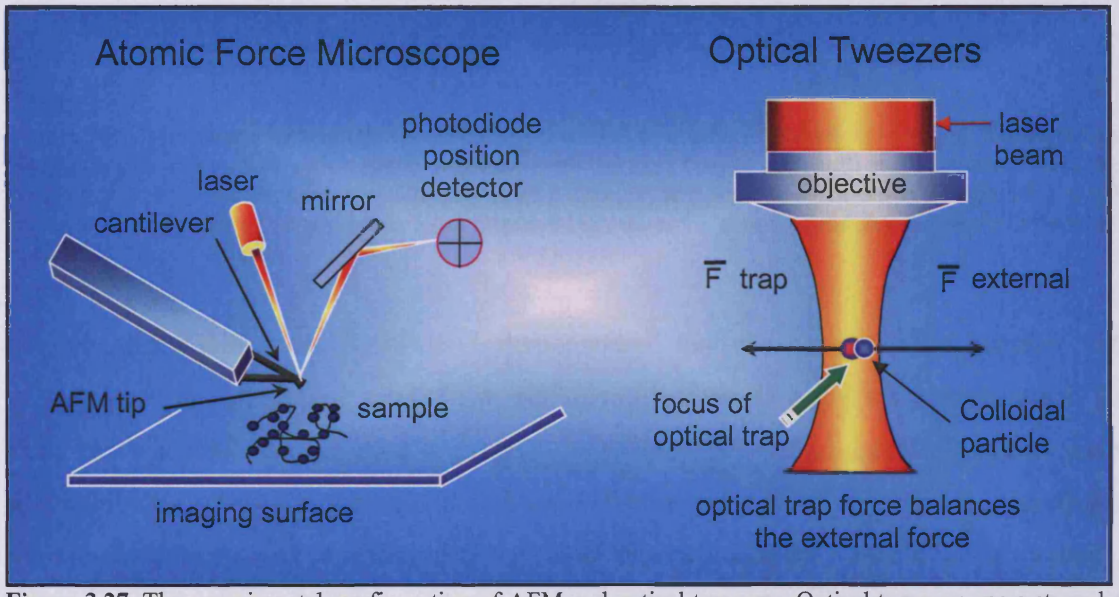

Figure 3.27. The experimental configuration of AFM and optical tweezers. Optical tweezers use a strongly focused beam of light to trap objects. Intensity gradients in the converging beam draw small objects such as a colloidal particle, towards the focus, whereas the radiation pressure of the beam tends to blow them down the optical axis. Under conditions where the gradient force dominates, a particle can be trapped, in three dimensions, near the focal point. In AFM, a sharp tip at the free end of a flexible cantilever generates a local deformation on the cell surface. The resulting deflection of the cantilever tip can be calibrated to estimate the applied force.

A protein conformational change that involves a change in hydrophobic mismatch between the protein's hydrophobic exterior with the hydrophobic thickness of the bilayer (Figure 3.28) will be sensitive to both membrane thickness and local membrane curvature (Mouritsen and Bloom, 1984; Mouritsen and Bloom, 1993). The membrane thickness and curvature can be altered by changing either the lipid bilayer composition or by mechanically stretching or bending the membrane (Huang et al., 1996; Mouritsen and Bloom, 1984) resulting in conformational changes of proteins within the membrane.

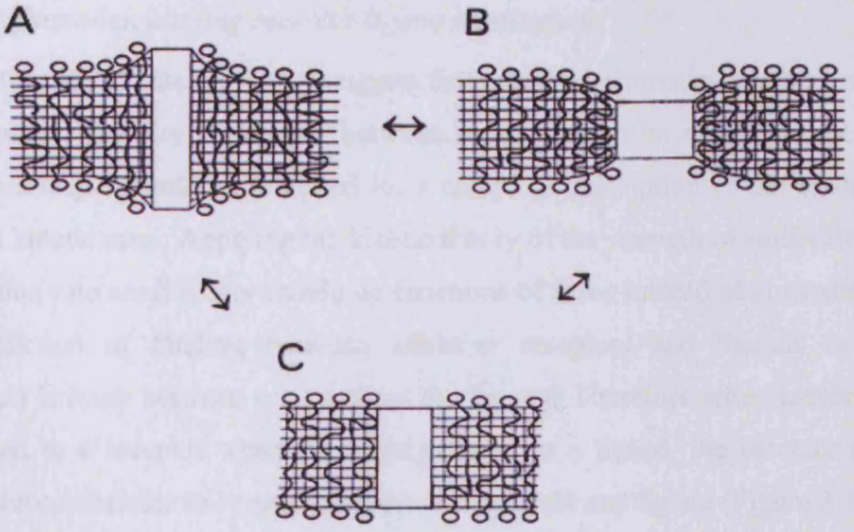

Figure 3.28. Membrane hydrophobicity and conformation. A membrane protein in changing conformation also undergoes changes in hydrophobic mismatch with the lipid bilayer (Hammill and Martinac, 2001). A) positive hydrophobic mismatch in which the protein promotes local positive curvature in the lipid bilayer. B) a protein conformation that promotes local negative curvature. C) neutral mismatch in which the protein does not distort the bilayer.

Experiments (Gudi et al., 1998) have demonstrated that shear stress force and physical properties of the membrane bilayer can modulate the activation of G-protein by shear. In these experiments, reconstituted G-proteins were activated within seconds of flow onset and exhibited 3-5 fold enhancement of basal GTPase under shear stress conditions in the absence of G-protein coupled receptors and ligand molecules (Gudi et al., 1998), supporting the idea of conformational deformation of proteins resulting from stretching of the membrane that leads to changes in their signalling activity (Figure 3.29).

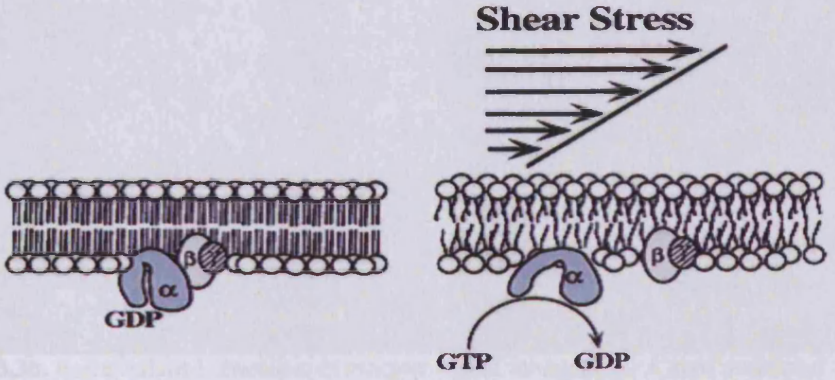

Figure 3.29. Schematic representation of protein receptor-independent activation of G proteins by fluid shear stress (Gudi et al 1998). Increase in the rotational and translational mobility in the lipid bilayer and the accompanying decrease in microviscosity activate membrane-bound G proteins by facilitating exchange of GDP for GTP.

3.6.3 *Deformation altering receptor-ligand interactions*

G.Bell (Bell, 1978) was the first to suggest that protein deformation plays an essential role in determining the rate of binding between molecules, so its effects on the changes of energy landscape should be included for a complete description of the relation between force and kinetic rates. Applying the kinetic theory of the strength of solids Bell suggested that reaction rate coefficients should be functions of force instead of constants, because a major function of binding between adhesive receptors and ligands is to provide mechanical linkage between cells against the force *f*. Therefore when mechanical forces are applied to a receptor which is already bound to a ligand, the receptor may deform altering the conformational match between the receptor and ligand (Figure 3.30). This can result in changes in the energy landscape of the bond and alter the associated kinetic rates. Even a small amount of deformation could significantly alter the binding strength of hydrogen bonds between the molecules.

For hydrogen bonds, increasing the distance between the hydrogen binding atoms by 1.2 angstroms can reduce binding strength (in terms of free energy) from 1 kcal/mole (~7 pN.nm) to almost zero and this suggests that small deformations can have large influences (Bao and Suresh, 2003; Krammer et al., 1999; Shafrir and Forgacs, 2002; Zhu et al., 2000). Deformation could in theory change the kinetic rates but it is also possible that deformation also changes the specificity of a receptor for a ligand or an intracellular target (Zhu et al., 2000).

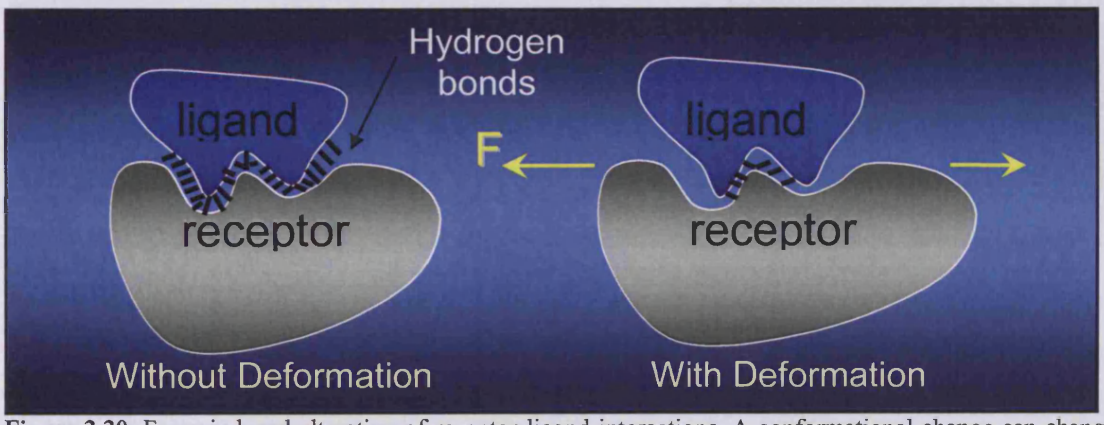

Figure 3.30. Force-induced alteration of receptor-ligand interactions. A conformational change can change if the receptor deforms under force. The deformation need not be large.

3.6.4 *Deformation altering conformation of intracellular tails*

It has also been observed that mechanical force can result in conformational changes in the intracellular tail of membrane receptors with subsequent effects in affinity and signalling rates for downstream targets. Investigators have (Osawa et al., 2002) attached microscopic magnetic beads coated with antibodies to the surface of endothelial cells which formed bonds with PECAM-1 receptors. It was observed that solely binding of the beads to the endothelial membrane receptors did not have any effect on signalling. The attached beads were then subjected to pulling force from optical tweezers (Figure 3.27) which was transmitted to the endothelial surface and the bound PECAM-1 receptors. It was then observed that when the receptors were stretched by the optical tweezers pulling the attached beads, there was a highly increased level of phosphorylation on two phosphotyrosines (Y663 and Y686) of the PECAM-1 receptors by tyrosine kinases (Osawa et al., 2002) which led to activation of the ERK pathway (Figure 3.31).

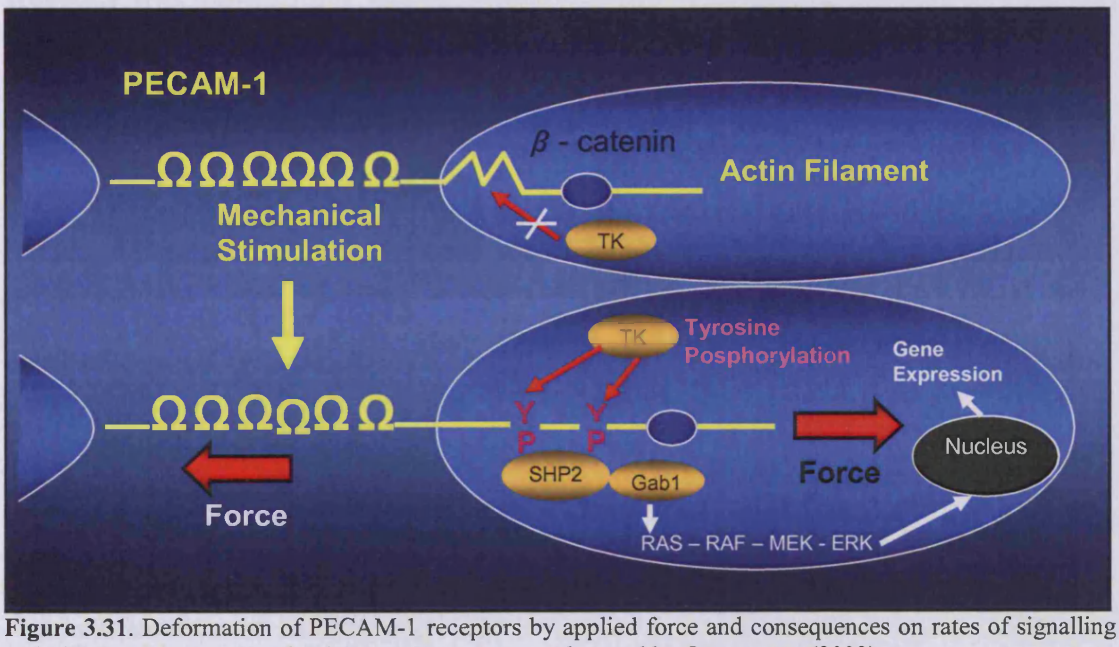

Figure 3.31. Deformation of PECAM-1 receptors by applied force and consequences on rates of signalling and affinity of the receptor for downstream targets as observed by Osawa et at (2002).

The observed elevated phosphorylation levels for the two PECAM-1 phosphotyrosines were unattainable in the absence of applied mechanical force, suggesting that stretching of molecular structures by force possibly reveals or enhances the affinity of binding/transformation sites in the intracellular tail of the receptors that were either not accessible or had low affinity rates prior to application of mechanical force.

3.6.5 The hypothesis for molecular deformation in shear stress

Based on the experimental observations described above, it was hypothesized that deformation of transmembrane receptors by shear stress results in alteration of the reaction rates for specific interactions involving the receptors. The reaction rates are altered either by enhancing or reducing the affinity of the receptor for certain intracellular target molecules or by revealing and activating (or the opposite) 'cryptic' binding sites (Bershadsky et al., 2003) that were previously inaccessible (before certain conformational changes occurred to the structure of receptor, Figure 3.31). This hypothesis allows for consideration of different modes of deformation for each different type of receptor (Figure 3.32). For example, force-induced deformation of integrins outside the cell could push the α and β tails apart (Figure 3.32a) so that they bind talin, or paxillin and FAK with higher affinity. PECAM-1 receptors on the other hand could undergo domain unfolding in response to shear stress that results in enhancement or even novel generation of molecular reactions with downstream targets (Figure 3.32b). Unfolding of secondary structures (Figure 3.32c) is not considered for either of the two receptors.

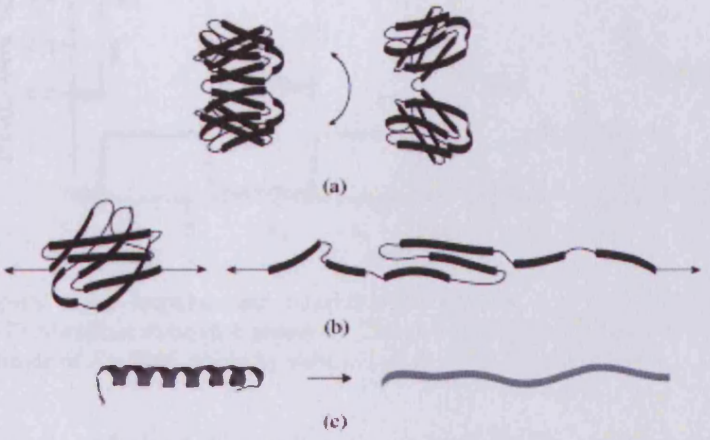

Figure 3.32. Modes of protein deformation (Zhu et al., 2000). (*a*) Domain motion (e.g. Integrins); (*b*) domain deformation and unfolding (e.g. PECAM-1 receptors); (*c*) unfolding of secondary structures (not applied).

This hypothesis supports that the length of the protein can be altered in response to force and that certain membrane molecular structures can deform in a viscoelastic-like manner. Viscoelasticity is not a novel attribute in cellular biology as it known that cells change morphologically and move in a viscoelastic manner (Bao and Suresh, 2003). When endothelial cells are suctioned with a small pipette, a portion of the cell exhibits an

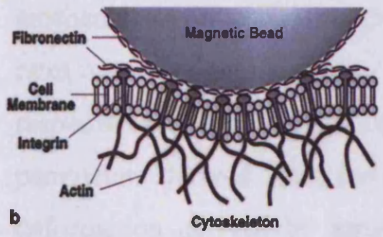

Figure 3.33. Fibronectin coated beads bound to integrins. Bauch et al., 1998

immediate elastic deformation followed by a slow viscous deformation (Sato and Ohashi, 2005; Sato et al., 1996). Viscoelastic response curves have also been observed in other studies (Bausch et al., 2001; Bausch et al., 1999; Bausch et al., 1998) that used magnetic colloidal bead microrheometry to investigate the response curves of the adhering cell surface of fibroblasts and HUVECs (Bausch et al., 1998; Bausch et al., 2001) under applied mechanical force. The magnetic beads coated with fibronectin were attached to cell surface and bound to integrin receptors via fibronectin-integrin bonds (Figure 3.33). Subsequently creep responses and relaxation curves were measured for the beads bound to the membrane. Overall a triphasic viscoelastic response was observed (Figure 3.34) which did not differ between fibroblasts and HUVECs (Bausch et al., 1998; Bausch et al., 2001).

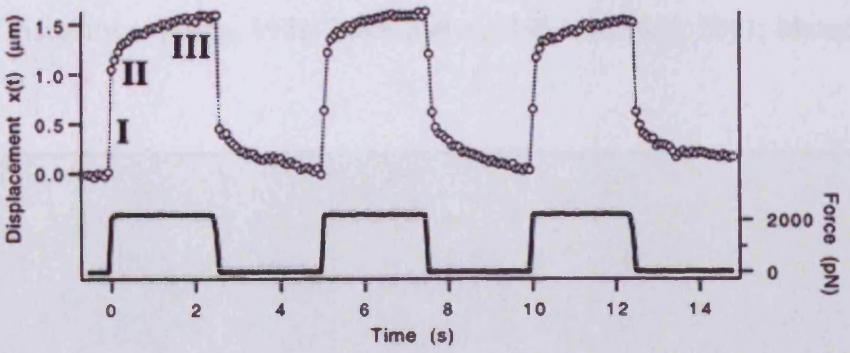

Figure 3.34. Typical creep response and relaxation curves observed for a 4.5-μm bead bound to the membrane of a 3T3 fibroblast through a presumed fibronectin-integrin linkage (Bausch et al., 1998). Force pulses of an amplitude of $F = 2000$ pN and a duration of $\Delta t = 2.5$ s were applied.

Thus, a combination of elasticity applied to account for the mechanical properties of the molecular structures and viscosity to account for the bilayer's fluidic rearrangement is considered optimal as a model to account for deformation of membrane structures that result in progressive but not spontaneous (e.g. increased phosphorylation of PECAM-1 in time upon force application and resulting deformation) activity changes (Osawa et al., 2002). Viscoelastic three-dimensional models for whole cell deformation (Karcher et al., 2003) and theoretical models for molecular deformation of molecular structure (Barakat, 2001) have been previously created but not models that combine both chemistry and

mechanics by investigating the effects of mechanical force and molecular deformation on rates of molecular signalling. Thereby, a viscoelastic model of deformation of receptors in response to mechanical force (shear stress) was created here based on the observations and parameters derived from the experiments described for PECAM-1 and the equations of deformation derived by force-based investigation of integrin responses (Bausch et al., 1999). These were used to formulate the model for calculation of the deformation of proteins and subsequently altered reaction rates. The mathematical formulation for the model of deformation is described in the following section.

3.6.6 Mathematical formulation of the receptor deformation model

The viscoelastic response curves are analyzed here in terms of a standard linear viscoelastic solid also called Kelvin body (Figure 3.35). A Kelvin body consists of a linear spring with spring constant k_1 (spring 1) in parallel with a Maxwell body, which consists of a linear spring with spring constant k_2 (spring 2) in series with a dashpot with coefficient of viscosity m (Fung, 1981; Bausch et al., 1998; Barakat, 2001; Mazzag et al., 2003).

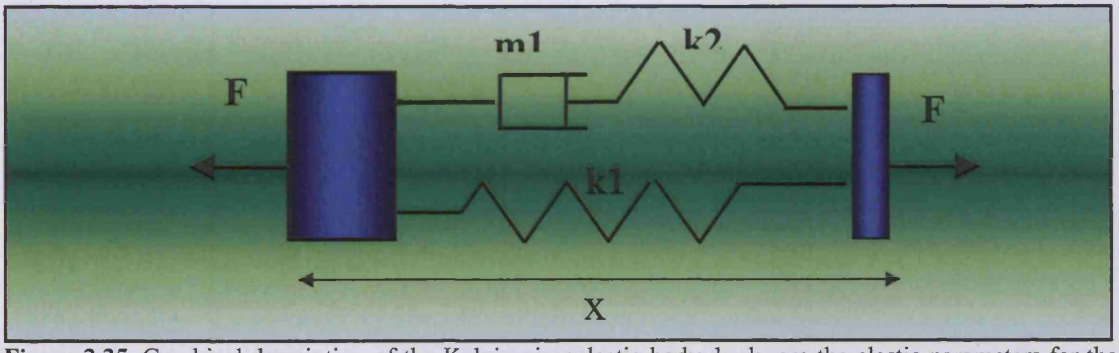

Figure 3.35. Graphical description of the Kelvin viscoelastic body. k_1, k_2 are the elastic parameters for the springs and m the viscosity coefficient of the dashpot. X represents the total length of the body.

This viscoelastic formation was specifically chosen as a template model for the dynamics of receptor deformation because it mimics best the response curves derived from experimental observations (Bausch et al., 1998). Bausch et al modeled their magnetic bead microrheometry results using a viscoelastic model consisting of a standard linear solid and an additional dashpot in a row and they demonstrated that this circuit captures the experimentally observed triphasic creep response of the cell surface consisting of an

elastic domain, a relaxation regime, and a viscous flow domain. The additional dashpot included in the model by Bausch et al (1998) however was not included in this study as it is responsible for the slow relaxation decay of deformation (mediated by rearrangement of internal bonds) upon removal of applied mechanical force (i.e. pulsatile flow) which is not relevant to the study of steady force by laminar force which is the focus in this project. The standard linear solid (Figure 3.35) as described by Barakat (2001) is used here to model the deformation responses of integrins. The deformation x(t) of the Kelvin body (Figure 3.35) given a force function F(t) across the body is governed by the following first-order linear differential equation shown (Fung, 1981; Barakat, 2001):

$$m_1\left(1+\frac{k_1}{k_2}\right)\frac{dx}{dt}+k_1x=F+\frac{m_1}{k_2}\frac{dF}{dt}, \qquad (3.34)$$

where x is the measure of deformation (length of the deformed protein – length of the protein prior to deformation) and F the amount of force applied (dF/dt becomes zero for steady force). The above equation can also be written in the form:

$$k_1\left(x+\tau_\sigma\frac{dx}{dt}\right)=F+\tau_\varepsilon\frac{dF}{dt}, \qquad (3.35)$$

where $\tau_\varepsilon=\frac{m_1}{k_2}$, (3.36)

and $\tau_\sigma=\frac{m_1}{k_1}\left(1+\frac{k_1}{k_2}\right)$, (3.37)

τ_ϵ represents the relaxation time for the viscoelastic Kelvin body under constant strain conditions whereas τ_σ represents the relaxation time for constant stress (Fung, 1981).

According to equation 3.34, the deformation x of the Kelvin body representing molecular structures can be calculated upon knowing the values of the elastic and viscosity

parameters of the Kelvin body and the applied force F. By approximating the molecular sensors of the membrane as spheres, Barakat (2001) has shown that the drag force F under the viscosity-dominated flow conditions near the endothelial surface is given by:

$$F = 10.2\pi GR^2\eta\,, \quad (3.38)$$

where R is the radius of the sphere approximating the membrane proteins modelled by the Kelvin body, η is the dynamic viscosity of the fluid (i.e. blood or cell culture medium) and G is the wall shear rate.

The work applied (i.e. energy imparted) to the viscoelastic body for a force-induced deformation x is given by Newton's equation (work applied when force F moves a body for distance X) as:

$$\frac{dW}{dt} = F(t)\frac{dx}{dt}, \quad (3.39)$$

Protein deformation is only meaningful if it has an effect on the affinity of membrane protein for their targets. The hypothesis predicts that the reaction rates of the deformed membrane proteins for their downstream targets are altered after a certain level of deformation has taken place. According to this, increased amount of mechanical force applied, increases the rate of molecular deformation which subsequently increases the rate of affinity changes for the protein structures (Figure 3.36).

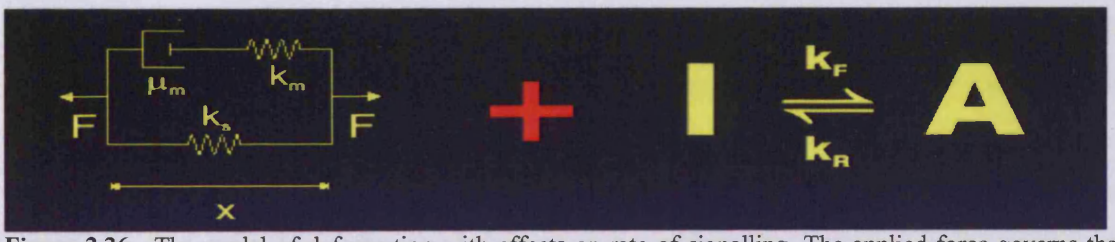

Figure 3.36. The model of deformation with effects on rate of signalling. The applied force governs the amount of deformation resulted on the protein structures which transit from undeformed/inactive (I) to deformed/active (A) states.

The deformation reaction is reversible upon reduction of the force applied and the calculation of the species concentration in deformed or normal states can now be given by the following equations:

$$\frac{d[A]}{dt} = k_f(x)[I] - k_r(x)[A] \qquad (3.40)$$

$$\frac{d[I]}{dt} = k_r(x)[A] - k_f(x)[I] \qquad (3.41)$$

where $k_f(x)$ and $k_r(x)$ the forward and reverse reaction rates of transition between inactive/undeformed *(I)* and active/deformed *(A)* states of membrane proteins depending on the amount of relative deformation x (equation 3.34) of the membrane proteins upon force F applied. The reaction rates governing the transition are now functions of molecular deformation. This allows for a coupling of protein deformation to protein function. However a critical step in the model is to define how much deformation is required for each protein to make an equivalent transition between inactive (normal conformation and kinetic rates) and active states (altered conformation with altered kinetic rates or altered affinity for molecular targets).

It is believed that there is a threshold of force that must be reached or exceeded to result in deformation that affects the function of proteins. This amount of force will be different for each protein and depends on the three-dimensional configuration of the protein. Proteins domains deform upon forces between 1-100 pN (Zhu et al., 2000) where the value of 100pN for F_t is considered to be the force value where spontaneous protein domain unfolding and protein-protein dissociation occurs for multidomain proteins such as tiun and tenascin (Zhu et al., 2000).

Ideally, the calculation of the rates of transition ($k_f(x)$, $k_r(x)$) should be based on experimental results (e.g. measured integrin-talin affinity in presence and absence of mechanical force). However little is known regarding the amount of force required to deform proteins such as integrins and PECAM-1 with subsequent alterations in affinity rates or binding site specificity.

The transition switch that turns on/off the reverse and forward rates activating or inactivating proteins by deformation is given here by a logistic sigmoidal function to allow examination of the transition rates upon increased deformation in a sigmoidal manner (see also section 3.2), which exhibits both plateau and sudden increase (Figure 3.37). The transition between plateau and increased rates is the threshold of required deformation and can be investigated with parametric studies. The equation for the sigmoidal function is given by a standard formula as:

$$LS(x) = \frac{1}{b + k\exp(-ax)}, \qquad (3.42)$$

where LS(x) is the transition equation as a function of the relative deformation x (altered protein length) and *a, b, k* represent the logistic function parameters chosen according to constraints that put LS(x) in the range restricted to interval (0, 1) for the deformation.

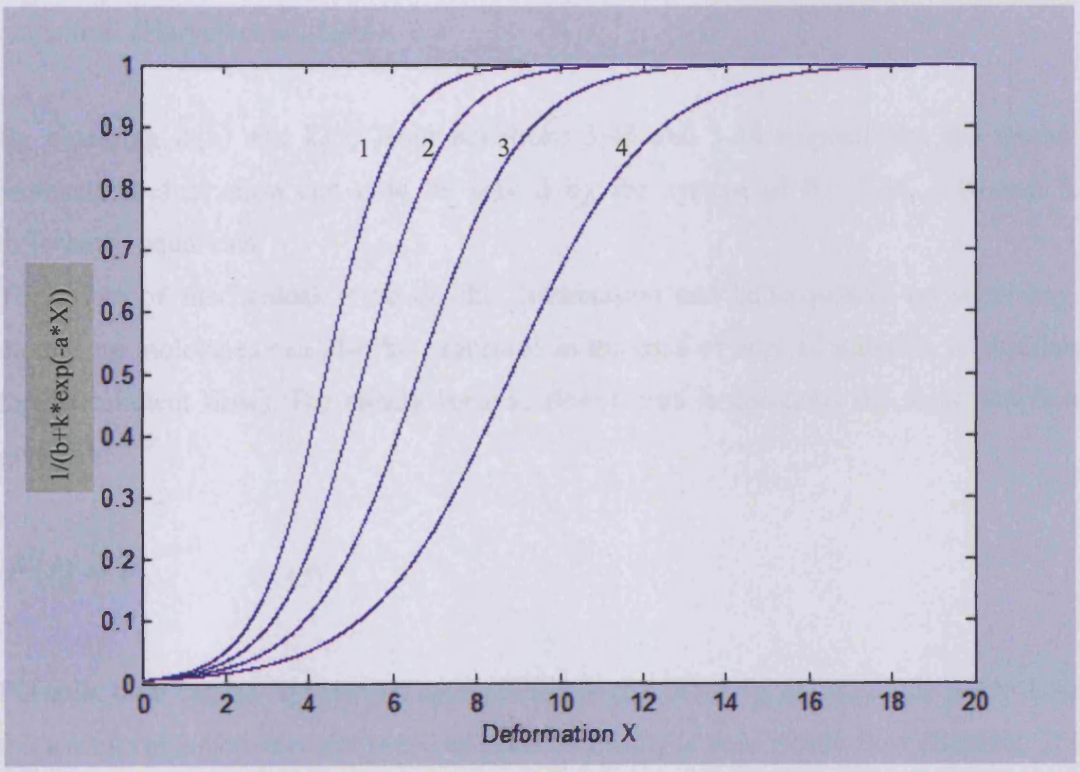

Figure 3.37. Plot of the sigmoid function (Y axis) for hypothetical deformation X of arbitrary values between 1 and 20, where a (amplitude) = 1, k (right bias) = 200 and b (left bias) = 1.2, 1, 0.8, 0.6 for plotted sigmoid lines 1 - 4 respectively.

The forward and reverse rates can now be expressed as a function of deformation resulting from applied shear force, acting as on/off switches where the speed depends on deformation level and amount of applied force:

$$k_f(x) = LS(x)k_f^0 , \qquad (3.43)$$

$$k_r(x) = (1 - LS(x))k_r^0 , \qquad (3.44)$$

where k_f^0 and k_r^0 are the initial steady state rates of transition prior to application of external force by fluid flow. These rates exist under physiological conditions at all times as all proteins are dynamic and undergo constant motions and structural changes in cells. These changes include large-scale movements of domains (e.g. caused by insertion of protein in the membrane bilayer which results in conformational changes) as well as small-scale random movement of secondary structures or domains due to thermal forces, known as molecular breathing. The time scales of such processes span many orders of magnitude (Harvey et al., 1984).

By obtaining $k_f(x)$ and $k_r(x)$ from equations 3.43 and 3.44 respectively, the model of molecular deformation can now be solved by the system of the 3.34, 3.40 and 3.41 differential equations.

The effect of mechanical force on the deformation and subsequently on signalling of membrane molecules can also be examined in the case of applied pulsatile or oscillatory force (turbulent flow). For steady laminar flow (force is constant) the force function is given by:

$$F(t) = F_0 , \qquad (3.45)$$

Pulsatile flow can be represented by superimposing a sinusoid of amplitude A (A<1 since the waveform is non-reversing) and angular frequency ω onto steady flow (Barakat, 2001) to yield a force function of the form:

$$F(t) = F_0(1 + A\sin(\omega t)), \quad (3.46)$$

Oscillatory flow can be represented by a sinusoidal function with an angular frequency ω (Barakat, 2001):

$$F(t) = F_0 \cos(\omega t), \quad (3.47)$$

where F_0 in each of the above cases is the magnitude of the applied force at time t = 0.
The notion of differential responsiveness to different types of shear stress is especially significant to development of atherosclerotic lesions, which localize preferentially in arterial regions subjected to low and/or oscillatory shear stress, while regions subjected to high and unidirectional shear stress remain largely unaffected (Cunningham and Gotlieb, 2005).

3.6.7 Implied assumptions of the mechanosensitive model

There are several assumptions inherent in the model formulation described above:

- It is recognised that the magnetic bead microrheometry measurements described in the above experiments (Bausch et al., 1998; Bausch et al., 2001) do not represent the mechanical properties of integrins alone but also include the contribution of cytoskeletal elements to which integrins are coupled to. Within this context, the Kelvin body is used to model the deformation of integrin receptors along with any coupled cytoskeletal elements as one molecular entity. This also implies that it is the amount of deformation and not the relative molecular position (which could be altered by hinge motion between molecules) that determines signalling.
- Experiments on cultured endothelial cells (Sato et al., 1996; Bausch et al., 1998) have demonstrated that the elastic viscosity parameter values of the membrane change after cells are exposed to shear stress for a certain period of time (e.g. values are double after 24 h of shear stress exposure). This is in agreement with our treatment of membrane stiffening (i.e. due to changes in membrane fluidity and cytoskeletal rearrangements) after few minutes upon application of shear stress

as has been applied in the calcium dynamics module (section 3.2). However for the simulation time scales (~20 minutes) of the deformation model it is assumed that the elastic constants of the individual membrane molecules subjected to force do not change over and their values are the same for both normal and deformed states. Therefore for constant force applied, the deformation x of the proteins is the only variable that varies in time.

- Since proteins are in constant motion due to thermal energy fluctuations, the membrane proteins modelled as Kelvin bodies must be sufficiently large structures for the energy imparted to their bodies by shear stress to significantly exceed the energy associated with the thermal fluctuations of the proteins so the imparted energy can be felt. Barakat (2001) calculates that the characteristic dimension of the membrane molecular sensors must be of order 100 nm for the energy imparted to them to be an order of magnitude larger than the thermal energy of the molecules (i.e. ~10 KT). Therefore in order to fulfil this criterion it is assumed that the dimension of the receptors (e.g. integrins) is of order ~100nm. This dimension is not expected to deviate much from physiologic reality as the membrane receptors are generally larger than the average size of whole cytosolic proteins in the cell which vary in size between 5 and 200 nm (Zhu et al., 2000).
- Since the observed elastic parameters for the mechanical properties of membrane molecules (Sato et al., 1996; Bausch et al., 1998) have been reported for the whole length/body of these molecules (e.g. integrins), each membrane protein is accordingly modelled here as a single domain by the Kelvin body (allowing for usage of the reported parameter values of viscoelasticity). Therefore, the deformation model is not applied to each individual domain of the proteins separately due to unavailability of information regarding the mechanical properties of these domains. Although, the elastic and viscosity parameter values have been experimentally derived for integrin receptors (Bausch et al., 1998), we assume that the same values apply also for PECAM-1 receptors.

3.6.8 Parameter values

For the viscoelastic body modeled, the values of the two spring constants k_1 and k_2 as well as the dashpot coefficient of viscosity m must be specified. The parameter values for the mechanical properties of cell-surface transmembrane receptors were based on published magnetic bead microrheometry measurements (Bausch et al., 1999; Bausch et al., 1998). A second set of equivalent values for the mechanical properties of actin filaments were also collected from the measurements of Sato et al (1996). The parameter values in both cases are given in Pa and Pa-s for the spring constants and the viscosity coefficient respectively in Table 3.06

Kelvin body	k_1 (Pa)	k_2 (Pa)	m (Pa-s)	Source
Transmembrane proteins	100	200	7.5	Bausch et al., 1998; Mazzag et al., 2003

Table 3.06. Parameter values for integrins and actin filaments. 1 dyne/cm^2 = 10 μN/cm^2 and 1 Pa = 10 dynes/cm^2.

Mazzag et al (2003) have used the experimental observations of Sato et al (1996) and Bausch et al (1998) to calculate the equivalent value for initial deformation in the Kelvin body as:

$$x_0 = \frac{F}{k_1 + k_2}, \qquad (3.48)$$

They also give the deformation for the Kelvin body at steady state ($t \rightarrow \infty$) as:

$$x_0 = \frac{F}{k_1}, \qquad (3.49)$$

The baseline value of the angular frequency in the oscillatory and pulsatile flow simulations is taken as $\omega = 2\pi$ rad/s which corresponds to a heart beat frequency $f = 1$ Hz ($\omega = 2\pi f$). The pulsatile flow amplitude A was taken after Barakat (2001) as A = 0.25 (dimensionless).

For an approximate size R of 150 nm for a transmembrane and for a typical arterial shear stress τ = 3 Pa (30 dyne/cm^2 or 3 N/m^2) and dynamic viscosity of blood fluid η =0.32 Pa-s (section 1.3.1) where the shear rate G = shear stress τ /viscosity η, equation 3.38 yields a total hydrodynamic force F of ~2 pN (2.2 pN) applied on each membrane molecular body. In typical experimental conditions where shear stress τ = 1.2 Pa (12 dyne/cm^2) and dynamic viscosity of cell culture medium η = 0.1 Pa-s, the total hydrodynamic force *F* applied on each mechanosensor is F = ~1 pN (0.9 pN).

By incorporating G = τ/ η in equation 3.38, τ can be given as: τ = F/10.2πR^2, which when used in the standard equation for wall shear stress in Newtonian fluids (refer to section 1.3.1, page 46) gives: F= μ10.2πR2(dU)/dy. Taken that fluid velocity increases uniformly in the tube this readily establishes that the force *F* applied is directly proportional to the rate of fluid flow. Thus, the effect of different levels of shear stress on molecular def rmation can be simulated by simply proportionaly scaling the value of *F* in the model. N te here that the force applied on cell surfaces by bead microrheometry, optical tweezers c AFM experiments is much larger than the force applied by physiological fluid flow onditions. Unit conversions for parameter values were performed according to Table 3.07.

Unit conversions		
1 N = 10^5 dynes	1 dyne = 1g-cm/sec^2	1 Pa = 1 N/m^2
1 N = 1Kg-m/sec^2	1 dyne/cm^2 = 0.1 Pa	1 dyne/cm^2 = 0.1 N/m^2

Table 3.07. Unit conversions

The concentration of available integrins in endothelial cells has been estimated as 0.16 μM in section 3.4 or 10^5 receptor molecules per cell. The potential deformation influence which might be caused by molecular breathing has been excluded and it is assumed that before application of shear stress all integrin receptors are undeformed, therefore: [I] = 0.16 μM and [A] = 0.0 μM.

Solution of the equations 3.40 and 3.41 require the values of $k_f(x)$ and $k_r(x)$ which are given by equations 3.43 and 3.44 respectively. The determination of $k_f(x)$ and $k_r(x)$ however requires values for the initial steady state rates of transition k_f^0 and k_r^0 prior to application of external force by fluid flow. Based on the model governing that molecular

deformation is force-dependent and not permanent, appropriate initial values for k_d ratio ($k_d = k_r^0 / k_f^0$) were chosen to satisfy the following two conditions for steady state:

1. When no external force is present:
If *[I]* = 0.16 μM and *[A]* = 0.0 μM at time t = 0, then *[I]* = 0.16 μM and *[A]* = 0.0 μM at time $t = 0 \rightarrow \infty$
2. When the applied force is removed:
If *[I]* = 0.00 μM and *[A]* = 0.16 μM at time t = 0, then *[I]* = 0.16 μM and *[A]* = 0.0 μM at time $t = 0 \rightarrow \infty$

Condition 2 implies that if force is applied for a certain amount of time and then it is removed, the receptors return quickly to their normal state. This recovery is different between different molecular species and depends on their elastic and viscosity parameters.

3.6.9 Simulation results, analysis and discussion

The amount of force applied to each integrin receptor was first calculated upon fluid flow-induced shear-stress as F_o = 1 pN (shear stress τ = 12 dyne/cm^2). The model was then tested by applying F_o = 1 pN on the membrane mechanosensors at time t = 0 and calculated the resulting deformation of integrins according to equation 3.34 as: final length of the receptors - initial length = 450m/N = 0.45 nm/pN.

The amount of molecular deformation observed in the simulation results matches the equivalent experimental observations previously reported (Bausch et al., 1998). After measuring the force-induced deformation, the concentration of the molecular species that switch between inactive/undeformed (basal kinetic rates for downstream signalling) and deformed/active states (sufficiently deformed for altered kinetic rates for downstream signalling) could be calculated.
As the peak value of the sigmoidal function (equation 3.42) is dependent on the overall amount of deformation, the calculated deformed lengths for the molecular species were used to adjust the parameter values of the logistic function to provide the sigmoidal switch that simulates the transition between inactive and active states of the receptors. The

sigmoidal function was then used to modify the values of k_f^0 and k_r^0 according to equations 3.43 and 3.44 from $F_0 = 0$ to $F_0 = 1$ (pN).

As a result, when the deformation value x exceeds a certain value it causes the sigmoid function to switch from the plateau region towards its peak region. The forward reaction rate producing active deformed integrins is then 'switched on' and its rate increased to switch the bias of the reaction towards the deformed state (Figure 3.37).

The velocity of deformation, which depends on the elastic and viscosity constants and thus is different for each molecular species, governs how early in time t the switch will take place (i.e. accelerates the initiation of transition). On the other hand, the amount of deformation which is linearly related to the amount of force applied, governs the respective values of the transition rates between inactive and active states of the receptors (i.e. accelerates the reaction speed of the transition).

As observed in Figure 3.38 there is no deformation at steady state in the absence of mechanical force. No energy is imparted on the molecules and all the receptors exist in the normal undeformed state.

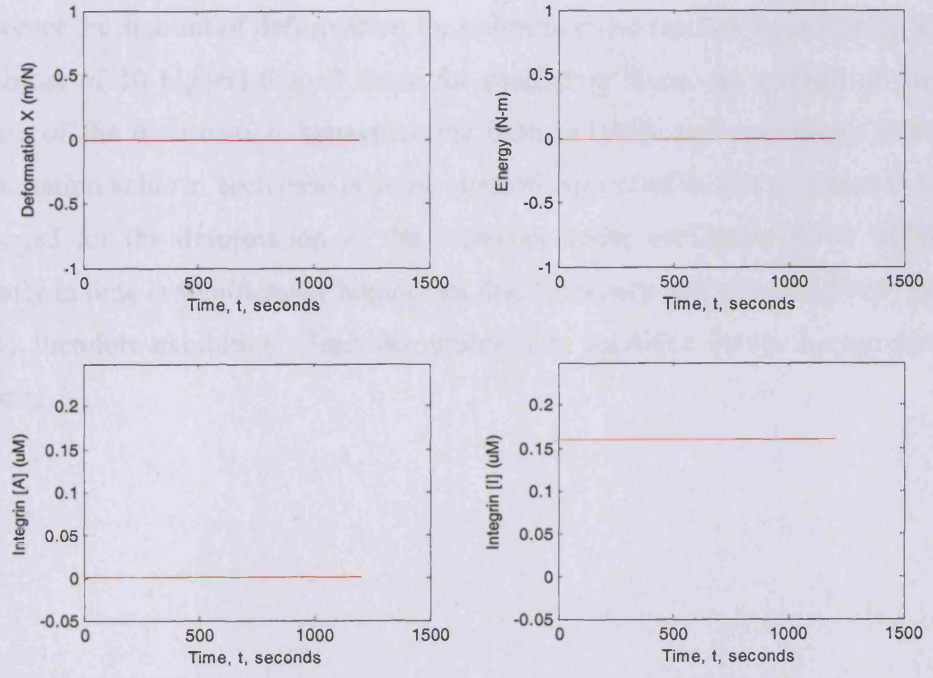

Figure 3.38. Deformation, energy and concentration of species at steady state $F_o = 0$.

Figures (3.39-3.41) demonstrate the deformation of integrin receptors as a function of time for steady, pulsatile and oscillatory force respectively. For all three types of force there is an immediate deformation. According to the Kelvin body this immediate response is given by the instantaneous deflection of the elastic springs followed by gradual creeping of the dashpot towards the long-term deformation behaviour (this is not visible in the graphs as it occurs within the first 5 seconds).

The results of the model show that in response to a suddenly (t = 0) applied steady fluid mechanical force, the integrin transmembrane receptors deform instantaneously by a certain amount dictated by the elastic constants as derived from the experimental observations of Bausch et al (1998). The time constant characterising the rate at which the deformation approaches its long-term steady state behaviour depends on the values of the three viscoelastic constants, which in the case of steady force occurs within few seconds. The peak deformation of the receptors is given by the long-term steady-state deformation value which once attained remains unchanged as long as the cells are subjected to flow.

On the other hand, both pulsatile and oscillatory flows lead to sinusoidal oscillations in the deformation of integrins of period 1 second, similar to the period of the imposed flow. However the amount of deformation for pulsatile pulse reaches significantly larger values (an order of 10 higher) that of those for oscillatory force. As a result of the sinusoidal nature of the deformation behaviour for both pulsatile and oscillatory force, the peak deformation value in each case is being attained periodically. It is observed that the energy imparted for the deformation of the receptors under oscillatory force which increases linearly in time is significantly higher that that for steady and pulsatile force (Figures 3.39-3.41), therefore exhibiting a least favourable flow condition for the human cardiovascular system.

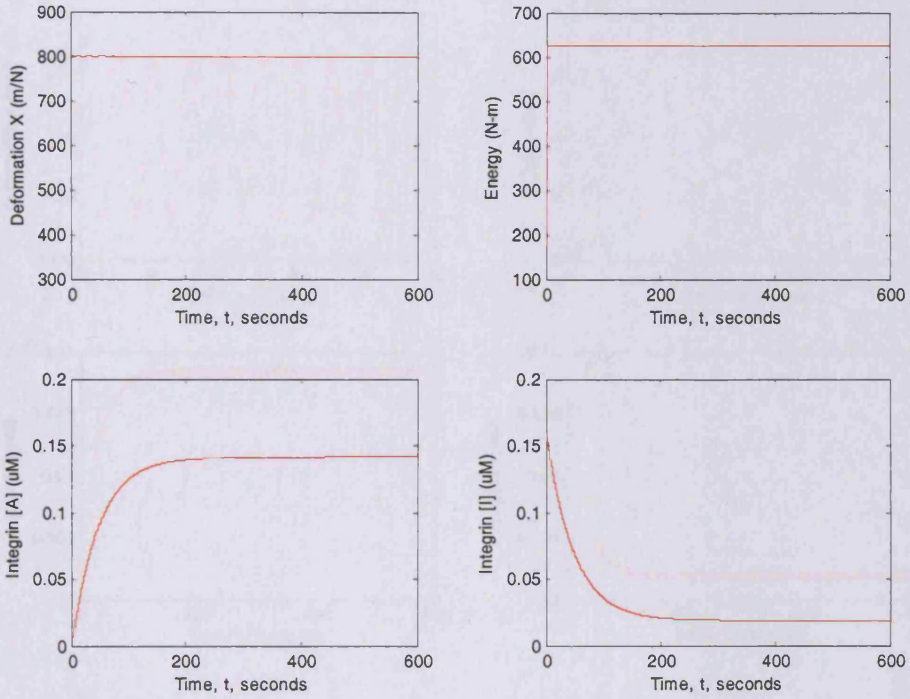

Figure 3.39. Deformation, energy and concentration of species after application of steady force F_o = 1 pN.

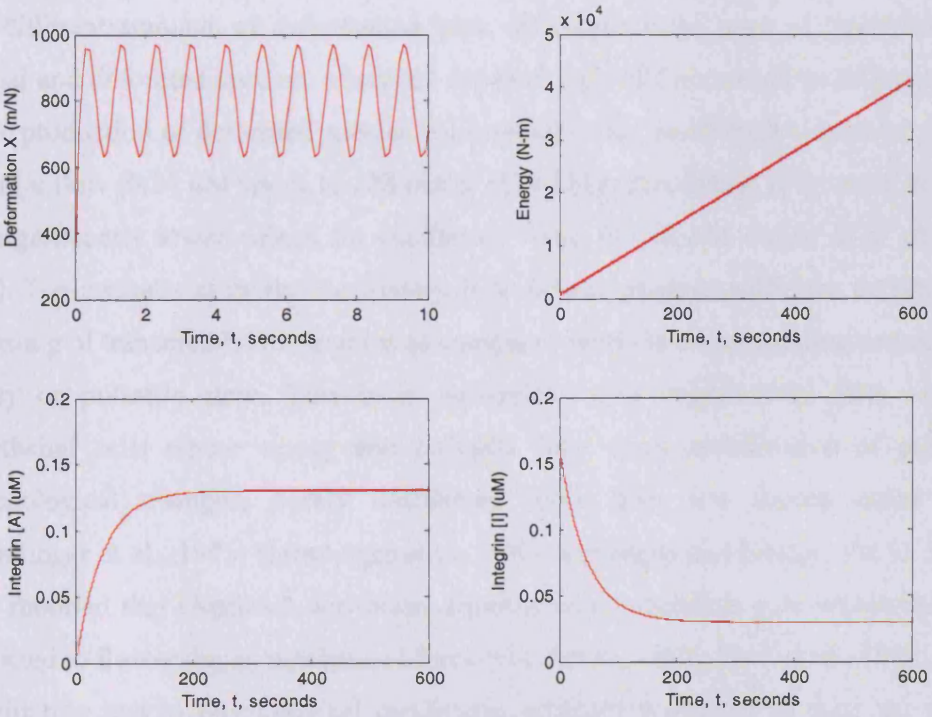

Figure 3.40. Deformation, energy and concentration of species at applied pulsatile force $F(t) = F_0(1 + A\sin(\omega t))$.

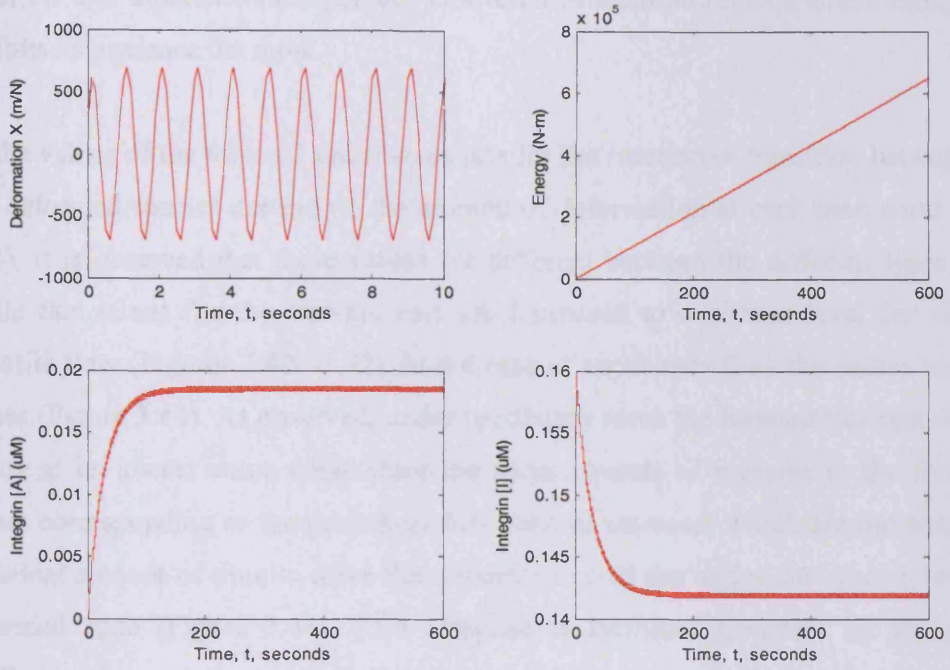

Figure 3.41. Deformation, energy and concentration of species at applied oscillatory force $F(t) = F_0 \cos(\omega t)$.

The different amounts of deformation (that differentiate the rates of transition between normal and deformed species) observed for each type of force result in different amounts in the production of deformed species concentration that reach high values for steady and pulsatile flow (0.14 μM and 0.13 μM out of 0.16 μM respectively) (Figures 3.39 and 3.40) but significantly lower values for oscillatory force (0.018 nM out of 0.16 μM) (Figure 3.41). These results show that oscillatory flow fails to produce sufficient deformation and signalling of transmembrane proteins as compared with the corresponding responses under steady or pulsatile flow. This is in agreement with experimental data on cultured endothelial cells where steady and pulsatile flow elicit mobilisation of calcium and morphological changes, purely oscillatory force does not induce either response (Helmlinger et al., 1995; Helmlinger et al., 1991; Levesque and Nerem, 1985). It has also been reported that G-protein activation depends on the duration over which the cells are subjected to flow-induced mechanical force (Gudi et al., 1998; Gudi et al., 1996).

Considering that in physiological conditions, oscillatory patterns of flow are frequently observed in regions of turbulent flow (Cunningham and Gotlieb, 2005; Gimbrone et al., 2000; Liu, 1999; Prado et al., 2006), the model predictions correlate with the higher

occurrence of atherosclerotic plaques at arterial bifurcation regions where turbulent flow exhibits its presence the most.

As the values of the forward and reverse rate for the reaction of transition between normal and deformed species depend on the amount of deformation at each time point (equation 3.34), it is observed that these values are different between the different types of force. While the values for the forward rate are increased to a similar level for steady and pulsatile flow (Figures 3.42 –3.43), in the case of oscillatory flow the values reach lower values (Figure 3.44). As observed, under oscillatory force the forward rate remains mostly steady at its lowest value while there are certain bursts of increase in the forward rate values corresponding to the periodical deformation increases which are not sustained for sufficient amount of time to drive the concentration of the molecular species towards the deformed state (Figure 3.44). This response is therefore governed by the period of oscillation (frequency) which if it is increased significantly can result to a response similar to that resulting from pulsatile/steady force.

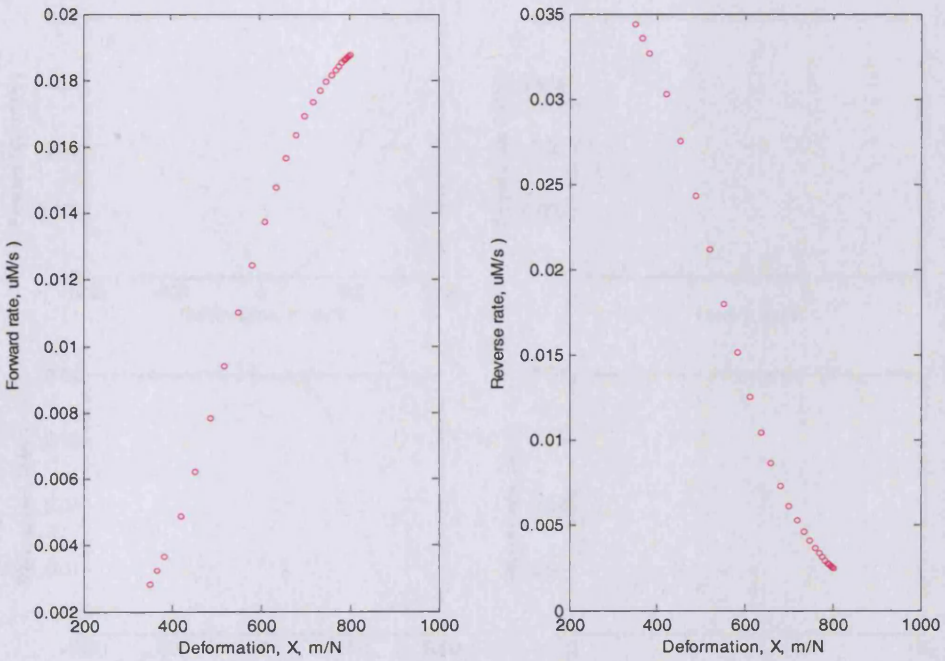

Figure 3.42. Evolution of forward/reverse rate values at steady force. Values are dependent on deformation.

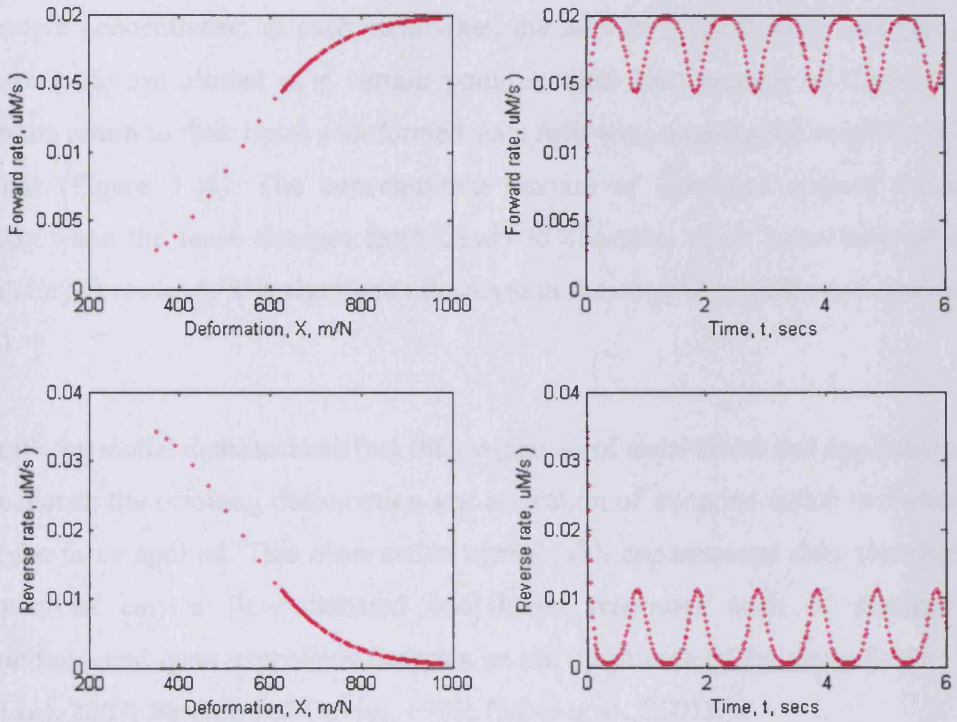

Figure 3.43. Evolution of forward/ reverse rate values under pulsatile force.

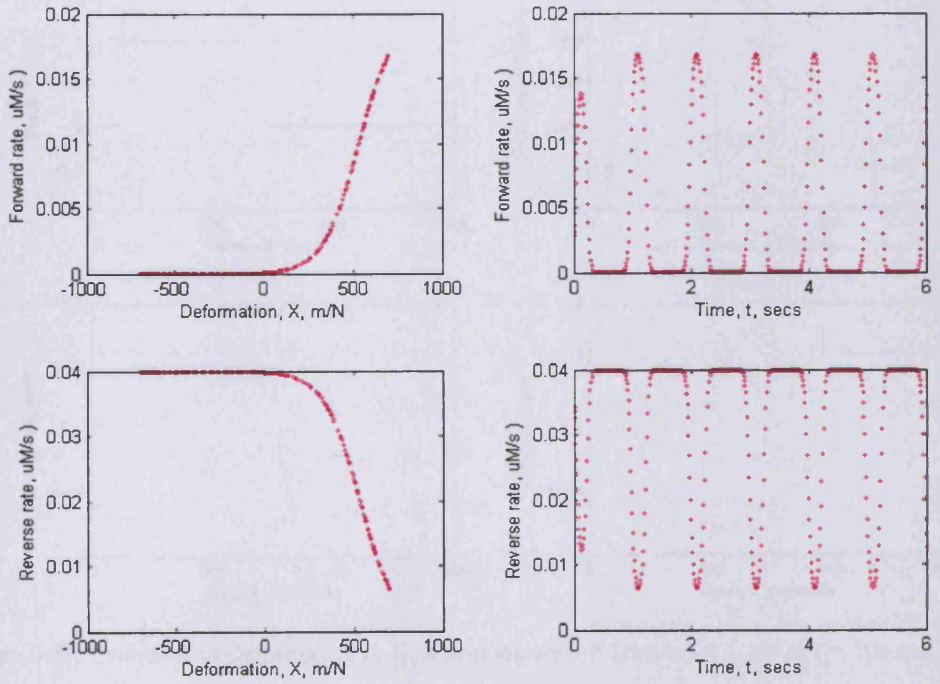

Figure 3.44. Evolution of forward/ reverse rate values under oscillatory force.

Figures 3.45-3.46 demonstrate the evolution of deformation of molecular species and their respective concentration in each state when the amount (Figure 3.45) and type of force (Figure 3.46) are altered at a certain point in time. On removal of force all integrin receptors return to their basal undeformed state following a relaxation response within 100 seconds (Figure 3.45). The concentration amount of deformed species reduced only slightly when the force changes from steady to pulsatile, while conversion of steady to oscillatory force leads to a significant decrease in the amount of deformed species (Figure 3.46).

Overall, the model demonstrates that the magnitude of shear stress and applied mechanical force dictate the resulting deformation and activation of integrins which increases linearly with the force applied. This observation agrees with experimental data showing that the intensity of certain flow-mediated endothelial responses such as changes in cell morphology and gene expression depends on the magnitude of the applied force (Barakat and Lieu, 2003; Barakat and Davies, 1998; Fisher et al., 2001).

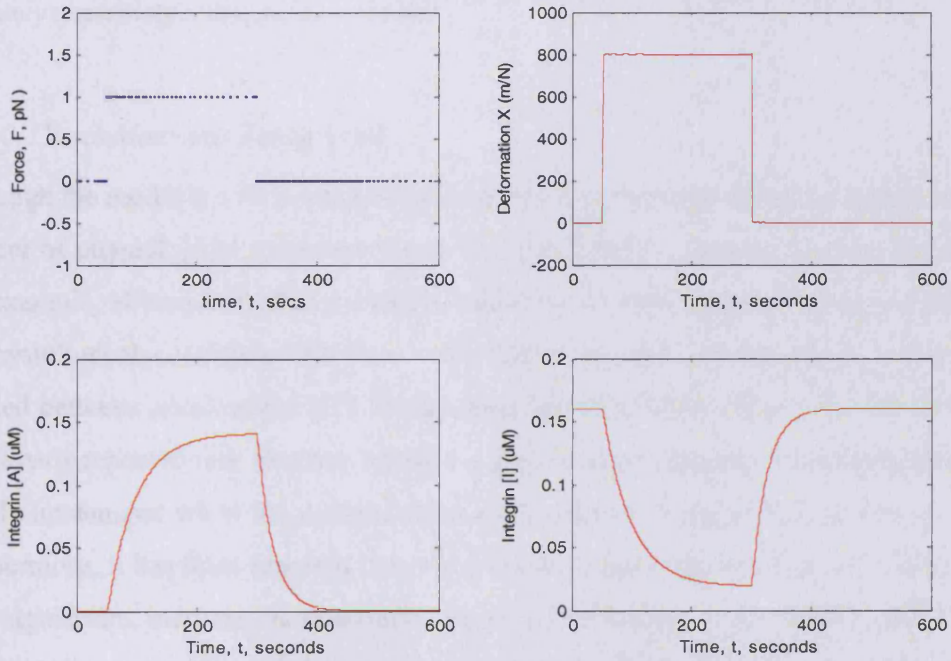

Figure 3.45. Evolution of deformation & [] of species upon F (steady) = 1 pN at t = 50s and $F = 0$ at t = 300s.

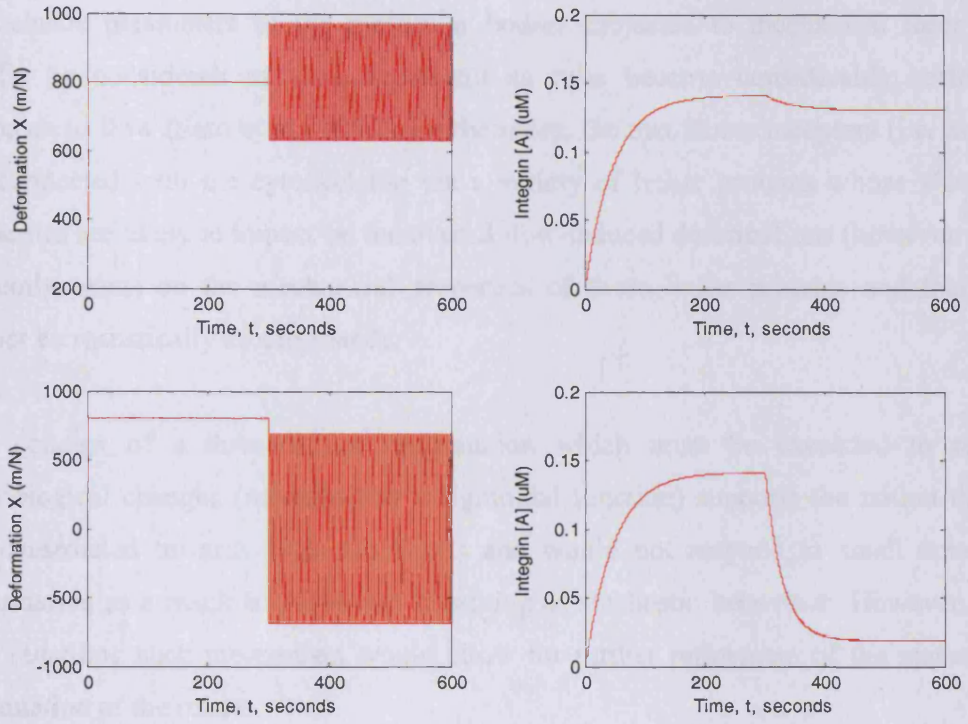

Figure 3.46. Evolution of deformation and [] of species when force F changes from steady to pulsatile and oscillatory respectively at time point $t = 300$ secs.

3.6.10 Conclusions and future work

Although the model is able to match results derived experimentally and is able to explain a number of physiological responses it can be significantly improved in a number of ways. For example, although oscillatory and pulsatile flows were modelled as sinusoidal flows, in physiological conditions the flow pulse differs in that the waveform is not equally divided between acceleration and deceleration (Barakat, 2001). However, Barakat (2001) has already reported that the flow behaviour simulated by sinusoidal functions will remain largely unchanged when the computations are applied to a physiological flow waveform. Furthermore, it has been reported that exposure of cultured endothelial cells to flow leads to a significant increase in membrane fluidity (Haidekker et al., 2000) as also in the activity of transmembrane receptors (Tzima et al., 2005). It would therefore be very interesting to incorporate the impact of mechanical force on the endothelial membrane fluidity.

As discussed in the assumptions, experimental observations have suggested that the viscoelastic parameters of the molecular bodies subjected to mechanical force should ideally be considered as time dependent as cells become considerably stiffer upon exposure to flow (Sato et al., 1996). Furthermore, the membrane receptors (i.e. integrins) are connected with the cytoskeleton via a variety of linker proteins whose viscoelastic properties are likely to impact on the overall flow-induced deformations (however, no data currently exists on the mechanical properties of these linker proteins and their effect cannot be realistically incorporated).

The concept of a threshold of deformation which must be exceeded to result in physiological changes (modelled by a sigmoidal function) supports the notion that cells are constructed towards high robustness and would not respond to small amounts of deformation as a result of molecular breathing or stochastic behaviour. However, further data regarding such mechanism would allow for further refinement of the mathematical formulation of the model.

3.7 Effects of deformation on integrin and FAK activation (Module 6)

3.7.1 Module description

Recent studies (section 3.5.5) have suggested that stretch-induced conformational changes can influence the dynamics of proteins (Kumar et al., 2006; Lele et al., 2006a; Lele et al., 2006b). For example, molecular dynamics simulations suggested that the focal adhesion targeting domain of FAK changes conformation in response to mechanical force, resulting in an increase in its binding affinity for paxillin (Kamm and Kaazempur-Mofrad, 2004). Stretch-induced conformational changes could also cause unfolding of domains in proteins, exposing cryptic binding sites for partners. This has been shown for fibronectin fibril assembly where cytoskeletal tension can cause fibronectin extension and unfolding of specific domains (Baneyx et al., 2002). Applied force could alter integrin signalling using any one or all of these mechanisms. For example, stretching detergent-insoluble cytoskeletons alters the binding of several cytoplasmic proteins, including paxillin and FAK, to the cytoskeleton (Sawada and Sheetz, 2002). Based on this evidence, and the inability of the model to match the experimentally observed changes in integrin activity (2-fold increase) (Tzima et al., 2001) and FAK phosphorylation (3-fold increase) (Li et al., 1997) in conditions of shear stress (12 dynes/cm^2) using Ca^{2+} influx alone, it seems likely that shear stress (mechanical force) is transduced directly into changes in molecular binding kinetics of critical signalling/integrin-associated proteins. A viscoelastic model was formulated in the previous section to examine properties of stretch-induced deformation for membrane receptors. The influence of this deformation on the binding kinetics of molecules is investigated in this section by introducing enhanced affinities for certain molecules resulting from stretching of integrins.

3.7.2 Influences of deformation on signalling

Shear stress is transmitted onto the membrane bilayer and results in deformation of transmembrane receptors and associated proteins. It is estimated that about 10% of integrins are active (bound to ligand e.g. fibronectin) prior to shear stress stimulation (section 3.5). This pool of active integrins (Figure 3.47) is subject to outside-in activation by force-induced deformation. It is assumed that deformation of integrins takes place only

when integrins are engaged to fibronectin bonds resulting in force-induced stretching. Release of integrins from fibronectin caused by either talin or fibronectin dissociation from integrins results in the removal of the force sensed by integrins and their rapid return to their basal undeformed state.

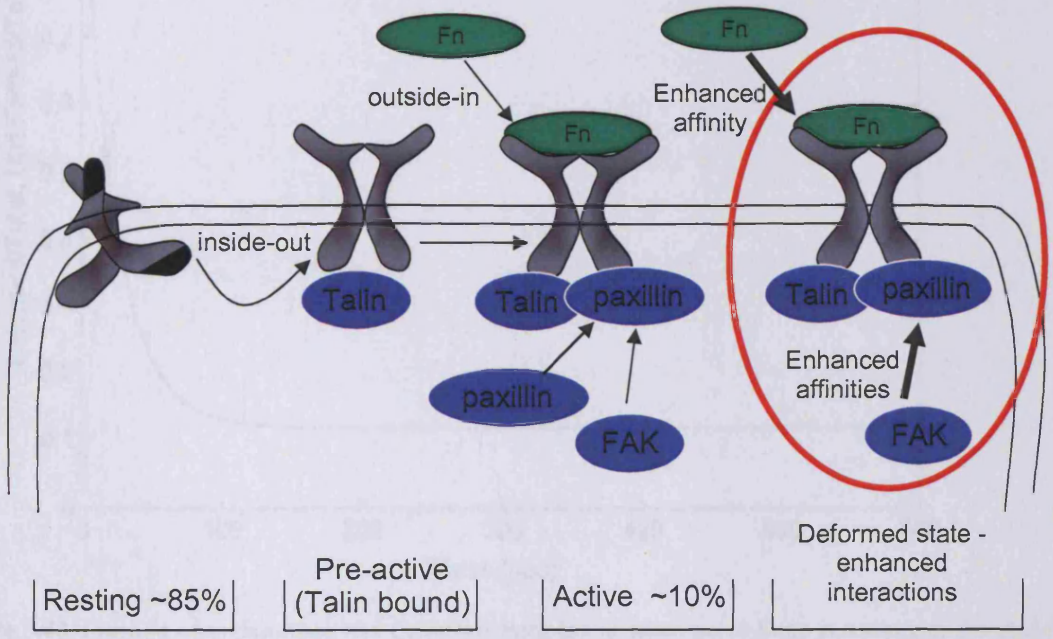

Figure 3.47. Overview of integrin activation including deformation and effects on signalling. There are three major pools of integrins. Integrins unbound (inactive), integrin bound to talin (pre-active) and integrin bound to talin and fibronectin (active). Integrins bound to fibronectin are subject to further activity enhancement resulting from stretch-induced deformation.

To avoid additional model complexity, the stretch-deformed integrins were not introduced in the model as a separate species, instead a fraction of ligand-bound integrins (bound to fibronectin) were assumed to be deformed. Using the model of integrin deformation for (section 3.6), the fraction of deformed and undeformed integrins was calculated for every time point for the duration of the applied shear stress (Figure 3.48).

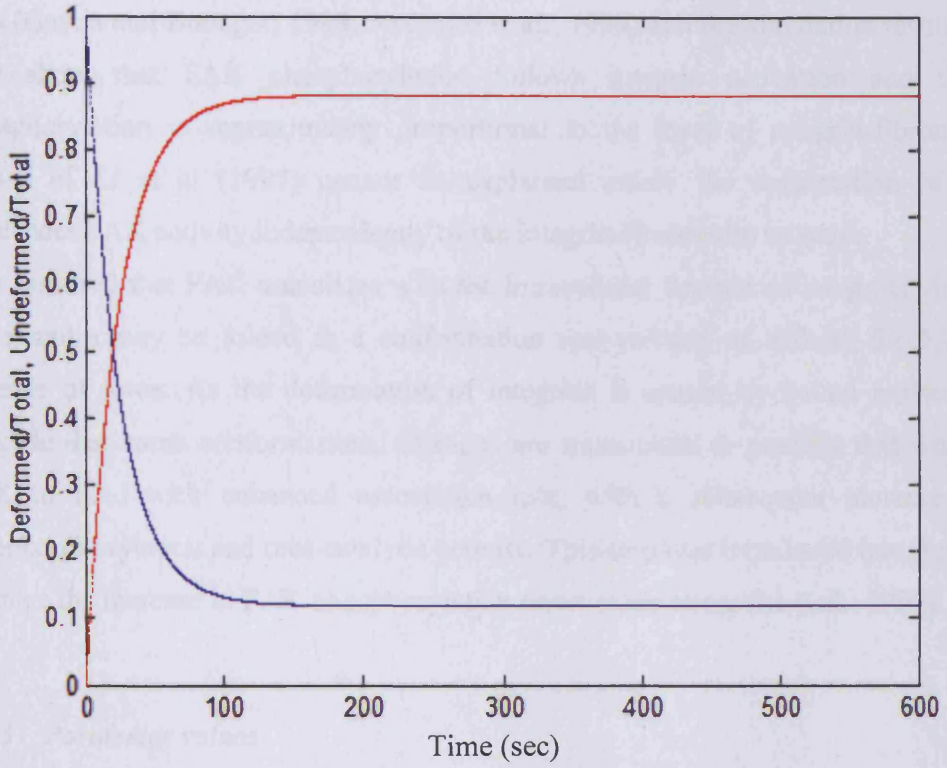

Figure 3.48. Fraction of undeformed and deformed integrins in response to force according to the model formulated in section 3.6. Deformed and undeformed integrins are shown in red and blue respectively. Total = the amount of integrins that are bound to fibronectin. For 12 dynes/cm^2 shear stress, approximately 90% of active integrins deform within 2 minutes (120 secs).

The effects of integrin deformation on signalling were based on the assumption that the conformational changes to integrins are sensed by molecules bound to the integrin complex. Consequently, the two states of active integrins were assumed to exhibit different affinities for extracellular (i.e. fibronectin) and intracellular (paxillin/FAK) partners. In order to produce increased activation of integrins in response to shear stress and since receptor deformation only applies to integrins that are bound to fibronectin, the affinity of integrins for fibronectin was increased for the deformed species by decreasing the dissociation rate of integrins to fibronectin.

An increase in integrin activation by enhanced fibronectin binding will lead to an elevation of FAK bound to integrin complexes and thus increased FAK phosphorylation. However, the published experimental data have shown that although integrin activity is increased by 1-fold within 2 minutes and 2-fold after 5 minutes (Figure 3.19) the changes in FAK phosphorylation take place much more rapidly, exhibiting and increase of 3-fold

within 1 minute of shear stress stimulation (Li et al., 1997). Because both experimental data (Garcia and Boetiger, 1999; Asthagiri et al., 1999) and the simulation results (section 3.5) show that FAK phosphorylation follows integrin activation and that FAK phosphorylation is approximately proportional to the level of integrin-fibronectin, the results of Li et al (1997) cannot be explained unless the deformation of integrins influences FAK activity independently of the integrin-fibronectin increase.

It is assumed that FAK associates with the intracellular domain of integrins via paxillin, but paxillin may be folded in a conformation that reduces its affinity for FAK in the absence of force. As the deformation of integrins is sensed by bound molecules, it is possible that some conformational changes are transmitted to paxillin that would allow FAK to bind with enhanced association rate, with a subsequent increase in FAK autophosphorylation and thus catalytic activity. This step was introduced into the model to produce the increase in FAK phosphorylation under shear stress (Li et al., 1997).

3.7.3 Parameter values

These effects are introduced in the model as new reaction rates for fibronectin dissociation and FAK association for the deformed species.

Two parameter values were estimated in order to reproduce the experimentally observed dynamics. The dissociation rate of fibronectin from integrin was reduced by 10-fold for the deformed integrins, and the affinity of FAK for paxillin was increased by 100-fold by increasing its association rate.

Parameter values before deformation				
Constant	Description	Value	Units	Source
kfi_r	Dissociation of fibronectin from integrins	0.01	s^{-1}	Akiyama and Yamada, 1985
kpF_f	Association of FAK to paxillin	0.083	$\mu M^{-1} s^{-1}$	Thomas et al., 1999
Parameter values after deformation				
Constant	Description	Value	Units	Source
Kfi_r2	Dissociation of fibronectin from integrins	0.001	s^{-1}	estimated
kpF_f2	Association of FAK to paxillin	8.3	$\mu M^{-1} s^{-1}$	estimated

Table 3.08. The parameter value modifications for the deformed species.

3.7.4 *Simulation results and discussion*

Simulations were run for conditions of 12 dynes/cm^2 shear stress (combining the deformation model and altered rate constants).

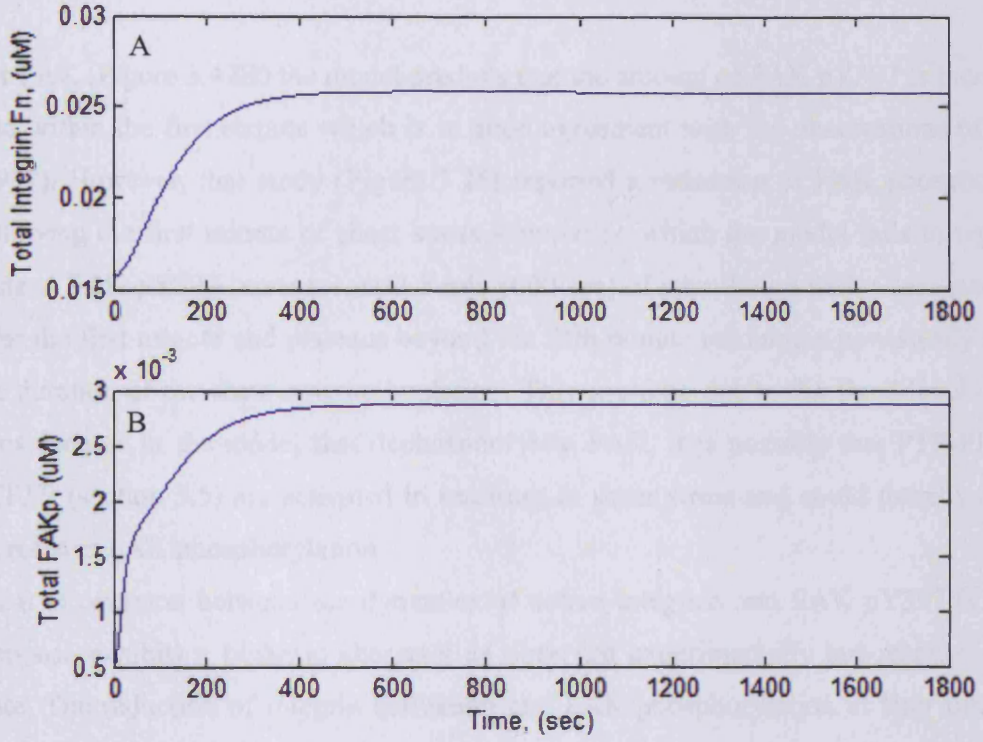

Figure 3.49. Dynamics of integrin activation and FAK phosphorylation after introducing integrin deformation. FAKp = FAK pY397.

The simulated dynamics for active integrins (Figure 3.49A) were compared with the data of Tzima et al (2001) (Figure 3.19) which were obtained at 12 dynes/cm^2 shear stress. The model predicts that activation of integrins peaks at 5 minutes (600 sec) which is in good agreement with the experimental data. The slope of activation is also similar: the model predicts that the amount of integrins that are activated between 120 sec and 600 sec of shear stress is approximately equal to the amount of integrins that get activated within the first 2 minutes. The model deviates from the results of Tzima et al (2001) in that the peak fold-activation of integrins is 1.8 in contrast to the 3-fold increase observed experimentally. The lower fold-activation of integrin in the model results from the limited availability of integrin:talin complexes since the amount of fully active integrins cannot exceed the amount of talin-integrin complexes. Further inputs are therefore required to reproduce the fold activation observed experimentally. If integrins could be activated

independently of talin then it would be possible to obtain higher levels of integrin activation. Integrin activity is also controlled via the GTPase Rap1, which is believed to enhance talin binding to integrins (McLeod et al., 2004; Reedquist et al., 2000; Shimonaka et al., 2003).

For FAK (Figure 3.47B) the model predicts that the amount of FAK pY397 is increased 3-fold within the first minute which is in good agreement with the observations of Li et al (1997). However, that study (Figure 3.25) reported a reduction of FAK phosphorylation following the first minute of shear stress stimulation which the model fails to reproduce. Instead FAK pY397 increases until 5 min (600 sec) of stimulation with a less steep slope after the first minute and plateaus beyond the fifth minute reaching a new steady state for the duration of the shear stress stimulation. This could be due to the fixed level of active phosphatases in the model that dephosphorylate FAK. It is possible that PTP-PEST and PTP1B (section 3.5) are activated in response to shear stress and could thereby limit the increase in FAK phosphorylation.

What is common between the dynamics of active integrins and FAK pY397 is that the response exhibits a biphasic character as observed experimentally but reaches a steady state. The reduction of integrin activation and FAK phosphorylation at later time points must involve a negative feedback loop (i.e. where an increase in signalling triggers feedback inhibition). This is discussed in section 3.9.

3.8 Activation of Src by FAK and the PKC – RPTPα pathway (Module 7)

3.8.1 Module description

The autophosphorylation of FAK on Y397 creates a high-affinity binding site for the SH2 domain of Src (Schaller et al., 1994). In addition, there is a proline-rich sequence upstream of Y397 on FAK that conforms to a high-affinity binding site for the SH3 domain of Src (Thomas et al., 1998). Src kinase is also known to be activated in response to shear stress (Jalali et al., 1998), however, the Src SH2 domain is not always accessible to substrates (Frame, 2004) and it is thus necessary to first examine the pathway responsible for the activation of Src kinase prior to its interaction with FAK.

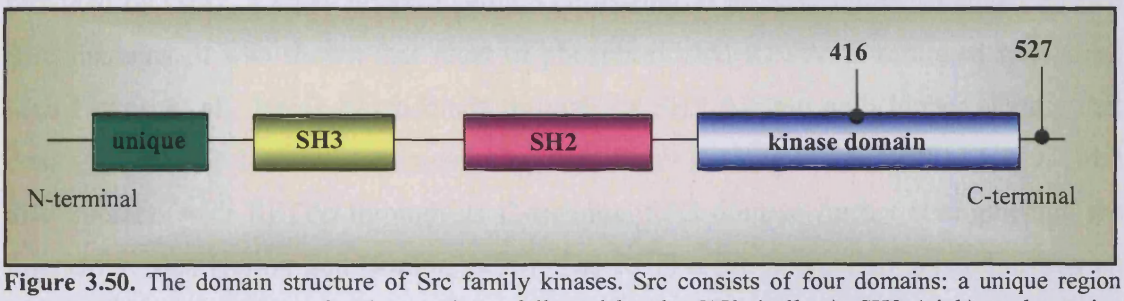

Figure 3.50. The domain structure of Src family kinases. Src consists of four domains: a unique region (green), which varies among family members, followed by the SH3 (yellow), SH2 (pink), and tyrosine kinase domains (light blue). The activating (Tyr 416) and autoinhibitory (Tyr 527) phosphorylation sites are indicated.

The catalytic activity of Src is normally suppressed by intramolecular folding, frequently called "tail-bite" conformation, in which a phosphorylated tyrosine residue near the C-terminus, Y527, binds to the SH2 domain (Boggon and Eck, 2004; Playford and Schaller, 2004) (Figure 3.50). This conformation, which is stabilised by the kinase's own SH3 domain, forces the catalytic domain into a locked state where catalytic residues are out of alignment and substrate access is blocked (Thomas and Brugge, 1997; Xu et al., 1997). The inhibitory phosphorylation that keeps Src in an inactive state is carried out by the tyrosine kinase Csk (Cooper et al., 1986; Okada and Nakagawa, 1989). Conversely, dephosphorylation of Y527 can be catalysed by the transmembrane receptor-like protein tyrosine phosphatase RPTPα (Pallen, 1993; Pallen, 2003; Zheng et al., 1992) which has two catalytic domains, D1 and D2. Although other protein tyrosine phosphatases (e.g. SHP2) have also been reported to dephosphorylate Src, RPTPα appears to be the main Src

phosphatase in vivo, because in RPTPα $^{-/-}$ cells, Src has reduced activity (Ponniah et al., 1999; Zeng et al., 2003). Structural analysis revealed a direct interaction between the Src SH2 domain and the catalytic domains of RPTPα (Sonnenburg et al., 2003) that is likely to disrupt the intramolecular interaction within Src, thus exposing Y527 for dephosphorylation by RPTPα (Sicheri and Kuriyan, 1997). The Src SH2 domain binds to the phosphorylated Y789 on RPTPα (Zheng et al., 2000). Normally, about 90% of the total RPTPα is phosphorylated at Y789 (den Hertog et al., 1994). Evidence as to which kinases are responsible for the tyrosine phosphorylation of RPTPα does not exist to date.

This RPTPα-induced displacement mechanism of Src activation is assumed not to operate at full capacity normally and the vast majority of Src is phosphorylated at Y527 and remains catalytically dormant. Inhibition of the RPTPα dephosphorylation of Src is provided by Grb2, a small adaptor protein consisting of an SH2 domain flanked by two SH3 domains. It was shown that most of phosphorylated RPTPα is saturated with Grb2 (den Hertog et al., 1994) which binds through its SH2 domain with higher affinity that does the Src SH2 domain, thus preventing significant binding of Src SH2 to Y789. Grb2 also interacts with RPTPα through its C-terminal SH3 domain further strengthening the interaction (den Hertog and Hunter, 1996). The RPTPα-Src interaction is regulated by an additional mechanism: RPTPα is also phosphorylated at one or more serines which results in reduced binding of Grb2 and exposure of Y789 that is needed for attracting Src to RPTPα (Zheng and Shalloway, 2001). In addition, serine phosphorylation causes a two-fold activation of RPTPα to further increase its ability to dephosphorylate Y527 on Src. Although it is not certain yet which kinase is responsible for serine phosphorylation of RPTPα, the serine/threonine kinase, protein kinase C, is the most likely candidate because RPTPα is phosphorylated on S180 and S204 in treated cells with phorbol ester (den Hertog et al., 1995; Tracy et al., 1995). These two sites are located in the juxtamembrane region of RPTPα, adjacent to the active D1 catalytic domain (den Hertog et al., 1995). There are multiple PKC isoforms, some of which are known to be activated by Ca^{2+} and DAG, a lipid located in the cell membrane produced by phospholipace C (Bhalla and Iyengar, 1999). Dephosphorylation of Y527 by RPTPα allows Src to associate with substrates, one of which is FAK. At this point modules 7 and 4 converge to allow for full activation of Src kinase (Figure 3.50). FAK is bound to the integrin complexes (or free in the cytosol) and has been activated by autophosphorylation on Y397. Binding of Src on

FAK pY397 induces further conformational changes to the molecular structure of Src and reveals its active kinase site (Schlaepfer et al., 2004). Src gets fully activated by autophosphorylation of Y416 (Schlaepfer et al., 2004) and proceeds to catalyse subsequent phosphorylation of its substrates.

3.8.1 Considerations for mathematical description

The PKC pathway (Figure 3.51) originates from the work of Bhalla and Lyengar (1999). There are four ways of activating PKC (assuming PKC α, β, γ, which are included in the model, conventional PKC isoforms – not atypical or novel): 1) by binding of Ca^{2+} (output from module 1) to PKC, forming an intermediate complex (PKC-Ca) which translocates to the membrane 2) by association of PKC-Ca with DAG, to form a second intermediate (PKC-Ca-DAG) which is a much more active kinase 3) by calcium-independent association of PKC with DAG and subsequent activation of PKC and 4) by a slow basal reversible conversion of inactive to active PKC (Bhalla and Iynegar, 1999). Active PKC is a sum of all active intermediates and is degraded at a constant rate.

Binding of PKC to RPTPα and subsequent phosphorylation is included in the model as a one-step catalytic event (i.e. *Michaelis Menten* equation). Nothing is known of serine phosphatase that dephosphorylates RPTPα. This dephosphorylation event had to be included to avoid irreversible serine phosphorylation and permanent saturation of RPTPα in the active state in response to PKC activation. A hypothetical phosphatase (PPX) of fixed concentration was introduced in the model to dephosphorylate RPTPα promoting its binding to Grb2 (Figure 3.51).

Dephosphorylation of Src Y416 is also needed in the model for similar reasons. This phosphatase could be SHP2, RPTPα or PTP-PEST (Roskoski, 2005) although it is possible they are all involved. Experimental observations (Jalali et al., 1998) have reported a decrease of tyrosine phosphorylation of Src kinase after the initial increase in response to shear stress, consistent with action of phosphatase. A hypothetical phosphatase PTPX was introduced in the model (which may be RPTPα or SHP2) that dephosphorylates Src Y416. It is important to note here that these assumptions are essentially predictions from the model and are generated by the inability of the model to match the reported dynamics of kinase molecules. Almost all experimental observations of Src and FAK

phosphorylation measurements indicate a transient increase which cannot be reproduced if phosphorylation and activation of kinases is not reversible. In the model, association of Src kinase with integrin complexes is treated as a reversible reaction as well. However the complex can dissociate further by spontaneous dissociation of talin or paxillin. Upon full activation of Src by auto-phosphorylation of Y416, Src is released from the integrin complexes (Figure 3.52). It is assumed that phosphorylation of Src Y416 prevents Csk phosphorylation of Y527 and inactivation of Src can result only by dephosphorylation of Y416. In the model Csk is given a fixed concentration as not much is known regarding the regulation of Csk by other molecular interactions.

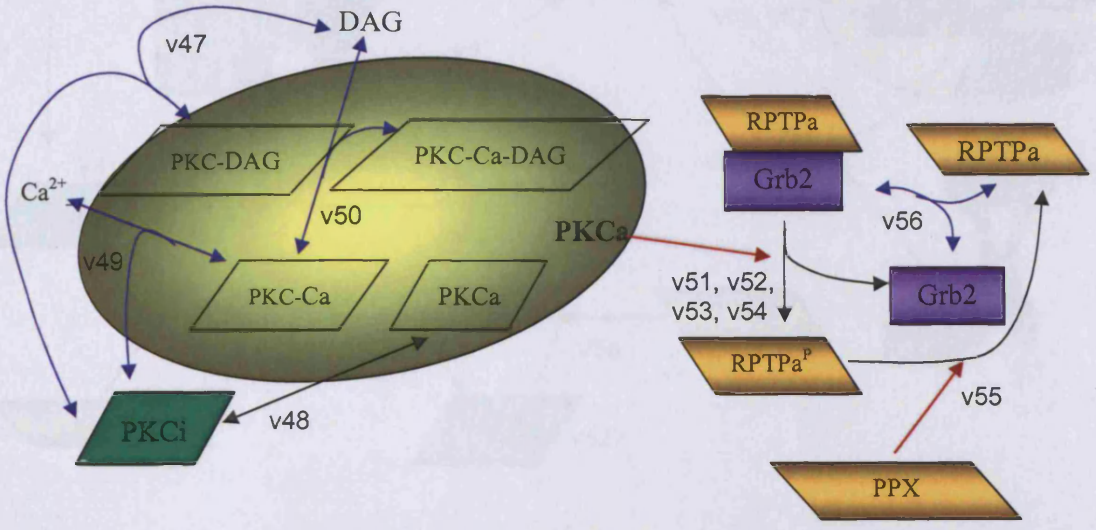

Figure 3.51. Activation of PKC and subsequent interactions with RPTPα. PPX = hypothetical serine/threonine phosphatase. PKCi = inactive PKC, PKCa = active PKC, RPTPα^{P} = RPTPα pS180/204.

The activation of PKC and regulation of RPTPα are given by the following reactions:

v47, [PKCi] + [DAG] ↔ [PKC-DAG]

v48, [PKCi] ↔ [PKCa]

v49, [Ca^{2+}] + [PKCi] ↔ [PKC-Ca]

v50, [PKC-Ca] + [DAG] ↔ [PKCCa-DAG]

v51 [PKC-DAG] + [RPTPα-Grb2] → [PKC-DAG] + [RPTPα^{P}] +[Grb2]

v52, [PKCa] + [RPTPα-Grb2] → [PKCa] + [RPTPα^{P}] + [GRB2]

v53, [PKC-Ca] + [RPTPα-Grb2] → [PKC-Ca] + [RPTPα^{P}] + [Grb2]

v54 [PKC-Ca-DAG] + [RPTPα-Grb2] → [PKC-Ca-DAG] + [RPTPα^{P}] +[Grb2]

v55, $[PPX] + [RPTP\alpha^P] \rightarrow [PPX] + [RPTP\alpha]$

v56, $[RPTP\alpha] + [Grb2] \leftrightarrow [RPTP\alpha\text{-}Grb2]$

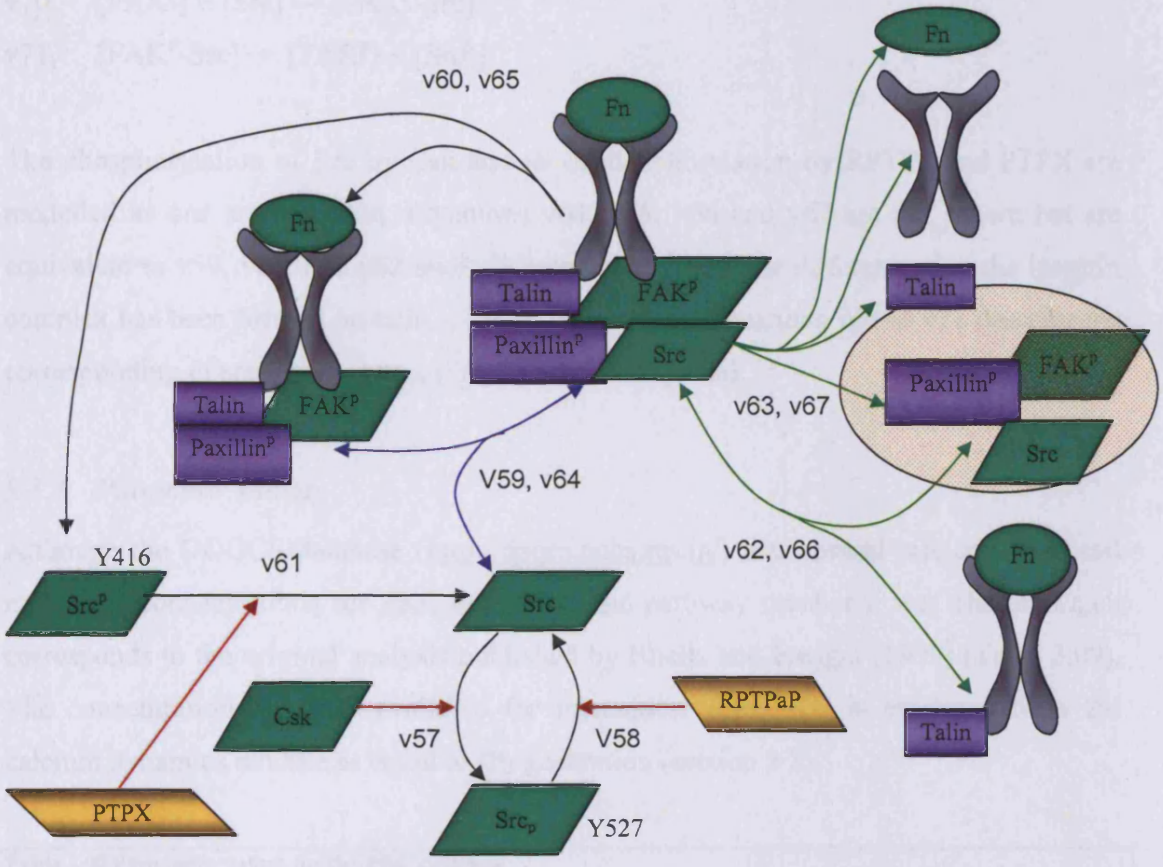

Figure 3.52. Activation of Src kinase and interaction with FAK and integrin complex. Src^P = active Src pY416, Src_p = inactive Src pY527.

Equations for regulation of Src and its interaction with FAK^P both at the membrane and cytosol that activate Src (Src^P) are given by:

v57, $[Csk] + [Src] \rightarrow [Src_p] + [Csk]$

v58, $[RPTP\alpha^P] + [Src_p] \rightarrow [Src] + [RPTP\alpha^P]$

v59, $[Tn_{Int}\text{-}\alpha_v\beta_3\text{-Fn-paxillin}^P\text{-FAK}^P] + [Src] \leftrightarrow [Tn_{Int}\text{-}\alpha_v\beta_3\text{-Fn-paxillin}^P\text{-FAK}^P\text{-Src}]$

v60, $[Tn_{Int}\text{-}\alpha_v\beta_3\text{-Fn-paxillin}^P\text{-FAK}^P\text{-Src}] \rightarrow [Tn_{Int}\text{-}\alpha_v\beta_3\text{-Fn-paxillin}^P\text{-FAK}^P] + [Src^P]$

v61, $[Src^P] + [PTPX] \rightarrow [Src] + [PTPX]$

v62, $[Tn_{Int}\text{-}\alpha_v\beta_3\text{-Fn-paxillin}^P\text{-FAK}^P\text{-Src}] \leftrightarrow [Tn_{Int}\text{-}\alpha_v\beta_3\text{-Fn}] + [\text{paxillin}^P\text{-FAK}^P\text{-Src}]$

v63, $[Tn_{Int}\text{-}\alpha_v\beta_3\text{-Fn-paxillin}^P\text{-FAK}^P\text{-Src}] \rightarrow [Tn_{Int}]+[\alpha_v\beta_3]+[Fn] + [\text{paxillin}^P\text{-FAK}^P\text{-Src}]$

v68, $[paxillin^{P}\text{-}FAK^{P}] + [Src] \leftrightarrow [paxillin^{P}\text{-}FAK^{P}\text{-}Src]$

v69, $[paxillin^{P}\text{-}FAK^{P}\text{-}Src] \rightarrow [paxillin^{P}\text{-}FAK^{P}] + [Src^{P}]$

v70, $[FAK^{P}] + [Src] \leftrightarrow [FAK^{P}\text{-}Src]$

v71, $[FAK^{P}\text{-}Src] \rightarrow [FAK^{P}] + [Src^{P}]$

The phosphorylation of Src by Csk and its dephosphorylation by RPTPα and PTPX are modelled as one step-reaction. Equations v64, v65, v66 and v67 are not shown but are equivalent to v59, v60, and v62 and v63 respectively with the difference that the integrin complex has been formed on $talin_{Clv}$ rather than $talin_{Int}$. Equations v68 to v71 describe the corresponding events in the cytosol (not shown in diagram).

3.8.3 Parameter values

Although the DOQCS database (http://doqcs.ncbs.res.in/) lists several rate constants and molecular concentrations for PKC activation, the pathway number 2 was chosen which corresponds to the original analysis published by Bhalla and Iyengar (1999) (Table 3.09). The concentration of DAG available for interaction with PKC is produced from the calcium dynamics module as equal to IP_3 generation (section 3.2).

Table 3.09 Parameter values for the PKC pathway

Constant	Description	Value	Units	Source
PKCa_k_f	PKCa basal activation rate	1	$\mu M^{-1}s^{-1}$	DOQCS, Bhalla & Iyengar 1999
PKCa_k_r	PKCa basal inactivation rate	50	s^{-1}	DOQCS, Bhalla & Iyengar 1999
PKC-Ca_k_f	PKC – Ca^{2+} association rate	0.6	$\mu M^{-1}s^{-1}$	DOQCS, Bhalla & Iyengar 1999
PKC-Ca_k_r	PKC – Ca^{2+} dissociation rate	0.5	s^{-1}	DOQCS, Bhalla & Iyengar 1999
PKC-Caact_k_f	Activation of PKC by PKC- Ca^{2+} complex	1.27	$\mu M^{-1}s^{-1}$	DOQCS, Bhalla & Iyengar 1999
PKC-Caact_k_r	Inactivation of PKC by PKC- Ca^{2+} complex	3.5	s^{-1}	DOQCS, Bhalla & Iyengar 1999
PKC-Ca-DAG_k_f	PKC - Ca^{2+} - DAG association rate	0.008	$\mu M^{-1}s^{-1}$	DOQCS, Bhalla & Iyengar 1999
PKC-Ca-DAG_k_r	Dissociation rate to PKC - Ca^{2+} and DAG	8.6348	s^{-1}	DOQCS, Bhalla & Iyengar 1999
PKC-Ca-DAGact_k_f	Activation of PKC by PKC- Ca^{2+}- DAG	1	$\mu M^{-1}s^{-1}$	DOQCS, Bhalla & Iyengar 1999
PKC-Ca-DAGact_k_r	Inactivation of PKC by PKC- Ca^{2+} DAG	0.1	s^{-1}	DOQCS, Bhalla & Iyengar 1999
PKC-DAGk_f	Association of PKC with DAG	0.006	$\mu M^{-1}s^{-1}$	DOQCS, Bhalla & Iyengar 1999
PKC-DAGk_f	Dissociation of POKC with DAG	0.1	s^{-1}	DOQCS, Bhalla & Iyengar 1999
PKC_kcat	Kcat for PKC phosphorylation	4	s^{-1}	DOQCS, Bhalla & Iyengar 1999
PKC_km	Km for PKC phosphorylation	3.33	μM	DOQCS, Bhalla & Iyengar 1999
PKC	Total PKC	0.1	μM	DOQCS, Bhalla & Iyengar 1999

Table 3.09. Parameter values for the PKC pathway. The parameter values for the PKC pathway were extracted from an online source, the Database of Quantitative Cellular Signalling (http://doqcs.ncbs.res.in/).

Table 3.10 Parameter values for RPTPα-Src pathway				
$Grb2k_f$	Association rate of Grb2 to RPTPα	10	$\mu M^{-1}s^{-1}$	Schoeberl et al., 2002
$Grb2k_r$	Dissociation rate of Grb2 from RPTPα	0.55	s^{-1}	Schoeberl et al., 2002
Csk_{kcat}	Kcat of Csk	1.2	s^{-1}	Wang et al., 2001
Csk_{km}	Km for Csk catalysis	3.5	μM	Wang et al., 2001
$RPTP\alpha^{P}_{kcat}$	RPTPαdephosphorylation rate	4.9	s^{-1}	Lim et al., 1998; Lim et al., 1997
$RPTP\alpha^{P}_{km}$	Dephosphorylation Km from $RPTP\alpha^{P}$	33	μM	Lim et al., 1998; Lim et al., 1997
Src_{kf}	Association of Src with substrate	0.037	$\mu M^{-1}s^{-1}$	Bradshaw et al., 1999
Src_{kr}	Dissociation of Src with substrate	0.0074	s^{-1}	Bradshaw et al.
Src_{kcat}	Phosphorylation rate of Src	2.53	s^{-1}	Bradshaw et al.
Src_{Km}	Km for Src phosphorylation	69	μM	Bradshaw et al.
$PPX1_{km}$	Km for PTPX1 serine dephosphorylation	65	μM	Estimated
$PPX1_{kcat}$	Kcat for PTPX1 serine dephosphorylation	1	s^{-1}	Estimated
$PTPX_{km}$	Km for Src Y416 dephosphorylation	33	μM	As RPTPα, Lim et al 1997, 1998
$PTPX_{kcat}$	Kcat for Src Y416 dephosphorylation	4.9	s^{-1}	As RPTPα, Lim et al 1997, 1998
Grb2	Total Grb2	0.2	μM	Schoeberl et al., 2002
RPTPα	Total RPTPα	0.1	μM	Estimated
Csk	Total Csk	0.1	μM	Estimated
Src	Total Src	0.17	μM	Estimated
PPX	Total PPX	0.1	μM	Estimated
PTPX	Total PTPX	0.1	μM	Estimated

Table 3.10. Parameter values for the RPTPα-Src pathway.

The kinetic rates of Grb2 were taken from the model of Schoeberl et al (2002). Grb2 appears to have a high affinity (K_d=~ 0.05 μM) for known substrates such as EGFR, SOS and Shc and interacts with forward and reverse rates in the range of k_f=1 to 10 $\mu M^{-1}s^{-1}$ and k_r = 0.055 to 0.55 s^{-1} respectively. Although the rates of Grb2 binding to RPTPα are not available in the literature, studies have shown that Grb2 also binds very tightly to RPTPα (den Hertog et al., 1994; den Hertog and Hunter, 1996). The values of $Grb2k_f$=10 $\mu M^{-1}s^{-1}$ and $Grb2k_r$ = 0.55 s^{-1} were used for the forward and reverse rates of Grb2 binding in the model.

The kinetic rates of Csk phosphorylation were extracted from the work of Wang et al (2001). Analysis of the reaction kinetics of Csk for Src revealed a phosphorylation rate of Csk for Src at Csk_{kcat} = 1.2 s^{-1} and a K_m value at Csk_{km} = 3.5 μM with little variation between wild-type and mutants (Wang et al., 2001). These values were used in the model.

Based on kinetic analysis, (Lim et al., 1998; Lim et al., 1997) the kinetic rates of RPTPα for Src kinase were reported as Km = 33 μM and k_{cat} = 4.9 s^{-1}. The kinetic rates of phosphorylation and affinity of Src kinase for substrates have been previously determined (Bradshaw et al., 1999) as Src_{kcat} = 2.53 s^{-1}, Src_{km}= 69 μM and K_d = 0.2 μM. By definition of Km = (k_{cat}+ k_r)/k_f and K_d = k_r/k_f, the forward and reverse rates of association were calculated as Src_{kf} = 0.037 $\mu M^{-1}s^{-1}$ and Src_{kr} = 0.0074 s^{-1}. These values were applied in the model.

Although the identity of the phosphatase that dephosphorylates Y416 on Src (PTPX) is not clear yet (Zheng et al., 1992; den Hertog et al., 1993) observed RPTPα-dependent dephosphorylation of Src Tyr527 and Tyr416, suggesting that RPTPα is the most likely candidate for dephosphorylation of Src Y416. Thus the kinetic rates used for RPTPα (Table 3.10) were thus also used for PTPX.

The kinetic rates of PPX were set to values K_m = 65 μM and K_{cat} = 1 s^{-1} that allowed a ~0.2-fold activation of RPTPα phosphorylation by PKC (see section 3.8.5).

Total concentrations for the phosphatases of this module were not available in the literature. Concentrations for Csk, RPTPα and the unknown phosphatases were given at 0.1 μM and for Src kinase equal to the concentration of FAK at 0.17 μM.

3.8.4 *Steady state analysis*

Simulations were first run in the absence of shear stress but in the presence of fibronectin to obtain the basal levels of PKC, RPTPα and Src activity (Figure 3.53).

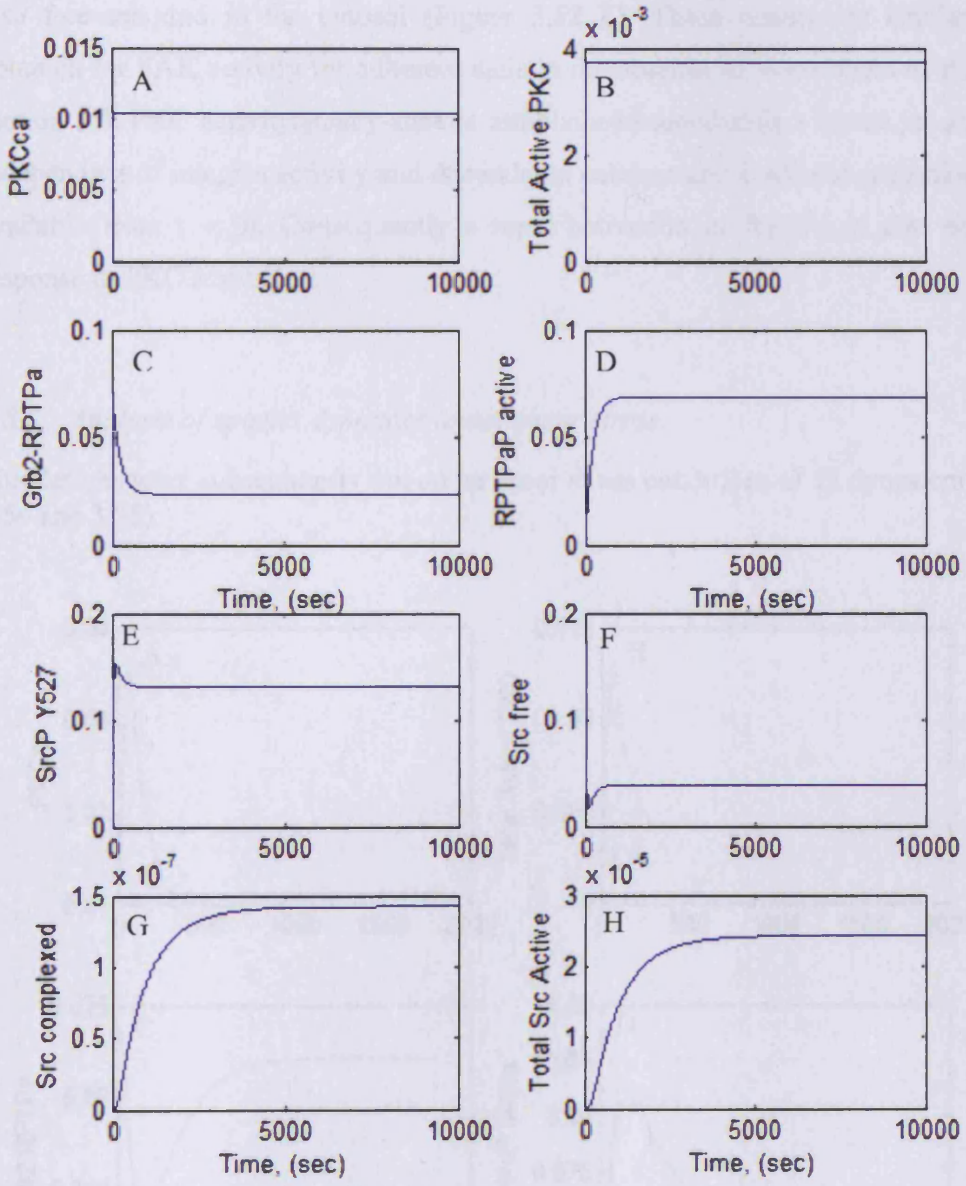

Figure 3.53. Steady state analysis of species dynamics. PKC activity (A and B) is established instantly due to the presence of basal cytosolic [Ca^{2+}]. RPTPα activity (C and D) is established within seconds while Src plateau levels are also reached within 1 hours (3600 seconds). PKCca (PKC-Ca) = PKC complexed with calcium. Src complexed = Src bound to FAK not yet activated. Src free = Src unbound. Total Src active = Src pY416. RPTPα active = RPTPα pS180/204. PKC active = the PKC intermediates that have translocated to the membrane. All the concentrations shown are in μM units.

Steady state analysis indicates an existing basal level of active Src in adherent cells in the absence of shear stress (Figure 3.52 G and H). The amount of active Src however is very low, in the order of 0.1%. The simulations predict that most of Src is inactive and in closed conformation resulting from phosphorylation of Y527 (Figure 3.52 E) by Csk and also free-unbound in the cytosol (Figure 3.52 F). These results are similar to those obtained for FAK activity for adherent cells in the absence of shear stress as discussed in section 3.5. PKC activity/steady-state is established immediately because its activation is independent of integrin activity and depends on calcium and DAG concentration which is available from t = 0). Consequently a rapid activation of RPTPα is also observed in response to PKC activation.

3.8.5 Analysis of species dynamics under shear stress

Simulations were subsequently run under shear stress conditions of 12 dynes/cm^2 (Figure 3.54 and 3.55).

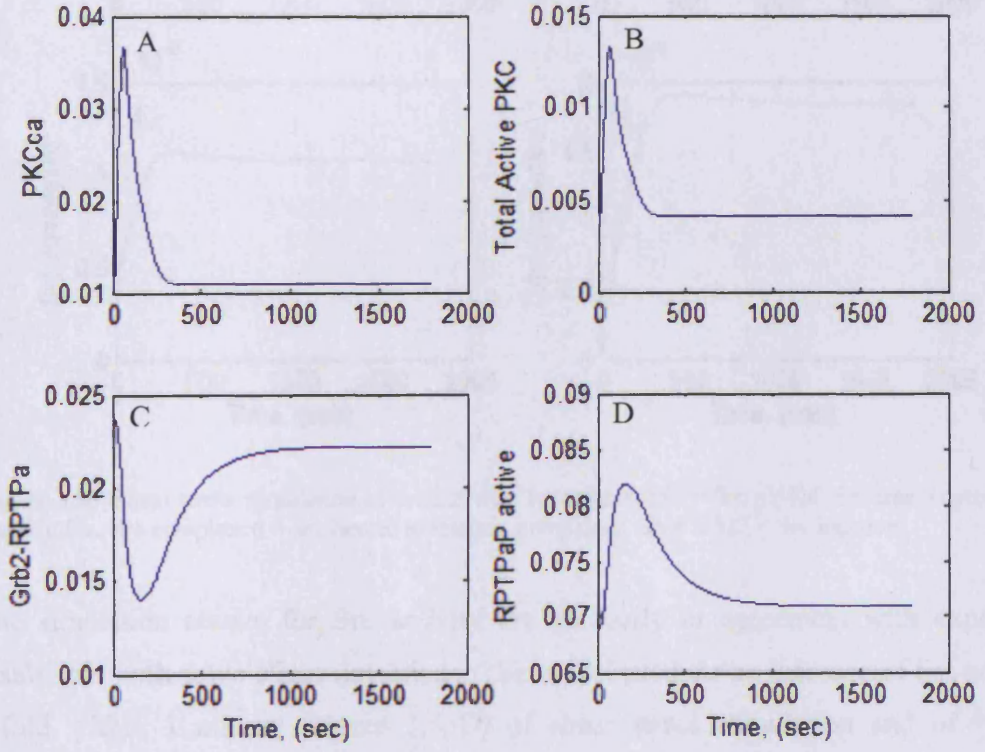

Figure 3.54. Shear stress stimulation of PKC and RPTPα activity. RPTPα active = RPTPα pS180/204. PKC active = the PKC intermediates that have translocated to the membrane. All the concentrations shown are in μM units.

According to the model, PKC activation is very fast (Figure 3.54A and B) comparable to the dynamic regulation of cytosolic [Ca^{2+}]. Increased PKC activity in turn leads to phosphorylation of RPTPα and a small increase of its activity by 0.2-fold (3.53D). RPTPα activity returns to basal levels slowly (approximately after 10 minutes) due to the low catalytic activity of PPX that reverses the serine phosphorylation by PKC on RPTPα. There has not been any phosphatase identified to date that performs such a function and it may be that RPTPα activation is not immediately reversible. The concentration of phosphorylated RPTPα may be also reduced by degradation. The low catalytic activity given to PPX prevents it from influencing the model significantly (which may be invalid).

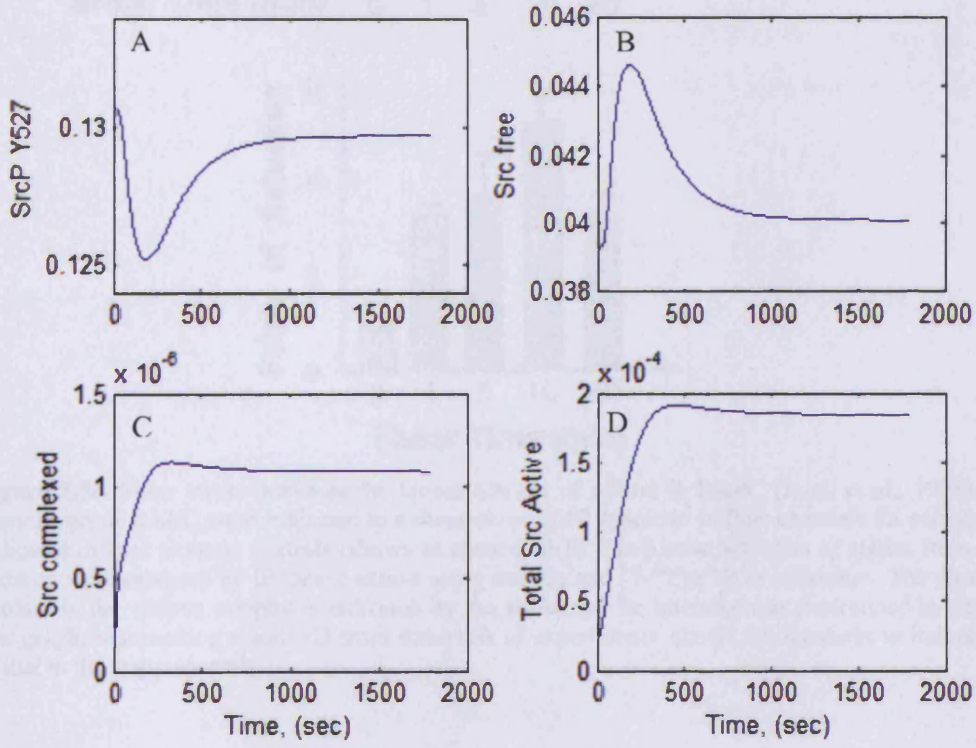

Figure 3.55. Shear stress stimulation of Src activity. Total Src active = Src pY416, Src free = cytosolic inactive Src. Src complexed = Src bound to integrin complexes. SrcP Y527 = Src inactive.

The simulation results for Src activity are generally in agreement with experimental results but with some slight deviations. The model predicts an increase of Src activity of 3-fold within 1 minute (Figure 3.55D) of shear stress stimulation and of 5.5 fold activation within 5 min (300 sec) of stimulation (Figure 3.55D). Both the fold activation of Src and the slope of increase are in good agreement with the experimental results of

Jalali et al (1998) (Figure 3.56) measured at 12 dynes/cm^2 shear stress. However, Jalali et al (1998) have also observed that the increase in Src activity is sustained up to 10 minutes at which point it returns to a new non-basal steady state by 20 minutes of stimulation. In contrast, in the model the non-basal state is reached at 5 minutes.

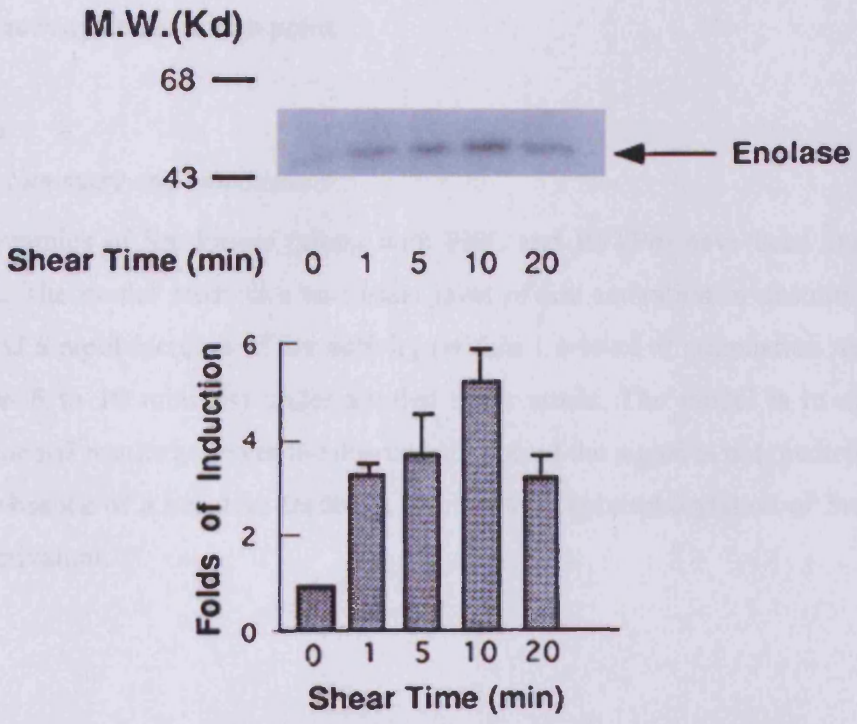

Figure 3.56. Shear stress increases the kinase activity of p60src in BAEC (Jalali et al., 1998). Confluent monolayers of BAEC were subjected to a shear stress of 12 dyne/cm^2 in flow channels for periods of time as indicated or kept as static controls (shown as shear time 0). The kinase activities of p60src from the various samples were assessed by IP kinase assays using enolase and [γ-^{32}P]ATP as substrates. The phosphorylated enolase in the various samples is indicated by the arrow and the intensity was determined by densitometry. Bar graph, representing mean±SD from three sets of experiments, shows the increases in induction relative to that in the static controls.

This is due to lack of negative feedback on Src activation that would inhibit/reduce its activation. Its dephosphorylation is fixed (phosphatase PTPX not regulated) and thus reaches a plateau near the peak of activation. If PTPX were activated after 10 minutes of shear stimulation, this would reproduce more accurately the complete dynamic response of Src activity as observed experimentally by Jalali et al (1998). It is also interesting to note that the amount of active Src exceeds that of pre-active bound Src to integrin complexes. This is because free active Src cannot be further inhibited by Csk

phosphorylation which results in accumulation of Src in active cytosolic free form. However, its levels are also limited by the available amount of FAK $Y397^P$ and thus Src activity is controlled and kept at relatively low levels. Src kinase is known to have more than 80 interacting partners and is also known to be activated by multiple pathways (Frame, 2004). This module demonstrates how two pathways converge and regulate Src kinase activity at a common point.

3.8.6 Summary and conclusions

The dynamics of Src kinase (along with PKC and RPTPα) have been examined in this section. The model predicts a non-basal level of Src activation in unstimulated adhering cells and a rapid increase of Src activity (within 1 minute of stimulation reaching plateau between 5 to 10 minutes) under applied shear stress. The model is in agreement with experimental results however the downregulation of the signal is not predicted. This is due to the absence of a negative feedback or elevated dephosphorylation of Src following its peak activation.

3.9 Src negative feedback on integrin/Fak/Src signalling (Module 8)

3.9.1 Module description

Apart from post-translationally modifying FAK and paxillin, Src may also downregulate the signal (negative feedback) initiated by integrins. This postulated negative feedback loop results from action of Src kinase on talin and integrins and involves phosphatidyl-inositol-4-phosphate 5-kinase isoform 1γ661 (PIPKIγ661). PIPK1γ661 is a splice variant of PIPKIγ with a unique carboxy-terminal tail that associates with talin and localizes at focal adhesions (Di Paolo et al., 2002; Ling et al., 2002; Ling et al., 2003). PIPKIγ661 is phosphorylated on Y644 directly by Src (Di Paolo et al., 2002; Ling et al., 2002; Ling et al., 2003), an event that is necessary for efficient association of PIPKIγ661 with talin and for localization to focal adhesions (Ling et al., 2003). The Src phosphorylation on PIPKIγ661 is regulated by FAK, which enhances the association between PIPKIγ661 and Src. The phosphorylation of Y644 on PIPKIγ661 results in a ~15 fold increase in affinity of PIPKIg661 for talin. It has been reported that this could potentially reduce (by competitive action) β-integrin binding to talin because the binding of the integrin subdomain and PIPKIγ661 kinase to talin F3 FERM are mutually exclusive (Barsukov et al., 2003). This defines a novel phosphotyrosine binding site on the talin F3 domain and a molecular switch for talin binding between PIPKIg661 and β-integrin that provides one way of regulating integrin signalling by negative feedback. PIPKIg661 is also phosphorylated on Y649 (possibly also by Src) however its influence on PIPKIg661 is still uncertain.

It has also been reported that Src phosphorylation affects the integrin-fibronectin linkage. Src was shown to phosphorylate integrin β3 receptors (directly) on Y747 and Y759 resulting in reduction of αvβ3 binding to fibronectin (Datta et al., 2002). Src also phosphorylates β1 integrins which may exclude them from focal adhesions and prevent strong-integrin-cytoskeleton and integrin-ligand interactions (Datta et al., 2002). Thus phosphorylation of either integrin by Src constitutes a mechanism by which the integrin-induced signal is attenuated in time (i.e. negative feedback).

3.9.2 *Considerations for mathematical description*

Since the model focuses on results related to $\beta 3$ integrins the direct phosphorylation of $\alpha v\beta 3$ integrins by Src kinase was included. The reduction of integrin binding to fibronectin can result from either reduced affinity of integrins for fibronectin or reduced affinity of talin to integrins thus reducing the pre-active pool of integrins that can associate with fibronectin. Since there is no evidence as to which of those two mechanisms occurs, the second mechanism was implemented in the model.

The phosphorylation of PIPKIγ661 by Src (Figure 3.57) is reversed in the model via action of PTPX2 (Figure 3.57), a phosphatase introduced this reaction since the hypothetical phosphatase responsible for this dephosphorylation is not known.

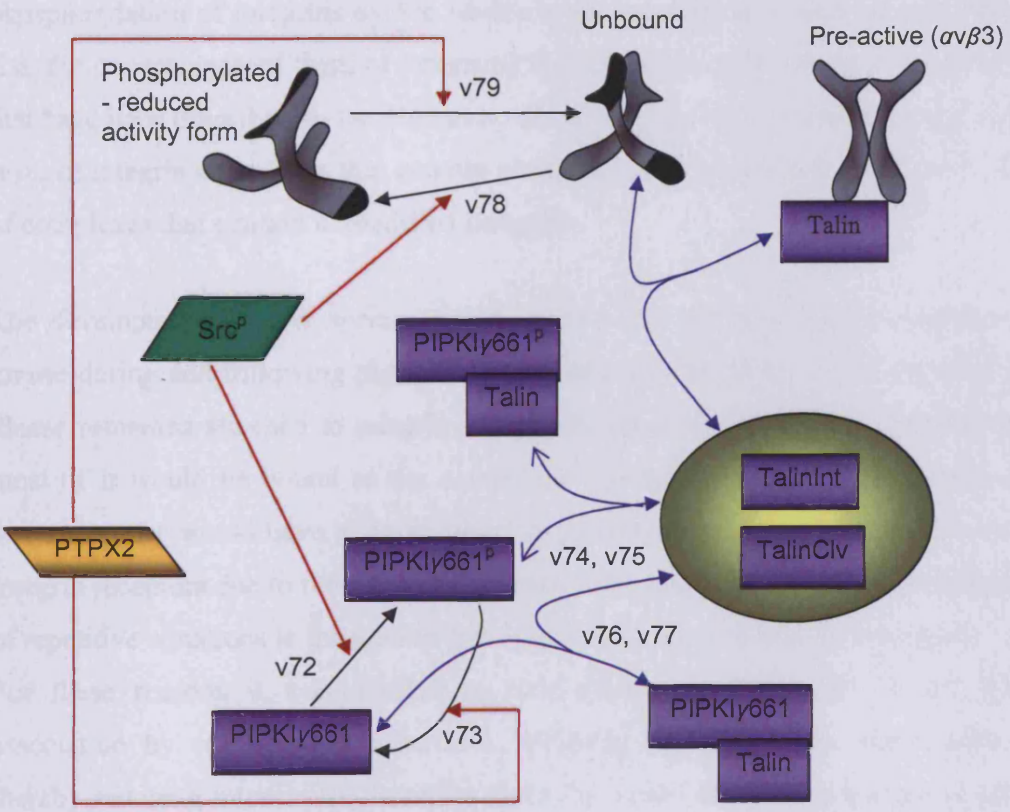

Figure 3.57. Src negative feedback loop on integrin signalling.

The reactions described above are given by the following equations:

v72, $[PIPKI\gamma661] + [Src^{p}] \rightarrow [PIPKI\gamma661^{p}] + [Src^{p}]$

v73, $[PIPKI\gamma661^{p}] + [PTPX2] \rightarrow [PIPKI\gamma661] + [PTPX2]$

v74, $[PIPKI\gamma661^{p}] + [TalinInt] \leftrightarrow [PIPKI\gamma661^{p}\text{-}TalinInt]$

v75, $[PIPKI\gamma661^{p}] + [TalinClv] \leftrightarrow [PIPKI\gamma661^{p}\text{-}TalinClv]$

v76, $[PIPKI\gamma661] + [TalinInt] \leftrightarrow [PIPKI\gamma661\text{-}TalinInt]$

v77, $[PIPKI\gamma661] + [TalinClv] \leftrightarrow [PIPKI\gamma661\text{-}TalinClv]$

v78, $[\alpha v\beta3] + [Src^{p}] \rightarrow [\alpha v\beta3_{p}] + [Src^{p}]$

v79, $[\alpha v\beta3_{p}] + [PTPX2] \rightarrow [\alpha v\beta33] + [PTPX2]$

Equation v78 specifically has fundamental effects on the model structure. The phosphorylation of integrins by Src results in the production of new a molecular species (i.e. the phosphorylated form of integrins) that can be included in all downstream events that have been described so far. However, the affinity for talin is reduced and therefore the level of integrin complexes that contain phosphorylated integrins is much lower than that of complexes that contain unmodified integrins.

The development of new species raised another concern regarding the location of Src kinase during and following phosphorylation of integrins. If the model assumed that Src kinase remained attached to integrin complexes upon the second phosphorylation event, most of it would be bound to the complexes and not free. Furthermore, each complex containing Src would have to be involved in phosphorylation of all complexes containing integrin receptors due to the negative feedback loop, therefore adding a significant amount of repetitive equations to the system that would make simulations very complex.
For these reasons it was decided to treat each phosphorylation of Src (following association by collision) as a reaction involving its spontaneous dissociation of Src thereby reducing unnecessary complexity in the model and also keeping and amount of active Src kinase concentration available for interactions that involve molecules that are not part of the focal complexes. This was the only time model simplification was applied in the model. The phosphorylation of the complexes containing integrins by Src kinase was modelled as a typical catalytic reaction using standard *Michaelis Menden* kinetics (as the also activity of PPX and PTPX have been modeled). The above assumption does not

affect the mechanism of whereby Src kinase is dephosphorylated since there are no detailed data regarding the PTP responsible for dephosphorylation that contradicts in any way the applied mechanism (i.e. if dephosphorylation of Src required it to be bound to the integrin complexes).

3.9.3 Parameter values

Table 3.11. Parameter values for Src negative feedback pathway				
PIPIg_kf	Association rate of PIPKγ to talin	4.4	$\mu M^{-1}s^{-1}$	Barsukov et al., 2003
PIPIg_kr	Dissociation rate of PIPKγ from talin	27	s^{-1}	Barsukov et al., 2003
PIPIg_kf2	Association rate of $PIPK\gamma^{(p)}$ to talin	0.29	$\mu M^{-1}s^{-1}$	Barsukov et al., 2003; Ling et al., 2003
Src_{kcat}	Phosphorylation rate of PIPIγ by Src	2.53	s^{-1}	Bradshaw et al., 1999
Src_{Km}	Km for Src phosphorylation of PIPIγ	69	μM	Bradshaw et al., 1999
Src_{Km}	Km for Src phosphorylation of integrins	1	μM	Estimated
$PTPX2_{km}$	Dephosphorylation rate of integrins	63	μM	Estimated
$PTPX2_{kcat}$	Km for dephosphorylation of integrins	4.9	s^{-1}	As RPTPα, Lim et al 1997., 1998
PTPX2	Total PTPX2	0.1	μM	Estimated
PIPIg661	Total PIPIγ661	0.1	μM	Estimated

Table 3.11. Parameter values for the Src negative feedback

The association/dessociation rates of talin and PIPKIγ661 were extracted from Barsukov et al (2003) and Ling et al (2003). Based on kinetic studies, Barsukov et al (2003) reported the association rate of PIPKIγ for talin to be $k_f = 4.4\ \mu M^{-1}s^{-1}$ and the dissociation rate $k_r = 27\ s^{-1}$. These values were extracted from kinetic studies in normal conditions where presumably Src kinase is active. Although these values were given for the PIPKIγ91 isoform it was taken here that these values also apply for the PIPKIγ661 isoform. Ling et al also reported that in the absence of Src kinase and when PIPKIγ661 is not phosphorylated the affinity of PIPKIγ661 is reduced by 15-fold. Thus by extrapolation the association rate of $PIPKI\gamma661^p$ was calculated as $k_f = 0.29\ \mu M^{-1}s^{-1}$. The reaction rates for integrin dephosphorylation by postulated PTP, PTPX2, of integrins were given similar to those for RPTPα activity (see section 3.8.3).

The catalytic acitivity of Src was extracted from (Bradshaw et al., 1999) who gives both Kcat = 2.53 s^{-1} and Km = 69 μM. As described in the previous section a simplification was applied in the model (i.e. Src dettaches from integrin complexes following its

phosphorylation and activation) to allow for easier investigation. However the existence of this simlification in the model should not have an impact on the dynamics of signalling. Thus, assuming that Src remains attached to the complexes following its phosphorylation in cells, it would be able to phosphorylate integrins without the need to bind to the complexes again. For this reason the Km value for Src activity was significanlty reduced and given a value of 1 μM in order to avoid adding additional delay to integrin phosphorylation that may not take place in cells. The original Km value however (Km = 69 μM) was used for phosphorylation of PIPKIγ661 by Src.

In order to reproduce the biphasic behaviour observed for shear stress-induced integrin activity by Tzima et al (2001), reduced (affinity) rates of talin for integrins were applied following phosphorylation of integrins by Src. This was implemented in the model by increasing the dissociation rate of talin from phosphorylated integrins by an order of 100. Concentration values for PTPX2 and PIPKIγ661 were given at 0.1 μM.

3.9.5 Analysis of species dynamics

The incorporation of the negative feedback loops in the model allowed the dynamics of phosphorylation of PIPKIγ661 to be investigated first at steady state (Figure 3.58) and subsequently for shear stress conditions (Figure 3.59).

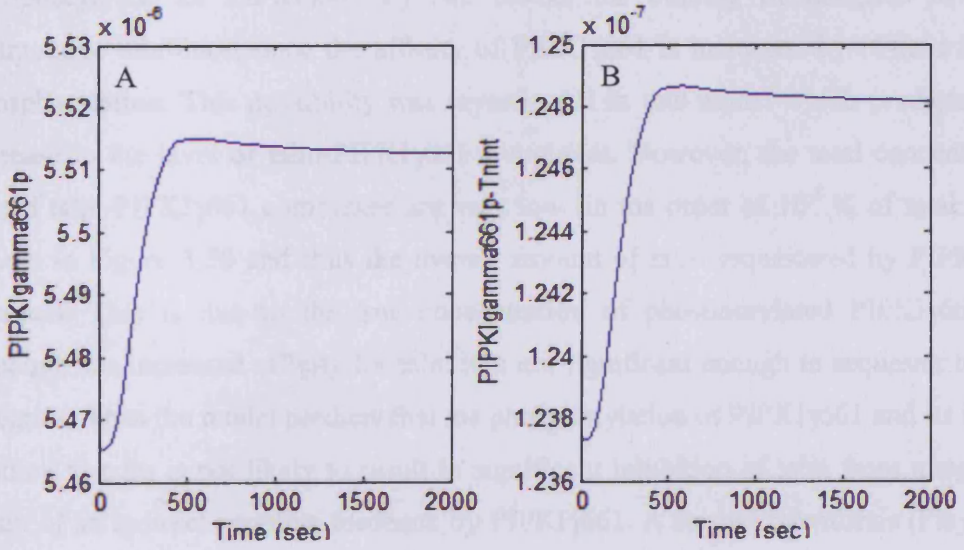

Figure 3.58. Dynamics of PIPKIγ661 phosphorylation (A) and binding to talin (B) at steady state. Basal concentrations of species in the absence of shear stress stimulus are simulated.

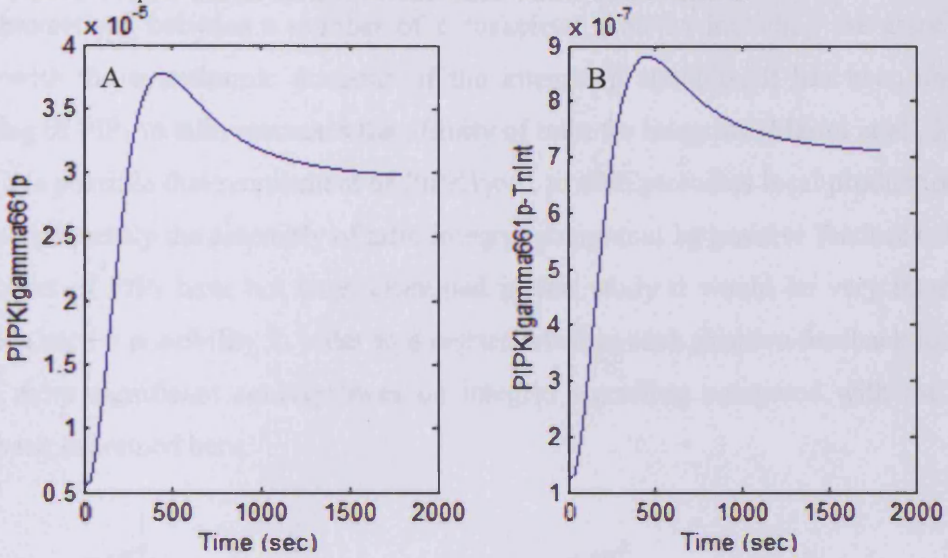

Figure 3.59. Dynamics of phosphorylation of PIPKIγ661 (A) and binding to talin (B) under shear stress. Activation of Src leads to an increase of PIPKIγ661 by 9-fold and an increase in formation of [PIPKIγ661-$Talin_{int}$] by approximately 7 fold. Dynamics of [PIPKIγ661-$Talin_{Clv}$] are not included as $Talin_{Clv}$ only involves a very small fraction of total talin (i.e. not significant).

Although it is believed that PIPKIγ661 phosphorylation is important for the efficient association of talin with PIPKIγ661 (Ling et al., 2003), there has been much debate as to the role and consequences of the interaction of talin with the PIPKIγ (Cram and Schwarzbauer, 2004; Playford and Schaller, 2004). One hypothesis proposes that phosphorylation of PIPKIγ661 by Src blocks the binding of integrins to talin by competitive inhibition since the affinity of PIPKIγ661 is increased by 15-fold following phosphorylation. This possibility was investigated in this model which predicts a 7-fold increase in the level of talin-PIPKIγ661 complexes. However, the total concentration of bound talin-PIPKIγ661 complexes are very low (in the order of 10^{-5} % of total talin), as shown in Figure 3.58 and thus the overall amount of talin sequestered by PIPKIγ661 is minimal. This is due to the low concentration of phosphorylated PIPKIγ661 which although has increased affinity for talin it is not significant enough to sequester talin from integrins. Thus the model predicts that the phosphorylation of PIPKIγ661 and its increased binding to talin is not likely to result in significant inhibition of talin from integrins as a result of an indirect negative feedback by PIPKIγ661. A second hypothesis (Playford and Schaller, 2004) proposes a positive feedback loop generated by PIPKIγ661 on integrin

signalling. PIP_2 is generated by phosphorylation of PI(4)P by PIP kinases and regulates the interactions between a number of cytoskeletal proteins including the association of talin with the cytoplasmic domains of the integrin β subunits. It has been shown that binding of PIP_2 to talin increases the affinity of talin for integrins (Martel et al., 2001) and thus it is possible that recruitment of PIPKIγ661 to talin promotes local production of PIP_2 and consequently the assembly of talin-integrin complexes by positive feedback. Although dynamics of PIP_2 have not been examined in this study it would be very interesting to include such a possibility in order to compare whether such positive feedback loop would have more significant consequences on integrin signalling compared with the negative feedback examined here.

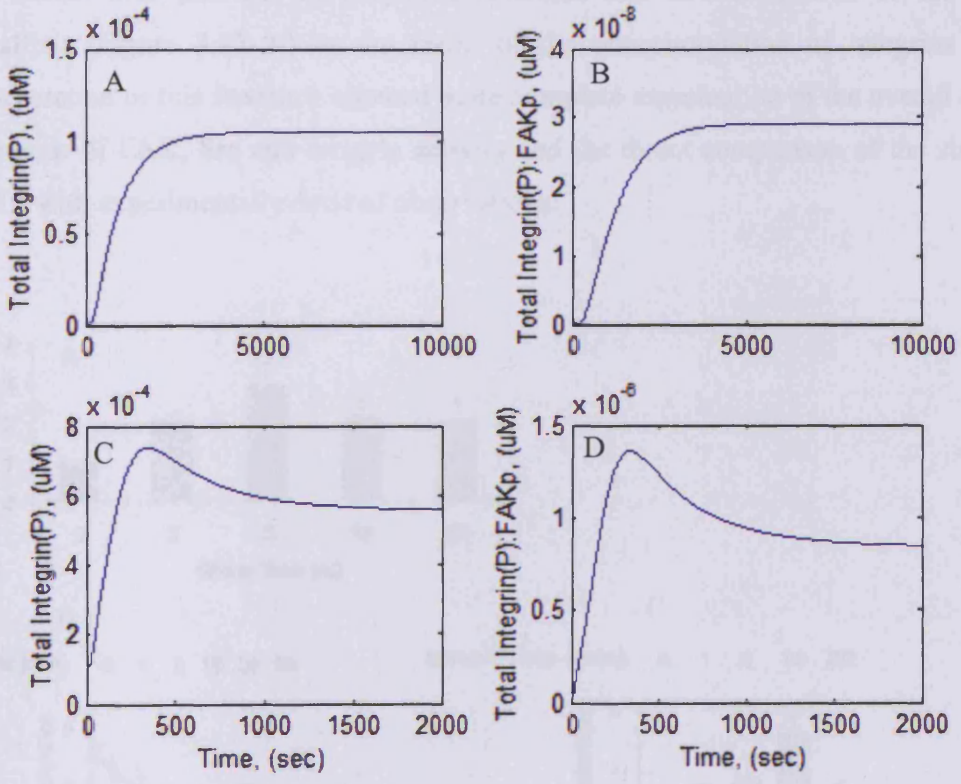

Figure 3.60. Dynamics of phosphorylation of integrins by Src. Concentration of species is shown at steady state (A and B) and under shear stress conditions (C and D).

The dynamics of phosphorylated integrins were also examined at steady state and under 12 dynes/cm^2 shear stress conditions (Figure 3.60). Phosphorylated integrins reach a steady state after approximately 20 to 30 minutes in the absence of shear stress. In the

presence of shear stress an increase of 8-fold is observed for the concentration of phosphorylated integrins (Figure 3.60 C) and a 15-fold increase is observed for the complexes containing phosphorylated integrins and FAK. This increase results from increased activation of integrins and Src in response to shear stress. Therefore, the higher the activation of integrins (as shear stress increases) results in higher negative feedback. The action of PTPX2 however prevents unlimited phosphorylation of integrins and the increased phosphorylation is followed by a decrease at approximately 10 to 12 minutes as the amount of total active integrins begins to reduce due to the negative feedback loop.

3.9.5 Re-evaluation of species dynamics under negative feedback

The model here presents the negative feedback and downregulation of the integrin signalling (Figure 3.62 A) as the result of the phosphorylation of integrins by Src. Incorporation of this feedback allowed more complete examination of the overall dynamic behaviour of FAK, Src and integrin activity and the direct comparison of the simulation results with experimentally derived observations.

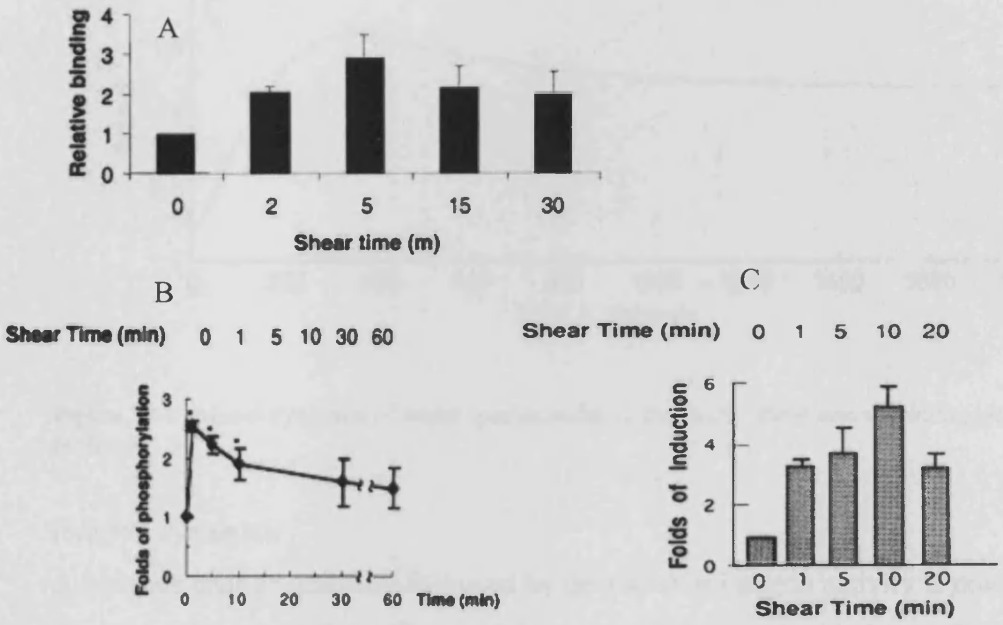

Figure 3.61. Experimentally observed dynamics of integrin (A) (Tzima et al., 2001), FAK (B) (Li et al., 1997) and Src (C) (Jalali et al., 1998) as observed experimentally. Refer to sections 3.4.5, 3.5.6 and 3.8.5 for original Figures.

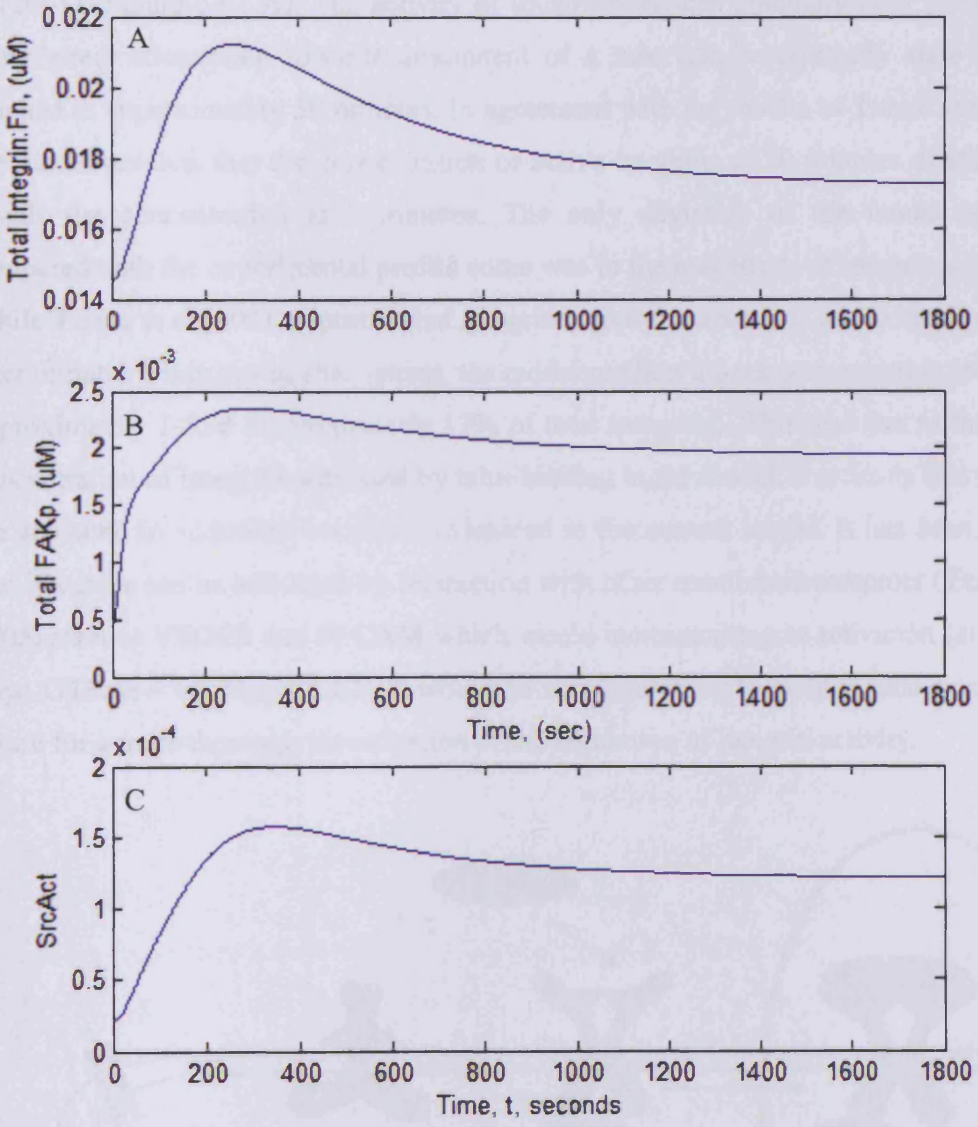

Figure 3.62. Model dynamics of major species under 12 dynes/cm^2 shear stress including negative feedback.

Integrin dynamics:

A biphasic change (increase followed by decrease) in integrin activity is now predicted by the model (Figure 3.62 A). The model graph was compared with the results of Tzima et al (2001) for the same experimental conditions (Figure 3.61 A). The dynamic behaviour of integrin activity predicted by the model was overall in very good agreement with what has

been observed experimentally. Integrin activation is observed within 2 minutes of shear stress application and peaks exactly at 5 minutes of stimulation as also shown by Tzima et al (2001) (Figure 3.61 A). The activity of integrins reduces gradually after 5 minutes of shear stress stimulation towards attainment of a new non-basal steady state that was reached at approximately 30 minutes. In agreement with the results of Tzima et al (2001) the model predicts that the concentration of active integrins at 30 minutes of stimulation equals the concentration at 2 minutes. The only deviation of the model prediction compared with the experimental profile come was in the magnitude of integrin activations. While Tzima et al (2001) reported that integrin activity increased to a maximum of 2-fold after minutes 5 minutes of shear stress, the model predicts a peak concentration increase of approximately 1-fold (approximately 17% of total integrins). This was due to the limited concentration of integrins activated by talin-binding in the model. It is likely that integrins are activated in additional ways not examined in the current model. It has been reported that integrins can be activated by interaction with other membrane receptors (Tzima et al 2005) such as VEGFR and PECAM which would increase integrin activation (and by the Rap1 GTPase – see Figure 3.62). It would be very interesting to include such events in the future for a more thorough investigation of the regulation of integrin activity.

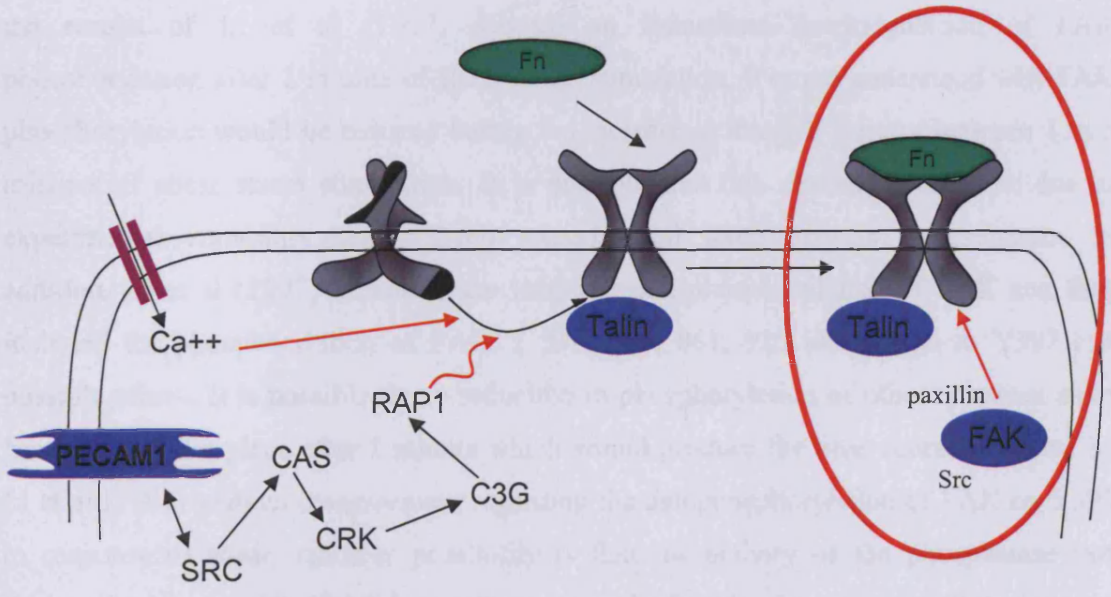

Figure 3.62. Model for regulation of Src activity and integrin activation via PECAM-1 and Rap1 GTPase. PECAM-1 binds Src, which phosphorylates Cas allowing Crk SH2 domain to bind. In turn Crk binds to C3G which is an exchange factor for Rap1 thus activating it. This pathway would upregulate integrin integrin and therefore FAK and Src.

FAK dynamics:

The dynamic profile of FAK Y397 phosphorylation (Figure 3.62 B) as predicted by the model was compared to the results of Li et al (1997) (Figure 3.61 B). The model showed a significant increase of FAK phosphorylation by 3-fold within 1 minute of shear stress stimulation. This was in very good agreement with the result of Li et al (1997). A similar rapid activation of FAK (within 1 minute of stimulation) has also been reported by Lehoux et al., 2005) thus strengthening the confidence in the prediction by the model. The simulations however deviated in the timing and levels of peak activity compared with those of Li et al (1997). The simulations showed a rapid increase in phosphorylation of FAK Y397 which was produced by enchanced affinity of FAK for paxillin following deformation of integrins. As has already been discussed (sections 3.6, 3.7) it is unlikely that the increase of FAK phosphorylation by 3-fold preceding the activation of integrins could be achieved by other means. In the model, the increase in FAK phosphorylation continued beyond the first minute of shear stress stimulation at a reduced rate and peaked at 5 minutes of shear stress stimulation. This was essentially the result of increased integrin activation which drives the phosphorylation of FAK by increasing the amount of paxillin and FAK bound to the integrin complexes. Phosphorylation of FAK then decreased due to the negative feedback downregulation of integrin signalling. In contrast, the results of Li et al (1997) showed an immediate downregulation of FAK phosphorylation after 1 minute of shear stress stimulation. It is not understood why FAK phosphorylation would be reduced during the increase in integrin activity between 1 to 5 minutes of shear stress stimulation. It is possible that this deviation might be due to experimental variability and different experimental setup between investigators. In addition, Li et al (1997) measured the total tyrosine phosphorylation of FAK and thus included the phosphorylation of FAK Y 576, 577, 861, 925 in addition to Y397 and possible others. It is possible that a reduction in phosphorylation of other tyrosines apart from Y397 takes place after 1 minute which would produce the time course provided by Li et al (1997) without disagreement regarding the autophosphorylation of FAK on Y397 in response to shear. Another possibility is that the activity of the phosphatase that dephosphorylates FAK Y397 is rapidly increased after the first minute of shear stress stimulation thus downregulating FAK phosphorylation after the first minute. Phosphatase activity following shear stress has not been reported to date and it would be interesting to

identify whether changes do occur. In any case the experimental profiles used for comparison against the model here are taken from separate experiments produced by different laboratories and there is not enough independent experimental verification or a set of protein activity profiles available for all the molecular species produced by the same laboratory that could be compared with the simulation results with greater confidence.

Src dynamics:

Finally simulations of Src activity (Figure 3.62 C) were compared against the experimental observations of Jalali et al (1998) (Figure 3.61 C). Jalali et al (1998) reported that Src is rapidly and transiently activated by shear stress. A 3-fold increase was observed within 1 to 2 minutes of stimulation which reached a 5-fold increase after 5 minutes and peaked at approximately 6-fold after 10 minutes (Figure 3.61 C). Beyond 10 minutes Src activity decreased to a 3-fold increase over basal levels after 20 minutes. The simulation results were in good agreement for most of the above experimental observations. The model also predicted a 3-fold increase in Src acivity within 1 to 2 minutes of shear stress stimulation reaching a peak of approximately 6-fold increase after 5 minutes of applied shear stress, which was 1-fold higher compared with the experimental profile. According to the model however, Src activity was limited by the availability of FAK Y397 and thus reduced after 5. The slight increase between 5 to 10 minutes observed by Jalali et al (1998) is not considered as contradictory to the model as Src kinase is involved in many molecular interactions and is regulated by other pathways. It is possible that PECAM-1 signalling also contributes to Src activation as PECAM-1 (Figure 3.62) is activated very rapidly in response to shear stress and Src kinase is known to directly interact with PECAM-1 (Cao et al., 1998). This would make a very interesting addition to the model to determine if a further increase in Src activity beyond 5 minutes of shear stress stimulation takes place.

Overall, considering the potential for experimental variability between different investigators and lack of sufficient independent verification the model predictions are in good agreement with experimental results. Furthermore, throughout analysis of the dynamics of the various molecules examined in all modules, the model has made

predictions pointing to further experimental investigations; for example: cleavage of talin is not sufficient to influence integrin signalling significantly; activation of molecules by stretch-induced deformation is likely to play a significant role in pathway dynamics; integrin activation is likely influenced by additional events that possibly involve the action of other membrane receptors or Rap1 GTPase (that enhance activation and binding of integrins to talin); the action of phosphatases is critical in the dynamics of the pathways which makes very interesting the investigation of known and unknown phosphatases under shear stress; PIPKIγ661 is more likely to play a significant role in positive feedback as its negative effect is minimal for the overall integrin signalling; integrin inhibition by Src phosphorylation (as a negative feedback loop) seems to be a potent way of downregulating integrin signalling and should be further investigated.

4 CHAPTER 4 – CONCLUSIONS AND DISCUSSION

4.1.1 Modelling the shear stress response

Cell signalling pathways pose a formidable challenge in our efforts to understand how cells function. Once they were drawn as simple chains, or cascades – a result of both linear powers of reasoning and the pattern of experimental study. Now these have been replaced by highly interconnected networks of reactions, regarded as an inevitable outcome of over three billion years of evolution, with organisms striving to re-use components of existing pathways in order to exploit their environment more successfully. Although still limited, recent experimental observations on the responses of endothelial cells to shear stress stimulus afforded an opportunity to investigate how these signalling pathways could be integrated into a coherent model, providing an insight into the mechanisms responsible for signal processing in the shear stress response. A greater appreciation of the complexity of the shear stress response could be gained by contemplating its unique characteristics (e.g. adaptation to magnitude of shear stress, see sections 3.3, 3.4) and by trying to reconcile the expanse of experimental data describing it. Mathematical modelling was therefore applied in order to investigate, understand and predict the immediate responses of endothelial cells to shear stress that precede phenotypic alterations (e.g. cell morphology alterations, migration). A continuous mechanistic model of 92 ordinary differential equations was developed and used to resolve the dynamic behaviour of molecular species under various conditions (e.g. cells in suspension, adherent cells, cells under shear stress), some that have been experimentally applied, and therefore allowing for validation, and some that remain to be verified (e.g. deformation of receptors).

To simulate the dynamics of cellular pathways in a realistic manner, great effort was put both in identifying the molecular interrelationships and reactions involved in the response from which the molecular network was created, but also resolving the relationships between shear stress stimuli (e.g. calcium influx, molecular deformation) and the endothelial molecular response. Biological principles of signalling were investigated and

established in the model to match cellular reality (e.g. combinatorial complexity) and the model was constructed from both published knowledge and from newly formed ideas and hypotheses that were suggested from the model itself. Putting all this together allowed, for the first time, a model of integrin signalling to be simulated in response to fluid flow-induced shear stress on endothelial cells.

The model allowed for better understanding of the sequence of events that take place within the cell, identified which events are significant for amplification of information signal from synergistic stimuli and which are not (e.g. cleavage of talin) and identified pathway conversion points (e.g. integrin→ Src, PKC → Src). Much was also learned from the inability of the model to reproduce (correctly) all the behaviours demonstrated experimentally. Without any discrepancies, the rather bland conclusion would be drawn that the model represents a possible mechanism that could underlie the system under scrutiny. Mathematicians however would attest to the fact that it is much easier to show that a given solution is correct than it is to prove that no other solution exists. Thus if the model had not failed at certain points (e.g. FAK^P dynamics under shear stress without protein deformation) the model would not easily disprove other solutions and, most importantly would not imply the way that real system had to operate this way. Where the model failed, investigation of the possible reasons and exploration of alternative mechanisms took place. The necessary additional mechanisms considered in the model (e.g. addition of unknown phosphatases, application of molecular deformation) highlighted the importance of certain post-translational modifications (e.g. dephosphorylation) that have not been thoroughly investigated to date, and provided hypotheses and explanations for experimentally observed events that are currently under examination but have not yet been fully elucidated (e.g. deformation influence on signalling, FAK^P and integrin dynamics, role of calcium influx in the shear stress response).

The model represents a plausible mechanism for part of the molecular response of endothelial cells to shear stress. The new hypotheses extrapolated from published observations and data has left a conclusion that the real system is likely to operate similarly to the mechanisms given by the model. Furthermore, the biological principles

given in this model (e.g. combinatorial complexity) and much of the knowledge gained (e.g. receptor regulation, dynamic behaviour of kinases) can also be applied to other molecules and signalling pathways.

Preliminary modelling has taken place for additional modules of the shear stress response (refer to Figures 2.05, 2.12) including involvement of CAS, Crk and DOCK180 leading to FAK/Src signal amplification, PI3K pathway leading to activation of Vav1 (a GEF for Rac GTPase), and analysis of the dynamics of PECAM-1 and Rac GTPase pathways. Furthermore, frameworks were built a) for multivariate statistical analysis of the simulation results (involving clustering, PCA and PLS analyses), b) for one-by-one and combinatorial sensitivity analyses and c) for examining the contribution of ligand transport (from the fluid media to the apical cell surface) by convection-diffusion to the shear stress response. Although time limitations prevented completion of these modules (not discussed here), their addition will improve greatly the predictive power of the model in the future.

4.1.2 Evaluation of fluid flow-induced stimuli

Fluid flow can potentially influence endothelial behaviour by several distinct mechanisms (Figure 4.01) including:

a) calcium influx from shear stress gated ion channels (Figure 3.02). It was found that although calcium influx regulates the activity of calpain and levels of talin cleavage it is not in isolation significant for increasing integrin activity due to the limited talin cleavage. Calcium influx however is important for PKC and RPTPα activation which in turns controls the feedback and integrin downregulation dynamics via Src kinase activity.

b) molecular deformation of receptors and receptor-associated proteins with subsequent influences in signalling rates. Both experimental evidence and simulations from the model strongly indicate that molecular deformation is likely to regulate the signalling response of endothelial cells to a certain extent. This hypothesis is based on the idea that endothelial cells have the ability to adapt and differentiate the intensity of the response in terms of cellular signalling according to the level of the shear stress applied. Although it is possible that many cell surface receptors such as VEGFR (Tzima et al., 2005; Wang et al., 2004; Wang et al., 2002), EGFR (Ogata, 2003), PECAM-1 (Naganuma et al., 2004; Osawa et al.,

2002), RPTPα (von Wichert et al., 2003b), and GPCRs (Makino et al., 2006) contribute to the shear stress response, experimental examination of such properties will be required to reveal the role of molecular deformation on signalling. Finally, analysis of the deformation model provided a novel explanation regarding the differences in endothelial responses between laminar and turbulent flow and the corresponding differences in regional occurrence of atherosclerotic plaques (section 3.6.9).

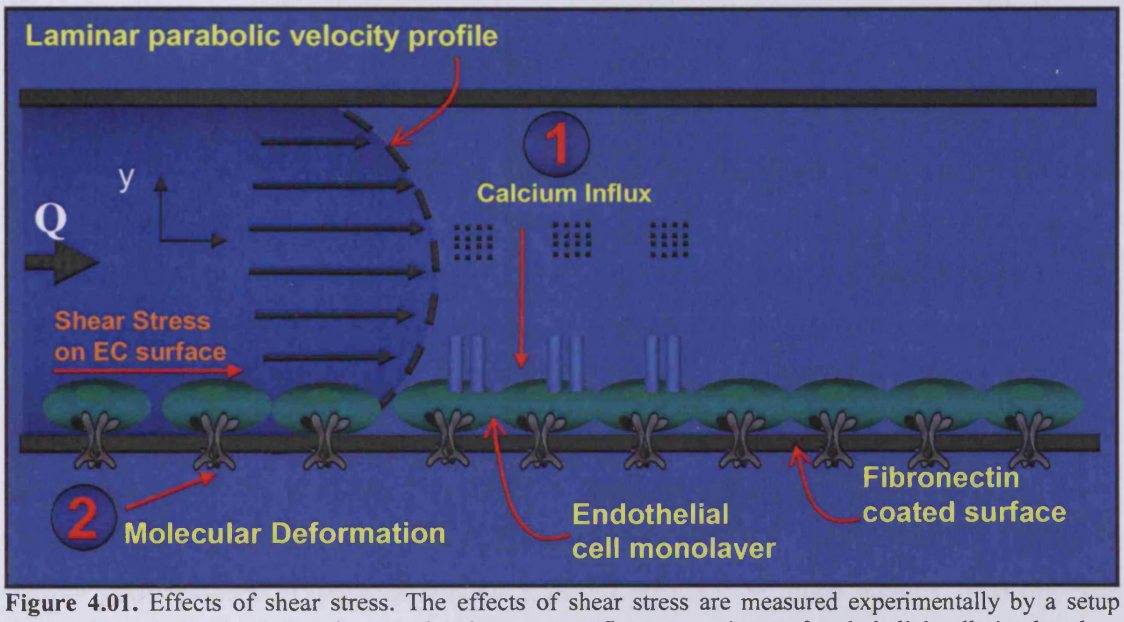

Figure 4.01. Effects of shear stress. The effects of shear stress are measured experimentally by a setup designed to mimic blood flow in vascular tissue. A confluent monolayer of endothelial cells is placed on ligand coated surface and positioned in parallel flow enclosed chambers. The cells form adherent junctions to the surface by binding of receptors to the ligand surface. The chamber is perfused with medium in steady defined laminar flow with known concentrations of ligand molecules and extracellular calcium. Flow of the media exerts a viscous shear force upon the monolayer. Effects of shear stress (direct and indirect) on endothelial cells are shown.

4.1.3 Emergent properties of the pathways examined

The model assumes that both talin and ECM proteins (e.g. fibronectin) are required for association of integrins with downstream molecules. After adhesion of integrins to fibronectin, integrins transiently associate in a macromolecular complex, which contains talin, paxillin, FAK and Src kinase. Formation of the macromolecular complex is required for activation of both FAK and Src. Integrin signalling exhibits a biphasic behaviour that includes a negative feedback loop where the molecules that have been activated in response to integrin activation downregulate in turn the amount of active integrins.

Progression of the signal to successive pathways (e.g. Rac GTPase) requires additional information which is transmitted through PKC and RPTPα to Src kinase (Sicheri and Kuriyan, 1997). Although all the above events take place at the cell membrane, many of the model's molecular interactions take place in the cytosol even in the absence of shear stress (also in presence of shear stress) keeping signalling at a resting state (which could allow stochastic changes to cell behaviour).

The signalling interplay between molecules results in various properties (Bhalla and Iynegar, 1999) that are not visible in individual pathway modules. These include:
i) extended signal duration. For example, coupling of fast responses to slower responses confers on the system the ability to regulate output for considerable time after withdrawal of the original signal (e.g. Ca^{2+} dynamics). Similar behaviour is also exhibited by reactions that provide slow reversibility of activation events as in the case of Src activation/inactivation by RPTPα and Csk respectively.
ii) activation of feedback loops. These occur frequently in biochemical pathways as a means of internal control of the magnitude of signal propagation. The magnitude of the negative feedback exhibited by phosphorylation of integrin by Src in the model is limited directly by the concentration of Src but also indirectly by the concentration of FAK. The role of phosphatases in negative feedback might possibly be much greater in reality than the limited role of dephosphorylation (due to lack of available data) that phosphatases exhibit in the model.
iii) Definition of threshold stimulation for signal propagation and biological robustness. Various responses in the model require signals of defined magnitude and duration. For example, shear stress of 18 dynes/cm^2 is required for significant contribution of calpain-induced talin cleavage to signalling while shear stress of 2 dynes/cm^2 does not induce significant deformation of integrin receptors. Thus the system itself governs what the threshold stimulation needs to be and which stimuli are capable of evoking an appropriate biological response. This is essentially a feature of biological robustness that makes the cell insensitive to changes and perturbations of certain magnitude while very sensitive to others (Kitano, 2004). It is important to note however that the current model has limited robustness because it does not include alternative pathways to regulate each component of the network. Therefore perturbations such as protein knock-outs or kinase inhibition

would prevent most of the simulated changes of the shear stress response, although it is likely that in reality the consequences would be equally devastating.

iv) multiple signal inputs/outputs and regulatory conversion points. These provide a mechanism to ensure that only appropriate signals are transmitted into corresponding molecular responses. For example, both FAK autophosphorylation (Schlaepfer and Mitra, 2004; Schlaepfer et al., 2004), resulting from ligand-induced activation of integrin receptors, and Src dephosphorylation by RPTPα (Sicheri and Kuriyan, 1997), resulting from calcium elevation and activation of the PKC pathway, are required for Src activation resulting in tight regulation of Src activity. This would provide a safety mechanism that limits the amount of active Src (if mutated) according to the amount of receptor engagement and does not allow excessive activation. Similar behaviour is observed for the activation of integrins by both external (fibronectin binding) and internal (talin binding) events, which might also be regulated (e.g. regulation of talin cleavage by calcium influx). Similar regulation has been shown for many other signalling proteins where uncontrollable stimulation would make cells susceptible to internal damage. In this respect the model provided a framework to understand the biological consequence of multiple inputs for single components.

v) amplification. This commonly results either from the utilization of a positive feedback loop or a change of stoichoiometry in molecular reactions in favour of production of downstream species. Neither of these is present in the current model, although they occur at later stages of the pathway (Figure 2.12). For example, for every macromolecular complex in the model, two Crk molecules can associate, one binds on paxillin pY31 (Turner, 2000b) (phosphorylated by FAK) and another that binds on the adaptor molecule CAS (Bouton et al., 2001) (which binds to FAK) resulting in amplified signal propagation towards activation of Rac GTPase (Figure 2.12). Nevertheless, the enhanced activation of FAK in response to molecular deformation can be envisaged as an indirect signal amplification event in the current model that takes place under shear stress.

vi) adaptation. Mechanisms of adaptation are prevalent throughout biology and allow organisms to respond to a change in the environment, which is often of greater interest to the organism than the magnitude of the stimulus itself, and is more economical than persistent activation of a signalling pathway. Adaptation also extends the range of stimuli that can be detected as cells employ physical and chemical mechanisms to respond

accordingly to different stimuli. The ability of cells to adapt to external signals is apparent in the model. For example simulations show how cells can adapt to applied force by mechanisms of deformation and how subsequently signalling molecules such as FAK can also adapt to deformation. The negative feedback residing in the pathways is also a mechanism of adaptation.

4.1.4 Advantages of research approach and evaluation of the model

The approach applied and the current model, both have certain distinct qualities: model composition invoked extensive literature research and the pathways were assembled from peer-reviewed publications. The newly synthesized portions of the comprehensive model are the most likely to contain molecular mistakes however great emphasis was put on limiting such possibility by following general biological principles and rules (e.g. reversibility of post-translational modifications).

The computational requirements of the model are generally low and do not pose limitations on computing power needed for the simulations. However, as the number of interactions and mathematical equations increase with further expansion of the model, it is not limitations in computing power but complexity and size of the model that can potentially make investigation very complicated. Accordingly, the construction of the model and its analysis were performed in modular way, thus allowing each pathway to serve as a distinct stand alone module that can be investigated separately from others thereby reducing the difficulty of investigation.

Most of the parameter values needed for simulations were extracted from the literature, whereas some were extrapolated from experimental results and information and others were estimated, when considered vital for the model, such as the parameter values of certain phosphatases in the model. The model relies relatively little on parameter estimation by optimization techniques and mostly on experimentally derived data for its performance. The numerical accuracy of simulations is considered high and was considerably aided by employment of the Matlab ODE routines. The model was run at different time steps (e.g. 0.1 sec to 1 sec) and the resulting simulated values were found to be equal (not shown) demonstrating a sufficient stability for providing convergent solutions for the range of time steps used in the study.

Overall, the performance and accuracy of model are satisfactory as judged by the ability of the model to explain molecular mechanisms and accommodate new ideas and hypotheses, thus achieving the first objective of this thesis which was to obtain a better understanding of the molecular pathways underlying the shear stress response. The simulation results have been found highly interesting in matching comparisons with experimental data (section 3.9) and by providing explanations for things that have not been yet clearly understood (sections 3.6, 3.7) thus establishing a model of good predictive power. Equally however, the model was also helpful in the cases where it failed to match or explain experimental data by forming new questions that need to be answered. The model will allow expansion to include regulation of Rho GTPases, actin polymerisation and myosin-light chain activation that together form the tools that control dynamic cytoskeletal rearrangements and subsequently cell morphology and cell migration (Ridley, 2004; Ridley et al., 2003).

4.1.5 Data limitations and further information requirements

Experimental data for the major molecules in the model exist in the literature which made the model predictions testable. However, it is not the compatibility of the model results with experimental data but rather the compatibility of different experimental results that is problematic because each set of data originates from a different research group.

Furthermore it is not known whether the experimental data used (i.e. FAK vs. Src) are accurate enough (i.e. timing/activation slope) when also considering the reported experimental uncertainty (e.g. error bars). This could significantly affect the numerical robustness of the model as experimental error and variability between preparations introduces uncertainty in parameter estimates. Although these issues could not be addressed or avoided in this study, it must be said that it is becoming apparent that signalling pathways are not very sensitive to internal perturbations (Bhalla and Iyengar, 1999; Schoeberl et al., 2002): the properties of the system must be sufficiently robust to withstand the inherent degree of variability resulting from stochastic events which are present at various degrees for almost all biochemical reactions.

Another limitation comes from the lack of available time-dependent quantitative observations. Although some experimental molecular activity profiles were available, it is clear that a lot more are required to refine and increase both the accuracy and predictive power of the model and in particular experimental data regarding the dynamic behaviour of phosphatases. To date the function of around 38 PTPs out of 107 PTP genes and ~85 PTKs out of 90 PTK genes has been elucidated to a certain extent (Alonso et al., 2004; Andersen et al., 2004), and thus PTPs have received much less attention. Due to their ability to regulate protein phosphotyrosine levels, PTPs are undoubtedly essential for robust regulation of intracellular signalling. However, the roles of specific PTPs in the regulation of receptor-initiated signal transduction events and cell adhesion remain poorly understood. Analysis of pathway dynamics in the current model allowed the evaluation of the ability of the receptor-like phosphatase RPTPα to co-regulate calcium-induced activation of Src kinase along with the regulation induced by activation of integrins in response to shear stress. Furthermore, the model also clearly demonstrated the importance of dephosphorylation events in the shear stress response and thus phosphatases need to be further investigated if we are to understand better how these biological responses are controlled.

Finally, there are various knowledge limitations in the current model. For example, clustering of integrins and associated molecules was not investigated in the model. This is because it is not yet known whether signalling is different depending on size of clustering. Furthermore, there have been reports that RPTPα is also subject to molecular deformation (von Wichert et al., 2003b) believed to govern its activity rates, but this was not included as the data is not sufficient and parameter values that describe the molecular elasticity of RPTPα or other receptors is not yet available. In addition, a combination of model results and experimental findings (Di Paolo et al., 2002) suggested that PIP_2 generation and PIPKγ activity are likely to constitute a positive feedback present in the pathways leading to further activation of talin. Such was not included however due to time limitations. It is anticipated that adding these molecular events to the model may significantly change the dynamics of signalling and also increase our understanding of the shear stress response.

4.1.6 Conceptual limitations

The model is subject to some inherent limitations because of the general deterministic approach followed in this project. Under certain circumstances, deterministic models no longer represent the physical system adequately and cannot be used to predict the concentrations of chemical species. If we could focus on the microscopic scale of a chemical reaction, we could see the individual molecules randomly bumping into others and react (assuming the kinetic energies of the colliding molecules were sufficient). To convert this probabilistic system with its molecular graininess, into a continuous, deterministic model, one must make several assumptions (i.e. examined system has infinite volume). These hold within a defined regime, where the discrete, stochastic nature of a chemical system is not apparent. However, certain properties of a system may cause these assumptions to break down (e.g. modelling small volumes such as small organelles within the cell), with the result that the use of continuous deterministic models leads to a loss in predictive power.

Fluctuations, arising from the stochastic behaviour of the physical system are often negligible and can be ignored. However, they can be amplified and cause observable macroscopic effects if the system operates close to points of unstable equilibria. Biological pathways frequently employ positive feedback and other more complex relationships which lead to instabilities in state-space. This for example can be demonstrated from the fact that individual cells under the same stimuli exhibit different morphological changes between them and do not exhibit identical patterns migration. This unfortunately is a limitation that it is not easily bypassed.

4.1.7 Potential additions and improvements to the current model

There is considerable potential for additions and improvements to the model. Improvements can be applied to the model of deformation, by considering the direction of force relative to focal contacts. It is not exactly understood whether cells sense applied force on the apical or the basal membrane (or both) and the point or angle of force application is not considered in the current model (Figure 4.02). However, it is possible that these could significantly govern both the amount of deformation and the rate by which it is applied on molecular bodies.

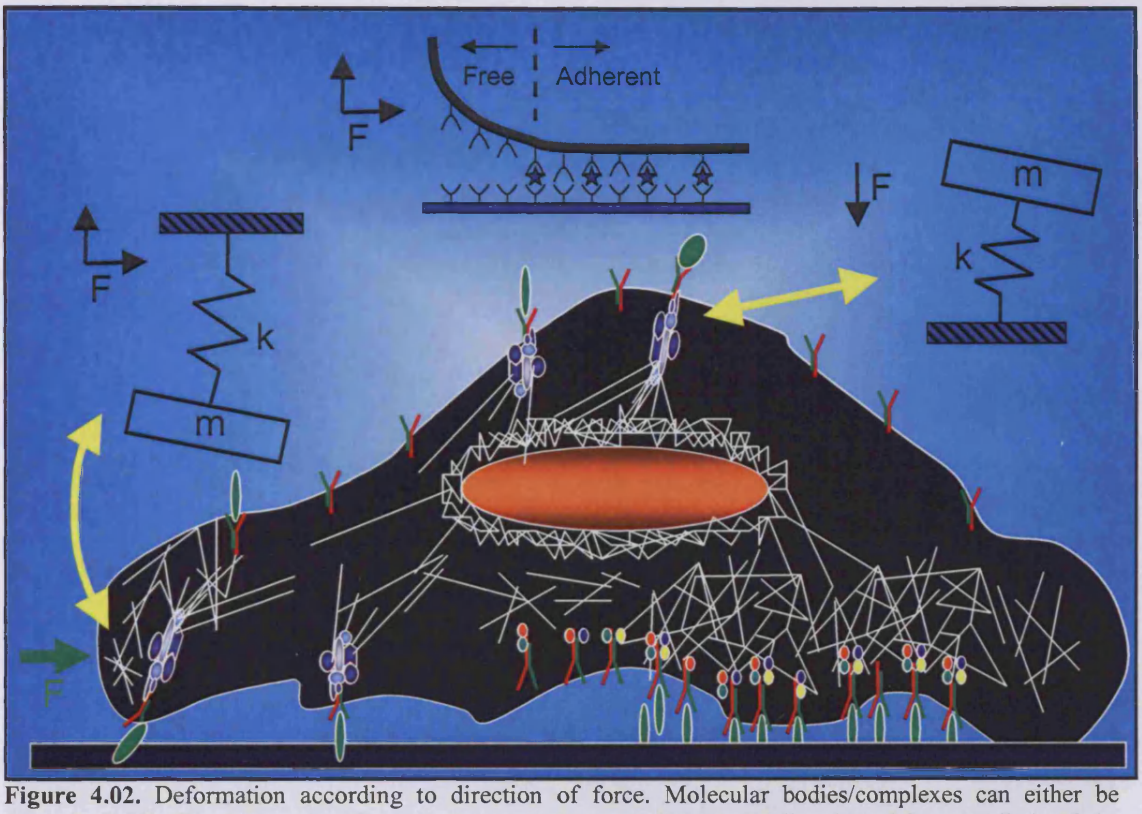

Figure 4.02. Deformation according to direction of force. Molecular bodies/complexes can either be "stretched/pulled" or "compressed" similarly to a spring according to the direction of force applied and the surface the molecular body is attached too.

A significant improvement to the deformation model would come from considering a macromolecular complex (e.g. integrin, talin, FAK, paxillin) that is deformed using the same viscoelastic principles (Figure 4.03). This would allow more accurate and realistic calculation of the force transition between attached molecules and consequent deformation of every molecule that is present in the complex, including structural molecules such as vinculin and actin (as deformable bodies).

Further expansion of the model could also include: a) regulation of Rho GTPases. This would shed light into how cell morphology is regulated by Rho GTPases (see Figure 4.04). b) regulation of critical transcription factors. This could be used to identify long term responses to shear stress including mechanisms that could be manipulated (e.g. by chemical intervention) in order to suppress and inhibit disease causing genes without negatively affecting any other beneficial molecules.

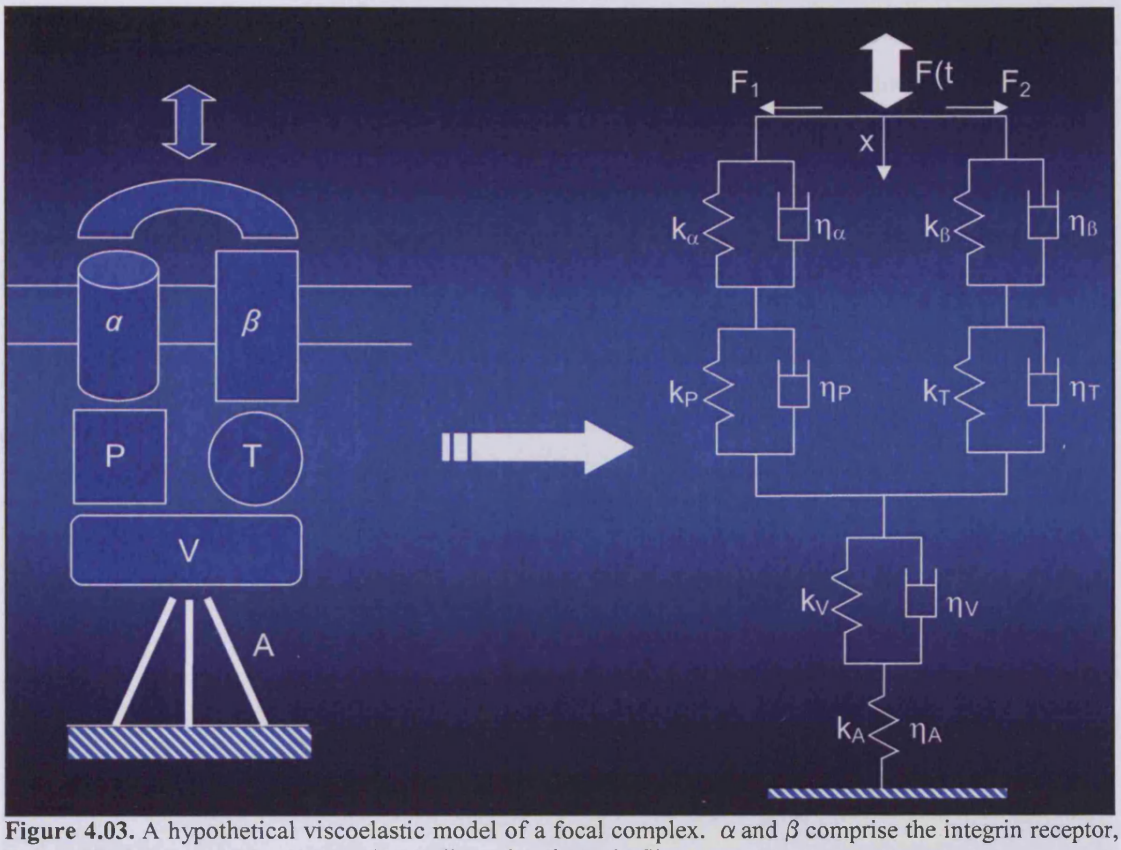

Figure 4.03. A hypothetical viscoelastic model of a focal complex. α and β comprise the integrin receptor, P, T and V denote paxillin, talin and vinculin and A the actin filaments.

For example, the ability to predict the expression levels of the protein troponin at different time points (Figure 4.04) would be interesting because troponin is one of the major clinical risk predictors of heart failure (Bueti et al., 2006; Valgimigli et al., 2005) and can be easily measured by blood test examinations. The dynamics of each molecular component in the system could be used not only to predict the effect of single perturbations to the dynamic signature of the whole system, but potentially also to measure the effect each perturbation would have in influencing positively or negatively the risk for a heart attack (e.g. by affecting the levels of expressed troponin).

Finally, the endothelium plays a crucial role in maintaining vascular homeostasis and regulating the passage of materials between the blood and the vessel wall (Traub and Berk, 1998). EC are sensitive not only to mechanical stimuli such as wall shear stress, but also biochemical stimuli such as blood-borne agonists and are also a source of vasoactive factors such as nitric oxide (NO), prostaglandin, endothelin and angiotensin (Schachter, 1997a; Schachter, 1997b). Atherosclerosis is also significantly affected by environmental

toxins that insert the human body via smoking or poor (high cholesterol) diet. In the long term, modelling the effects of these stimuli on the endothelium may allow us to find better ways for curing and preventing diseases.

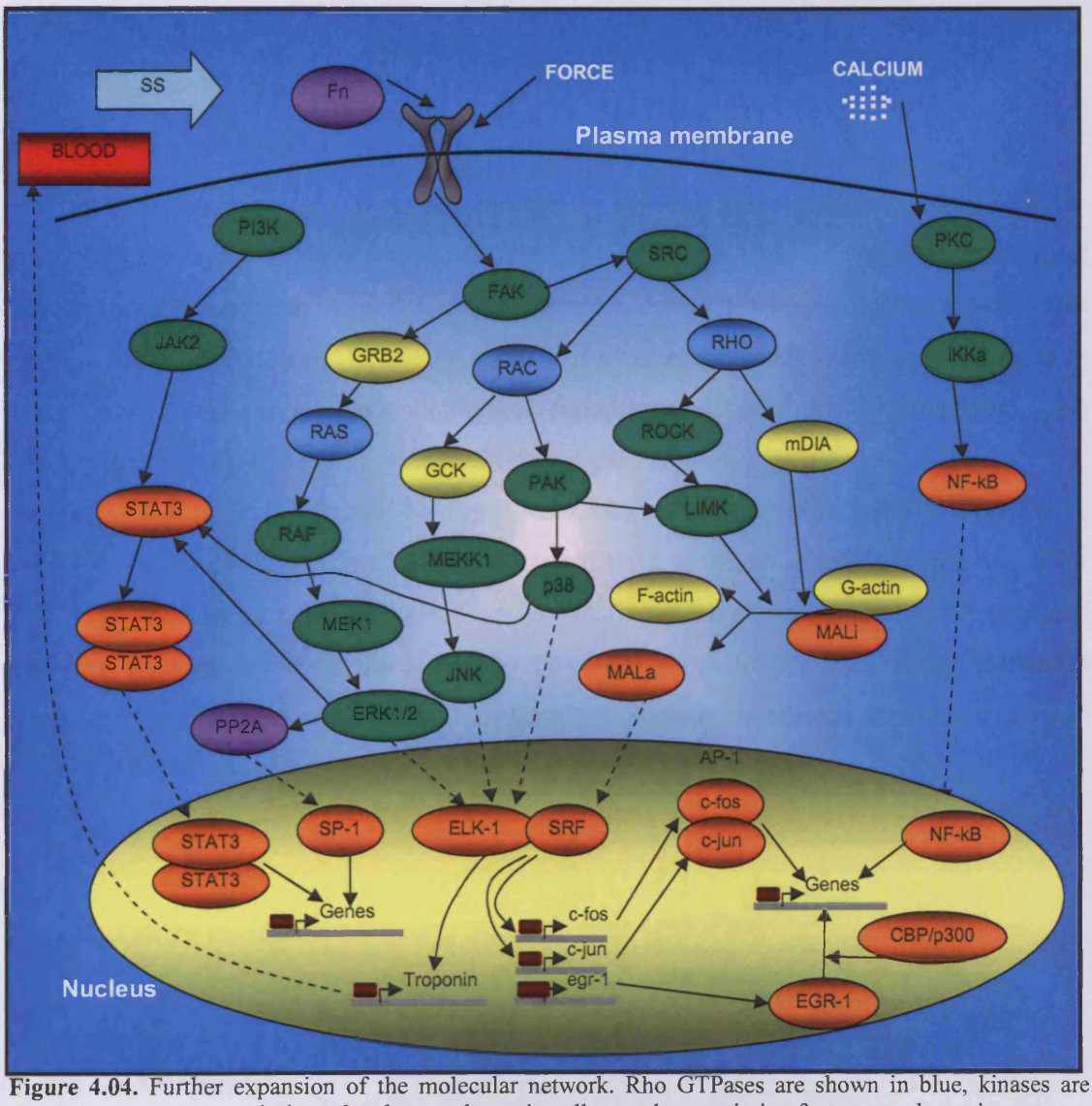

Figure 4.04. Further expansion of the molecular network. Rho GTPases are shown in blue, kinases are shown in green, non-catalytic molecules are shown in yellow and transcription factors are shown in orange.

It is thereby clear that the quest for finding the mechanisms that regulate the properties and function of endothelial cells in response to shear stress stimulation has certainly not ended. We are probably just at the tip of the iceberg, surfing over the few pathways that are today known to cell biology. Much remains to be learnt about the clustering and

interactions of different signalling molecules in cellular membranes and in the cytosol, in order to understand the functions and responses of endothelial cells in the vascular system. A model that extends beyond signalling pathways and immediate responses to investigate a disease in all its breadth and properties would be a long term goal and certainly require such knowledge.

4.1.8 Towards the future

Potential applications of the model lie not in the qualified modelling of a common pathway to understand its function, but the use of the model to link applied mechanical stimuli to molecular activation and gene expression in a cell mathematically, as a function of time and applied force. In theory, such a mathematical relationship can be useful to form novel tools for studying biological function such as fluid flow-mediated gene therapies and applications in tissue gradients (Figure 4.05).

Assuming that the model could be expanded sufficiently, it could be used to model gene therapies for diseases of the circulatory system such as atherosclerosis (refer to section 1.3.1). If endothelial cells contained an artificial gene that was activated via a signal transduction pathway upon the sustained presence of oscillatory shear stress (turbulent flow), and such a gene was designed to stimulate degradation of such deposits, this could treat atherosclerosis effectively.

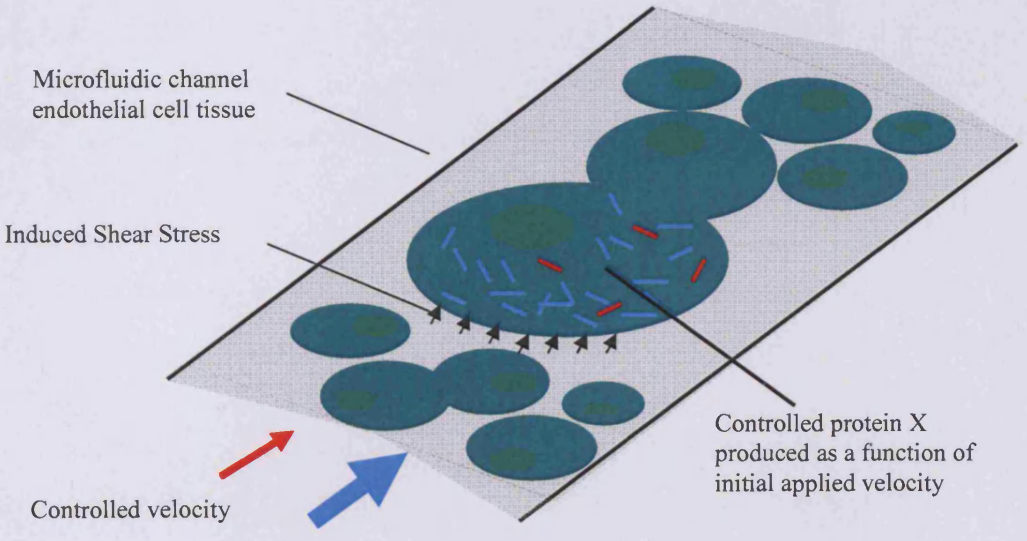

Figure 4.05. Controlling shear stress-induced protein activity and/or gene expression.

Twenty-five years ago, if someone had predicted that computer simulation would invade biology to the extent it has, his or her grant application would not have been taken seriously. Likewise, it is difficult to know where it will take us in the decades to come. Pharmaceutical companies have already turned towards computational biology to help them interpret vast quantities of experimental data related to signal transduction pathways, which are central to processes of disease and illness. Modelling and simulation will promote a new understanding of how drugs work and how their effectiveness and specificity can be improved.

REFERENCES

Adams, D. J., Barakeh, J., Laskey, R., and Van Breemen, C. (1989). Ion channels and regulation of intracellular calcium in vascular endothelial cells. Faseb J *3*, 2389-2400.

Akiyama, S. K., and Yamada, K. M. (1985). Synthetic peptides competitively inhibit both direct binding to fibroblasts and functional biological assays for the purified cell-binding domain of fibronectin. J Biol Chem *260*, 10402-10405.

Alberts, B. (1994). Molecular biology of the cell, 3rd edn (New York: Garland Pub.).

Ali, M. H., and Schumacker, P. T. (2002). Endothelial responses to mechanical stress: where is the mechanosensor? Crit Care Med *30*, S198-206.

Alon, U., Surette, M. G., Barkai, N., and Leibler, S. (1999). Robustness in bacterial chemotaxis. Nature *397*, 168-171.

Alonso, A., Sasin, J., Bottini, N., Friedberg, I., Friedberg, I., Osterman, A., Godzik, A., Hunter, T., Dixon, J., and Mustelin, T. (2004). Protein tyrosine phosphatases in the human genome. Cell *117*, 699-711.

Andersen, J. N., Jansen, P. G., Echwald, S. M., Mortensen, O. H., Fukada, T., Del Vecchio, R., Tonks, N. K., and Moller, N. P. (2004). A genomic perspective on protein tyrosine phosphatases: gene structure, pseudogenes, and genetic disease linkage. Faseb J *18*, 8-30.

Ando, J., Komatsuda, T., and Kamiya, A. (1988). Cytoplasmic calcium response to fluid shear stress in cultured vascular endothelial cells. In Vitro Cell Dev Biol *24*, 871-877.

Arkin, A., Ross, J., and McAdams, H. H. (1998). Stochastic kinetic analysis of developmental pathway bifurcation in phage lambda-infected Escherichia coli cells. Genetics *149*, 1633-1648.

Arthur, J. S., and Crawford, C. (1996). Investigation of the interaction of m-calpain with phospholipids: calpain-phospholipid interactions. Biochim Biophys Acta *1293*, 201-206.

Asthagiri, A. R., Nelson, C. M., Horwitz, A. F., and Lauffenburger, D. A. (1999). Quantitative relationship among integrin-ligand binding, adhesion, and signaling via focal adhesion kinase and extracellular signal-regulated kinase 2. J Biol Chem *274*, 27119-27127.

Bader, G. D., Donaldson, I., Wolting, C., Ouellette, B. F., Pawson, T., and Hogue, C. W. (2001). BIND--The Biomolecular Interaction Network Database. Nucleic Acids Res *29*, 242-245.

Baneyx, G., Baugh, L., and Vogel, V. (2002). Fibronectin extension and unfolding within cell matrix fibrils controlled by cytoskeletal tension. Proc Natl Acad Sci U S A *99*, 5139-5143.

Bao, G., and Suresh, S. (2003). Cell and molecular mechanics of biological materials. Nat Mater *2*, 715-725.

Barakat, A., and Lieu, D. (2003). Differential responsiveness of vascular endothelial cells to different types of fluid mechanical shear stress. Cell Biochem Biophys *38*, 323-343.

Barakat, A. I. (2001). A model for shear stress-induced deformation of a flow sensor on the surface of vascular endothelial cells. J Theor Biol *210*, 221-236.

Barakat, A. I., and Davies, P. F. (1998). Mechanisms of shear stress transmission and transduction in endothelial cells. Chest *114*, 58S-63S.

Barnoy, S., Zipser, Y., Glaser, T., Grimberg, Y., and Kosower, N. S. (1999). Association of calpain (Ca(2+)-dependent thiol protease) with its endogenous inhibitor calpastatin in myoblasts. J Cell Biochem *74*, 522-531.

Barsukov, I. L., Prescot, A., Bate, N., Patel, B., Floyd, D. N., Bhanji, N., Bagshaw, C. R., Letinic, K., Di Paolo, G., De Camilli, P., *et al.* (2003). Phosphatidylinositol phosphate kinase type 1gamma and beta1-integrin cytoplasmic domain bind to the same region in the talin FERM domain. J Biol Chem *278*, 31202-31209.

Bausch, A. R., Hellerer, U., Essler, M., Aepfelbacher, M., and Sackmann, E. (2001). Rapid stiffening of integrin receptor-actin linkages in endothelial cells stimulated with thrombin: a magnetic bead microrheology study. Biophys J *80*, 2649-2657.

Bausch, A. R., Moller, W., and Sackmann, E. (1999). Measurement of local viscoelasticity and forces in living cells by magnetic tweezers. Biophys J *76*, 573-579.

Bausch, A. R., Ziemann, F., Boulbitch, A. A., Jacobson, K., and Sackmann, E. (1998). Local measurements of viscoelastic parameters of adherent cell surfaces by magnetic bead microrheometry. Biophys J *75*, 2038-2049.

Bayley, P., Ahlstrom, P., Martin, S. R., and Forsen, S. (1984). The kinetics of calcium binding to calmodulin: Quin 2 and ANS stopped-flow fluorescence studies. Biochem Biophys Res Commun *120*, 185-191.

Belansky, R, Wanser, K. (1993). Laser doppler velocimetry using a bulk optic Michelson interferometer: a student laboratory experiment. American J Phys *61*, 1014–1019.

Bell, G. I. (1978). Models for the specific adhesion of cells to cells. Science *200*, 618-627.
Berridge, M. J. (1990). Calcium oscillations. J Biol Chem *265*, 9583-9586.

Berridge, M. J. (1997). Elementary and global aspects of calcium signalling. J Physiol *499 (Pt 2)*, 291-306.

Bershadsky, A. D., Balaban, N. Q., and Geiger, B. (2003). Adhesion-dependent cell mechanosensitivity. Annu Rev Cell Dev Biol *19*, 677-695.

Bhalla, U. S., and Iyengar, R. (1999). Emergent properties of networks of biological signaling pathways. Science *283*, 381-387.

Bhalla, U. S., Ram, P. T., and Iyengar, R. (2002). MAP kinase phosphatase as a locus of flexibility in a mitogen-activated protein kinase signaling network. Science *297*, 1018-1023.

Blanchard, H., Grochulski, P., Li, Y., Arthur, J. S., Davies, P. L., Elce, J. S., and Cygler, M. (1997). Structure of a calpain Ca(2+)-binding domain reveals a novel EF-hand and Ca(2+)-induced conformational changes. Nat Struct Biol *4*, 532-538.

Boggon, T. J., and Eck, M. J. (2004). Structure and regulation of Src family kinases. Oncogene *23*, 7918-7927.

Bolouri, H., and Davidson, E. H. (2002). Modeling DNA sequence-based cis-regulatory gene networks. Dev Biol *246*, 2-13.

Booij ,W., de Jongh A,, de Mul F. (1995). Flow profile study using miniature laser-doppler velocimetry. American J Phys *63*, 1028–1033.

Borisuk, M. T., and Tyson, J. J. (1998). Bifurcation analysis of a model of mitotic control in frog eggs. J Theor Biol *195*, 69-85.

Bouton, A. H., Riggins, R. B., and Bruce-Staskal, P. J. (2001). Functions of the adapter protein Cas: signal convergence and the determination of cellular responses. Oncogene *20*, 6448-6458.

Bradshaw, J. M., Mitaxov, V., and Waksman, G. (1999). Investigation of phosphotyrosine recognition by the SH2 domain of the Src kinase. J Mol Biol *293*, 971-985.

Brakemeier, S., Kersten, A., Eichler, I., Grgic, I., Zakrzewicz, A., Hopp, H., Kohler, R., and Hoyer, J. (2003). Shear stress-induced up-regulation of the intermediate-conductance Ca(2+)-activated K(+) channel in human endothelium. Cardiovasc Res *60*, 488-496.

Bray, D. (1998). Signaling complexes: biophysical constraints on intracellular communication. Annu Rev Biophys Biomol Struct *27*, 59-75.

Bray, D., and Bourret, R. B. (1995). Computer analysis of the binding reactions leading to a transmembrane receptor-linked multiprotein complex involved in bacterial chemotaxis. Mol Biol Cell *6*, 1367-1380.

Breitkreutz, B. J., Stark, C., and Tyers, M. (2003). Osprey: a network visualization system. Genome Biol *4*, R22.

Brown, M. C., Perrotta, J. A., and Turner, C. E. (1996). Identification of LIM3 as the principal determinant of paxillin focal adhesion localization and characterization of a novel motif on paxillin directing vinculin and focal adhesion kinase binding. J Cell Biol *135*, 1109-1123.

Brown, T. D. (2000). Techniques for mechanical stimulation of cells in vitro: a review. J Biomech *33*, 3-14.

Bruggeman, F. J., and Kholodenko, B. N. (2002). Modular interaction strengths in regulatory networks; an example. Mol Biol Rep *29*, 57-61.

Bruggeman, F. J., Westerhoff, H. V., Hoek, J. B., and Kholodenko, B. N. (2002). Modular response analysis of cellular regulatory networks. J Theor Biol *218*, 507-520.

Brugnera, E., Haney, L., Grimsley, C., Lu, M., Walk, S. F., Tosello-Trampont, A. C., Macara, I. G., Madhani, H., Fink, G. R., and Ravichandran, K. S. (2002). Unconventional Rac-GEF activity is mediated through the Dock180-ELMO complex. Nat Cell Biol *4*, 574-582.

Bueti, J., Krahn, J., Karpinski, M., Bohm, C., Fine, A., and Rigatto, C. (2006). Troponin I testing in dialysis patients presenting to the emergency room: does troponin I predict the 30-day outcome? Nephron Clin Pract *103*, c129-136.

Burrage, K., Tian, T., and Burrage, P. (2004). A multi-scaled approach for simulating chemical reaction systems. Prog Biophys Mol Biol *85*, 217-234.

Burridge, K., Turner, C. E., and Romer, L. H. (1992). Tyrosine phosphorylation of paxillin and pp125FAK accompanies cell adhesion to extracellular matrix: a role in cytoskeletal assembly. J Cell Biol *119*, 893-903.

Calalb, M. B., Polte, T. R., and Hanks, S. K. (1995). Tyrosine phosphorylation of focal adhesion kinase at sites in the catalytic domain regulates kinase activity: a role for Src family kinases. Mol Cell Biol *15*, 954-963.

Calderwood, D. A. (2004a). Integrin activation. J Cell Sci *117*, 657-666.

Calderwood, D. A. (2004b). Talin controls integrin activation. Biochem Soc Trans *32*, 434-437.

Calderwood, D. A., Yan, B., de Pereda, J. M., Alvarez, B. G., Fujioka, Y., Liddington, R. C., and Ginsberg, M. H. (2002). The phosphotyrosine binding-like domain of talin activates integrins. J Biol Chem *277*, 21749-21758.

Calderwood, D. A., Zent, R., Grant, R., Rees, D. J., Hynes, R. O., and Ginsberg, M. H. (1999). The Talin head domain binds to integrin beta subunit cytoplasmic tails and regulates integrin activation. J Biol Chem *274*, 28071-28074.

Campbell, I. D., and Ginsberg, M. H. (2004). The talin-tail interaction places integrin activation on FERM ground. Trends Biochem Sci *29*, 429-435.

Cannell, M. B. (1997). New insights into cardiac excitation-contraction coupling in normal and hypertension/failure animal models. J Hum Hypertens *11*, 555-558.

Cao, M. Y., Huber, M., Beauchemin, N., Famiglietti, J., Albelda, S. M., and Veillette, A. (1998). Regulation of mouse PECAM-1 tyrosine phosphorylation by the Src and Csk families of protein-tyrosine kinases. J Biol Chem *273*, 15765-15772.

Carlson, J. M., and Doyle, J. (2000). Highly optimized tolerance: robustness and design in complex systems. Phys Rev Lett *84*, 2529-2532.

Carman, C. V., and Springer, T. A. (2003). Integrin avidity regulation: are changes in affinity and conformation underemphasized? Curr Opin Cell Biol *15*, 547-556.

Caro, C.G., Fitz-Gerald, J.M., and Schrode RC. (1971). Atheroma and arterial wall shear stress. Observations, correlations and proposal of a shear stress dependent mass transfer mechanism for atherogeneis. Procs Ro Soc London. (Biol) *117*, 109-159

Carragher, N. O., Levkau, B., Ross, R., and Raines, E. W. (1999). Degraded collagen fragments promote rapid disassembly of smooth muscle focal adhesions that correlates with cleavage of pp125(FAK), paxillin, and talin. J Cell Biol *147*, 619-630.

Charest, A., Wagner, J., Shen, S. H., and Tremblay, M. L. (1995). Murine protein tyrosine phosphatase-PEST, a stable cytosolic protein tyrosine phosphatase. Biochem J *308 (Pt 2)*, 425-432.

Chen, K. D., Li, Y. S., Kim, M., Li, S., Yuan, S., Chien, S., and Shyy, J. Y. (1999). Mechanotransduction in response to shear stress. Roles of receptor tyrosine kinases, integrins, and Shc. J Biol Chem *274*, 18393-18400.

Chen, Q., Cannell, M., and van Breemen, C. (1992). The superficial buffer barrier in vascular smooth muscle. Can J Physiol Pharmacol *70*, 509-514.

Cheng, K., Kurzrock, R., Qiu, X., Estrov, Z., Ku, S., Dulski, K. M., Wang, J. Y., and Talpaz, M. (2002). Reduced focal adhesion kinase and paxillin phosphorylation in BCR-ABL-transfected cells. Cancer *95*, 440-450.

Chiarugi, P. (2003). Reactive oxygen species as mediators of cell adhesion. Ital J Biochem *52*, 28-32.

Chicurel, M. E., Singer, R. H., Meyer, C. J., and Ingber, D. E. (1998). Integrin binding and mechanical tension induce movement of mRNA and ribosomes to focal adhesions. Nature *392*, 730-733.

Cluzel, C., Saltel, F., Lussi, J., Paulhe, F., Imhof, B. A., and Wehrle-Haller, B. (2005). The mechanisms and dynamics of (alpha)v(beta)3 integrin clustering in living cells. J Cell Biol *171*, 383-392.

Cobb, B. S., Schaller, M. D., Leu, T. H., and Parsons, J. T. (1994). Stable association of pp60src and pp59fyn with the focal adhesion-associated protein tyrosine kinase, pp125FAK. Mol Cell Biol *14*, 147-155.

Cong, J., Goll, D. E., Peterson, A. M., and Kapprell, H. P. (1989). The role of autolysis in activity of the Ca2+-dependent proteinases (mu-calpain and m-calpain). J Biol Chem *264*, 10096-10103.

Cooley, M. A., Broome, J. M., Ohngemach, C., Romer, L. H., and Schaller, M. D. (2000). Paxillin binding is not the sole determinant of focal adhesion localization or dominant-negative activity of focal adhesion kinase/focal adhesion kinase-related nonkinase. Mol Biol Cell *11*, 3247-3263.

Cooper, J. A., Gould, K. L., Cartwright, C. A., and Hunter, T. (1986). Tyr527 is phosphorylated in pp60c-src: implications for regulation. Science *231*, 1431-1434.

Cooray, P., Yuan, Y., Schoenwaelder, S. M., Mitchell, C. A., Salem, H. H., and Jackson, S. P. (1996). Focal adhesion kinase (pp125FAK) cleavage and regulation by calpain. Biochem J *318 (Pt 1)*, 41-47.

Corana, A., Marchesi, M., Martini, C and Ridella S (1987). Minimizing multimodal functions of continuous variables with the 'simulated annealing' algorithm. ACM Trans.Math.Soft *13*, 262-280

Cote, J. F., Turner, C. E., and Tremblay, M. L. (1999). Intact LIM 3 and LIM 4 domains of paxillin are required for the association to a novel polyproline region (Pro 2) of protein-tyrosine phosphatase-PEST. J Biol Chem *274*, 20550-20560.

Cram, E. J., and Schwarzbauer, J. E. (2004). The talin wags the dog: new insights into integrin activation. Trends Cell Biol *14*, 55-57.

Crawford, C., Brown, N. R., and Willis, A. C. (1990). Investigation of the structural basis of the interaction of calpain II with phospholipid and with carbohydrate. Biochem J *265*, 575-579.

Critchley, D. R. (2000). Focal adhesions - the cytoskeletal connection. Curr Opin Cell Biol *12*, 133-139.

Critchley, D. R. (2004). Cytoskeletal proteins talin and vinculin in integrin-mediated adhesion. Biochem Soc Trans *32*, 831-836.

Critchley, D. R. (2005). Genetic, biochemical and structural approaches to talin function. Biochem Soc Trans *33*, 1308-1312.

Cunningham, K. S., and Gotlieb, A. I. (2005). The role of shear stress in the pathogenesis of atherosclerosis. Lab Invest *85*, 9-23.

D'Haeseleer, P., Liang, S., and Somogyi, R. (2000). Genetic network inference: from co-expression clustering to reverse engineering. Bioinformatics *16*, 707-726.

Dartnell, L., Simeonidis, E., Hubank, M., Tsoka, S., Bogle, I. D., and Papageorgiou, L. G. (2005). Robustness of the p53 network and biological hackers. FEBS Lett *579*, 3037-3042.

Datta, A., Huber, F., and Boettiger, D. (2002). Phosphorylation of beta3 integrin controls ligand binding strength. J Biol Chem *277*, 3943-3949.

Davidson, E. H., Rast, J. P., Oliveri, P., Ransick, A., Calestani, C., Yuh, C. H., Minokawa, T., Amore, G., Hinman, V., Arenas-Mena, C., *et al.* (2002). A genomic regulatory network for development. Science *295*, 1669-1678.

Davies, P. F. (1995). Flow-mediated endothelial mechanotransduction. Physiol Rev *75*, 519-560.

Davies, P. F., Mundel, T., and Barbee, K. A. (1995). A mechanism for heterogeneous endothelial responses to flow in vivo and in vitro. J Biomech *28*, 1553-1560.

Davis, G. E., Black, S. M., and Bayless, K. J. (2000). Capillary morphogenesis during human endothelial cell invasion of three-dimensional collagen matrices. In Vitro Cell Dev Biol Anim *36*, 513-519.

de Atauri, P., Orrell, D., Ramsey, S., and Bolouri, H. (2005). Is the regulation of galactose 1-phosphate tuned against gene expression noise? Biochem J *387*, 77-84.

de Jong, H. (2002). Modeling and simulation of genetic regulatory systems: a literature review. J Comput Biol *9*, 67-103.

Dejana, E. (1993). Endothelial cell adhesive receptors. J Cardiovasc Pharmacol *21 Suppl 1*, S18-21.

Dejana, E., Raiteri, M., Resnati, M., and Lampugnani, M. G. (1993). Endothelial integrins and their role in maintaining the integrity of the vessel wall. Kidney Int *43*, 61-65.

den Hertog, J., and Hunter, T. (1996). Tight association of GRB2 with receptor protein-tyrosine phosphatase alpha is mediated by the SH2 and C-terminal SH3 domains. Embo J *15*, 3016-3027.

den Hertog, J., Pals, C. E., Peppelenbosch, M. P., Tertoolen, L. G., de Laat, S. W., and Kruijer, W. (1993). Receptor protein tyrosine phosphatase alpha activates pp60c-src and is involved in neuronal differentiation. Embo J *12*, 3789-3798.

den Hertog, J., Sap, J., Pals, C. E., Schlessinger, J., and Kruijer, W. (1995). Stimulation of receptor protein-tyrosine phosphatase alpha activity and phosphorylation by phorbol ester. Cell Growth Differ *6*, 303-307.

den Hertog, J., Tracy, S., and Hunter, T. (1994). Phosphorylation of receptor protein-tyrosine phosphatase alpha on Tyr789, a binding site for the SH3-SH2-SH3 adaptor protein GRB-2 in vivo. Embo J *13*, 3020-3032.

Dennis, J.E., Gay, D.M., and Welsch RE (1981). An adaptive nonlinear least squares algorithm. ACM Trans on Mathem Soft *7*, 348-368

Dewey, C. F., Jr., Bussolari, S. R., Gimbrone, M. A., Jr., and Davies, P. F. (1981). The dynamic response of vascular endothelial cells to fluid shear stress. J Biomech Eng *103*, 177-185.

Di Paolo, G., Pellegrini, L., Letinic, K., Cestra, G., Zoncu, R., Voronov, S., Chang, S., Guo, J., Wenk, M. R., and De Camilli, P. (2002). Recruitment and regulation of phosphatidylinositol phosphate kinase type 1 gamma by the FERM domain of talin. Nature *420*, 85-89.

Doherty, T.M., Fitzpatrick, L.A., Shaeen, A., Rajavashisth, T.B., Detrano, R.C. (2004). Genetic determinants of arterial clacification associated with atherosclerosis. Mayo Clin Procs *79*,197-210

Dull, R. O., and Davies, P. F. (1991). Flow modulation of agonist (ATP)-response (Ca2+) coupling in vascular endothelial cells. Am J Physiol *261*, H149-154.

Dupont, G., and Goldbeter, A. (1992). Oscillations and waves of cytosolic calcium: insights from theoretical models. Bioessays *14*, 485-493.

Edmunds, T., Nagainis, P. A., Sathe, S. K., Thompson, V. F., and Goll, D. E. (1991). Comparison of the autolyzed and unautolyzed forms of mu- and m-calpain from bovine skeletal muscle. Biochim Biophys Acta *1077*, 197-208.

Edwards, J. S., and Palsson, B. O. (2000). Robustness analysis of the Escherichia coli metabolic network. Biotechnol Prog *16*, 927-939.

Evans, E. A., and Skalak, R. (1979a). Mechanics and thermodynamics of biomembranes: part 1. CRC Crit Rev Bioeng *3*, 181-330.

Evans, E. A., and Skalak, R. (1979b). Mechanics and thermodynamics of biomembranes: part 2. CRC Crit Rev Bioeng *3*, 331-418.

Faller, D., Klingm¨uller, U., Timmer, J. (2003). Simulation methods for optimal experimental design in systems biology. Simulation *79*, 717–725.

Faull, R. J., Kovach, N. L., Harlan, J. M., and Ginsberg, M. H. (1993). Affinity modulation of integrin alpha 5 beta 1: regulation of the functional response by soluble fibronectin. J Cell Biol *121*, 155-162.

Fell, D.A. (1997). Understanding the Control of Metabolism. London Portland Press.

Fisher, A. B., Chien, S., Barakat, A. I., and Nerem, R. M. (2001). Endothelial cellular response to altered shear stress. Am J Physiol Lung Cell Mol Physiol *281*, L529-533.

Flaherty, J. T., Pierce, J. E., Ferrans, V. J., Patel, D. J., Tucker, W. K., and Fry, D. L. (1972). Endothelial nuclear patterns in the canine arterial tree with particular reference to hemodynamic events. Circ Res *30*, 23-33.

Fletcher, R. (1987). Practical Methods of Optimization, 2nd edn, John Willey and Sons, Chichester

Flint, A. J., Tiganis, T., Barford, D., and Tonks, N. K. (1997). Development of "substrate-trapping" mutants to identify physiological substrates of protein tyrosine phosphatases. Proc Natl Acad Sci U S A *94*, 1680-1685.

Fogel, D.B, Fogel, L.J. and Atmar JW. (1992). Meta-evolutionary programming. In Chen, R.R (ed), 25th Asilomar Conference on Signals, Systems and Computers, IEEE Computer society, Asilomar 540-545

Frame, M. C. (2004). Newest findings on the oldest oncogene; how activated src does it. J Cell Sci *117*, 989-998.

Franco, S. J., and Huttenlocher, A. (2005). Regulating cell migration: calpains make the cut. J Cell Sci *118*, 3829-3838.

Franco, S. J., Rodgers, M. A., Perrin, B. J., Han, J., Bennin, D. A., Critchley, D. R., and Huttenlocher, A. (2004). Calpain-mediated proteolysis of talin regulates adhesion dynamics. Nat Cell Biol *6*, 977-983.

Freeman, M. (2000). Feedback control of intercellular signalling in development. Nature *408*, 313-319.

Freeman, R. M., Jr., Plutzky, J., and Neel, B. G. (1992). Identification of a human src homology 2-containing protein-tyrosine-phosphatase: a putative homolog of Drosophila corkscrew. Proc Natl Acad Sci U S A *89*, 11239-11243.

Friedman, N., Linial, M., Nachman, I., and Pe'er, D. (2000). Using Bayesian networks to analyze expression data. J Comput Biol *7*, 601-620.

Friedrich, P. (2004). The intriguing Ca2+ requirement of calpain activation. Biochem Biophys Res Commun *323*, 1131-1133.

Fujiwara, K., Masuda, M., Osawa, M., Kano, Y., and Katoh, K. (2001). Is PECAM-1 a mechanoresponsive molecule? Cell Struct Funct *26*, 11-17.

Fung, Y. C. (1981). The lung--a perspective of biomechanics development. J Biomech Eng *103*, 91-96.

Fung, Y. C., and Liu, S. Q. (1993). Elementary mechanics of the endothelium of blood vessels. J Biomech Eng *115*, 1-12.

Furuta, Y., Ilic, D., Kanazawa, S., Takeda, N., Yamamoto, T., and Aizawa, S. (1995). Mesodermal defect in late phase of gastrulation by a targeted mutation of focal adhesion kinase, FAK. Oncogene *11*, 1989-1995.

Garcia, A. J., and Boettiger, D. (1999). Integrin-fibronectin interactions at the cell-material interface: initial integrin binding and signaling. Biomaterials *20*, 2427-2433.

Garcia, A. J., Takagi, J., and Boettiger, D. (1998). Two-stage activation for alpha5beta1 integrin binding to surface-adsorbed fibronectin. J Biol Chem *273*, 34710-34715.

Garcia, A. J., Vega, M. D., and Boettiger, D. (1999). Modulation of cell proliferation and differentiation through substrate-dependent changes in fibronectin conformation. Mol Biol Cell *10*, 785-798.

Geiger, B., Bershadsky, A., Pankov, R., and Yamada, K. M. (2001). Transmembrane crosstalk between the extracellular matrix--cytoskeleton crosstalk. Nat Rev Mol Cell Biol *2*, 793-805.

George, E. L., Baldwin, H. S., and Hynes, R. O. (1997). Fibronectins are essential for heart and blood vessel morphogenesis but are dispensable for initial specification of precursor cells. Blood *90*, 3073-3081.

Giannone, G., Jiang, G., Sutton, D. H., Critchley, D. R., and Sheetz, M. P. (2003). Talin1 is critical for force-dependent reinforcement of initial integrin-cytoskeleton bonds but not tyrosine kinase activation. J Cell Biol *163*, 409-419.

Giannone, G., Ronde, P., Gaire, M., Beaudouin, J., Haiech, J., Ellenberg, J., and Takeda, K. (2004). Calcium rises locally trigger focal adhesion disassembly and enhance residency of focal adhesion kinase at focal adhesions. J Biol Chem *279*, 28715-28723.

Gibson, J. M. (1989). Simulated evolution and artificial selection. Biosystems *23*, 219-228; discussion 229.

Gillespie, D.T. (1977). Exact stochastic simulation of coupled chemical reactions. J Phys Chem *81*, 2340–2361.

Gimbrone, M. A., Jr., Topper, J. N., Nagel, T., Anderson, K. R., and Garcia-Cardena, G. (2000). Endothelial dysfunction, hemodynamic forces, and atherogenesis. Ann N Y Acad Sci *902*, 230-239; discussion 239-240.

Goldbeter, A., Dupont, G., and Berridge, M. J. (1990). Minimal model for signal-induced Ca2+ oscillations and for their frequency encoding through protein phosphorylation. Proc Natl Acad Sci U S A *87*, 1461-1465.

Goldmann, W. H. (2000). Kinetic determination of focal adhesion protein formation. Biochem Biophys Res Commun *271*, 553-557.

Goll, D. E., Thompson, V. F., Li, H., Wei, W., and Cong, J. (2003). The calpain system. Physiol Rev *83*, 731-801.

Goll, D. E., Thompson, V. F., Taylor, R. G., and Zalewska, T. (1992). Is calpain activity regulated by membranes and autolysis or by calcium and calpastatin? Bioessays *14*, 549-556.

Gough, N. R. (2002). Science's signal transduction knowledge environment: the connections maps database. Ann N Y Acad Sci *971*, 585-587.

Gu, J., Sumida, Y., Sanzen, N., and Sekiguchi, K. (2001). Laminin-10/11 and fibronectin differentially regulate integrin-dependent Rho and Rac activation via p130(Cas)-CrkII-DOCK180 pathway. J Biol Chem *276*, 27090-27097.

Gu, Y. Q., Anderson, O. D., Londeore, C. F., Kong, X., Chibbar, R. N., and Lazo, G. R. (2003). Structural organization of the barley D-hordein locus in comparison with its orthologous regions of wheat genomes. Genome *46*, 1084-1097.

Guan, J. L., and Shalloway, D. (1992). Regulation of focal adhesion-associated protein tyrosine kinase by both cellular adhesion and oncogenic transformation. Nature *358*, 690-692.

Gudi, S., Nolan, J. P., and Frangos, J. A. (1998). Modulation of GTPase activity of G proteins by fluid shear stress and phospholipid composition. Proc Natl Acad Sci U S A *95*, 2515-2519.

Gudi, S. R., Clark, C. B., and Frangos, J. A. (1996). Fluid flow rapidly activates G proteins in human endothelial cells. Involvement of G proteins in mechanochemical signal transduction. Circ Res *79*, 834-839.

Guet, C. C., Elowitz, M. B., Hsing, W., and Leibler, S. (2002). Combinatorial synthesis of genetic networks. Science *296*, 1466-1470.

Hagel, M., George, E. L., Kim, A., Tamimi, R., Opitz, S. L., Turner, C. E., Imamoto, A., and Thomas, S. M. (2002). The adaptor protein paxillin is essential for normal development in the mouse and is a critical transducer of fibronectin signaling. Mol Cell Biol *22*, 901-915.

Haidekker, M. A., L'Heureux, N., and Frangos, J. A. (2000). Fluid shear stress increases membrane fluidity in endothelial cells: a study with DCVJ fluorescence. Am J Physiol Heart Circ Physiol *278*, H1401-1406.

Hamill, O. P., and Martinac, B. (2001). Molecular basis of mechanotransduction in living cells. Physiol Rev *81*, 685-740.

Harada, N., Masuda, M., and Fujiwara, K. (1995). Fluid flow and osmotic stress induce tyrosine phosphorylation of an endothelial cell 128 kDa surface glycoprotein. Biochem Biophys Res Commun *214*, 69-74.

Hardy, S., and Robillard, P. N. (2004). Modeling and simulation of molecular biology systems using petri nets: modeling goals of various approaches. J Bioinform Comput Biol *2*, 595-613.

Harte, M. T., Hildebrand, J. D., Burnham, M. R., Bouton, A. H., and Parsons, J. T. (1996). p130Cas, a substrate associated with v-Src and v-Crk, localizes to focal adhesions and binds to focal adhesion kinase. J Biol Chem *271*, 13649-13655.

Hartwell, L. H., Hopfield, J. J., Leibler, S., and Murray, A. W. (1999). From molecular to modular cell biology. Nature *402*, C47-52.

Harvey, S. C., Prabhakaran, M., Mao, B., and McCammon, J. A. (1984). Phenylalanine transfer RNA: molecular dynamics simulation. Science *223*, 1189-1191.

Hawkins, J., and Boden, M. (2006). Detecting and sorting targeting peptides with neural networks and support vector machines. J Bioinform Comput Biol *4*, 1-18.

Helmlinger, G., Berk, B. C., and Nerem, R. M. (1995). Calcium responses of endothelial cell monolayers subjected to pulsatile and steady laminar flow differ. Am J Physiol *269*, C367-375.

Helmlinger, G., Berk, B. C., and Nerem, R. M. (1996). Pulsatile and steady flow-induced calcium oscillations in single cultured endothelial cells. J Vasc Res *33*, 360-369.

Helmlinger, G., Geiger, R. V., Schreck, S., and Nerem, R. M. (1991). Effects of pulsatile flow on cultured vascular endothelial cell morphology. J Biomech Eng *113*, 123-131.

Hildebrand, J. D., Schaller, M. D., and Parsons, J. T. (1993). Identification of sequences required for the efficient localization of the focal adhesion kinase, pp125FAK, to cellular focal adhesions. J Cell Biol *123*, 993-1005.

Hildebrand, J. D., Schaller, M. D., and Parsons, J. T. (1995). Paxillin, a tyrosine phosphorylated focal adhesion-associated protein binds to the carboxyl terminal domain of focal adhesion kinase. Mol Biol Cell *6*, 637-647.

Hlavacek, W.S., Faeder, J.R., Blinov, M.L., Perelson, A.S., Goldstein B. (2003). The complexity of complexes in signal transduction. Biotech Bioeng *84*, 783-794

Hocking, D. C., Smith, R. K., and McKeown-Longo, P. J. (1996). A novel role for the integrin-binding III-10 module in fibronectin matrix assembly. J Cell Biol *133*, 431-444.

Hoffmann, A., Levchenko, A., Scott, M. L., and Baltimore, D. (2002). The IkappaB-NF-kappaB signaling module: temporal control and selective gene activation. Science *298*, 1241-1245.

Hoffmann, R., Krallinger, M., Andres, E., Tamames, J., Blaschke, C., and Valencia, A. (2005). Text mining for metabolic pathways, signaling cascades, and protein networks. Sci STKE *2005*, pe21.

Hooke, R., and Jeeves TA. (1961). 'Direct search' solution of numerical and statistical problems. J Assoc Comp Mach *8*, 212-229

Hotchin, N. A., Kidd, A. G., Altroff, H., and Mardon, H. J. (1999). Differential activation of focal adhesion kinase, Rho and Rac by the ninth and tenth FIII domains of fibronectin. J Cell Sci *112 (Pt 17)*, 2937-2946.

Hoyer, J., Distler, A., Haase, W., and Gogelein, H. (1994). Ca2+ influx through stretch-activated cation channels activates maxi K+ channels in porcine endocardial endothelium. Proc Natl Acad Sci U S A *91*, 2367-2371.

Hua, C. T., Gamble, J. R., Vadas, M. A., and Jackson, D. E. (1998). Recruitment and activation of SHP-1 protein-tyrosine phosphatase by human platelet endothelial cell adhesion molecule-1 (PECAM-1). Identification of immunoreceptor tyrosine-based inhibitory motif-like binding motifs and substrates. J Biol Chem *273*, 28332-28340.

Huang, H. W., Goldberg, E. M., and Zidovetzki, R. (1996). Ceramide induces structural defects into phosphatidylcholine bilayers and activates phospholipase A2. Biochem Biophys Res Commun *220*, 834-838.

Huang, S. (1999). Gene expression profiling, genetic networks, and cellular states: an integrating concept for tumorigenesis and drug discovery. J Mol Med *77*, 469-480.

Hughes, P. E., Diaz-Gonzalez, F., Leong, L., Wu, C., McDonald, J. A., Shattil, S. J., and Ginsberg, M. H. (1996). Breaking the integrin hinge. A defined structural constraint regulates integrin signaling. J Biol Chem *271*, 6571-6574.

Humphries, M. J., McEwan, P. A., Barton, S. J., Buckley, P. A., Bella, J., and Mould, A. P. (2003). Integrin structure: heady advances in ligand binding, but activation still makes the knees wobble. Trends Biochem Sci *28*, 313-320.

Hwang, K. B., and Zhang, B. T. (2005). Bayesian model averaging of Bayesian network classifiers over multiple node-orders: application to sparse datasets. IEEE Trans Syst Man Cybern B Cybern *35*, 1302-1310.

Hynes, R. O. (1992). Integrins: versatility, modulation, and signaling in cell adhesion. Cell *69*, 11-25.

Ideker, T., Thorsson, V., Siegel, A. F., and Hood, L. E. (2000a). Testing for differentially-expressed genes by maximum-likelihood analysis of microarray data. J Comput Biol *7*, 805-817.

Ideker, T., Winslow, L. R., and Lauffenburger, A. D. (2006). Bioengineering and systems biology. Ann Biomed Eng *34*, 257-264.

Ideker, T. E., Thorsson, V., and Karp, R. M. (2000b). Discovery of regulatory interactions through perturbation: inference and experimental design. Pac Symp Biocomput, 305-316.

Imajoh, S., Kawasaki, H., and Suzuki, K. (1986). The amino-terminal hydrophobic region of the small subunit of calcium-activated neutral protease (CANP) is essential for its activation by phosphatidylinositol. J Biochem (Tokyo) *99*, 1281-1284.

Ingber, D. E. (2003). Mechanosensation through integrins: cells act locally but think globally. Proc Natl Acad Sci U S A *100*, 1472-1474.

Ingham, K. C., Brew, S. A., Huff, S., and Litvinovich, S. V. (1997). Cryptic self-association sites in type III modules of fibronectin. J Biol Chem *272*, 1718-1724.

Isenberg, G., and Goldmann, W. H. (1998). Peptide-specific antibodies localize the major lipid binding sites of talin dimers to oppositely arranged N-terminal 47 kDa subdomains. FEBS Lett *426*, 165-170.

Ishida, T., Peterson, T. E., Kovach, N. L., and Berk, B. C. (1996). MAP kinase activation by flow in endothelial cells. Role of beta 1 integrins and tyrosine kinases. Circ Res *79*, 310-316.

Jafri, M. S., Vajda, S., Pasik, P., and Gillo, B. (1992). A membrane model for cytosolic calcium oscillations. A study using Xenopus oocytes. Biophys J *63*, 235-246.

Jalali, S., del Pozo, M. A., Chen, K., Miao, H., Li, Y., Schwartz, M. A., Shyy, J. Y., and Chien, S. (2001). Integrin-mediated mechanotransduction requires its dynamic interaction with specific extracellular matrix (ECM) ligands. Proc Natl Acad Sci U S A *98*, 1042-1046.

Jalali, S., Li, Y. S., Sotoudeh, M., Yuan, S., Li, S., Chien, S., and Shyy, J. Y. (1998). Shear stress activates p60src-Ras-MAPK signaling pathways in vascular endothelial cells. Arterioscler Thromb Vasc Biol *18*, 227-234.

Jeong, H., Tombor, B., Albert, R., Oltvai, Z. N., and Barabasi, A. L. (2000). The large-scale organization of metabolic networks. Nature *407*, 651-654.

Joshi-Tope, G., Gillespie, M., Vastrik, I., D'Eustachio, P., Schmidt, E., de Bono, B., Jassal, B., Gopinath, G. R., Wu, G. R., Matthews, L., *et al.* (2005). Reactome: a knowledgebase of biological pathways. Nucleic Acids Res *33*, D428-432.

Kaazempur Mofrad, M. R., Abdul-Rahim, N. A., Karcher, H., Mack, P. J., Yap, B., and Kamm, R. D. (2005). Exploring the molecular basis for mechanosensation, signal transduction, and cytoskeletal remodeling. Acta Biomater *1*, 281-293.

Kamm, R. D. (2002). Cellular fluid mechanics. Annu Rev Fluid Mech *34*, 211-232.

Kamm, R. D., and Kaazempur-Mofrad, M. R. (2004). On the molecular basis for mechanotransduction. Mech Chem Biosyst *1*, 201-209.

Kanai, A.J., Strauss, H.C., Truskey, G.A., Crews, A.L., Grunfeld, S., Malinski, T. (1995). Shear stress induces ATP-independent transient nitric oxide release from vascular endothelial cells, measured directly with a porphyrinic microsensor. Circ Res *77*, 284-93

Kanehisa, M. (2002). The KEGG database. Novartis Found Symp *247*, 91-101; discussion 101-103, 119-128, 244-152.

Kapprell, H. P., and Goll, D. E. (1989). Effect of Ca2+ on binding of the calpains to calpastatin. J Biol Chem *264*, 17888-17896.

Karcher, H., Lammerding, J., Huang, H., Lee, R. T., Kamm, R. D., and Kaazempur-Mofrad, M. R. (2003). A three-dimensional viscoelastic model for cell deformation with experimental verification. Biophys J *85*, 3336-3349.

Karp, P. D., Ouzounis, C. A., Moore-Kochlacs, C., Goldovsky, L., Kaipa, P., Ahren, D., Tsoka, S., Darzentas, N., Kunin, V., and Lopez-Bigas, N. (2005). Expansion of the BioCyc collection of pathway/genome databases to 160 genomes. Nucleic Acids Res *33*, 6083-6089.

Katsumi, A., Orr, A. W., Tzima, E., and Schwartz, M. A. (2004). Integrins in mechanotransduction. J Biol Chem *279*, 12001-12004.

Katz, B. Z., Miyamoto, S., Teramoto, H., Zohar, M., Krylov, D., Vinson, C., Gutkind, J. S., and Yamada, K. M. (2002). Direct transmembrane clustering and cytoplasmic dimerization of focal adhesion kinase initiates its tyrosine phosphorylation. Biochim Biophys Acta *1592*, 141-152.

Kauffman, S., Peterson, C., Samuelsson, B., and Troein, C. (2003). Random Boolean network models and the yeast transcriptional network. Proc Natl Acad Sci U S A *100*, 14796-14799.

Kholodenko, B. N. (2006). Cell-signalling dynamics in time and space. Nat Rev Mol Cell Biol *7*, 165-176.

Kholodenko, B. N., Demin, O. V., Moehren, G., and Hoek, J. B. (1999). Quantification of short term signaling by the epidermal growth factor receptor. J Biol Chem *274*, 30169-30181.

Kim, M., Carman, C. V., and Springer, T. A. (2003). Bidirectional transmembrane signaling by cytoplasmic domain separation in integrins. Science *301*, 1720-1725.

Kitano, H. (2002). Computational systems biology. Nature *420*, 206-210.

Kitano, H. (2003). Cancer robustness: tumour tactics. Nature *426*, 125.

Kitano, H. (2004). Biological robustness. Nat Rev Genet *5*, 826-837.

Kitano, H., Funahashi, A., Matsuoka, Y., and Oda, K. (2005). Using process diagrams for the graphical representation of biological networks. Nat Biotechnol *23*, 961-966.

Kohn, K. W. (1998). Functional capabilities of molecular network components controlling the mammalian G1/S cell cycle phase transition. Oncogene *16*, 1065-1075.

Kolpakov, F. A., Ananko, E. A., Kolesov, G. B., and Kolchanov, N. A. (1998). GeneNet: a gene network database and its automated visualization. Bioinformatics *14*, 529-537.

Kornberg, L., Earp, H. S., Parsons, J. T., Schaller, M., and Juliano, R. L. (1992). Cell adhesion or integrin clustering increases phosphorylation of a focal adhesion-associated tyrosine kinase. J Biol Chem *267*, 23439-23442.

Krammer, A., Lu, H., Isralewitz, B., Schulten, K., and Vogel, V. (1999). Forced unfolding of the fibronectin type III module reveals a tensile molecular recognition switch. Proc Natl Acad Sci U S A *96*, 1351-1356.

Krull, M., Pistor, S., Voss, N., Kel, A., Reuter, I., Kronenberg, D., Michael, H., Schwarzer, K., Potapov, A., Choi, C., *et al.* (2006). TRANSPATH: an information resource for storing and visualizing signaling pathways and their pathological aberrations. Nucleic Acids Res *34*, D546-551.

Krull, M., Voss, N., Choi, C., Pistor, S., Potapov, A., and Wingender, E. (2003). TRANSPATH: an integrated database on signal transduction and a tool for array analysis. Nucleic Acids Res *31*, 97-100.

Ku, D.N. (1997) Blood flow in arteries. Ann Rev Fluid Mech *29*, 399-434

Kumar, S., Maxwell, I. Z., Heisterkamp, A., Polte, T. R., Lele, T. P., Salanga, M., Mazur, E., and Ingber, D. E. (2006). Viscoelastic retraction of single living stress fibers and its impact on cell shape, cytoskeletal organization, and extracellular matrix mechanics. Biophys J *90*, 3762-3773.

Kutalik, Z., Cho, K.H.,Wolkenhauer, O., (2004). Optimal sampling time selection for parameter estimation in dynamic pathway modeling. BioSystems *75,* 43–55.

Kwan, H. Y., Leung, P. C., Huang, Y., and Yao, X. (2003). Depletion of intracellular Ca2+ stores sensitizes the flow-induced Ca2+ influx in rat endothelial cells. Circ Res *92*, 286-292.

Lane, R. D., Allan, D. M., and Mellgren, R. L. (1992). A comparison of the intracellular distribution of mu-calpain, m-calpain, and calpastatin in proliferating human A431 cells. Exp Cell Res *203*, 5-16.

Lauffenburger, D. A., and Linderman, J. J. (1993). Receptors : models for binding, trafficking, and signaling (New York: Oxford University Press).

Lee, R.M.K.W. (1989). Blood Vessel Changes in Hypertension: Structure and Function, Volume I, CRC Press.

Lehoux, S., Esposito, B., Merval, R., and Tedgui, A. (2005). Differential regulation of vascular focal adhesion kinase by steady stretch and pulsatility. Circulation *111*, 643-649.

Lele, T. P., Pendse, J., Kumar, S., Salanga, M., Karavitis, J., and Ingber, D. E. (2006a). Mechanical forces alter zyxin unbinding kinetics within focal adhesions of living cells. J Cell Physiol *207*, 187-194.

Lele, T. P., Thodeti, C. K., and Ingber, D. E. (2006b). Force meets chemistry: analysis of mechanochemical conversion in focal adhesions using fluorescence recovery after photobleaching. J Cell Biochem *97*, 1175-1183.

Lelkes, P., Samet, M. (1999). The Hemodynamic Environment of the Endothelium. In mechanical Forces and the Endothelium, edited by Peter Lelkes, Amsterdam: Gordon and Breach Publishing Group 1-28.

Levenberg, K. (1944). A method for the solution of certain non linear problems in least squares. Q. Applied Mathematics *2*, 164-168

Levesque, M. J., and Nerem, R. M. (1985). The elongation and orientation of cultured endothelial cells in response to shear stress. J Biomech Eng *107*, 341-347.

Li, S., Guan, J. L., and Chien, S. (2005a). Biochemistry and biomechanics of cell motility. Annu Rev Biomed Eng *7*, 105-150.

Li, S., Huang, N. F., and Hsu, S. (2005b). Mechanotransduction in endothelial cell migration. J Cell Biochem *96*, 1110-1126.

Li, S., Kim, M., Hu, Y. L., Jalali, S., Schlaepfer, D. D., Hunter, T., Chien, S., and Shyy, J. Y. (1997). Fluid shear stress activation of focal adhesion kinase. Linking to mitogen-activated protein kinases. J Biol Chem *272*, 30455-30462.

Liang, F., Lee, S. Y., Liang, J., Lawrence, D. S., and Zhang, Z. Y. (2005). The role of protein-tyrosine phosphatase 1B in integrin signaling. J Biol Chem *280*, 24857-24863.

Libby, P. (2003). Vascular biology of atherosclerosis: overview and state of the art. Am J Cardiol *91*, 3A-6A.

Liddington, R. C., and Ginsberg, M. H. (2002). Integrin activation takes shape. J Cell Biol *158*, 833-839.

Lim, K. L., Kolatkar, P. R., Ng, K. P., Ng, C. H., and Pallen, C. J. (1998). Interconversion of the kinetic identities of the tandem catalytic domains of receptor-like protein-tyrosine phosphatase PTPalpha by two point mutations is synergistic and substrate-dependent. J Biol Chem *273*, 28986-28993.

Lim, K. L., Lai, D. S., Kalousek, M. B., Wang, Y., and Pallen, C. J. (1997). Kinetic analysis of two closely related receptor-like protein-tyrosine-phosphatases, PTP alpha and PTP epsilon. Eur J Biochem *245*, 693-700.

Ling, K., Doughman, R. L., Firestone, A. J., Bunce, M. W., and Anderson, R. A. (2002). Type I gamma phosphatidylinositol phosphate kinase targets and regulates focal adhesions. Nature *420*, 89-93.

Ling, K., Doughman, R. L., Iyer, V. V., Firestone, A. J., Bairstow, S. F., Mosher, D. F., Schaller, M. D., and Anderson, R. A. (2003). Tyrosine phosphorylation of type Igamma phosphatidylinositol phosphate kinase by Src regulates an integrin-talin switch. J Cell Biol *163*, 1339-1349.

Lipfert, L., Haimovich, B., Schaller, M. D., Cobb, B. S., Parsons, J. T., and Brugge, J. S. (1992). Integrin-dependent phosphorylation and activation of the protein tyrosine kinase pp125FAK in platelets. J Cell Biol *119*, 905-912.

Liu, S. Q. (1999). Biomechanical basis of vascular tissue engineering. Crit Rev Biomed Eng *27*, 75-148.

Loeffler, M., Herkenrath, P., Wichmann, H. E., Lord, B. I., and Murphy, M. J., Jr. (1984). The kinetics of hematopoietic stem cells during and after hypoxia. A model analysis. Blut *49*, 427-439.

Lollar, P., Hoak, J. C., and Owen, W. G. (1980). Binding of thrombin to cultured human endothelial cells. Nonequilibrium aspects. J Biol Chem *255*, 10279-10283.

Longabaugh, W. J., Davidson, E. H., and Bolouri, H. (2005). Computational representation of developmental genetic regulatory networks. Dev Biol *283*, 1-16.

Lu, T. T., Barreuther, M., Davis, S., and Madri, J. A. (1997). Platelet endothelial cell adhesion molecule-1 is phosphorylatable by c-Src, binds Src-Src homology 2 domain, and exhibits immunoreceptor tyrosine-based activation motif-like properties. J Biol Chem *272*, 14442-14446.

Luo, B. H., Springer, T. A., and Takagi, J. (2004). A specific interface between integrin transmembrane helices and affinity for ligand. PLoS Biol *2*, e153.

Mackerle, J. (2005). Finite element modelling and simulations in cardiovascular mechanics and cardiology: a bibliography 1993-2004. Comput Methods Biomech Biomed Engin *8*, 59-81.

Mahadevan, L., and Matsudaira, P. (2000). Motility powered by supramolecular springs and ratchets. Science *288*, 95-100.

Makino, A., Prossnitz, E. R., Bunemann, M., Wang, J. M., Yao, W., and Schmid-Schonbein, G. W. (2006). G protein-coupled receptors serve as mechanosensors for fluid shear stress in neutrophils. Am J Physiol Cell Physiol *290*, C1633-1639.

Marieb, E.N. (2004). Human Anatomy and Physiology Laboratory Manual, 7th Edition, Benjamin-Cummings Publishing Co.

Martel, V., Racaud-Sultan, C., Dupe, S., Marie, C., Paulhe, F., Galmiche, A., Block, M. R., and Albiges-Rizo, C. (2001). Conformation, localization, and integrin binding of talin depend on its interaction with phosphoinositides. J Biol Chem *276*, 21217-21227.

Masuda, M., Osawa, M., Shigematsu, H., Harada, N., and Fujiwara, K. (1997). Platelet endothelial cell adhesion molecule-1 is a major SH-PTP2 binding protein in vascular endothelial cells. FEBS Lett *408*, 331-336.

Matthews, B. D., Overby, D. R., Alenghat, F. J., Karavitis, J., Numaguchi, Y., Allen, P. G., and Ingber, D. E. (2004). Mechanical properties of individual focal adhesions probed with a magnetic microneedle. Biochem Biophys Res Commun *313*, 758-764.

Mazzag, B. M., Tamaresis, J. S., and Barakat, A. I. (2003). A model for shear stress sensing and transmission in vascular endothelial cells. Biophys J *84*, 4087-4101.

McAdams, H. H., and Arkin, A. (1999). It's a noisy business! Genetic regulation at the nanomolar scale. Trends Genet *15*, 65-69.

McKeown-Longo, P. J., and Mosher, D. F. (1985). Interaction of the 70,000-mol-wt amino-terminal fragment of fibronectin with the matrix-assembly receptor of fibroblasts. J Cell Biol *100*, 364-374.

McLeod, S. J., Shum, A. J., Lee, R. L., Takei, F., and Gold, M. R. (2004). The Rap GTPases regulate integrin-mediated adhesion, cell spreading, actin polymerization, and Pyk2 tyrosine phosphorylation in B lymphocytes. J Biol Chem *279*, 12009-12019.

Melloni, E., Michetti, M., Salamino, F., Minafra, R., and Pontremoli, S. (1996). Modulation of the calpain autoproteolysis by calpastatin and phospholipids. Biochem Biophys Res Commun *229*, 193-197.

Melloni, E., Michetti, M., Salamino, F., and Pontremoli, S. (1998). Molecular and functional properties of a calpain activator protein specific for mu-isoforms. J Biol Chem *273*, 12827-12831.

Mendes, P. (1993). GEPASI: a software package for modelling the dynamics, steady states and control of biochemical and other systems. Comput Appl Biosci *9*, 563-571.

Mendes, P., Kell, D.B., (1998). Non-linear optimization of biochemical pathways: applications to metabolic engineering and parameter estimation. Bioinformatics *14*, 869–883.

Meyer, T., and Stryer, L. (1988). Molecular model for receptor-stimulated calcium spiking. Proc Natl Acad Sci U S A *85*, 5051-5055.

Michalewicz, Z. (1994). Genetic algorithms + Data structures = Evolution programs, 3rd edn, Springer-Verlag, Berlin

Michetti, M., Viotti, P. L., Melloni, E., and Pontremoli, S. (1991). Mechanism of action of the calpain activator protein in rat skeletal muscle. Eur J Biochem *202*, 1177-1180.

Mitra, S. K., Hanson, D. A., and Schlaepfer, D. D. (2005). Focal adhesion kinase: in command and control of cell motility. Nat Rev Mol Cell Biol *6*, 56-68.

Moldoveanu, T., Hosfield, C. M., Lim, D., Elce, J. S., Jia, Z., and Davies, P. L. (2002). A Ca(2+) switch aligns the active site of calpain. Cell *108*, 649-660.

Moles, C.G., Mendes, P., Banga, J.R., (2003). Parameter estimation in biochemical pathways: a comparison of global optimization methods. Genome Research *13,* 2467–2474.

Moon, S. Y., and Zheng, Y. (2003). Rho GTPase-activating proteins in cell regulation. Trends Cell Biol *13*, 13-22.

Morla, A., Zhang, Z., and Ruoslahti, E. (1994). Superfibronectin is a functionally distinct form of fibronectin. Nature *367*, 193-196.

Morohashi, M., Winn, A. E., Borisuk, M. T., Bolouri, H., Doyle, J., and Kitano, H. (2002). Robustness as a measure of plausibility in models of biochemical networks. J Theor Biol *216*, 19-30.

Morton-Firth, C. J., and Bray, D. (1998). Predicting temporal fluctuations in an intracellular signalling pathway. J Theor Biol *192*, 117-128.

Mouritsen, O. G., and Bloom, M. (1984). Mattress model of lipid-protein interactions in membranes. Biophys J *46*, 141-153.

Mouritsen, O. G., and Bloom, M. (1993). Models of lipid-protein interactions in membranes. Annu Rev Biophys Biomol Struct *22*, 145-171.

Munevar, S., Wang, Y. L., and Dembo, M. (2004). Regulation of mechanical interactions between fibroblasts and the substratum by stretch-activated Ca2+ entry. J Cell Sci *117*, 85-92.

Naganuma, Y., Satoh, K., Yi, Q., Asazuma, N., Yatomi, Y., and Ozaki, Y. (2004). Cleavage of platelet endothelial cell adhesion molecule-1 (PECAM-1) in platelets exposed to high shear stress. J Thromb Haemost *2*, 1998-2008.

Nagasaki, M., Doi, A., Matsuno, H., and Miyano, S. (2004). A versatile petri net based architecture for modeling and simulation of complex biological processes. Genome Inform *15*, 180-197.

Nakache, M., and Gaub, H. E. (1988). Hydrodynamic hyperpolarization of endothelial cells. Proc Natl Acad Sci U S A *85*, 1841-1843.

Nash, S.G. (1984). Newton-type minimization via the Lanczos method. SIAM J. Numer. Anal *21*, 770-788

Nerem, R. M., Levesque, M. J., and Cornhill, J. F. (1981). Vascular endothelial morphology as an indicator of the pattern of blood flow. J Biomech Eng *103*, 172-176.

Neves, S. R., and Iyengar, R. (2002). Modeling of signaling networks. Bioessays *24*, 1110-1117.

Ng, A., Bursteinas, B., Gao, Q., Mollison, E., and Zvelebil, M. (2006). pSTIING: a 'systems' approach towards integrating signalling pathways, interaction and transcriptional regulatory networks in inflammation and cancer. Nucleic Acids Res *34*, D527-534.

Nilius, B., and Droogmans, G. (2001). Ion channels and their functional role in vascular endothelium. Physiol Rev *81*, 1415-1459.

Noble, D. (1960). Cardiac action and pacemaker potentials based on the Hodgkin-Huxley equations. Nature *188*, 495-497.

Noble, D. (2002). Modelling the heart: insights, failures and progress. Bioessays *24*, 1155-1163.

Noble, D. (2004). Modeling the heart. Physiology (Bethesda) *19*, 191-197.

Noble, D. (2006). Systems biology and the heart. Biosystems *83*, 75-80.

Novartis_Foundation, 2001. Complexity in biological information processing.. Chichester, Wiley.

Oda, K., Matsuoka, Y., Funahashi, A., and Kitano, H. (2005). A comprehensive pathway map of epidermal growth factor receptor signaling. Mol Syst Biol *1*, 2005 0010.

Ogata, T. (2003). Increase in epidermal growth factor receptor protein induced in osteoblastic cells after exposure to flow of culture media. Am J Physiol Cell Physiol *285*, C425-432.

Okada, M., and Nakagawa, H. (1989). A protein tyrosine kinase involved in regulation of pp60c-src function. J Biol Chem *264*, 20886-20893.

Olesen, S. P., Clapham, D. E., and Davies, P. F. (1988). Haemodynamic shear stress activates a K+ current in vascular endothelial cells. Nature *331*, 168-170.

Osawa, M., Masuda, M., Harada, N., Lopes, R. B., and Fujiwara, K. (1997). Tyrosine phosphorylation of platelet endothelial cell adhesion molecule-1 (PECAM-1, CD31) in mechanically stimulated vascular endothelial cells. Eur J Cell Biol *72*, 229-237.

Osawa, M., Masuda, M., Kusano, K., and Fujiwara, K. (2002). Evidence for a role of platelet endothelial cell adhesion molecule-1 in endothelial cell mechanosignal transduction: is it a mechanoresponsive molecule? J Cell Biol *158*, 773-785.

Otsuka, Y., and Goll, D. E. (1987). Purification of the Ca2+-dependent proteinase inhibitor from bovine cardiac muscle and its interaction with the millimolar Ca2+-dependent proteinase. J Biol Chem *262*, 5839-5851.

Owen, J. D., Ruest, P. J., Fry, D. W., and Hanks, S. K. (1999). Induced focal adhesion kinase (FAK) expression in FAK-null cells enhances cell spreading and migration requiring both auto- and activation loop phosphorylation sites and inhibits adhesion-dependent tyrosine phosphorylation of Pyk2. Mol Cell Biol *19*, 4806-4818.

Ozbudak, E. M., Thattai, M., Lim, H. N., Shraiman, B. I., and Van Oudenaarden, A. (2004). Multistability in the lactose utilization network of Escherichia coli. Nature *427*, 737-740.

Pal, G. P., Elce, J. S., and Jia, Z. (2001). Dissociation and aggregation of calpain in the presence of calcium. J Biol Chem *276*, 47233-47238.

Palecek, S. P., Horwitz, A. F., and Lauffenburger, D. A. (1999). Kinetic model for integrin-mediated adhesion release during cell migration. Ann Biomed Eng *27*, 219-235.

Pallen, C. J. (1993). The receptor-like protein tyrosine phosphatase alpha: a role in cell proliferation and oncogenesis. Semin Cell Biol *4*, 403-408.

Pallen, C. J. (2003). Protein tyrosine phosphatase alpha (PTPalpha): a Src family kinase activator and mediator of multiple biological effects. Curr Top Med Chem *3*, 821-835.

Papadaki, M., and Eskin, S. G. (1997). Effects of fluid shear stress on gene regulation of vascular cells. Biotechnol Prog *13*, 209-221.

Parsons, J. T. (2003). Focal adhesion kinase: the first ten years. J Cell Sci *116*, 1409-1416.

Parsons, J. T., Martin, K. H., Slack, J. K., Taylor, J. M., and Weed, S. A. (2000). Focal adhesion kinase: a regulator of focal adhesion dynamics and cell movement. Oncogene *19*, 5606-5613.

Patuzzi, R. (1998). The Goldman-Hodgkin-Katz equation and graphical 'load-line' analysis of ionic flow through outer hair cells. Hear Res *125*, 71-97.

Pe'er, D., Regev, A., Elidan, G., and Friedman, N. (2001). Inferring subnetworks from perturbed expression profiles. Bioinformatics *17 Suppl 1*, S215-224.

Peleg, M., Yeh, I., and Altman, R. B. (2002). Modelling biological processes using workflow and Petri Net models. Bioinformatics *18*, 825-837.

Pelham, R. J., Jr., and Wang, Y. (1997). Cell locomotion and focal adhesions are regulated by substrate flexibility. Proc Natl Acad Sci U S A *94*, 13661-13665.

Peri, S., Navarro, J. D., Kristiansen, T. Z., Amanchy, R., Surendranath, V., Muthusamy, B., Gandhi, T. K., Chandrika, K. N., Deshpande, N., Suresh, S., *et al.* (2004). Human protein reference database as a discovery resource for proteomics. Nucleic Acids Res *32*, D497-501.

Playford, M. P., and Schaller, M. D. (2004). The interplay between Src and integrins in normal and tumor biology. Oncogene *23*, 7928-7946.

Ponniah, S., Wang, D. Z., Lim, K. L., and Pallen, C. J. (1999). Targeted disruption of the tyrosine phosphatase PTPalpha leads to constitutive downregulation of the kinases Src and Fyn. Curr Biol *9*, 535-538.

Popp, R., Hoyer, J., Meyer, J., Galla, H. J., and Gogelein, H. (1992). Stretch-activated non-selective cation channels in the antiluminal membrane of porcine cerebral capillaries. J Physiol *454*, 435-449.

Prado, C. M., Ramos, S. G., Alves-Filho, J. C., Elias, J., Jr., Cunha, F. Q., and Rossi, M. A. (2006). Turbulent flow/low wall shear stress and stretch differentially affect aorta remodeling in rats. J Hypertens *24*, 503-515.

Putney, J. W., Jr., Broad, L. M., Braun, F. J., Lievremont, J. P., and Bird, G. S. (2001). Mechanisms of capacitative calcium entry. J Cell Sci *114*, 2223-2229.

Rand, D. A., and Wilson, H. B. (1991). Chaotic stochasticity: a ubiquitous source of unpredictability in epidemics. Proc Biol Sci *246*, 179-184.

Ratnikov, B. I., Partridge, A. W., and Ginsberg, M. H. (2005). Integrin activation by talin. J Thromb Haemost *3*, 1783-1790.

Reedquist, K. A., Ross, E., Koop, E. A., Wolthuis, R. M., Zwartkruis, F. J., van Kooyk, Y., Salmon, M., Buckley, C. D., and Bos, J. L. (2000). The small GTPase, Rap1, mediates CD31-induced integrin adhesion. J Cell Biol *148*, 1151-1158.

Reguera, D., Rubi, J. M., and Vilar, J. M. (2005). The mesoscopic dynamics of thermodynamic systems. J Phys Chem B Condens Matter Mater Surf Interfaces Biophys *109*, 21502-21515.

Resnick, N., Yahav, H., Shay-Salit, A., Shushy, M., Schubert, S., Zilberman, L. C., and Wofovitz, E. (2003). Fluid shear stress and the vascular endothelium: for better and for worse. Prog Biophys Mol Biol *81*, 177-199.

Reverter, D., Sorimachi, H., and Bode, W. (2001a). The structure of calcium-free human m-calpain: implications for calcium activation and function. Trends Cardiovasc Med *11*, 222-229.

Reverter, D., Strobl, S., Fernandez-Catalan, C., Sorimachi, H., Suzuki, K., and Bode, W. (2001b). Structural basis for possible calcium-induced activation mechanisms of calpains. Biol Chem *382*, 753-766.

Ridley, A.J.(2001). Rho GTPases and cell migration J Cell Sci. *114*, 2713-2722

Ridley, A. J. (2004). Pulling back to move forward. Cell *116*, 357-358.

Ridley, A. J., Schwartz, M. A., Burridge, K., Firtel, R. A., Ginsberg, M. H., Borisy, G., Parsons, J. T., and Horwitz, A. R. (2003). Cell migration: integrating signals from front to back. Science *302*, 1704-1709.

Rodriguez-Fernandez, M., Mendes, P., Banga J.R. (2005). A hybrid approach for efficient and robust parameter estimation in biochemical pathways. BioSystems 1-18

Roskoski, R., Jr. (2005). Src kinase regulation by phosphorylation and dephosphorylation. Biochem Biophys Res Commun *331*, 1-14.

Rott, N. (1990) "Note on the history of the Reynolds number,". Ann Rev of Fluid Mechs *22,* 1–11.

Rupp, P. A., and Little, C. D. (2001). Integrins in vascular development. Circ Res *89*, 566-572.

Sachs, F. (1986). Biophysics of mechanoreception. Membr Biochem *6*, 173-195.

Sachs, F. (1988). Mechanical transduction in biological systems. Crit Rev Biomed Eng *16*, 141-169.

Sachs, K., Perez, O., Pe'er, D., Lauffenburger, D. A., and Nolan, G. P. (2005). Causal protein-signaling networks derived from multiparameter single-cell data. Science *308*, 523-529.

Sai, X., Naruse, K., and Sokabe, M. (1999). Activation of pp60(src) is critical for stretch-induced orienting response in fibroblasts. J Cell Sci *112 (Pt 9)*, 1365-1373.

Saido, T. C., Nagao, S., Shiramine, M., Tsukaguchi, M., Yoshizawa, T., Sorimachi, H., Ito, H., Tsuchiya, T., Kawashima, S., and Suzuki, K. (1994a). Distinct kinetics of subunit autolysis in mammalian m-calpain activation. FEBS Lett *346*, 263-267.

Saido, T. C., Sorimachi, H., and Suzuki, K. (1994b). Calpain: new perspectives in molecular diversity and physiological-pathological involvement. Faseb J *8*, 814-822.

Sastry, S. K., and Horwitz, A. F. (1993). Integrin cytoplasmic domains: mediators of cytoskeletal linkages and extra- and intracellular initiated transmembrane signaling. Curr Opin Cell Biol *5*, 819-831.

Sato, M., Levesque, M. J., and Nerem, R. M. (1987). An application of the micropipette technique to the measurement of the mechanical properties of cultured bovine aortic endothelial cells. J Biomech Eng *109*, 27-34.

Sato, M., and Ohashi, T. (2005). Biorheological views of endothelial cell responses to mechanical stimuli. Biorheology *42*, 421-441.

Sato, M., Ohshima, N., and Nerem, R. M. (1996). Viscoelastic properties of cultured porcine aortic endothelial cells exposed to shear stress. J Biomech *29*, 461-467.

Sauro, H. M. (1993). SCAMP: a general-purpose simulator and metabolic control analysis program. Comput Appl Biosci *9*, 441-450.

Sawada, Y., and Sheetz, M. P. (2002). Force transduction by Triton cytoskeletons. J Cell Biol *156*, 609-615.

Schacherer, F., Choi, C., Gotze, U., Krull, M., Pistor, S., and Wingender, E. (2001). The TRANSPATH signal transduction database: a knowledge base on signal transduction networks. Bioinformatics *17*, 1053-1057.

Schachter, M. (1997a). Calcium antagonists and atherosclerosis. Int J Cardiol *62 Suppl 2*, S9-15.

Schachter, M. (1997b). Vascular smooth muscle cell migration, atherosclerosis, and calcium channel blockers. Int J Cardiol *62 Suppl 2*, S85-90.

Schaller, M. D. (2001). Biochemical signals and biological responses elicited by the focal adhesion kinase. Biochim Biophys Acta *1540*, 1-21.

Schaller, M. D., Hildebrand, J. D., and Parsons, J. T. (1999). Complex formation with focal adhesion kinase: A mechanism to regulate activity and subcellular localization of Src kinases. Mol Biol Cell *10*, 3489-3505.

Schaller, M. D., Hildebrand, J. D., Shannon, J. D., Fox, J. W., Vines, R. R., and Parsons, J. T. (1994). Autophosphorylation of the focal adhesion kinase, pp125FAK, directs SH2-dependent binding of pp60src. Mol Cell Biol *14*, 1680-1688.

Schaller, M. D., Otey, C. A., Hildebrand, J. D., and Parsons, J. T. (1995). Focal adhesion kinase and paxillin bind to peptides mimicking beta integrin cytoplasmic domains. J Cell Biol *130*, 1181-1187.

Schaller, M. D., and Parsons, J. T. (1995). pp125FAK-dependent tyrosine phosphorylation of paxillin creates a high-affinity binding site for Crk. Mol Cell Biol *15*, 2635-2645.

Schilling, W. P., and Elliott, S. J. (1992). Ca2+ signaling mechanisms of vascular endothelial cells and their role in oxidant-induced endothelial cell dysfunction. Am J Physiol *262*, H1617-1630.

Schlaepfer, D. D., Hanks, S. K., Hunter, T., and van der Geer, P. (1994). Integrin-mediated signal transduction linked to Ras pathway by GRB2 binding to focal adhesion kinase. Nature *372*, 786-791.

Schlaepfer, D. D., and Hunter, T. (1998). Integrin signalling and tyrosine phosphorylation: just the FAKs? Trends Cell Biol *8*, 151-157.

Schlaepfer, D. D., and Mitra, S. K. (2004). Multiple connections link FAK to cell motility and invasion. Curr Opin Genet Dev *14*, 92-101.

Schlaepfer, D. D., Mitra, S. K., and Ilic, D. (2004). Control of motile and invasive cell phenotypes by focal adhesion kinase. Biochim Biophys Acta *1692*, 77-102.

Schlichting, H., (1968). Boundary Layer Theory. McGraw-Hill, New York.

Schoeberl, B., Eichler-Jonsson, C., Gilles, E. D., and Muller, G. (2002). Computational modeling of the dynamics of the MAP kinase cascade activated by surface and internalized EGF receptors. Nat Biotechnol *20*, 370-375.

Scholey, J. M., Brust-Mascher, I., and Mogilner, A. (2003). Cell division. Nature *422*, 746-752.

Schomburg, I., Chang, A., Hofmann, O., Ebeling, C., Ehrentreich, F., and Schomburg, D. (2002). BRENDA: a resource for enzyme data and metabolic information. Trends Biochem Sci *27*, 54-56.

Schwartz, M. A., and Ginsberg, M. H. (2002). Networks and crosstalk: integrin signalling spreads. Nat Cell Biol *4*, E65-68.

Schwartz, M. A., Schaller, M. D., and Ginsberg, M. H. (1995). Integrins: emerging paradigms of signal transduction. Annu Rev Cell Dev Biol *11*, 549-599.

Scott, J. (2004). Pathophysiology and biochemistry of cardiovascular disease. Curr Opin Gen & Dev *14*, 271-279

Selkov, E., Basmanova, S., Gaasterland, T., Goryanin, I., Gretchkin, Y., Maltsev, N., Nenashev, V., Overbeek, R., Panyushkina, E., Pronevitch, L., *et al.* (1996). The metabolic pathway collection from EMP: the enzymes and metabolic pathways database. Nucleic Acids Res *24*, 26-28.

Senger, D. R., Claffey, K. P., Benes, J. E., Perruzzi, C. A., Sergiou, A. P., and Detmar, M. (1997). Angiogenesis promoted by vascular endothelial growth factor: regulation through alpha1beta1 and alpha2beta1 integrins. Proc Natl Acad Sci U S A *94*, 13612-13617.

Shafrir, Y., and Forgacs, G. (2002). Mechanotransduction through the cytoskeleton. Am J Physiol Cell Physiol *282*, C479-486.

Shannon, P., Markiel, A., Ozier, O., Baliga, N. S., Wang, J. T., Ramage, D., Amin, N., Schwikowski, B., and Ideker, T. (2003). Cytoscape: a software environment for integrated models of biomolecular interaction networks. Genome Res *13*, 2498-2504.

Sheetz, M. P., Felsenfeld, D. P., and Galbraith, C. G. (1998). Cell migration: regulation of force on extracellular-matrix-integrin complexes. Trends Cell Biol *8*, 51-54.

Shen, J., Luscinskas, F. W., Connolly, A., Dewey, C. F., Jr., and Gimbrone, M. A., Jr. (1992). Fluid shear stress modulates cytosolic free calcium in vascular endothelial cells. Am J Physiol *262*, C384-390.

Shen, Y., Lyons, P., Cooley, M., Davidson, D., Veillette, A., Salgia, R., Griffin, J. D., and Schaller, M. D. (2000). The noncatalytic domain of protein-tyrosine phosphatase-PEST targets paxillin for dephosphorylation in vivo. J Biol Chem *275*, 1405-1413.

Shen, Y., Schneider, G., Cloutier, J. F., Veillette, A., and Schaller, M. D. (1998). Direct association of protein-tyrosine phosphatase PTP-PEST with paxillin. J Biol Chem *273*, 6474-6481.

Shi, Q., and Boettiger, D. (2003). A novel mode for integrin-mediated signaling: tethering is required for phosphorylation of FAK Y397. Mol Biol Cell *14*, 4306-4315.

Shimaoka, M., Takagi, J., and Springer, T. A. (2002). Conformational regulation of integrin structure and function. Annu Rev Biophys Biomol Struct *31*, 485-516.

Shimonaka, M., Katagiri, K., Nakayama, T., Fujita, N., Tsuruo, T., Yoshie, O., and Kinashi, T. (2003). Rap1 translates chemokine signals to integrin activation, cell polarization, and motility across vascular endothelium under flow. J Cell Biol *161*, 417-427.

Shmulevich, I., Dougherty, E. R., Kim, S., and Zhang, W. (2002a). Probabilistic Boolean Networks: a rule-based uncertainty model for gene regulatory networks. Bioinformatics *18*, 261-274.

Shmulevich, I., Dougherty, E. R., and Zhang, W. (2002b). Gene perturbation and intervention in probabilistic Boolean networks. Bioinformatics *18*, 1319-1331.

Shvartsman, S. Y., Muratov, C. B., and Lauffenburger, D. A. (2002). Modeling and computational analysis of EGF receptor-mediated cell communication in Drosophila oogenesis. Development *129*, 2577-2589.

Shyy, J. Y., and Chien, S. (2002). Role of integrins in endothelial mechanosensing of shear stress. Circ Res *91*, 769-775.

Sicheri, F., and Kuriyan, J. (1997). Structures of Src-family tyrosine kinases. Curr Opin Struct Biol *7*, 777-785.

Silkworth, J. B., McLean, B., and Stehbens, W. E. (1975). The effect of hypercholesterolemia on aortic endothelium studied en face. Atherosclerosis *22*, 335-348.
Skalak, R., Tozeren, A., Zarda, R. P., and Chien, S. (1973). Strain energy function of red blood cell membranes. Biophys J *13*, 245-264.

Sneyd, J., Keizer, J., and Sanderson, M. J. (1995). Mechanisms of calcium oscillations and waves: a quantitative analysis. Faseb J *9*, 1463-1472.

Somogyi, R., and Sniegoski, C.A. (1996). Modeling the complexity of genetic networks: Understanding multigene and pleiotropic regulation. Complexity *1*, 45

Sonnenburg, E. D., Bilwes, A., Hunter, T., and Noel, J. P. (2003). The structure of the membrane distal phosphatase domain of RPTPalpha reveals interdomain flexibility and an SH2 domain interaction region. Biochemistry *42*, 7904-7914.

Spiro, P. A., Parkinson, J. S., and Othmer, H. G. (1997). A model of excitation and adaptation in bacterial chemotaxis. Proc Natl Acad Sci U S A *94*, 7263-7268.

Spitzfaden, C., Grant, R. P., Mardon, H. J., and Campbell, I. D. (1997). Module-module interactions in the cell binding region of fibronectin: stability, flexibility and specificity. J Mol Biol *265*, 565-579.

Stelling, J., Sauer, U., Szallasi, Z., Doyle, F. J., 3rd, and Doyle, J. (2004). Robustness of cellular functions. Cell *118*, 675-685.

Stupack, D. G., and Cheresh, D. A. (2002). ECM remodeling regulates angiogenesis: endothelial integrins look for new ligands. Sci STKE *2002*, PE7.

Subramaniam, S. (2002). Bioinformatics of cellular signalling. Novartis Found Symp *247*, 104-116; discussion 116-108, 119-128, 244-152.

Suzuki, K. (1991). Nomenclature of calcium dependent proteinase. Biomed Biochim Acta *50*, 483-484.

Suzuki, K., Hata, S., Kawabata, Y., and Sorimachi, H. (2004). Structure, activation, and biology of calpain. Diabetes *53 Suppl 1*, S12-18.

Suzuki, K., Saido, T. C., and Hirai, S. (1992). Modulation of cellular signals by calpain. Ann N Y Acad Sci *674*, 218-227.

Suzuki, K., Shimizu, K., Hamamoto, T., Nakagawa, Y., Hamakubo, T., and Yamamuro, T. (1990). Biochemical demonstration of calpains and calpastatin in osteoarthritic synovial fluid. Arthritis Rheum *33*, 728-732.

Szallasi, Z. (1999). Genetic network analysis in light of massively parallel biological data acquisition. Pac Symp Biocomput, 5-16.

Tachibana, K., Sato, T., D'Avirro, N., and Morimoto, C. (1995). Direct association of pp125FAK with paxillin, the focal adhesion-targeting mechanism of pp125FAK. J Exp Med *182*, 1089-1099.

Tadokoro, S., Shattil, S. J., Eto, K., Tai, V., Liddington, R. C., de Pereda, J. M., Ginsberg, M. H., and Calderwood, D. A. (2003). Talin binding to integrin beta tails: a final common step in integrin activation. Science *302*, 103-106.

Takano, E., Ma, H., Yang, H. Q., Maki, M., and Hatanaka, M. (1995). Preference of calcium-dependent interactions between calmodulin-like domains of calpain and calpastatin subdomains. FEBS Lett *362*, 93-97.

Tanaka, T., Yamaguchi, R., Sabe, H., Sekiguchi, K., and Healy, J. M. (1996). Paxillin association in vitro with integrin cytoplasmic domain peptides. FEBS Lett *399*, 53-58.

Tang, Y., and Othmer, H. G. (1994). A G protein-based model of adaptation in Dictyostelium discoideum. Math Biosci *120*, 25-76.

Thomas, J. W., Cooley, M. A., Broome, J. M., Salgia, R., Griffin, J. D., Lombardo, C. R., and Schaller, M. D. (1999). The role of focal adhesion kinase binding in the regulation of tyrosine phosphorylation of paxillin. J Biol Chem *274*, 36684-36692.

Thomas, J. W., Ellis, B., Boerner, R. J., Knight, W. B., White, G. C., 2nd, and Schaller, M. D. (1998). SH2- and SH3-mediated interactions between focal adhesion kinase and Src. J Biol Chem *273*, 577-583.

Thomas, S. M., and Brugge, J. S. (1997). Cellular functions regulated by Src family kinases. Annu Rev Cell Dev Biol *13*, 513-609.

Thorburn WM. (1915). "Occam's razor," Mind *24,* 287-288

Tompa, P., Emori, Y., Sorimachi, H., Suzuki, K., and Friedrich, P. (2001). Domain III of calpain is a ca2+-regulated phospholipid-binding domain. Biochem Biophys Res Commun *280*, 1333-1339.

Tompa, P., Mucsi, Z., Orosz, G., and Friedrich, P. (2002). Calpastatin subdomains A and C are activators of calpain. J Biol Chem *277*, 9022-9026.

Tracy, S., van der Geer, P., and Hunter, T. (1995). The receptor-like protein-tyrosine phosphatase, RPTP alpha, is phosphorylated by protein kinase C on two serines close to the inner face of the plasma membrane. J Biol Chem *270*, 10587-10594.

Tran, Q. K., Ohashi, K., and Watanabe, H. (2000). Calcium signalling in endothelial cells. Cardiovasc Res *48*, 13-22.

Traub, O., and Berk, B. C. (1998). Laminar shear stress: mechanisms by which endothelial cells transduce an atheroprotective force. Arterioscler Thromb Vasc Biol *18*, 677-685.

Tseng, H., Peterson, T. E., and Berk, B. C. (1995). Fluid shear stress stimulates mitogen-activated protein kinase in endothelial cells. Circ Res *77*, 869-878.

Tullio, R. D., Passalacqua, M., Averna, M., Salamino, F., Melloni, E., and Pontremoli, S. (1999). Changes in intracellular localization of calpastatin during calpain activation. Biochem J *343 Pt 2*, 467-472.

Tumbarello, D. A., Brown, M. C., and Turner, C. E. (2002). The paxillin LD motifs. FEBS Lett *513*, 114-118.

Turner, C. E. (2000a). Paxillin and focal adhesion signalling. Nat Cell Biol *2*, E231-236.

Turner, C. E. (2000b). Paxillin interactions. J Cell Sci *113 Pt 23*, 4139-4140.

Turner, C. E., and Miller, J. T. (1994). Primary sequence of paxillin contains putative SH2 and SH3 domain binding motifs and multiple LIM domains: identification of a vinculin and pp125Fak-binding region. J Cell Sci *107 (Pt 6)*, 1583-1591.

Tyson, J. J., Csikasz-Nagy, A., and Novak, B. (2002). The dynamics of cell cycle regulation. Bioessays *24*, 1095-1109.

Tzima, E., Del Pozo, M. A., Kiosses, W. B., Mohamed, S. A., Li, S., Chien, S., and Schwartz, M. A. (2002). Activation of Rac1 by shear stress in endothelial cells mediates both cytoskeletal reorganization and effects on gene expression. Embo J *21*, 6791-6800.

Tzima, E., del Pozo, M. A., Shattil, S. J., Chien, S., and Schwartz, M. A. (2001). Activation of integrins in endothelial cells by fluid shear stress mediates Rho-dependent cytoskeletal alignment. Embo J *20*, 4639-4647.

Tzima, E., Irani-Tehrani, M., Kiosses, W. B., Dejana, E., Schultz, D. A., Engelhardt, B., Cao, G., DeLisser, H., and Schwartz, M. A. (2005). A mechanosensory complex that mediates the endothelial cell response to fluid shear stress. Nature *437*, 426-431.

Ugarova, T., Agbanyo, F. R., and Plow, E. F. (1995a). Conformational changes in adhesive proteins modulate their adhesive function. Thromb Haemost *74*, 253-257.

Ugarova, T. P., Zamarron, C., Veklich, Y., Bowditch, R. D., Ginsberg, M. H., Weisel, J. W., and Plow, E. F. (1995b). Conformational transitions in the cell binding domain of fibronectin. Biochemistry *34*, 4457-4466.

Valant, P. A., Adjei, P. N., and Haynes, D. H. (1992). Rapid Ca2+ extrusion via the Na+/Ca2+ exchanger of the human platelet. J Membr Biol *130*, 63-82.

Valgimigli, M., Squasi, P. A., Gaitani, S., Arcozzi, C., Martano, S., and Ferrari, R. (2005). [Markers of coronary damage. From diagnosis to prognosis]. Recenti Prog Med *96*, 566-572.

Valkema, R., and Van Haastert, P. J. (1994). A model for cAMP-mediated cGMP response in Dictyostelium discoideum. Mol Biol Cell *5*, 575-585.

Van Aelst, L., and D'Souza-Schorey, C. (1997). Rho GTPases and signaling networks. Genes Dev *11*, 2295-2322.

Varma, A., and Palsson, B. O. (1994). Stoichiometric flux balance models quantitatively predict growth and metabolic by-product secretion in wild-type Escherichia coli W3110. Appl Environ Microbiol *60*, 3724-3731.

Vinogradova, O., Velyvis, A., Velyviene, A., Hu, B., Haas, T., Plow, E., and Qin, J. (2002). A structural mechanism of integrin alpha(IIb)beta(3) "inside-out" activation as regulated by its cytoplasmic face. Cell *110*, 587-597.

Vinter, J.G., Gardner, M. (1994). Molecular modeling and drug design. McMillan, Basingstoke

von Bertalanffy, L. (1969). General System Theory, Revised Ed. (New York: George Braziller).

von Wichert, G., Haimovich, B., Feng, G. S., and Sheetz, M. P. (2003a). Force-dependent integrin-cytoskeleton linkage formation requires downregulation of focal complex dynamics by Shp2. Embo J *22*, 5023-5035.

von Wichert, G., Jiang, G., Kostic, A., De Vos, K., Sap, J., and Sheetz, M. P. (2003b). RPTP-alpha acts as a transducer of mechanical force on alphav/beta3-integrin-cytoskeleton linkages. J Cell Biol *161*, 143-153.

Vuori, K. (1998). Integrin signaling: tyrosine phosphorylation events in focal adhesions. J Membr Biol *165*, 191-199.

Wade, R., Bohl, J., and Vande Pol, S. (2002). Paxillin null embryonic stem cells are impaired in cell spreading and tyrosine phosphorylation of focal adhesion kinase. Oncogene *21*, 96-107.

Wang, D., Huang, X. Y., and Cole, P. A. (2001). Molecular determinants for Csk-catalyzed tyrosine phosphorylation of the Src tail. Biochemistry *40*, 2004-2010.

Wang, N., Butler, J. P., and Ingber, D. E. (1993). Mechanotransduction across the cell surface and through the cytoskeleton. Science *260*, 1124-1127.

Wang, Y., Chang, J., Li, Y. C., Li, Y. S., Shyy, J. Y., and Chien, S. (2004). Shear stress and VEGF activate IKK via the Flk-1/Cbl/Akt signaling pathway. Am J Physiol Heart Circ Physiol *286*, H685-692.

Wang, Y., Miao, H., Li, S., Chen, K. D., Li, Y. S., Yuan, S., Shyy, J. Y., and Chien, S. (2002). Interplay between integrins and FLK-1 in shear stress-induced signaling. Am J Physiol Cell Physiol *283*, C1540-1547.

Webb, D. J., Donais, K., Whitmore, L. A., Thomas, S. M., Turner, C. E., Parsons, J. T., and Horwitz, A. F. (2004). FAK-Src signalling through paxillin, ERK and MLCK regulates adhesion disassembly. Nat Cell Biol *6*, 154-161.

Wendt, A., Thompson, V. F., and Goll, D. E. (2004). Interaction of calpastatin with calpain: a review. Biol Chem *385*, 465-472.

Wiesner, T. F., Berk, B. C., and Nerem, R. M. (1996). A mathematical model of cytosolic calcium dynamics in human umbilical vein endothelial cells. Am J Physiol *270*, C1556-1569.

Wiesner, T. F., Berk, B. C., and Nerem, R. M. (1997). A mathematical model of the cytosolic-free calcium response in endothelial cells to fluid shear stress. Proc Natl Acad Sci U S A *94*, 3726-3731.

Winkler, J., Lunsdorf, H., and Jockusch, B. M. (1997). Energy-filtered electron microscopy reveals that talin is a highly flexible protein composed of a series of globular domains. Eur J Biochem *243*, 430-436.

Wixler, V., Laplantine, E., Geerts, D., Sonnenberg, A., Petersohn, D., Eckes, B., Paulsson, M., and Aumailley, M. (1999). Identification of novel interaction partners for the conserved membrane proximal region of alpha-integrin cytoplasmic domains. FEBS Lett *445*, 351-355.

Wojciak-Stothard, B., and Ridley, A. J. (2002). Rho GTPases and the regulation of endothelial permeability. Vascul Pharmacol *39*, 187-199.

Wojciak-Stothard, B., and Ridley, A. J. (2003). Shear stress-induced endothelial cell polarization is mediated by Rho and Rac but not Cdc42 or PI 3-kinases. J Cell Biol *161*, 429-439.

Wolkenhauer, O., Sreenath, S. N., Wellstead, P., Ullah, M., and Cho, K. H. (2005). A systems- and signal-oriented approach to intracellular dynamics. Biochem Soc Trans *33*, 507-515.

Wood, N. B. (1999). Aspects of fluid dynamics applied to the larger arteries. J Theor Biol *199*, 137-161.

Wu, C. (1997). Roles of integrins in fibronectin matrix assembly. Histol Histopathol *12*, 233-240.

Xenarios, I., Salwinski, L., Duan, X. J., Higney, P., Kim, S. M., and Eisenberg, D. (2002). DIP, the Database of Interacting Proteins: a research tool for studying cellular networks of protein interactions. Nucleic Acids Res *30*, 303-305.

Xing, B., Jedsadayanmata, A., and Lam, S. C. (2001). Localization of an integrin binding site to the C terminus of talin. J Biol Chem *276*, 44373-44378.

Xiong, J. P., Stehle, T., Goodman, S. L., and Arnaout, M. A. (2003). New insights into the structural basis of integrin activation. Blood *102*, 1155-1159.

Xu, W., Harrison, S. C., and Eck, M. J. (1997). Three-dimensional structure of the tyrosine kinase c-Src. Nature *385*, 595-602.

Yamamoto, K., Korenaga, R., Kamiya, A., Ando, J. (2000). Fluid shear stress activates Ca(2+) influx into human endothelial cells via P2X4 purinoceptors. Circ Res *87,* 385-91

Yan, B., Calderwood, D. A., Yaspan, B., and Ginsberg, M. H. (2001). Calpain cleavage promotes talin binding to the beta 3 integrin cytoplasmic domain. J Biol Chem *276*, 28164-28170.

Yang, H. Q., Ma, H., Takano, E., Hatanaka, M., and Maki, M. (1994). Analysis of calcium-dependent interaction between amino-terminal conserved region of calpastatin functional domain and calmodulin-like domain of mu-calpain large subunit. J Biol Chem *269*, 18977-18984.

Yang, Q., Co, D., Sommercorn, J., and Tonks, N. K. (1993). Cloning and expression of PTP-PEST. A novel, human, nontransmembrane protein tyrosine phosphatase. J Biol Chem *268*, 17650.

Yano, H., Mazaki, Y., Kurokawa, K., Hanks, S. K., Matsuda, M., and Sabe, H. (2004). Roles played by a subset of integrin signaling molecules in cadherin-based cell-cell adhesion. J Cell Biol *166*, 283-295.

Yano, Y., Geibel, J., and Sumpio, B. E. (1996). Tyrosine phosphorylation of pp125FAK and paxillin in aortic endothelial cells induced by mechanical strain. Am J Physiol *271*, C635-649.

Yi, T. M., Huang, Y., Simon, M. I., and Doyle, J. (2000). Robust perfect adaptation in bacterial chemotaxis through integral feedback control. Proc Natl Acad Sci U S A *97*, 4649-4653.

Yoshizawa, T., Sorimachi, H., Tomioka, S., Ishiura, S., and Suzuki, K. (1995). A catalytic subunit of calpain possesses full proteolytic activity. FEBS Lett *358*, 101-103.

Young, D., Munson, B., Okiishi, T (1997). A Brief Introduction to Fluid Mechanics. New York: John Wiley and Sons, Inc 323-367.

Yu, D. H., Qu, C. K., Henegariu, O., Lu, X., and Feng, G. S. (1998). Protein-tyrosine phosphatase Shp-2 regulates cell spreading, migration, and focal adhesion. J Biol Chem *273*, 21125-21131.

Zak, D.E., Gonye, G.E., Schwaber, J.S., Doyle III, F.J., 2003. Importance of input perturbations and stochastic gene expression in the reverse engineering of genetic regulatory networks: insights from an identifiability analysis of an in silico network. Genome Research *13,* 2396–2405.

Zamir, E., and Geiger, B. (2001). Molecular complexity and dynamics of cell-matrix adhesions. J Cell Sci *114*, 3583-3590.

Zarins, C.K., Giddens, D.P., Bharadvaj, B.K., Sottiural, V.S., Mabon, R.F. and Glagov S (1983). Carotid bifurcation atherosclerosis. Quantitative correlation of plaque localization with flow velocity profiles and wall shear stress. Circ Res *53,* 502-514

Zeng, L., Si, X., Yu, W. P., Le, H. T., Ng, K. P., Teng, R. M., Ryan, K., Wang, D. Z., Ponniah, S., and Pallen, C. J. (2003). PTP alpha regulates integrin-stimulated FAK autophosphorylation and cytoskeletal rearrangement in cell spreading and migration. J Cell Biol *160*, 137-146.

Zhao, J. H., Reiske, H., and Guan, J. L. (1998). Regulation of the cell cycle by focal adhesion kinase. J Cell Biol *143*, 1997-2008.

Zheng, X. M., Resnick, R. J., and Shalloway, D. (2000). A phosphotyrosine displacement mechanism for activation of Src by PTPalpha. Embo J *19*, 964-978.

Zheng, X. M., and Shalloway, D. (2001). Two mechanisms activate PTPalpha during mitosis. Embo J *20*, 6037-6049.

Zheng, X. M., Wang, Y., and Pallen, C. J. (1992). Cell transformation and activation of pp60c-src by overexpression of a protein tyrosine phosphatase. Nature *359*, 336-339.

Zhong, C., Chrzanowska-Wodnicka, M., Brown, J., Shaub, A., Belkin, A. M., and Burridge, K. (1998). Rho-mediated contractility exposes a cryptic site in fibronectin and induces fibronectin matrix assembly. J Cell Biol *141*, 539-551.

Zhu, C., Bao, G., and Wang, N. (2000). Cell mechanics: mechanical response, cell adhesion, and molecular deformation. Annu Rev Biomed Eng *2*, 189-226.